

For use in the Library only



Investigation of the Structure, Magnetic and Magnetoelastic Properties of Cobalt Ferrite and its Derivatives

Cajetan Ikenna Nlebedim

Wolfson Centre for Magnetism, School of Engineering,
Cardiff University, United Kingdom.

September, 2010.

Submitted in accordance with the requirements for the degree of Doctor of Philosophy



Cardiff School of Engineering



WOLFSON
CENTRE FOR MAGNETICS

UMI Number: U517302

All rights reserved

INFORMATION TO ALL USERS

The quality of this reproduction is dependent upon the quality of the copy submitted.

In the unlikely event that the author did not send a complete manuscript and there are missing pages, these will be noted. Also, if material had to be removed, a note will indicate the deletion.



UMI U517302

Published by ProQuest LLC 2013. Copyright in the Dissertation held by the Author.
Microform Edition © ProQuest LLC.


All rights reserved. This work is protected against
unauthorized copying under Title 17, United States Code.



ProQuest LLC
789 East Eisenhower Parkway
P.O. Box 1346
Ann Arbor, MI 48106-1346


Declaration

This work has not previously been accepted in substance for any degree and is not concurrently submitted in candidature for any other degree.

Signed:  (Candidate) Date: 08-September-2010


Statement 1

This thesis is being submitted in partial fulfilment of the requirements for the degree of*PhD*.....(insert Mch, MD, MPhil, PhD, etc, as appropriate)

Signed:  (Candidate) Date: 08-September-2010

Statement 2

This thesis is the result of my own independent work/investigation, except where otherwise stated. Other sources are acknowledged by explicit references.

Signed:  (Candidate) Date: 08-September-2010

Statement 3

I hereby give consent for my thesis, if accepted, to be available for photocopying, inter-library loan and for the title and summary to be made available to outside organisations.

Signed:  (Candidate) Date: 08-September-2010

Acknowledgement

This research was supported by the UK Engineering and Physical Science Research Council (EPSRC) under grant number EP/057094 and by the US National Science Foundation (NSF) under grant number DMR-0402716. It was also supported by the School of Engineering, Cardiff University under the Overseas Research Students Award Scheme (ORSAS).

As a Christian, I am pleased to thank God for the success of this research. I certainly cannot mention the names of everyone who contributed towards the success of this research, but as they have always known, I am very grateful. The completion of this research would have been more difficult without those supports.

I wish to thank my supervisor, Prof. A. J. Moses for his guidance from the inception to the end of this research. His supervision, counsels and expertise helped me to be focused and result oriented during the PhD period. Thanks to my second supervisor, Dr. F. Anayi for his support. I also wish to acknowledge the invaluable support from Prof. D. C. Jiles. Although he is not officially my supervisor, Prof. Jiles's expertise in magnetic and magnetostrictive properties contributed to the success of this research. I would like to thank Dr. J. E. Snyder, Dr. Y. Melikhov and Dr. P. I. Williams for their helpful supports, discussions and suggestions. My gratitude goes to all the members of staff and students at the Wolfson Centre for Magnetism who contributed to providing an enabling research environment for my PhD.

It certainly would have been very difficult completing this research without the support from my wife, Mrs. Lilian Nlebedim, my daughter, Glory Nlebedim, my mother Mrs. R. Nlebedim and my siblings. Their encouragements and supports inspired me to hold out to the end of this research. I would also appreciate Mr. T. Uwaogu and Mrs. A. N. Ekezie, who motivated me to undertake postgraduate studies.

Finally, I am grateful to the IEEE Magnetic Society and the UK Magnetic Society for financial support to travel and present my research results in various international conferences.

"The tragedy of life does not necessarily lie in not reaching one's goals but in having no goal to reach" [Bill Newman]

Abstract

The results of an investigation into the structure, magnetic and magnetostrictive properties of cobalt ferrite and its derivatives are presented in this thesis. The properties of these materials can be exploited for the development of high sensitivity stress sensors and energy efficient magnetomechanical actuators.

This study shows that the magnetostrictive properties of cobalt ferrite can be further enhanced by altering the oxygen content during preparation which resulted in the highest strain derivative reported for cobalt ferrite to date. Increase in annealing temperature before quenching the samples to ambient temperature resulted in changes in magnetic and magnetostrictive properties which were not accompanied by observable changes in crystal structure and microstructure. While the saturation magnetization increased, the anisotropy coefficient, coercive field, magnetostriction and strain derivative decreased. The changes show that annealing and quenching heat treatment resulted in cation redistribution between the tetrahedral and octahedral cation sites. Such redistribution can be exploited for property enhancement.

Further studies show that altering the processing parameters during sample preparation results in changes in the magnetostrictive properties of cobalt ferrite. Although the crystal structure, composition and saturation magnetization did not vary significantly with changes in processing parameters, coercive field decreased with increasing sintering temperature. The magnetostriction amplitude was dependent on holding time and powder compaction pressure. The strain derivative was found to depend on powder compaction pressure at any sintering temperature or holding time. The results show how the magnetoelastic properties can be varied by changing the processing parameters.

Cation substitution into cobalt ferrite is useful in optimizing the magnetomechanical properties for applications. Substituted cations altered the exchange and anisotropy energies depending on their preferences for either the octahedral or tetrahedral site. $\text{Co}_{1+x}\text{Ge}_x\text{Fe}_{2-2x}\text{O}_4$ is the only composition of all reported compositions with simultaneous improvement of magnetostriction amplitude and strain derivative. The highest strain

derivative of all cation substitution studies reported was obtained for $\text{CoGa}_x\text{Fe}_{2-x}\text{O}_4$. The strain derivative of $\text{CoAl}_x\text{Fe}_{2-x}\text{O}_4$ is higher than that for $\text{Co}_{1+x}\text{Ge}_x\text{Fe}_{2-2x}\text{O}_4$ but lower than that for $\text{CoGa}_x\text{Fe}_{2-x}\text{O}_4$. On the other hand, its magnetostriction is higher than that for $\text{CoGa}_x\text{Fe}_{2-x}\text{O}_4$ and lower than that for $\text{Co}_{1+x}\text{Ge}_x\text{Fe}_{2-2x}\text{O}_4$.

Samples sintered in vacuum developed a deleterious $\text{Co}_{1-x}\text{Fe}_x\text{O}$ second phase. The second phase, which is a solid solution of FeO in CoO is antiferromagnetic, resulted in decreased magnetostriction amplitude. This effect on magnetostriction was more pronounced with increase in sintering temperature than increase in holding time. Also, the sample sintered at higher temperatures and held for longer times showed the lowest anisotropy.

In this research, cobalt ferrite thin films were deposited at 523 K which eliminates the need for annealing at higher temperatures for homogeneity and crystallinity. This offers hope for integration of thin films based on cobalt ferrite into micro-electromechanical devices.

Table of Contents

Declaration i

Acknowledgement..... ii

Abstract iii

Table of Contents v

List of Figures ix

List of Tables xv

List of Equations xvi

Chapter 1. General Introduction 1

1.1 Introduction 1

1.2 Scope of the Research 4

References to Chapter 1: 5

Chapter 2. Magnetism in Magnetic Oxides 6

2.1 Introduction 6

2.2 Exchange Interaction in Magnetic Oxides 6

2.3 Magnetic Ordering 7

2.4 Magnetization Processes 8

2.4.1 Domain processes during magnetization 10

2.4.2 Curie temperature 12

2.5 Anisotropy 13

2.5.1 Magnetocrystalline anisotropy 13

2.5.2 Magnetoelastic anisotropy 16

2.5.3 Shape anisotropy 17

2.6 Law of Approach to Saturation Magnetization 18

2.7 Magnetostriction 20

2.7.1 Introduction 20

2.7.2 Spontaneous and field-induced magnetostriction 20

2.7.3 Magnetostriction in cubic materials 23

2.7.4 Strain derivative and stress sensitivity of magnetostrictive materials 25

References to Chapter 2: 27

Chapter 3. Ferrites..... 29

3.1 Introduction 29

3.2 Spinel Ferrites 29

3.3 Magnetization in Spinel Ferrites 34

3.4 Non-Spinel Ferrites 36

3.5	Cobalt Ferrite (CoFe ₂ O ₄).....	37
3.6	Preparation of Bulk Cobalt Ferrite	43
3.6.1	Traditional ceramic method.....	43
3.6.2	Other methods of preparing bulk CoFe ₂ O ₄	50
3.7	Preparation of Thin Film Cobalt Ferrite.....	51
3.7.1	Pulsed laser deposition (PLD).....	51
3.7.2	Other methods of preparing thin films of CoFe ₂ O ₄	52
	References to Chapter 3:	55
Chapter 4. Review of Previous Studies on Cobalt Ferrite for Magnetostrictive Applications		58
4.1	Introduction	58
4.2	Previous Researches on Magnetostrictive Application of Cobalt Ferrite	58
	References to Chapter 4:	69
Chapter 5. Experimental Procedure and Measurement Systems.....		71
5.1	Introduction	71
5.2	Preparation of Bulk Cobalt Ferrite Samples	71
5.2.1	Powder preparation for un-substituted cobalt ferrite	72
5.2.2	Preparation of substituted cobalt ferrite	73
5.2.3	Powder Compaction	76
5.2.4	Calcining.....	77
5.2.5	Sample milling and sieving.....	77
5.2.6	Sample sintering	79
5.3	Characterization of Bulk Cobalt Ferrite.....	81
5.3.1	Crystal structure determination.....	81
5.3.2	Microstructure and composition determination	85
5.3.3	Measurement of magnetic properties	88
5.3.4	Magnetostriction and strain derivative measurement	90
5.4	Preparation of Thin Film Cobalt Ferrite Samples	97
5.5	Characterization of Thin Film Cobalt Ferrite Samples	98
5.5.1	Crystal structure and film orientation.....	98
5.5.2	Film Thickness and Composition.....	98
5.5.3	Magnetic properties measurements.....	98
	References to Chapter 5:	99
Chapter 6. Experimental Results and Discussion: Dependence of Properties on Vacuum Sintering Environment.....		101
6.1	Introduction	101
6.2	Variation of Density with Sintering Conditions	101
6.3	Crystal Structure Determination	102
6.4	Microstructure Determination.....	104
6.5	Sample Composition	105
6.6	Effect of Vacuum Sintering on Coercive Field	106
6.7	Variation of First Cubic Anisotropy Constant with Vacuum Sintering	107

6.8	Influence of Vacuum Sintering on Magnetostriction	108
6.9	Effect of Vacuum Sintering on Strain Derivative	109
	References to Chapter 6:	110
Chapter 7. Experimental Results and Discussion: Dependence of Properties on Annealing and Quenching Heat Treatment..... 113		
7.1	Introduction	113
7.2	Influence of Heat Treatment on Crystal Structure and Lattice Parameter	114
7.3	Influence of Heat Treatment on Microstructure.....	115
7.4	Compositions of the Samples Before and After Heat Treatment.....	115
7.5	Variation of Saturation Magnetization due to Heat Treatment.....	116
7.6	Dependence of Anisotropy Constant and Coercive field on Heat Treatment	118
7.7	Influence of Heat Treatment on Magnetostriction	120
7.8	Strain Derivative	123
	References to Chapter 7:	126
Chapter 8. Experimental Results and Discussion: Effect of Variation of Processing Parameters on Properties of Cobalt ferrite..... 129		
8.1	Introduction	129
8.2	Determination of the Crystal Structure of the Samples	129
8.3	Effect of Processing Parameters on Microstructure	130
8.4	Composition of the samples	131
8.5	Effect of Variation of Processing Parameters on Saturation Magnetization	132
8.6	Variation of Coercive Field due to Variation in Processing Parameters	133
8.7	Dependence of Magnetostriction on Processing Parameters.....	134
8.8	Dependence of Strain Derivative on Processing Parameters	135
	References to Chapter 8:	137
Chapter 9. Experimental Results and Discussion: Structure, Magnetic and Magnetostrictive Properties of $\text{CoMe}_x\text{Fe}_{2-x}\text{O}_4$ (Me = Al, Ga and Ge/Co) 138		
9.1	Introduction	138
9.1.1	Influence of Al^{3+} substitution on the crystal structure of cobalt ferrite.....	139
9.1.2	Microstructure and compositions of cations in the $\text{CoAl}_x\text{Fe}_{2-x}\text{O}_4$ system	141
9.1.3	Curie temperature of the $\text{CoAl}_x\text{Fe}_{2-x}\text{O}_4$ system	142
9.1.4	Effect of Al^{3+} substitution on magnetization	143
9.1.5	Variation of magnetostriction of $\text{CoAl}_x\text{Fe}_{2-x}\text{O}_4$ as a function of Al^{3+} concentration	144
9.1.6	Variation of strain derivative of $\text{CoAl}_x\text{Fe}_{2-x}\text{O}_4$ as a function of Al^{3+} concentration	146
9.1.7	Dependence of magnetostriction of $\text{CoAl}_x\text{Fe}_{2-x}\text{O}_4$ on temperature [(x =0.0, 0.2, 0.5, 0.7) and (T = 50, 150, 250 and 350 K)]	148
9.1.8	Dependence of strain derivative of $\text{CoAl}_x\text{Fe}_{2-x}\text{O}_4$ on temperature [(x = 0.0, 0.2, 0.5, 0.7) and (T = 50, 150, 250 and 350 K)]	151
9.2	Structure, Magnetic and Magnetostrictive Properties of $\text{CoGa}_x\text{Fe}_{2-x}\text{O}_4$	152
9.2.1	Crystal structure of the $\text{CoGa}_x\text{Fe}_{2-x}\text{O}_4$ system.....	152
9.2.2	Composition of cations and microstructure of the $\text{CoAl}_x\text{Fe}_{2-x}\text{O}_4$ system	153
9.2.3	Variation of magnetization as a function of Ga^{3+} substitution	154

Table of Contents

9.2.4	Room temperature magnetostriction studies on $\text{CoGa}_x\text{Fe}_{2-x}\text{O}_4$	155
9.2.5	Dependence of maximum strain derivative of $\text{CoGa}_x\text{Fe}_{2-x}\text{O}_4$ on Ga^{3+} concentration.....	157
9.2.6	Temperature dependence of magnetostriction in $\text{CoGa}_x\text{Fe}_{2-x}\text{O}_4$ system [(x =0.0, 0.2, 0.4) and (T = 50, 150, 250 and 350 K)]	158
9.2.7	Temperature dependence of strain derivative of $\text{CoGa}_x\text{Fe}_{2-x}\text{O}_4$ system [(x =0.0, 0.2, 0.4) and (T = 50, 150, 250 and 350 K)]	159
9.3	Comparison of 300 K Magnetostrictive Properties of $\text{CoAl}_x\text{Fe}_{2-x}\text{O}_4$, $\text{CoGa}_x\text{Fe}_{2-x}\text{O}_4$ and $\text{Co}_{1+x}\text{Ge}_x\text{Fe}_{2-2x}\text{O}_4$	160
	References to Chapter 9:	163

Chapter 10. Experimental Results and Discussion: Dependence of Crystal Structure and Magnetic Properties of Thin Film Cobalt Ferrite on Deposition Temperature (T = 523, 623, 723, 823 and 873 K)	166
10.1 Introduction	166
10.2 Variation of Crystal Structure with Deposition Temperature.....	166
10.3 Film Composition and Thickness.....	167
10.4 Thermal Expansion Coefficient and Lattice Parameter Mismatch Strains.....	168
10.5 Magnetic Properties of the Thin Film Cobalt Ferrite Samples.....	170
10.5.1 Variation of magnetization with deposition temperature	170
10.5.2 Variation of coercive field with deposition temperature	172
References to Chapter 10:	172

Chapter 11. Conclusions and Recommended Future Research	175
11.1 Conclusions.....	175
11.2 Recommended Future Works	177
11.2.1 Mechanical properties of cobalt ferrite	177
11.2.2 Distribution of cations between the tetrahedral and octahedral sites	177
11.2.3 Oxygen content determination.....	178
11.2.4 Domain studies	178
11.2.5 Modelling the magnetostrictive properties of cobalt ferrite	178
11.2.6 Measuring the magnetostriction of thin film cobalt ferrite samples	179
References to Chapter 11:	180

Appendix I Determination of Mechanical Properties of Cobalt Ferrite by an Ultrasonic Method . 181

Appendix II Domain Studies in Cobalt Ferrite Samples

Appendix III Modelling the Magnetic and Magnetostrictive Properties of Cobalt Ferrite

Reference to Appendix III:

Appendix IV Journal Publications and Conference Presentations Based on this Research

List of Figures

Fig. 2.1: Summary of levels of magnetic ordering	8
Fig. 2.2: A typical hysteresis loop	9
Fig. 2.3: Schematic representation of the Bloch wall [2.7]	11
Fig. 2.4: Determination of Curie temperature of a cobalt ferrite sample from a magnetization vs. temperature plot	13
Fig. 2.5: Magnetic properties of iron and nickel measured in different crystallographic axes of the crystal structures. In S.I units, 1 Gauss = 10^{-4} T and 1 Oe = 79.58 A/m.	15
Fig.2.6: Schematic representation of the spontaneous and field-induced magnetostriction	21
Fig. 2.7: Magnetostriction as function of applied magnetic field [15].....	22
Fig.3.1: (a)Tetrahedral site surrounded by four oxygen ions (b) Octahedral site surrounded by six oxygen ions (c) Spinel crystal structure. Shaded and non-shaded parts represent octants of similar cation occupancy (d) Two octants showing cation and oxygen distribution. <i>After B. D. Cullity [3-2]</i>	30
Fig. 3.2: Schematic of the random distribution of cations between the octahedral and tetrahedral sites, in formula unit of a spinel structure.....	31
Fig. 3.3: Magnetization at 0 K in normal spinels with $ZnFe_2O_4$ and $NiFe_2O_4$ as examples .	36
Fig. 3.4: X-ray diffraction pattern for a Co-ferrite spinel structured sample	38
Fig. 3.5: Temperature dependence of first cubic magnetocrystalline anisotropy constant K_1 of $Co_xMn_{1-x}Fe_2O_4$ for $x = 0, 0.01, 0.02, 0.04, 0.06, 0.08, 0.1$ and 0.25 . 1 $ergcm^{-3}$ in S.I units is $10 Jm^{-3}$. <i>After R. F Pearson [19]</i>	39
Fig. 3.6: Typical magnetostriction curve of cobalt ferrite measured at 300 K. The hysteresis in this curve has been neglected for clarity of illustration.	41
Fig. 3.7: Temperature dependence of magnetostriction of $CoFe_2O_4$. 1 kOe = 79.58 kA/m. The figure shows that the amplitude of magnetostriction reduces with increasing measurement temperature [3-22].	42
Fig. 3.8: Steps for the preparation of $CoFe_2O_4$ via the traditional ceramic route	44
Fig. 3.9: Schematic showing voids between large and small powder particles. More work is required to eliminate voids between larger particles of the same volume.	45

Fig. 3.10: Stages in sintering [27].	46
Fig. 3.11: Typical microstructure of ceramic CoFe_2O_4	49
Fig. 3.12: A microstructure of CoFe_2O_4 material with two phases labelled 1 and 2.....	49
Fig. 3.13: Schematic of a basic pulsed laser deposition system	52
Fig. 4.1: λ -H plots obtained from Fig. 5 of the study by Bhamre et al. [4-14], for samples sintered at 1100 °C. Additional features were drawn to help determine the strain derivative.	64
Fig. 5.1: Ohaus precision balance used for measuring masses of the oxide powders	76
Fig. 5.2: Specac manual hydraulic press used for powder compaction.....	76
Fig. 5.3: Spetramill ball pestle impact grinder used for sample milling.....	78
Fig. 5.4: Air furnace used for calcining and sintering of the samples	80
Fig. 5.5: Conditions necessary for Bragg's law for X-ray diffraction	82
Fig. 5.6: Cobalt ferrite powder sample in the Goniometer for X-ray diffraction.....	83
Fig. 5.7: Schematic diagram of an X-ray diffractometer	83
Fig. 5.8: Interaction volume of the primary electron beam in a sample during SEM [5-5]	86
Fig. 5.9: Lakeshore model 7410 VSM with 740-H Head Drive	89
Fig.5.10: Wheatstone half-bridge configuration for cobalt ferrite magnetostriction measurement using the Quantum Design PPMS. A similar resistive strain that mounted on cobalt ferrite was also mounted on copper and was used as a dummy resistor.	91
Fig.5.11: Schematic diagram of the universal dC measurement system used for magnetostriction measurements.....	95
Fig.5.12: Schematic of the three-wire, quarter-bridge strain gauge circuit used for magnetostriction measurement with the universal dc measurement system ...	96
Fig. 6.1: Variation of sample densities with sintering temperature and time	102
Fig. 6.2: XRD patterns for the samples showing the sintering temperature and holding time at a particular sintering temperature. For each sample, unmarked peaks correspond to the spinel cobalt ferrite pattern. Peaks marked with ♠ correspond to the CoO pattern.....	103

Fig. 6.3: SEM micrographs of samples held at constant sintering temperature for different times (A, B and C) and for constant sintering times at different sintering temperatures. (I, II and III) 104

Fig. 6.4: Variation of coercive field with sintering temperature and at different sintering times..... 106

Fig. 6.5: Variation of the first cubic anisotropy coefficient with sintering temperature and at different sintering times 107

Fig. 6.6: Variation of magnetostriction with sintering times at constant sintering temperatures (upper) and variation of magnetostriction with sintering temperatures at constant sintering times (lower)..... 108

Fig. 6.7: Dependence of strain derivative on sintering temperature and time 110

Fig. 7.1: XRD pattern of the quenched and furnace cooled cobalt ferrite samples 114

Fig. 7.2: E-SEM micrographs of all the samples. The samples were annealed at temperatures shown before being quenched in water to ambient temperature. Images of the furnace cooled sample and the sample marked 1200 °C were obtained from diamond-sawed sample surfaces. The rest were obtained from fractured surfaces. 116

Fig. 7.3: Variation of magnetization at Field (H) = 4 MA/m with heat treatment temperature..... 117

Fig. 7.4: Variation of anisotropy constant and coercive field with heat treatment temperature..... 118

Fig. 7.5: Variation of peak to peak magnetostriction amplitude with applied magnetic field..... 120

Fig. 7.6: Comparing the magnetostriction curves of furnace cooled samples from this study and previous study..... 122

Fig. 7.7: Comparing the magnetostriction curves of furnace cooled samples from this study and previous study..... 123

Fig. 7.8: Variation of strain derivative with applied field..... 124

Fig. 7.9: Variation strain derivative with heat treatment 124

Fig. 8.1: X-ray diffraction patterns for a selected subset of representative samples showing the effect of varying sintering temperature (B, C and D), holding time (C and E) and powder compaction pressure (A and C). 130

Fig.8.2: Back scattered electron micrographs of samples after various sintering temperatures, holding times and powder compaction pressures for all the samples. Uniform image contrast indicates the presence of a single phase. ...	131
Fig. 8.3: First quadrants of the magnetization vs. hysteresis plots of the samples	132
Fig.8.4: Effects of compaction pressure, sintering temperature and holding time on coercive field	133
Fig. 8.5: Dependence of magnetostriction on processing parameters.....	135
Fig. 9.1: XRD patterns showing the influence of Al ³⁺ substitution on the crystal structure of cobalt ferrite. x is the proportion of Al ³⁺ in CoAl _x Fe _{2-x} O ₄	139
Fig. 9.2: Variation of lattice parameter with aluminium concentration (x) for CoAl _x Fe _{2-x} O ₄	140
Fig. 9.3: Scanning electron micrographs for different aluminium compositions (x) for the CoAl _x Fe _{2-x} O ₄ system.....	142
Fig. 9.4: Curie temperature of the samples for = 0.0, 0.2, 0.5 and 0.7	143
Fig. 9.5: Plots of magnetization against applied magnetic field. The inset is a plot of magnetization at 1250 kA/m as a function of Al ³⁺ concentration at 300 K.	144
Fig. 9.6: Variation of magnetostriction with applied magnetic field at 300 K for the CoAl _x Fe _{2-x} O ₄ system.....	145
Fig. 9.7: Variation of strain derivative with applied magnetic field at 300 K for the CoAl _x Fe _{2-x} O ₄ system (x = 0.0 to 0.9)	146
Fig. 9.8: Applied magnetic field at maximum strain derivative (dλ/dH) _{max} as a function of aluminium concentration. The field at (dλ/dH) _{max} are 101 kA/m, 19 kA/m and 11 kA/m for x = 0.0, 0.1 and 0.2 respectively.	147
Fig. 9.9 : Magnetostriction vs. field plots for CoAl _x Fe _{2-x} O ₄ system measure at different temperatures of 50, 150, 250 and 350 K. (a) Co _{1.02} Fe _{1.98} O ₄ (b) Co _{1.03} Al _{0.18} Fe _{1.79} O ₄ , (c) Co _{1.03} Al _{0.49} Fe _{1.48} O ₄ and (d) Co _{1.04} Al _{0.73} Fe _{1.23} O ₄	149
Fig. 9.10: Variation of strain sensitivity with concentration for the CoAl _x Fe _{2-x} O ₄ system (x = 0, 0.2, 0.5 and 0.7).....	151
Fig. 9.11: XRD patterns of the CoGa _x Fe _{2-x} O ₄ samples (x = 0.0, 0.2, 0.4, 0.5 and 0.6).....	153
Fig. 9.12: Backscattered electron images of the CoGa _x Fe _{2-x} O ₄	154

Fig. 9.13: Variation of magnetization at 300 K as a function of applied field for Ga ³⁺ concentrations x = 0.0 to 0.6. The inset shows the variation of saturation magnetization at 300 K with gallium concentration.....	155
Fig. 9.14: Variation of magnetostriction as a function of applied field for CoGa _x Fe _{2-x} O ₄	156
Fig. 9.15: Variation of maximum strain derivative as a function of applied field for CoGa _x Fe _{2-x} O ₄	157
Fig. 9.16: Dependence of magnetostriction in CoGa _x Fe _{2-x} O ₄ on temperature variation .	159
Fig. 9.17: Dependence of strain derivative in CoGa _x Fe _{2-x} O ₄ on temperature variation...	160
Fig. 9.18: Comparison of ambient temperature magnetostriction of Co _{1+x} Ge _x Fe _{2-2x} O ₄ , CoAl _x Fe _{2-x} O ₄ and CoGa _x Fe _{2-x} O ₄	162
Fig. 9.19: Dependence of (dλ/dH) _{max} of Ge ⁴⁺ /Co ²⁺ , Al ³⁺ and Ga ³⁺ on concentrations	163
Fig. 10.1: XRD pattern of the thin film cobalt ferrite deposited from 523 to 873 K. The pattern plotted in orange line is for a bulk sample fabricated by the traditional ceramic method. The peaks marked Si (substrate) are peaks from Si/SiO ₂ substrate.	167
Fig. 10.2: The cross-sectional micrograph of the thin film measured by SEM	168
Fig. 10.3: Dependence of thermal expansion mismatch strain on deposition temperature	169
Fig. 10.4: In-plane magnetization vs. field plots measured on the thin film samples at different deposition temperatures.	170
Fig. 10.5: Perpendicular magnetization vs. field plots measured on the thin film samples at different deposition temperatures.....	171
Fig. 10.6: Variation of maximum magnetization with deposition temperature of the thin film cobalt ferrite samples	171
Fig. 10.7: Variation of coercive field with deposition temperature.....	172
Fig. A1.1: Principle of measuring the mechanical properties of cobalt ferrite using the single probe ultrasonic method.....	181
Fig. A1.2: Using the ultrasonic wave method for flaw detection	182
Fig. A1.3: Measuring the mechanical properties of cobalt ferrite using the two probe ultrasonic method.....	183

Fig. A1.4: Experimental setup for determining the mechanical properties of cobalt ferrite via the ultrasonic method.....183

Fig. All. 1: Sample preparation instrumentation for domain imaging184

Fig. All. 2: Kerr microscope used for domain imaging185

Fig. All. 3: Bar domains of cobalt ferrite obtained using Kerr microscopy185

Fig. All. 4: Changes in domain with changes in magnetizing current186

Fig. All. 1: Model geometry.....196

Fig. All. 2: Model mesh.....197

Fig. All. 3: Variation with magnetic field strength (A/m) with current density (A/m²) ...198

Fig. All. 4: Variation with magnetic flux density (T) with current density (A/m²).....199

Fig. All. 5: Magnetization in the magnetostrictive rod at current densities $J_0 = 1$ to 1×10^7 A/m². Z-direction is the long axis of the magnetostrictive rod.....200

Fig. All. 6: Axial strain in the magnetostrictive rod at current densities $J_0 = 1$ to 1×10^7 A/m². Z-direction is the long axis of the magnetostrictive rod.....201

Fig. All. 7: Variation of magnetostriction with applied field along the magnetostrictive rod.....201

List of Tables

Table 3.1: Chemical compositions of different phases of hexaferrites	36
Table 5.1: Masses of compounds required for producing 15 g of $\text{CoAl}_x\text{Fe}_{2-x}\text{O}_4$. Mass was not conserved due to error in determining the masses of $\text{CoAl}_x\text{Fe}_{2-x}\text{O}_4$	74
Table 5.2: Masses of compounds required for producing 15 g of $\text{CoAl}_x\text{Fe}_{2-x}\text{O}_4$ with correction made for mass conservation.	75
Table 5.3: Method of determining cobalt ferrite sample composition using data from EDX result	88
Table 6.1: EDX results corresponding to electron images A, B and C	105
Table 6.2: EDX results corresponding to electron images I, II and III	105
Table 7.1: Influence of heat treatment of lattice parameters of the samples	115
Table 8.1: Dependence of strain derivative on processing parameters.....	136
Table 9.1: Concentration of cations in the $\text{CoAl}_x\text{Fe}_{2-x}\text{O}_4$ system as determined by EDX..	141
Table 9.2: Comparison of the magnitude of λ and $(d\lambda/dH)_{\text{max}}$ in $\text{CoAl}_x\text{Fe}_{2-x}\text{O}_4$, $\text{CoMn}_x\text{Fe}_{2-x}\text{O}_4$ [9-7], $\text{CoCr}_x\text{Fe}_{2-x}\text{O}_4$ [9-7] and $\text{CoGa}_x\text{Fe}_{2-x}\text{O}_4$ [9-5].	148
Table 9.3: Concentrations of the cations in $\text{CoGa}_x\text{Fe}_{2-x}\text{O}_4$ system as determined by EDX	153
Table 9.4: Comparison of the $(d\lambda/dH)_{\text{max}}$ in $\text{CoAl}_x\text{Fe}_{2-x}\text{O}_4$, $\text{CoMn}_x\text{Fe}_{2-x}\text{O}_4$ [7], $\text{CoCr}_x\text{Fe}_{2-x}\text{O}_4$ [7] and $\text{CoGa}_x\text{Fe}_{2-x}\text{O}_4$ [9]. Sample from this study is shown in red font while those from previous studies are in black font.	158

List of Equations

$$D = D_0 \exp\left(\frac{-Q}{RT}\right) \quad (1-1) \dots\dots\dots 2$$

$$F = U - TS \quad (1-2) \dots\dots\dots 2$$

$$W_e = -2 \sum J_{ij} \sum S_i \cdot S_j \quad (2-1) \dots\dots\dots 7$$

$$\mathbf{B} = \mu_0 (\mathbf{H} + \mathbf{M}) \quad (2-2) \dots\dots\dots 9$$

$$E_{magcrystal} = K_0 + K_1(\alpha_1^2 \alpha_2^2 + \alpha_2^2 \alpha_3^2 + \alpha_3^2 \alpha_1^2) + K_2(\alpha_1^2 \alpha_2^2 \alpha_3^2) + \dots \quad (2-3) \dots\dots\dots 15$$

$$E_{magcrystal} = K_1(\alpha_1^2 \alpha_2^2 + \alpha_2^2 \alpha_3^2 + \alpha_3^2 \alpha_1^2) \quad (2-4) \dots\dots\dots 15$$

$$E_{magcrystal} = K'_1 \sin^2 \vartheta + K'_2 \sin^4 \vartheta + K'_3 \sin^6 \vartheta + \dots \quad (2-5) \dots\dots\dots 16$$

$$E_{magcrystal} = K'_1 \sin^2 \vartheta \quad (2-6) \dots\dots\dots 16$$

$$E_{magelastic} = -\frac{3}{2} \lambda_{100} \sigma (\alpha_1^2 \gamma_1^2 + \alpha_2^2 \gamma_2^2 + \alpha_3^2 \gamma_3^2) \quad (2-7) \dots\dots\dots 17$$

$$-3 \lambda_{111} \sigma (\alpha_1 \alpha_2 \gamma_1 \gamma_2 + \alpha_2 \alpha_3 \gamma_2 \gamma_3 + \alpha_3 \alpha_1 \gamma_3 \gamma_1)$$

$$E_{magelastic} = -\frac{3}{2} \lambda \sigma \cos^2 \theta \quad (2-8) \dots\dots\dots 17$$

$$E_{ani} = E_{magcrystal} + E_{magelastic} = K_1(\alpha_1^2 \alpha_2^2 + \alpha_2^2 \alpha_3^2 + \alpha_3^2 \alpha_1^2) - \frac{3}{2} \lambda \sigma \cos^2 \theta \quad (2-9) \dots\dots\dots 17$$

$$\mathbf{H}_d = -N_d \mathbf{M} \quad (2-10) \dots\dots\dots 18$$

$$\mathbf{H}_{eff} = \mathbf{H}_{app} - \mathbf{H}_d = \mathbf{H}_{app} - N_d \mathbf{M} \quad (2-11) \dots\dots\dots 18$$

$$M = M_s \left(1 - \frac{a}{H} - \frac{b}{H^2} - \dots \right) + \kappa H \quad (2-12) \dots\dots\dots 19$$

$$b = \frac{8}{105} \frac{K_1^2}{\mu_0^2 M_s^2} \quad (2-13) \dots\dots\dots 19$$

$$M = M_s \left[1 - \frac{8}{105} \left(\frac{K_1}{\mu_0 M_s H} \right)^2 \right] + \kappa H \quad (2-14) \dots\dots\dots 19$$

$$\lambda_0 = \frac{\epsilon}{3} \quad (2-15) \dots\dots\dots 21$$

$$\lambda_s = \epsilon - \frac{\epsilon}{3} = \frac{2\epsilon}{3} \quad (2-16) \dots\dots\dots 21$$

$$\varepsilon = \frac{3}{2} \lambda_S \quad (2-17) \dots\dots\dots 22$$

$$\lambda_S(\theta) = \frac{3}{2} \lambda_S \left(\cos^2 \theta - \frac{1}{3} \right) \quad (2-18) \dots\dots\dots 22$$

$$\lambda_{S\parallel} - \lambda_{S\perp} = \lambda_S + \frac{\lambda_S}{2} = \frac{3}{2} \lambda_S \quad (2-19) \dots\dots\dots 23$$

$$\lambda_S = \frac{3}{2} \lambda_{100} \left(\alpha_x^2 \beta_x^2 + \alpha_y^2 \beta_y^2 + \alpha_z^2 \beta_z^2 - \frac{1}{3} \right) \quad (2-20) \dots\dots\dots 23$$

$$+ 3\lambda_{111} (\alpha_x \alpha_y \beta_x \beta_y + \alpha_y \alpha_z \beta_y \beta_z + \alpha_z \alpha_x \beta_z \beta_x)$$

$$\lambda_S = \lambda_{100} + 3(\lambda_{111} - \lambda_{100}) (\alpha_x^2 \alpha_y^2 + \alpha_y^2 \alpha_z^2 + \alpha_z^2 \alpha_x^2) \quad (2-21) \dots\dots\dots 24$$

$$\lambda_{S_{Average}} = \frac{2}{5} \lambda_{100} + \frac{3}{5} \lambda_{111} \quad (2-22) \dots\dots\dots 24$$

$$\lambda_S(\theta) = \frac{3}{2} \lambda_{S_{Average}} \left(\cos^2 \theta - \frac{1}{3} \right) \quad (2-23) \dots\dots\dots 24$$

$$\frac{dI}{I} = \lambda_S \left[1 - \frac{8}{105} \left(\frac{K_1}{\mu_0 M_S H} \right)^2 \right] + \kappa H \quad (2-24) \dots\dots\dots 25$$

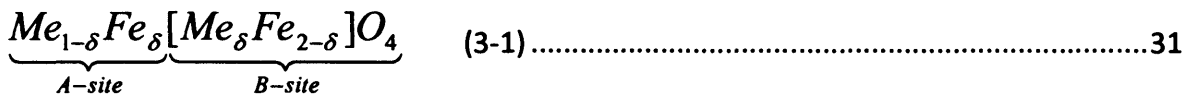
$$\lambda = s^H \sigma + dH \quad (2-25) \dots\dots\dots 25$$

$$B = d\sigma + \mu^\sigma H \quad (2-26) \dots\dots\dots 25$$

$$\left(\frac{\partial \lambda}{\partial H} \right)_\sigma = d \quad (\text{Strain derivative}) \quad (2-27) \dots\dots\dots 25$$

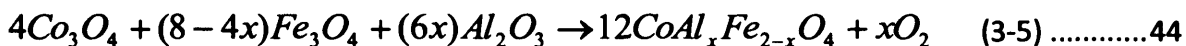
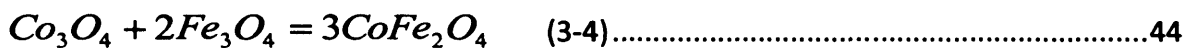
$$\left(\frac{\partial B}{\partial \sigma} \right)_H = d \quad (\text{Stress sensitivity}) \quad (2-28) \dots\dots\dots 25$$

$$\left(\frac{\partial \lambda}{\partial H} \right)_\sigma = \left(\frac{\partial B}{\partial \sigma} \right)_H \quad (2-29) \dots\dots\dots 26$$

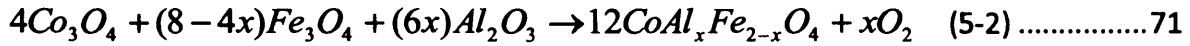


$$\delta = \left(\frac{1}{4} \right) \left(7 - \left[\frac{\mu_{FU}}{\mu_B} \right] \right) \quad (3-2) \dots\dots\dots 31$$

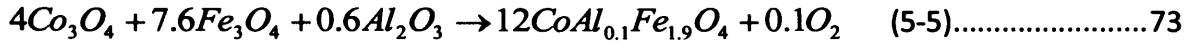
Inverse spinel structure is favoured (3-3).....34



$$\frac{dB}{d\sigma} \propto \frac{d\lambda}{dH} \propto \frac{\lambda_{\max}}{K_1} \quad (4-1) \dots\dots\dots 60$$



(5-3) 71



$$2d_{hkl} \sin \theta_{hkl} = n\lambda_{x\text{-ray}} \quad (5-12) \dots\dots\dots 81$$

$$d_{hkl} = \frac{a}{\sqrt{h^2 + k^2 + l^2}} \quad (5-13) \dots\dots\dots 82$$

$$\frac{4\sin^2 \theta}{\lambda_{x\text{-ray}}^2} = \frac{1}{d^2} \quad (5-14) \dots\dots\dots 84$$

$$h^2 + k^2 + l^2 = 3 * \left[\frac{d_1^2}{d_i^2} \right] \quad (5-15) \dots\dots\dots 85$$

$$\frac{V_o}{I} (H = 0) = R_{\text{measured}} \quad (5-16) \dots\dots\dots 92$$

$$I = I_1 + I_2 \quad (5-17) \dots\dots\dots 92$$

$$\frac{I_1}{I_2} = \frac{R_1 + R_2}{R_{\text{Co-ferrite}} + R_{\text{copper}}} \quad (5-18) \dots\dots\dots 92$$

$$I_1 = I_2 \frac{R_1 + R_2}{R_{\text{Co-ferrite}} + R_{\text{copper}}} \quad (5-19) \dots\dots\dots 92$$

$$I_2 = I_1 \frac{R_{Co-ferrite} + R_{copper}}{R_1 + R_2} \quad (5-20) \dots\dots\dots 92$$

$$I = I_1 + I_1 \frac{R_{Co-ferrite} + R_{copper}}{R_1 + R_2} = I_1 \left(1 + \frac{R_{Co-ferrite} + R_{copper}}{R_1 + R_2} \right) = I = I_1 \left(\frac{R_1 + R_2 + R_{Co-ferrite} + R_{copper}}{R_1 + R_2} \right) \dots\dots$$

(5-21)..... 92

$$I_1 = I \left(\frac{R_1 + R_2}{R_1 + R_2 + R_{Co-ferrite} + R_{copper}} \right) \quad (5-22) \dots\dots\dots 93$$

$$I_2 = I \left(\frac{R_{Co-ferrite} + R_{copper}}{R_1 + R_2 + R_{Co-ferrite} + R_{copper}} \right) \quad (5-23) \dots\dots\dots 93$$

$$V_o = V_A - V_B = I_1 R_{Co-ferrite} - I_2 R_1 \quad (5-24) \dots\dots\dots 93$$

$$\frac{V_o}{I} = \left(\frac{(R_1 + R_2) R_{Co-ferrite}}{R_1 + R_2 + R_{Co-ferrite} + R_{copper}} - \frac{(R_{Co-ferrite} + R_{copper}) R_1}{R_1 + R_2 + R_{Co-ferrite} + R_{copper}} \right) \quad (5-25) \dots\dots\dots 93$$

$$\frac{V_o}{I} (H = 0) = R_{measured} = \frac{R_2 R_{Co-ferrite} - R_{copper} R_1}{R_1 + R_2 + R_{Co-ferrite} + R_{copper}} \quad (5-26) \dots\dots\dots 93$$

(5-27) 94

$$\frac{V_o}{I} (H = H) = R_{measured} = \frac{\Delta R_{Co-ferrite}}{4} \quad (5-28) \dots\dots\dots 94$$

$$F_G = \frac{\Delta R}{R\epsilon} = \frac{\Delta R_{Co-ferrite}}{R\epsilon} = \frac{4R_{measured}}{R\epsilon} \quad (5-29) \dots\dots\dots 94$$

$$Magnetostriction = \epsilon = \frac{4R_{measured}}{F_G R} \quad (5-30) \dots\dots\dots 94$$

$$Magnetostriction = \epsilon = R_{measured} (5.58 * 10^{-3}) \quad (5-31) \dots\dots\dots 94$$

$$\frac{1}{2} * \left[\frac{\lambda_{i+1} - \lambda_i}{x_{i+1} - x_i} + \frac{\lambda_i - \lambda_{i-1}}{x_i - x_{i-1}} \right] \quad (5-32) \dots\dots\dots 97$$

$$M = \sum M_B - \sum M_A \quad (7-1) \dots\dots\dots 117$$

$$\epsilon = (\alpha_{film} - \alpha_{substrate}) (T_{Dep} - T_{Ambient}) \quad 10-1 \dots\dots\dots 169$$

Chapter 1. General Introduction

1.1 Introduction

Cobalt ferrite (CoFe_2O_4) and its derivatives $\text{CoMe}_x\text{Fe}_{2-x}\text{O}_4$ (where Me stands for a metal ion) are promising materials for use in devices such as transducers, vibration controllers and sound generators because of their high magnetostriction and high rate of change of strain with magnetic field. Their technological potential as alternatives to the rare earth based magnetostrictive materials has recently attracted much interest. Apart from suitable mechanical and chemical properties, it has been shown that composites based on CoFe_2O_4 have a higher sensitivity of strain to applied field compared to Terfenol based composites [1-1].

The magnetic and magnetostrictive properties of cobalt ferrite depend on how the cations are distributed in the lattice and as well as the structural properties. Both cation distribution and structural properties of CoFe_2O_4 can be altered by the processing route, heat treatment and cation substitution. Such alterations can cause changes in the amplitude of magnetostriction (λ) and sensitivity of magnetostrictive strain to applied magnetic field or strain sensitivity ($d\lambda/dH$). The objective of this research is to investigate how changes due to processing, heat treatment and cation substitution affect the structural, magnetic and magnetostrictive properties of bulk CoFe_2O_4 and magnetic properties of CoFe_2O_4 thin films. It also includes an investigation of temperature dependence of magnetic and magnetostrictive properties of CoFe_2O_4 and $\text{CoMe}_x\text{Fe}_{2-x}\text{O}_4$.

The stoichiometry composition of cobalt ferrite is CoFe_2O_4 . In preparing cobalt ferrite, compared with the stoichiometry composition, the processing route may result in a final composition ranging from $\text{Co}_{1-x}\text{Fe}_{2+x}\text{O}_4$ to $\text{Co}_{1+x}\text{Fe}_{2-x}\text{O}_4$ in the range $0 \leq x < 1$. This depends on the proportions of the constituent elements during sample production. While some authors did not present any result on the confirmation of how close to stoichiometry their samples were [1-2, 1-3], others produced samples which were off stoichiometry [1-4, 1-5]. It is important that magnetic and magnetostrictive properties of cobalt ferrite samples be

viewed with the actual sample composition in mind. This is because deviation of the final composition from the targeted composition could result in different cation distributions and hence different magnetic and magnetostrictive properties. It is also important to compare compositions to find the most suitable for different properties and applications.

Cation distribution in cobalt ferrite can be altered by heat treatment. Consistent with thermally activated processes, the formation of structurally uniform cobalt ferrite samples is diffusion dependent and can be expressed by an Arrhenius equation given by [1-6];

$$D = D_0 \exp\left(\frac{-Q}{RT}\right) \quad (1-1)$$

where D (m^2s^{-1}) is the diffusion coefficient, D_0 (m^2s^{-1}) is a constant for a given diffusion system, Q ($\text{J}\cdot\text{mol}^{-1}$) is the activation energy, R ($\text{J}\cdot\text{mol}^{-1}\text{K}^{-1}$) is the gas constant and T (K) is the temperature. The effect of heat treatment can be seen from equation 1-1; increase in temperature (thermal energy) increases $\exp\left(\frac{-Q}{RT}\right)$ thus increasing the diffusion coefficient.

Since the diffusion is time dependent, heat treatment time also plays a very crucial role. More time is necessary for atoms to diffuse to equilibrium positions at lower temperatures than higher temperatures. Thus the cation distribution in CoFe_2O_4 and its derivatives ($\text{CoMe}_x\text{Fe}_{2-x}\text{O}_4$), can be controlled which in turn offers the capability to systematically control magnetic and magnetostrictive properties.

Equilibrium positions of cations due to heat treatment can be explained by the Helmholtz free energy, F ;

$$F = U - TS \quad (1-2)$$

U is the internal energy associated with cation site preference, T is temperature while S is the entropy. If the U term is higher, cations will tend towards occupying their preferred sites. If the TS term is higher, this favours disorder (entropy). Equilibrium at a particular temperature represents a balance between the two effects. At higher temperatures, the TS

term is higher, thus, cations would be randomly distributed and would even be more randomly distributed if the temperature is increased further. At lower temperatures, cations would tend to occupy their preferred sites. If cooling occurs very slowly, the cations have time to migrate closer to their low temperature equilibrium positions. On the other hand, if the temperature falls quickly, cations are frozen at the equilibrium positions corresponding to the higher temperature from which the material was quenched. These two cases represent different heat treatments by which the cations in a material can be redistributed among the cation sites. Heat treatment can also result in a change in the microstructure and so it can be used to alter the magnetic and magnetostrictive properties of cobalt ferrite materials which are both affected by cation distribution and microstructure.

Substitution of non-magnetic cations for Fe^{3+} or Co^{2+} in the cobalt ferrite spinel lattice can also alter the magnetic and magnetoelastic properties. Different cations have different effects on the anisotropy and magnetostriction depending on the strengths of their preferences for either A-sites or B-sites. For example, while Ga has preference for the A-site, Cr prefers the B-sites. Since the high anisotropy and magnetostriction in cobalt ferrite is thought to be due to the Co^{2+} on the B-sites, substitution of non-magnetic cations with strong B-sites preference for Fe^{3+} may displace some Co^{2+} out of B-sites. Similarly, substitution of cations with strong A-sites preference may displace some Co^{2+} from A-sites to the B-sites. In either case, non magnetic cation substitution results in weakening the exchange interaction and anisotropy thus offering the opportunity to alter the magnetic and magnetostrictive properties.

Thin film CoFe_2O_4 and its derivative materials have a wide range of potential applications including magnetostrictive, magneto-electric, magneto-optical and magneto-transport applications. Preparation of high quality films and optimization of properties is necessary for these applications. Cation substitution and heat treatment can also be used to tune the desired properties of thin film CoFe_2O_4 to match the intended applications.

1.2 Scope of the Research

In order to study the variation of magnetic and magnetostrictive properties of cobalt ferrite and its derivative materials, the research covered the following;

- a. an investigation of how these properties depend on processing parameters used during sample preparation
- b. a comparison of changes in the properties due to changes in heat treatment conditions
- c. a systematic study of the contribution of cooling rate to the magnetic and magnetostrictive properties of CoFe_2O_4
- d. a comparison of how different cation substitutions into CoFe_2O_4 , and how variation of the cation compositions affects magnetic and magnetostrictive properties.
- e. a study of how these properties vary with temperature
- f. an investigation of magnetic properties of thin film CoFe_2O_4 samples.

The outcome of these research themes is presented and compared to previous studies.

References to Chapter 1:

- [1-1]. R. W. McCallum, K.W. Dennis, D. C. Jiles, J.E Snyder and Y. H. Chen, "Composite magnetostrictive materials for advanced automotive magnetomechanical sensor" *Low Temp. Phys.*, **27** (2001) 266
- [1-2]. J. G. Na, T. D. Lee and S. J. Park "Effects of cation distribution on magnetic properties in cobalt ferrite" *J. Mat. Sci.* **27** (1993) 961
- [1-3]. S.D. Bhame and P. A. Joy "Enhanced Magnetostrictive properties of CoFe_2O_4 synthesized by an autocombustion method" *Sens. & Act. A* **137** (2007) 256
- [1-4]. J. A. Paulsen, A. P. Ring, and C. C. H. Lo, J. E. Snyder and D. C. Jiles "Manganese-substituted cobalt ferrite magnetostrictive materials for magnetic stress sensor applications" *J. Appl. Phys.* **97** (2005) 044502
- [1-5]. S. H. Song, C. C. H. Lo and S. J. Lee, S. T. Aldini, J. E. Snyder and D. C. Jiles "Magnetic and magnetoelastic properties of Ga-substituted cobalt ferrite" *J. Appl. Phys.* **101** (2007) 09C517
- [1-6]. Donald R. Askeland, *The Science and Engineering of Materials*, UK, Chapman and Hall (1996)

Chapter 2. Magnetism in Magnetic Oxides

2.1 Introduction

A magnetic oxide can be thought to be made up of a lattice of oxygen ions (O^{2-}) in which cations with magnetic properties occupy the interstitial sites in an ordered manner [2-1]. In a magnetic oxide, those interstitial sites can be referred to as cation sites or positions. Since O^{2-} is non-magnetic, the magnetic signature of a magnetic oxide comes from the cations. A number of factors such as size of cation relative to the size of the interstice, electronegativity and thermal history can contribute to determining which cation occupies which site. Also the type of cation positions available in the lattice determines the type of magnetic interactions between the cations and thus the magnetic properties of the oxide. For example, CoO with the rock salt structure has only octahedral cation sites while Co_3O_4 and $CoFe_2O_4$ with spinel structure have both octahedral and tetrahedral cation sites. CoO and Co_3O_4 are antiferromagnetic [2-2] while $CoFe_2O_4$ is ferrimagnetic. Therefore magnetism in magnetic oxides is due to the availability of sites for cations to occupy, the magnetic properties of the cations occupying those sites and the super-exchange interaction.

2.2 Exchange Interaction in Magnetic Oxides

Since the ionic radius of O^{2-} in magnetic oxides is larger than the ionic radius of most cations, cations occupying the cation sites in the lattice have no direct contact with each other, being separated by O^{2-} . Nevertheless, due to the overlap of their electron clouds with that of O^{2-} , these cations still interact [2-3] through the intervening O^{2-} . Exchange interaction therefore refers to the interaction between the electron clouds associated with neighbouring magnetic atoms which influences the manner in which electrons can be allocated among the various spin states of partially filled inner sub-shells [2-4].

In spinel ferrites, exchange interaction describes the interaction between the electron clouds of cations through the intervening oxygen anion. If the orbitals of adjacent atoms are in direct contact, direct exchange interaction would be possible but this is unlikely in

magnetic oxides because of the relative ionic radii of oxygen and the cations. As a result, the interaction between magnetic cations in magnetic oxides is mostly indirect being mediated by the separating oxygen ion. Because the ionic radii of cations in magnetic oxides are different, the exchange interaction varies with the distance between the magnetic moments of the interacting atoms and the bond angle. For oxides containing transition elements ions, strong exchange interaction would occur where transition elements ions such as Fe^{3+} , Co^{2+} and Ni^{2+} , Cr^{3+} , Mn^{2+} , etc with extended orbitals (i.e their magnetic orbitals (3d orbitals) participate in bonding alongside the 4s and 4p orbitals), occupy the interstitial position.

2.3 Magnetic Ordering

Magnetic ordering of individual atomic moments arises as a consequence of exchange interaction in magnetic structures. It represents the competition between the alignment of moments due to exchange interaction energy and the resistance to the alignment due to thermal agitation energy. The alignment results in magnetic ordering in which, parallel alignment is called ferromagnetism and anti-parallel alignment is called antiferromagnetism.

The Curie temperature represents a transition point for ferromagnetic materials above which thermal agitation energy dominates but below which exchange interaction energy dominates and magnetic ordering takes place. For antiferromagnetic materials, this temperature is called the Néel temperature. Below the Curie temperature (or Néel temperature), the tendency for a magnetic ordering to result in ferromagnetic or antiferromagnetic ordering is usually described in literature by the exchange energy [2-1];

$$W_e = -2 \sum J_{ij} \sum S_i \cdot S_j \quad (2-1)$$

where W_e is the exchange energy, J_{ij} is the exchange integral linking atoms i and j , and S_i and S_j represents the spin angular momentum of the atoms. If the exchange integral is positive, then the magnetic moments are aligned parallel to each other resulting in ferromagnetic ordering. If the exchange integral is negative, magnetic moments will align in an anti-parallel

form which results in cancellation of moments leading to antiferromagnetic ordering. The antiferromagnetic ordering in which the net moment is greater than zero ($\sum m > 0$) is called ferrimagnetic ordering. CoFe_2O_4 is a ferrimagnetic ordered spinel structured material with antiferromagnetic coupling between the octahedral and tetrahedral sites. Fig. 2.1 [2-5] summarises the levels of magnetic ordering.

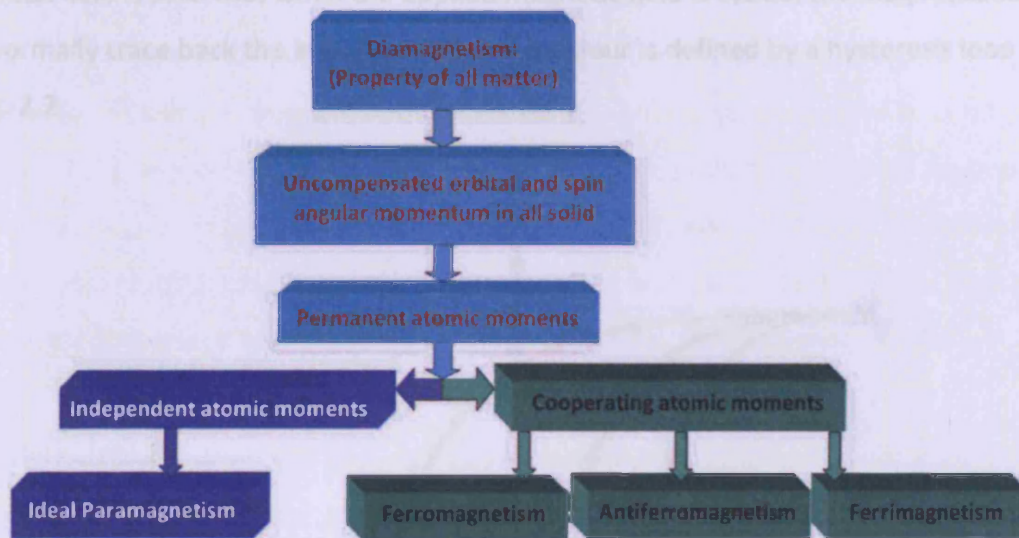


Fig. 2.1: Summary of levels of magnetic ordering

2.4 Magnetization Processes

Magnetization (M) is defined as the magnetic moments (m) per unit volume (V) of a material, ($M = \frac{m}{V}$). Ferromagnetic and ferrimagnetic materials are spontaneously

magnetized below their Curie temperatures resulting in the development of regions of uniform magnetization called magnetic domains. This spontaneous magnetization comes as a result of an internal magnetic field known as the Weiss molecular field. As a result, when magnetic field is applied, the effective magnetic field acting on a ferromagnetic material is the sum of the applied magnetic field and the Weiss molecular field. If the applied magnetic field is sufficiently large, domains are forced to align in the direction of the applied field. Magnetization in the material and the magnetic field (H) contribute such that the vector

sum of both gives the total magnetic induction (B) of a magnetic material. The constant μ_0 is the permeability of free space.

$$\mathbf{B} = \mu_0(\mathbf{H} + \mathbf{M}) \quad (2-2)$$

The behaviour of the magnetization of a ferrimagnetic material with respect to the applied magnetic field is such that when the applied magnetic field is cycled, the magnetization does not normally trace back the initial path. This behaviour is defined by a hysteresis loop shown in Fig. 2.2

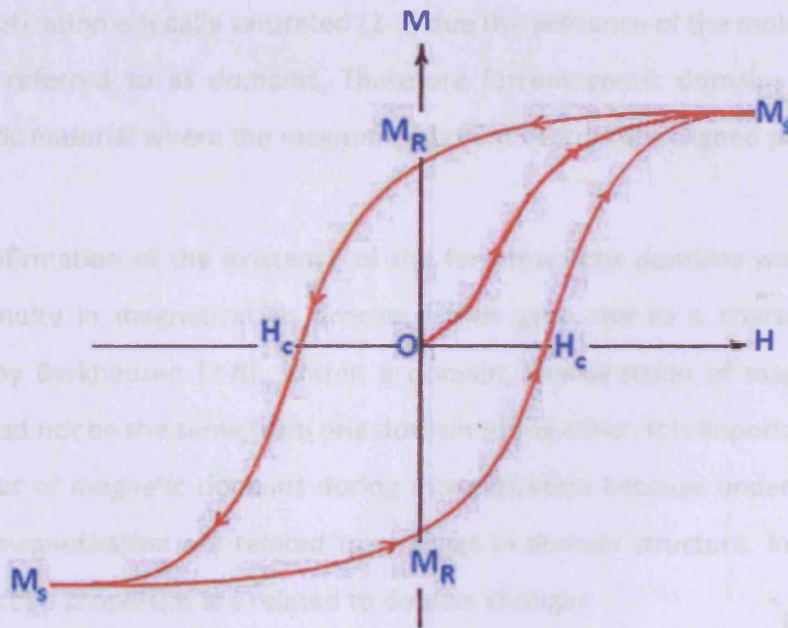


Fig. 2.2: A typical hysteresis loop

Changing the magnetic field of a material from zero to a positive peak value, back to a negative peak value and back again to the same positive peak, traces the hysteresis loop of the material. The path from zero to M_s ($O-M_s$) is the initial magnetization curve. M_s represents the saturation magnetization which is the state where all the magnetic moments are aligned parallel to the applied magnetic field. H_c represents the coercivity which is the

applied magnetic field at zero magnetization. M_R is the remanence which is the residual magnetization when the magnetic field has been reduced to zero. The area enclosed by the hysteresis loop is proportional to the hysteresis loss which represents the magnetic energy lost in the form of heat in the lattice of the material while tracing the hysteresis loop. The relationship between hysteresis loss and coercivity is such that reducing coercivity also reduces hysteresis loss [2-6].

2.4.1 Domain processes during magnetization

In order to explain the large magnetization of a ferromagnetic material in weak applied magnetic field, Weiss assumed that actual specimens are made up of small regions within which magnetization is locally saturated [2-7] due the presence of the molecular field. These regions are referred to as domains. Therefore ferromagnetic domains are regions in a ferromagnetic material where the magnetic moment vectors are aligned parallel.

The first confirmation of the existence of the ferromagnetic domains was associated with the discontinuity in magnetization process which gave rise to a characteristic noise as discovered by Barkhausen [2-8]. Within a domain, the direction of magnetization is the same but need not be the same from one domain to the other. It is important to understand the behaviour of magnetic domains during magnetization because under an applied field, changes in magnetization are related to changes in domain structure. In turn; changes in magnetostrictive properties are related to domain changes.

Domains are separated from each other by transition regions referred to as domain walls. The domain wall has associated surface magnetic energy which arises as a result of the competition between the exchange interaction and magnetocrystalline anisotropy energies of the material. The exchange interaction energy tends to align the magnetic moments parallel to one another while conversely, anisotropy energy tends to align them in preferred crystallographic directions called the magnetic easy directions. This competition between exchange interaction energy and anisotropy energy determines the thickness of the domain

wall. The width of the domain wall tends to be thicker when exchange energy is higher and thinner when magnetocrystalline anisotropy energy is higher. As shown in Fig. 2.3, within a domain wall (the region between the dotted lines), the direction of magnetic moments changes from its direction in one domain to its direction in another domain leading to the creation of a transitional region known as Bloch wall.

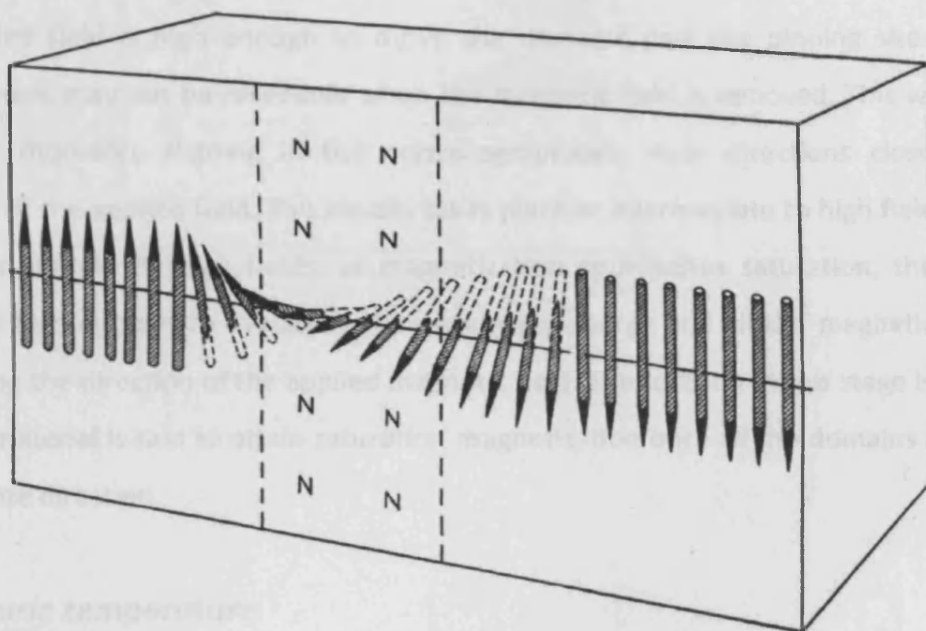


Fig. 2.3: Schematic representation of the Bloch wall [2.7]

In ferromagnets and ferrimagnets, the magnetic moments within the domains are ordered even in a demagnetized state. When a magnetic field is applied in the demagnetized state, the magnetic moments tend to align themselves along the direction of the applied field as a response to the need for energy minimization. This results in the growth of the domains aligning favourably, close to or along the direction of the applied field, at the expense of the unfavourably oriented domains. Domain rotation and domain wall displacement are terms used to describe the behaviour of domains to applied magnetic field.

Pinning sites are sites which obstruct the domain motion and arise due to material imperfections. If the applied magnetic field is low such that the energy required for moving the magnetic domains past pinning sites in the way of the magnetic domains is higher than the magnetic energy moving the domains, reversible domain rotation and reversible domain wall bowing take place. Under this condition, the magnetic moments return to their original easy directions as determined by the anisotropy energy when magnetic field is removed. If the applied field is high enough to move the domains past the pinning sites, the wall displacement may not be reversible when the magnetic field is removed. This will result in magnetic moments aligning in the crystallographically easy directions closest to the direction of the applied field. This usually takes place at intermediate to high field strengths [2-6]. At sufficiently high fields, as magnetization approaches saturation, the magnetic energy is high enough to overcome the anisotropy energy and all the magnetic moments align along the direction of the applied magnetic field. The rotation at this stage is reversible and the material is said to attain saturation magnetization once all the domains are aligned in the same direction.

2.4.2 Curie temperature

If a ferromagnetic or ferrimagnetic material is subjected to increase in temperature, the spontaneous magnetization within the magnetic domains decreases and vanishes at a temperature T_C called the Curie temperature. The Curie temperature is therefore the temperature at which magnetic ordering (i.e spontaneous magnetization) takes place on cooling resulting in paramagnetic to ferromagnetic (or ferrimagnetic) transition. Curie temperature can be determined by linear extrapolation of the region of maximum slope down to the temperature axis in a magnetization versus temperature measurement as shown in Fig. 2.4 for cobalt ferrite. The plot in Fig. 2.4 was made during the course of this research project to determine the Curie temperature of cobalt ferrite.

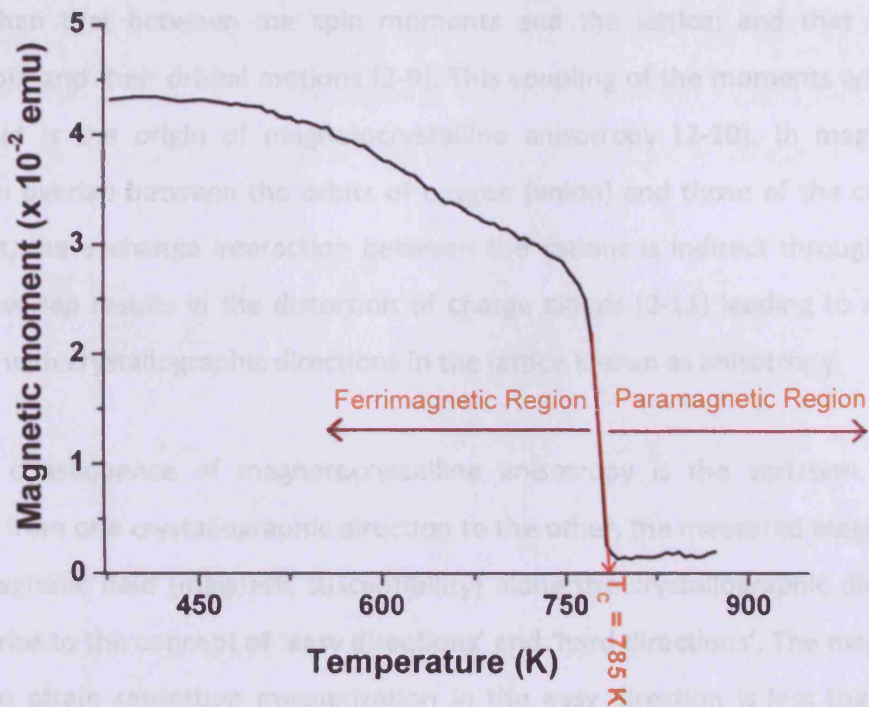


Fig. 2.4: Determination of Curie temperature of a cobalt ferrite sample from a magnetization vs. temperature plot

2.5 Anisotropy

Anisotropy is the term used to define the directional dependence of the properties of a material. Three types of anisotropy are usually considered in relation to magnetic materials;

- Magnetocrystalline anisotropy
- Magnetoelastic anisotropy
- Shape anisotropy

2.5.1 Magnetocrystalline anisotropy

Magnetism in solids arises from the contributions of the electron orbits and the spins of the electrons to the magnetic moments. The electron orbits can give rise to orbital moments while the spin gives rise to spin moments. There is no direct interaction between the spins and the lattice but the spin moments of electrons are coupled to the lattice via coupling to their orbital motions [2-1]. The coupling between the orbital motions and the lattice is

stronger than that between the spin moments and the lattice; and that between the electron spin and their orbital motions [2-9]. This coupling of the moments with the lattice of the solid is the origin of magnetocrystalline anisotropy [2-10]. In magnetic oxides, because an overlap between the orbits of oxygen (anion) and those of the cations (metal ions) exists, the exchange interaction between the cations is indirect through the oxygen ion. This overlap results in the distortion of charge clouds [2-11] leading to a variation of properties with crystallographic directions in the lattice known as anisotropy.

Since the consequence of magnetocrystalline anisotropy is the variation of magnetic properties from one crystallographic direction to the other, the measured magnetization for a given magnetic field (magnetic susceptibility) along the crystallographic directions vary. This gives rise to the concept of 'easy directions' and 'hard directions'. The magnetic energy required to attain saturation magnetization in the easy direction is less than the energy required to attain saturation magnetization in the hard direction. Easy and hard directions vary from one magnetic material to another and can be easily determined by measuring the magnetic properties of single crystals of materials magnetised along different directions.

Fig. 2.5 [2-12] shows magnetic properties measured along different crystallographic directions in single crystals of iron and nickel samples. The easy directions for iron are in the $\langle 100 \rangle$ while the hard directions are in the $\langle 111 \rangle$ with the $\langle 110 \rangle$ being intermediate. The easy, hard and intermediate magnetization directions in cobalt ferrite are same as that of iron. For nickel, the easy directions are in the $\langle 111 \rangle$, hard directions in the $\langle 100 \rangle$ and the intermediate being the $\langle 110 \rangle$. Nickel ferrite has similar easy, hard and intermediate directions as nickel.

The magnitude of magnetocrystalline anisotropy is usually represented in terms of energy density (Jm^{-3}) which varies with crystal structure due to different lattice symmetries. For the cubic crystal structure magnetocrystalline anisotropy energy is given by [2-1];

$$E_{magcrystal} = K_0 + K_1(\alpha_1^2\alpha_2^2 + \alpha_2^2\alpha_3^2 + \alpha_3^2\alpha_1^2) + K_2(\alpha_1^2\alpha_2^2\alpha_3^2) + \dots \quad (2-3)$$

$\alpha_1, \alpha_2, \alpha_3$ are the cosines the angles between M_s and the x, y and z axes of the cubic crystal structure. K_1 and K_2 are the first and second order cubic anisotropy constants, respectively.

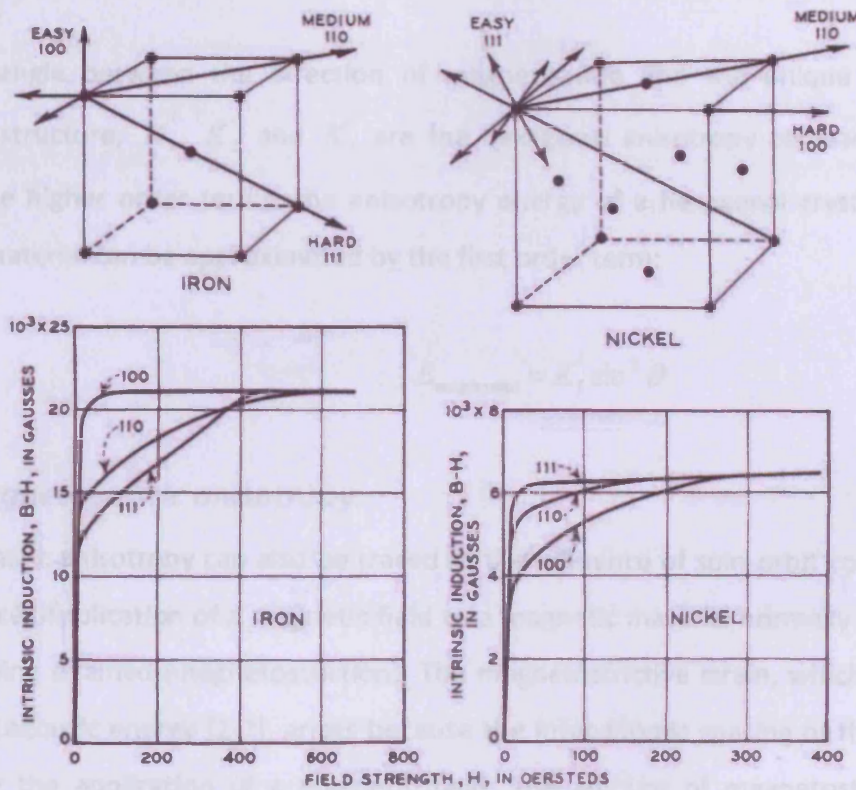


Fig. 2.5: Magnetic properties of iron and nickel measured in different crystallographic axes of the crystal structures. In S.I units, 1 Gauss = 10^{-4} T and 1 Oe = 79.58 A/m.

As an approximation when K_2 is negligible, it can be ignored and in which case, the anisotropy can be represented by the first order cubic anisotropy constant.

$$E_{magcrystal} = K_1(\alpha_1^2\alpha_2^2 + \alpha_2^2\alpha_3^2 + \alpha_3^2\alpha_1^2) \quad (2-4)$$

Considering the one-constant anisotropy, if $K_1 > 0$ (i.e. if K_1 is positive), the easy axis will be along $\langle 100 \rangle$ and if $K_1 < 0$ (i.e. if K_1 is negative), the easy axis will be along the $\langle 111 \rangle$. For a hexagonal crystal structure the magnetocrystalline anisotropy energy is given by;

$$E_{magcrystal} = K_1' \sin^2 \vartheta + K_2' \sin^4 \vartheta + K_3' \sin^6 \vartheta + \dots \quad (2-5)$$

ϑ is the angle between the direction of magnetization and the unique axes of the hexagonal structure, K_1' , K_2' and K_3' are the hexagonal anisotropy constants. Similarly, ignoring the higher order terms, the anisotropy energy of a hexagonal crystal structured magnetic material can be approximated by the first order term:

$$E_{magcrystal} = K_1' \sin^2 \vartheta \quad (2-6)$$

2.5.2 Magnetoelastic anisotropy

Magnetoelastic anisotropy can also be traced to the influence of spin-orbit coupling on the crystal lattice. Application of a magnetic field to a magnetic material normally results in the material being strained (magnetostriction). The magnetostrictive strain, which depends on the magnetoelastic energy [2-7], arises because the inter-atomic spacing of the material is strained by the application of a magnetic field. The amount of magnetostrictive strain exhibited by a crystal in a specific direction depends on the direction of the magnetization [2-13]. Similarly, if the lattice is altered by the application of stress, the spin-orbit coupling is altered also and an additional strain will be imposed on the material resulting in change in the direction of magnetization. For example, it has been shown that if 69 MPa compressive stress is applied to nickel (with negative magnetostriction), the magnetization doubles but under 69 MPa tensile stress, the magnetization reduces by a tenth [2-13]. This indicates that the direction and magnitude of stress affects the direction and magnitude of magnetization. The magnitude of magnetoelastic energy for a cubic crystal under uniform stress (σ) can be expressed as shown in equation (2-7).

$$E_{magelastic} = -\frac{3}{2} \lambda_{100} \sigma (\alpha_1^2 \gamma_1^2 + \alpha_2^2 \gamma_2^2 + \alpha_3^2 \gamma_3^2) - 3 \lambda_{111} \sigma (\alpha_1 \alpha_2 \gamma_1 \gamma_2 + \alpha_2 \alpha_3 \gamma_2 \gamma_3 + \alpha_3 \alpha_1 \gamma_3 \gamma_1) \quad (2-7)$$

λ_{100} and λ_{111} are the magnetostriction constants with strain measured in a magnetic field applied along the $\langle 100 \rangle$ and $\langle 111 \rangle$ directions respectively. γ_1 , γ_2 and γ_3 are the direction cosines of the stress components with respect to the crystal axes. If the material has isotropic elasticity with isotropic magnetostriction (λ), then magnetoelastic anisotropy reduces to;

$$E_{magelastic} = -\frac{3}{2} \lambda \sigma \cos^2 \theta \quad (2-8)$$

θ is the angle between magnetization and stress. Under the simultaneous effects of magnetic field and stress, the total anisotropy energy reflects the contributions of both magnetocrystalline anisotropy and magnetoelastic anisotropy (or stress anisotropy). Thus for a cubic structured crystalline material, considering only the first order term of the magnetocrystalline anisotropy and the isotropic elasticity and magnetostriction form of the magnetoelastic anisotropy, the total anisotropy energy is given by;

$$E_{ani} = E_{magcrystal} + E_{magelastic} = K_1 (\alpha_1^2 \alpha_2^2 + \alpha_2^2 \alpha_3^2 + \alpha_3^2 \alpha_1^2) - \frac{3}{2} \lambda \sigma \cos^2 \theta \quad (2-9)$$

If $K_1 \gg \lambda \sigma$, magnetocrystalline anisotropy dominates and if $K_1 \ll \lambda \sigma$, magnetoelastic anisotropy dominates.

2.5.3 Shape anisotropy

Shape anisotropy arises due to the dependence of demagnetizing field on the shape of magnetic materials. When magnetized, ferromagnetic and ferrimagnetic materials generate a magnetic field opposite in direction to the magnetization that created it. This magnetic

field is called the demagnetizing field. The demagnetizing field creates magnetostatic energy which depends on the shape of the material [2-14] which introduces shape anisotropy with an easy axis lying along the long axis of the material [2-15]. As a result of this, a spherical sample under uniform applied magnetic field would be magnetized equally easily in all directions because the demagnetizing field acting against the applied field is equal in all directions. An oblate spheroid shaped sample on the other hand would magnetize easier along the long axis than the short axis due the effect of demagnetizing field which is stronger along the short axis. Demagnetizing field (H_d) depends on both the shape of the material and the magnetization (M) in the material [2-6] and are related as shown:

$$\mathbf{H}_d = -N_d \mathbf{M} \quad (2-10)$$

The constant of proportionality N_d is called the demagnetization factor which depends on the shape of the material. This dependence of magnetization on the shapes of magnetic materials requires a correction for the effect of demagnetizing field especially in magnetized thin film and small particle sized materials due to the contribution of shape anisotropy. In this correction, the demagnetizing field H_d acting on a magnetized material is subtracted from the applied field H_{app} to obtain the effective field H_{eff} :

$$\mathbf{H}_{eff} = \mathbf{H}_{app} - \mathbf{H}_d = \mathbf{H}_{app} - N_d \mathbf{M} \quad (2-11)$$

In applications where shape anisotropy is much smaller than the magnetocrystalline anisotropy, it can be ignored. [2-16].

2.6 Law of Approach to Saturation Magnetization

The law of approach to saturation magnetization can be used to determine the first order cubic magnetocrystalline anisotropy coefficient (K_1) of a ferrimagnetic material. This method was used in determining the anisotropy constant of the samples used in this research work. The law assumes that as magnetization approaches saturation, all irreversible hysteretic

processes are completed and the magnetization process in that region would be due to reversible rotational processes only. These reversible rotational processes represent the results of rotation of magnetic domains to the direction of the applied field against magnetic anisotropy. The law of approach to saturation magnetization as was experimentally obtained is [2-17]

$$M = M_s \left(1 - \frac{a}{H} - \frac{b}{H^2} - \dots \right) + \kappa H \quad (2-12)$$

M_s and H are the saturation magnetization and applied field respectively, κH is the forced magnetization term representing the additional spontaneous magnetization induced in the domains under high field conditions and a is a constant representing the effect of inclusions and/or micro-stresses [2-13]. It is related to domain wall pinning and therefore in the higher field region of reversible rotation of magnetization, the value of $a \approx 0$. b is a constant representing the effect of magnetocrystalline anisotropy. For randomly oriented polycrystalline samples with a cubic crystal structure such as cobalt ferrite, the coefficient b is given as [2-12]

$$b = \frac{8}{105} \frac{K_1^2}{\mu_0^2 M_s^2} \quad (2-13)$$

This gives the law of approach to saturation magnetization as:

$$M = M_s \left[1 - \frac{8}{105} \left(\frac{K_1}{\mu_0 M_s H} \right)^2 \right] + \kappa H \quad (2-14)$$

The law of approach is said to be valid in the range $0.97M_s < M < M_s$ [2-18].

2.7 Magnetostriction

2.7.1 Introduction

The discovery of magnetostriction dates back to 1842 and is credited to Joule [2-13]. Magnetostriction is the strain produced when the shape of a ferromagnetic material changes during magnetization. This type of magnetostriction is called Joule magnetostriction. Magnetostriction arises when in response to applied magnetic field, domain rotation and domain wall motion result in a strain. This strain, usually measured in parts per million (ppm) is small but can be technologically harnessed to convert magnetic energy to mechanical energy. It is also possible to convert mechanical energy to magnetic energy in a mechanism called inverse magnetostriction. In this inverse magnetostriction, applied stress results in change in magnetization. While Joule magnetostriction can be harnessed in actuator development, inverse magnetostriction can be exploited for magnetomechanical stress sensors. Magnetostriction can be of volume or linear form but linear magnetostriction is more observable and probably more important than the volume magnetostriction and thus is comparatively more frequently studied.

2.7.2 Spontaneous and field-induced magnetostriction

Magnetostriction is also often classified as spontaneous or field-induced. The relation between spontaneous and field induced magnetostriction is schematically represented in Fig. 2.6. Spontaneous magnetostriction arises following magnetic ordering from paramagnetic to ferromagnetic or ferrimagnetic state. It is therefore the strain that is associated with the occurrence of spontaneous magnetization in materials. The occurrence of spontaneous bulk magnetostriction shows that strains within domains are anisotropic in nature and that the strain depends on the direction of saturation magnetization with respect to the crystal axes [2-1]. The spontaneous magnetostriction (λ_0) in a material is given by the integral of the spontaneous magnetostriction from all the domains in the material which equals one-third of the total amount of magnetostriction (ϵ) obtainable from the disordered-demagnetized state to ordered-saturation-magnetized state as given in equation (2-15).

$$\lambda_0 = \frac{\epsilon}{3} \quad (2-15)$$

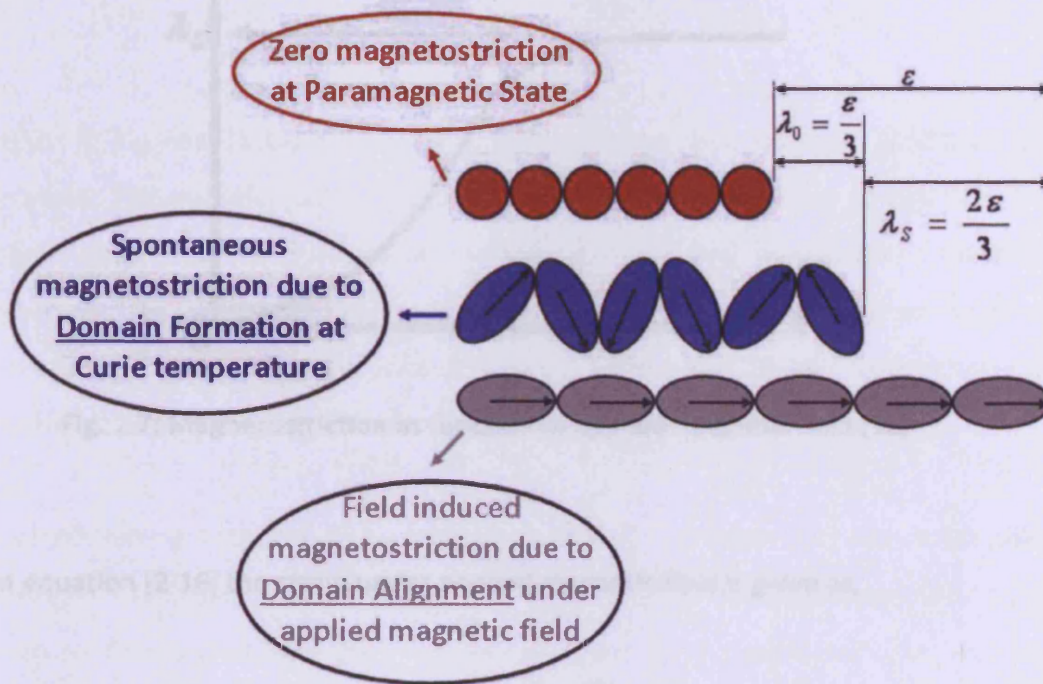


Fig. 2.6: Schematic representation of the spontaneous and field-induced magnetostriction

Also, from equations 2-15 and 2-16, it is easy to see that the magnitude of the saturation magnetostriction is twice that of the spontaneous magnetostriction. Equation (2-15) to (2-16) Field-induced magnetostriction is more important for development of devices such as sensors and actuators. It arises when, apart from ordering of the magnetic moment into domains below the Curie temperature, the domains align themselves along the direction of the magnetization in response to applied magnetic field. Fig. 2.7 [2-16] shows the dependence of magnetostriction on applied magnetic field. When a material is magnetized, magnetostriction increases with increase in the field strength until the material reaches saturation magnetostriction. If the material is magnetized to saturation, then saturation magnetostriction is given by;

$$\lambda_s = \epsilon - \frac{\epsilon}{3} = \frac{2\epsilon}{3} \quad (2-16)$$



Fig. 2.7: Magnetostriction as function of applied magnetic field [15]

From equation (2-16) the strain under applied magnetic field is given as,

$$\varepsilon = \frac{3}{2} \lambda_s \quad (2-17)$$

Also, from equations 2-15 and 2-16, it is easy to see that the magnitude of the saturation magnetostriction is twice that of the spontaneous magnetostriction. Equations (2-15) to (2-17) were obtained assuming isotropic conditions. Within the same restriction, the dependence of magnetostriction on the angle of inclination to the direction of magnetization is given by [2-6]

$$\lambda_s(\theta) = \frac{3}{2} \lambda_s \left(\cos^2 \theta - \frac{1}{3} \right) \quad (2-18)$$

Sometimes the change in strain is measured as the difference between magnetostriction measurements with field applied parallel ($\lambda_{s\parallel}$) and normal ($\lambda_{s\perp}$) to a given direction. When measured parallel to the field, $\cos^2 \theta = 1$ giving $\lambda_{s\parallel} = \lambda_s$, and when measured perpendicular,

$\cos^2\theta = 0$, yielding $\lambda_{s\perp} = -\lambda_s/2$. The difference between the values obtained in both directions is

$$\lambda_{s\parallel} - \lambda_{s\perp} = \lambda_s + \frac{\lambda_s}{2} = \frac{3}{2}\lambda_s \quad (2-19)$$

Equation (2-19) and (2-17) are similar which indicates that isotropic conditions are still maintained. The quantity $3/2 \lambda_s$ is called isotropic magnetostriction [2-16]. It is the total change in length caused by the change in magnetic field and is obtained as the difference between measured value of magnetostriction along the parallel and transverse directions. The reason for using this difference is to obtain the value of magnetostriction which is independent of the initial domain distribution in the demagnetized state [2-11].

It is worth noting that isotropic magnetostriction is only ideal and that most solids are anisotropic. For anisotropic materials, it is necessary to consider magnetostriction with respect to the crystal axis lying in the direction of magnetization. In such a case, magnetostriction varies, both in magnitude and sign from one crystallographic direction of magnetization to another and thus varies from one type of crystal structure to another.

2.7.3 Magnetostriction in cubic materials

The magnetostriction constant is dependent on crystallographic direction and its combinative effects along different crystallographic directions determine the magnitude of saturation magnetostriction in a domain. Because of the high symmetry in cubic materials, only two independent magnetostriction constants are required to represent magnetostriction. The saturation magnetostriction along an arbitrary axis for single crystal cubic material is given by equation (2-20) [2-9];

$$\lambda_s = \frac{3}{2}\lambda_{100}\left(\alpha_x^2\beta_x^2 + \alpha_y^2\beta_y^2 + \alpha_z^2\beta_z^2 - \frac{1}{3}\right) + 3\lambda_{111}\left(\alpha_x\alpha_y\beta_x\beta_y + \alpha_y\alpha_z\beta_y\beta_z + \alpha_z\alpha_x\beta_z\beta_x\right) \quad (2-20)$$

α_x , α_y and α_z are the directional cosines of magnetization measurement and β_x , β_y and β_z are the directional cosines magnetostriction measurement with respect to the cubic axes, x, y and z respectively. Equation (2-20) represents the total magnetostriction when a material is magnetized from a completely demagnetized state to saturation, which is obtainable from measurement on a single domain of a single crystal sample. If, like in many magnetostriction measurements, the sample is magnetized in the same direction as the magnetostriction is measured, then $\beta_x = \alpha_x$, $\beta_y = \alpha_y$, and $\beta_z = \alpha_z$ and equation (2-20) reduces to;

$$\lambda_s = \lambda_{100} + 3(\lambda_{111} - \lambda_{100})(\alpha_x^2\alpha_y^2 + \alpha_y^2\alpha_z^2 + \alpha_z^2\alpha_x^2) \quad (2-21)$$

For polycrystalline cubic structured materials with random grain orientation, saturation magnetostriction is obtained by taking an average of the contributions from individual crystals. This is still valid because the deformation in each crystallite averages to produce the overall strain resulting in an isotropic magnetostriction [2-16]. Assuming that the material is under uniformly applied stress or under uniform strain, the saturation magnetostriction obtained by averaging is

$$\lambda_{S_{Average}} = \frac{2}{5}\lambda_{100} + \frac{3}{5}\lambda_{111} \quad (2-22)$$

The value of saturation magnetostriction of a polycrystalline magnetic material measured at an angle to the direction of magnetization can still be determined by substituting $\lambda_{S_{Average}}$ for λ_s in equation (2-18) [2-9];

$$\lambda_s(\theta) = \frac{3}{2}\lambda_{S_{Average}}\left(\cos^2\theta - \frac{1}{3}\right) \quad (2-23)$$

It should be noted that all the magnetostriction expressions above are for samples at saturation (i.e at M_s). Below saturation, it is complex to completely represent

magnetostriction. An expression similar to the law of approach (equation (2-14)) can be used to represent magnetostriction as function of magnetization:

$$\frac{dl}{l} = \lambda_s \left[1 - \frac{8}{105} \left(\frac{K_1}{\mu_0 M_s H} \right)^2 \right] + \kappa H \quad (2-24)$$

2.7.4 Strain derivative and stress sensitivity of magnetostrictive materials

The constitutive equations for linear magnetostriction can be written as [2-9]

$$\lambda = s^H \sigma + dH \quad (2-25)$$

$$B = d\sigma + \mu^\sigma H \quad (2-26)$$

These equations couple the mechanical strain (λ) and stress (σ) to magnetic field (H) and flux density (B) through the coupling parameter d called the piezomagnetic constant. s^H is the elastic compliance (the reciprocal of Young's Modulus) of the material measured at constant applied field while μ^σ is the permeability measured at constant stress. In modelling magnetostrictive materials, it is important that equations (2-25) and (2-26) be solved simultaneously to produce a strong coupling which represents the true magnetomechanical effect in magnetostrictive materials. Partial differentiation of equation (2-25) with respect to magnetic field at constant stress and equation (2-26) with respect to mechanical stress at constant field give;

$$\left(\frac{\partial \lambda}{\partial H} \right)_\sigma = d \quad (\text{Strain derivative}) \quad (2-27)$$

$$\left(\frac{\partial B}{\partial \sigma} \right)_H = d \quad (\text{Stress sensitivity}) \quad (2-28)$$

As a result,

$$\left(\frac{\partial \lambda}{\partial H}\right)_{\sigma} = \left(\frac{\partial B}{\partial \sigma}\right)_H \quad (2-29)$$

Equation (2-29) indicates that the stress sensitivity of magnetic flux density is directly proportional to the strain derivative. This is only true assuming a reversible process under small applied stress and magnetic field [2-19]. The expression $\left(\frac{\partial \lambda}{\partial H}\right)_{\sigma}$ is a figure of merit that can be used as indication of the potential performance of a magnetostrictive material for actuator application because it gives the changes in magnetostriction due to changes in applied magnetic field.

References to Chapter 2:

- [2-1]. D.J. Craik, *Magnetic Oxides, -Part 1*, UK: John Wiley & Sons; Ltd, (1975)
- [2-2]. Aditi S. Risbud, Lauren P. Snedeker, Margaret M. Elcombe, Anthony K. Cheetham, and Ram Seshadri, "Wurtzite CoO" *Chem. Mater.* **17** (2005) 834
- [2-3]. W. Heisenberg, "Theory of Ferromagnetism" *Z. Phys.* **49** (1928) 619
- [2-4]. J. S. Blakemore, *Solid State Physics, 2nd ed.* UK: Cambridge University Press, (1985)
- [2-5]. H. P Myers, *Introduction to Solid States Physics, 2nd ed.* UK: Taylor and Francis, (1997)
- [2-6]. David Jiles, *Introduction to Magnetism and Magnetic Materials, 2nd ed.* USA, CRC Taylor and Francis (1998)
- [2-7]. Charles Kittel "Physical theory of ferromagnetic domains" *Rev. Mod. Phys.* **21** (1949) 541
- [2-8]. D. C Jiles "Dynamics of ferromagnetic domain and Barkhausen effect by D.C Jiles" *Czech. J. Phys.* **50** (2000) 893
- [2-9]. B.D Cullity and C.D Graham, *Introduction to Magnetic Materials, 2nd edn*, USA, Willey (2009)
- [2-10]. Göran Engdahl, *Handbook of Giant Magnetostrictive Materials*, USA, Academic Press (2000)
- [2-11]. J. Smit and H. P. J Wijn, *Ferrites: physical properties of ferrimagnetic oxides in relation to their technical application*, Netherlands, Philips Technical Library (1959)
- [2-12]. R. M. Bozorth, *Ferromagnetism*, New Yor, IEEE Press (1993)
- [2-13]. B. D. Cullity, *Introduction to Magnetic Materials*, USA, Addison-Wisley (1972)
- [2-14]. Nicola Spaldin, *Magnetic Materials, Fundamentals and Device Applications*, UK, Cambridge University Press (2003)
- [2-15]. J. Yu, U. Rüdiger, L. Thomas, S. S. P. Parkin, A. D. Kent "Micromagnetics of mesoscopic epitaxial (110) Fe elements with nanoshaped ends" *J. Appl. Phys.* **85** (1999) 5501

- [2-16]. L. J. Brandy "The determination of the demagnetization factor resulting from shape anisotropy in ferrite magnets" *J. Mat. Sci.* **10** (1975) 697
- [2-17]. S. Chikazumi, *Physics of Ferromagnetism*, 2nd ed. Oxford, UK.: Oxford Univ. Press, (1997)
- [2-18]. W. Lee "Magnetostriction and magnetomechanical effects" *Rep. Prog. Phys.* **18** (1955) 184
- [2-19]. C.C. Lo, A. P. Ring, J. E. Snyder and D. C. Jiles, "Improvement of magnetomechanical properties by magnetic annealing" *IEEE Trans. Magn.* **41** (2005) 3676

Chapter 3. Ferrites

3.1 Introduction

Ferrites are magnetic oxides which contain iron as the main metallic element. Pure ferrites such as FeO (wüstite or iron (II) oxide), Fe₂O₃ (haematite or iron (III) oxide) and Fe₃O₄ (magnetite or iron (II, III) oxide) contain only iron and oxygen. Magnetism was first discovered in Fe₃O₄ in the form of lodestone. Fe₃O₄ is sometimes written as FeO.Fe₂O₃ which indicates that it is made up in parts of 50% FeO and 50% Fe₂O₃ which is why Fe₃O₄ is called iron (II, III) oxide. The technological importance of ferrites is mainly in the tunability of magnetic properties which derives from the possibility of substituting Fe²⁺ with another divalent cation. In its tunable form, FeO.Fe₂O₃ can be written as MeO.Fe₂O₃ where Me represents divalent cations such as Mn²⁺, Co²⁺, Zn²⁺, Ni²⁺, etc. Another consequence of the substitution capability in ferrites is the fact it crystallizes in different crystal structures which include the spinel and non-spinel ferrites. The non-spinel ferrites include hexaferrites, garnets and orthoferrites.

3.2 Spinel Ferrites

Spinel ferrites are a large class of magnetic oxides possessing the crystal structure of the naturally occurring spinel (MgAl₂O₄). The chemical formula of spinel ferrites is MeFe₂O₄ (or MeOFe₂O₃) where Me represents a single or combination of divalent cations with ionic radius of about 0.06 nm to 0.1 nm [3-1]. Magnetite (FeO.Fe₂O₃), the earliest known magnetic material is a spinel structured ferrite. The spinel structure is a lattice of 32 oxygen ions forming a face centred cubic closed packed structure with tetrahedral and octahedral sites available for cation occupancy. Each unit cell comprises eight octants out of which four have tetrahedral coordination, the other having octahedral coordination. There are 64 tetrahedral sites (A-sites) and 32 octahedral (B-sites) sites in a unit cell of a spinel structure hence 2/3 of the available sites are tetrahedral and 1/3 of the sites are octahedral. Of the 64 tetrahedral and 32 octahedral sites, only 8 and 16 of the sites respectively are occupied by cations. Hence 2/3 of the cations occupy the octahedral sites and 1/3 of the cations occupy

tetrahedral sites. Altogether, there are 32 oxygen anions and 24 cations making a total of 56 ions in a unit cell. Fig. 3.1 [3-2] is the schematic of the spinel structure showing cations and oxygen sites.

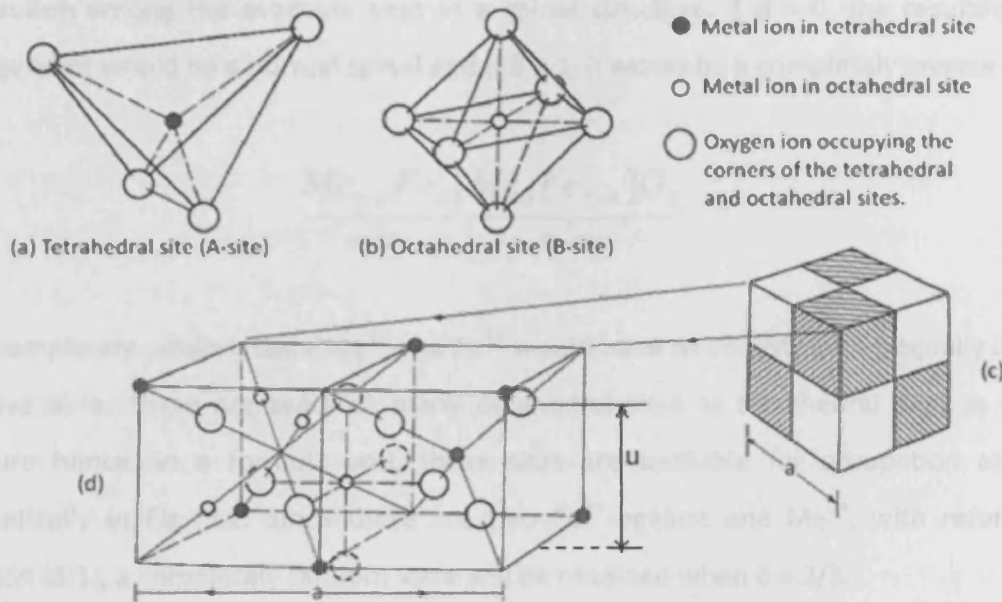
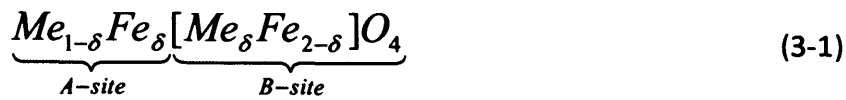


Fig. 3.1: (a) Tetrahedral site surrounded by four oxygen ions (b) Octahedral site surrounded by six oxygen ions (c) Spinel crystal structure. Shaded and non-shaded parts represent octants of similar cation occupancy (d) Two octants showing cation and oxygen distribution.

Spinel structured materials with all the trivalent cations occupying the octahedral sites and all the divalent cations occupying the tetrahedral sites are called normal or direct spinels. Deviation from the normal spinel arrangement can occur resulting in half of the trivalent cations occupying the tetrahedral site and the other half with all the divalent cations occupying the octahedral sites. This gives rise to a completely inverse spinel structure. Apart from ZnFe_2O_4 and CdFe_2O_4 , every other ferrite is inverse spinel structured [3-3]. Most inverse spinels, including cobalt ferrite [3-4] are known not to be completely inverse, i.e. the divalent cations occupy both octahedral and tetrahedral sites. Similarly, there are more trivalent cations on one site than the other. This deviation from the completely inverse

spinel arrangement gives rise to the concept of the degree of inversion which defines the percentage of each cation type occupying the tetrahedral and octahedral sites. The general formula for cation distribution in spinel ferrite is represented as shown in equation (3-1). Me stands for divalent metal ion and δ is the degree of inversion which represents the cation distribution among the available sites in a spinel structure. If $\delta = 0$, the resulting cation arrangement would be a normal spinel and if $\delta = 1$, it would be a completely inverse spinel.



For a completely random state Me^{2+} and Fe^{3+} would have to be distributed equally in all the sites available. There are twice as many octahedral sites as tetrahedral sites in a spinel structure hence, in a formula unit, three sites are available for occupation as shown schematically in Fig. 3.2. Since there are two Fe^{3+} against one Me^{2+} , with reference to equation (3-1), a completely random state will be obtained when $\delta = 2/3$.

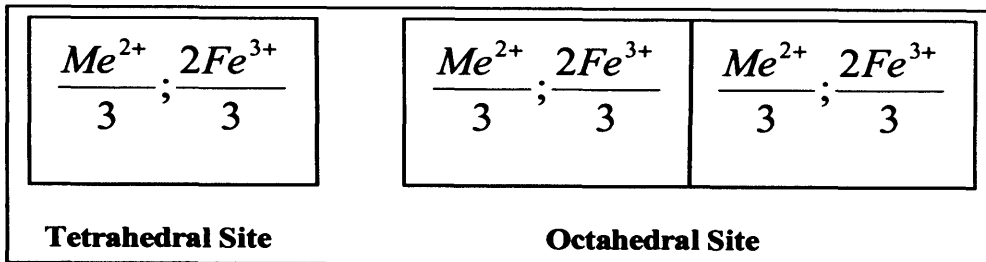


Fig. 3.2: Schematic of the random distribution of cations between the octahedral and tetrahedral sites, in formula unit of a spinel structure

A relation for determining the value of the degree of inversion [3-4], δ is

$$\delta = \left(\frac{1}{4} \right) \left(7 - \left[\frac{\mu_{FU}}{\mu_B} \right] \right) \quad (3-2)$$

The ratio $\frac{\mu_{FU}}{\mu_B}$ is the magnetic moment per formula unit in Bohr magnetons divided by 1 Bohr magneton. (The Bohr magneton is the strength of magnetic field associated with an isolated electron and equals $9.27 \times 10^{-24} \text{ Am}^2$ [3-5]) The degree of inversion plays an important role in determining the magnetic and magnetostrictive properties of spinel structured materials as it shows the cation distribution among the available cation sites. It can be altered by heat treatment, being dependent on cation diffusion processes and the cooling rate of the material from high temperature. δ tends towards $2/3$ with increase in cooling rate such as quenching from high temperature into a medium (such as in water). Quenching results in the cooling rate being much higher than the rate of cation diffusion and as a result, cations are trapped in their relatively random positions. Depending on the value of δ , some inverse spinel materials are more inverted than others leading to the concept of low inversion, high inversion and complete inversion. MnFe_2O_4 with $\delta = 0.2$ (20% of the Mn^{2+} on the octahedral sites) has a low inversion. CoFe_2O_4 on the other hand with $\delta = 0.68$ to 0.8 has a high inversion because 68 to 80% of the Co^{2+} cations are on the octahedral sites. NiFe_2O_4 is said to be completely inverted with $\delta = 1$ which means that all the Ni^{2+} cations are on octahedral sites [3-6].

The ionic radii of different cations occupying the tetrahedral and octahedral sites influence the degree of inversion i.e the cation site occupancies. A cation with an ionic radius larger than the size of the tetrahedral site will most likely occupy the octahedral site which is

larger. The chances of occupying the tetrahedral site increases if $0.225 \leq \frac{r_{ionic}}{R_{ionic}} < 0.414$

while the chances of occupying the octahedral site on the other hand increases if

$0.414 \leq \frac{r_{ionic}}{R_{ionic}} < 0.732$ [3-7]. For spinel ferrites R_{ionic} is the ionic radius of O^{2-} and r_{ionic} is the

ionic radius of Me^{2+} . The ionic radii of trivalent cations such Fe^{3+} ($r_A = 0.49\text{\AA}$, $r_B = 0.55\text{\AA}$) and Al^{3+} ($r_A = 0.39\text{\AA}$, $r_B = 0.53\text{\AA}$) are usually smaller than the ionic radii of divalent cations such as Mn^{2+} ($r_A = 0.66\text{\AA}$, $r_B = 0.83\text{\AA}$), Co^{2+} ($r_A = 0.58\text{\AA}$, $r_B = 0.65\text{\AA}$) and Ni^{2+}

($r_A = 0.55\text{\AA}$, $r_B = 0.69\text{\AA}$), where r_A = ionic radius of cation in tetrahedral sites and r_B = ionic radius of cation in octahedral sites. This difference in ionic radii of trivalent and divalent cations tends to favour inverse structures [3-1] and may explain why most spinel ferrites are inverted.

Though the differences in ionic radii explain why most spinel ferrites are inverted, it does not explain why some are not inverted (normal spinels) and why some are more inverted than others. Zn^{2+} ($r_A = 0.6\text{\AA}$, $r_B = 0.74\text{\AA}$) and Ni^{2+} ($r_A = 0.55\text{\AA}$, $r_B = 0.69\text{\AA}$) are both divalent cations with ionic radii larger than Fe^{3+} ($r_A = 0.49\text{\AA}$, $r_B = 0.55\text{\AA}$) but while ZnFe_2O_4 is a normal spinel (with $\delta = 0$), NiFe_2O_4 is fully inverted ($\delta = 1$). Considering only their ionic radii, both should be inverse structured spinel ferrites, which is not the case. The reason for this has been explained in terms of the crystal field stabilization energy. This is the energy required to stabilize a cation in either a tetrahedral or an octahedral site. Crystal field stabilization varies in such a way as to account for the changes in the degree of inversion in spinels. Cations with excess octahedral stabilization energy tend to form inverse spinels while those without excess octahedral stabilization energy tend to form normal spinels [3-8]. This simply means that the degree of inversion increases with increase in octahedral stabilization energies of cations. For ZnFe_2O_4 , Zn^{2+} has no excess stabilization energy which implies $\delta = 0$ and so forms a normal spinel structure. For NiFe_2O_4 on the other hand, the excess stabilization energy of Ni^{2+} at an octahedral site favours $\delta = 1$, hence NiFe_2O_4 is largely inverted [3-8, 3-1].

Another factor that can contribute to the determining the degree of inversion in spinel ferrites is the oxygen parameter which is denoted by u in Fig. 3.1. Occupation of the tetrahedral sites by cations usually results in the site being expanded due to the relative size of the cations compared to the size of the tetrahedral site. Using the relation

$$0.225 \leq \frac{r_{\text{ionic}}}{R_{\text{ionic}}} < 0.414$$

for tetrahedral site occupancy, it could be seen that the maximum ionic radius r_{ionic} that could be accommodated in the tetrahedral site is

$R_{ionic} * 0.414 = 1.38\text{\AA} * 0.414 = 0.571\text{\AA}$. This is smaller than the ionic radius of Zn^{2+} (0.60 Å) and Cd^{2+} (0.78 Å) which both result in normal spinels with both cations occupying the tetrahedral sites. The consequence of this is an expansion of the tetrahedral site and a contraction of the octahedral site resulting in the displacement of the position of oxygen ion. This displacement is called the oxygen parameter which is the distance between the oxygen ion and a face of the cube (see Fig. 3.1d). The theoretical value of the oxygen parameter for spinels is 0.375 [3-9]. For spinel ferrites consisting of only divalent and trivalent cations, the oxygen parameter contributes to the degree of inversion according to the following:

$$\begin{aligned}
 u < 0.379 &\rightarrow \text{Inverse spinel structure is favoured} & (3-3) \\
 u > 0.379 &\rightarrow \text{The normal spinel structure is favoured}
 \end{aligned}$$

3.3 Magnetization in Spinel Ferrites

Magnetization in spinel ferrites is strongly dependent on the distribution of cations between the octahedral sites (B-sites) and tetrahedral sites (A-sites) of the spinel structure. If A-sites and B-sites cations are magnetic, there exist two levels of interaction;

- interaction between the cations within each type of cation site
- interaction between the two different sites

The interaction between A-sites cations is called the A-A interaction; the interaction between the B-sites cations is called the B-B interaction and the interaction between the A-sites cations and B-sites cations is called A-B interaction. The strength of the exchange interaction between two cations on different sites of a spinel structure depends on the distance between the cations through the oxygen ion that connects them and the angle formed by the three ions; A-O-A, B-O-B and A-O-B. The interaction is strongest for the shortest distance between the cations and when the angle is 180° [3-10]. As a result, the shorter the distance and the closer the angle is to 180° , the stronger the interaction. In

spinel crystal structure, the angles formed by the cations with the interlinking oxygen ion are A-O-A (79°), B-O-B (90° and 125°) and A-O-B (125° and 154°). The distance between the cations for the B-O-B angle of 125° is more than that for the A-O-B angle of 125° . This means that the strength of the interaction decreases in the order, A-O-B > B-O-B > A-O-A. Consequently, the weak A-A, and B-B interactions result in no spin alignment while the strong A-B interaction results in spin alignment [3-11].

Due to the fact that thermal fluctuations reduce the net magnetic moments per unit volume, theoretically, the magnitude of magnetic moments are given as their value at 0 K. This is practically achieved by measuring the saturation magnetic moments at very low temperatures and extrapolating the data to 0 K. In spinels generally, the A-B interaction is antiferromagnetic, meaning that the spins from the cations on the A-sites align anti-parallel to the spins from the cations on the B-sites. At 0 K, when all the spins from A-sites cations are fully aligned anti-parallel to the spins from B-sites cations, the difference between the moments from both sites gives the resultant saturation magnetization for the material. As shown in Fig. 3.3, for normal spinels with non magnetic Me^{2+} cations, such as $ZnFe_2O_4$, there is no A-B interaction. As a result, the weaker B-B antiferromagnetic coupling causes the B-sites Fe^{3+} moments to align half in one direction, and the other half in antiparallel direction. Thus the magnetic moments of the $2Fe^{3+}$ which are on the B-sites cancel out and since Zn^{2+} has no moments, there is no resultant moment for $ZnFe_2O_4$. Thus $ZnFe_2O_4$ is antiferromagnetic with Néel temperature of 9 K [3-12]. For completely inverse spinels such $NiFe_2O_4$, the magnetic moments of the $2Fe^{3+}$ on the A- and B-sites cancel and the net moment becomes the magnetic moment of Ni^{2+} on the B-sites. $NiFe_2O_4$ is thus ferrimagnetic with a Curie temperature of 858 K [3-12].

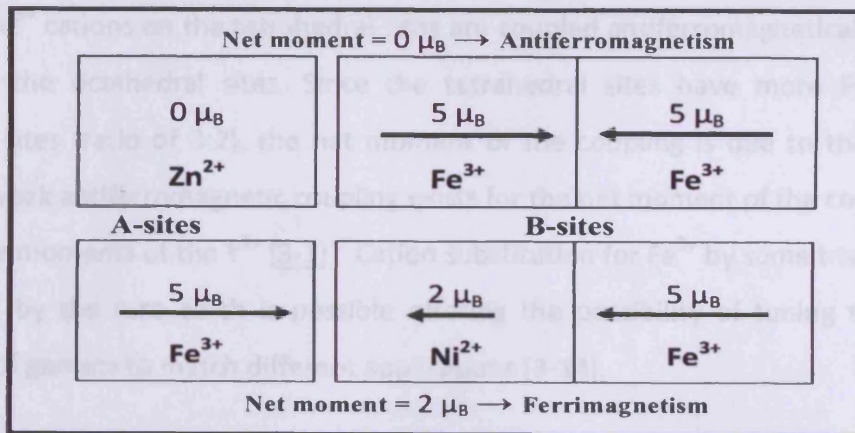


Fig. 3.3: Magnetization at 0 K in normal spinels with $ZnFe_2O_4$ and $NiFe_2O_4$ as examples

3.4 Non-Spinel Ferrites

Hexaferrites crystallize in the hexagonal crystal structure. They can exist as four phases depending on composition as shown in Table 3.1 [3-13]. The most studied and applied is the M-type (magnetoplumbite-type) material, barium hexaferrite ($BaFe_{12}O_{19}$). $BaFe_{12}O_{19}$ has three types of lattice sites; the tetrahedral, octahedral and trigonal. It has high uniaxial anisotropy and saturation magnetization, and is mainly used for permanent magnet and microwave applications.

Phase	Formula
M	$BaFe_{12}O_{19}$
W	$BaMe_2Fe_{16}O_{22}$
Y	$Ba_2Me_2Fe_{12}O_{22}$
Z	$Ba_3Me_2Fe_{24}O_{41}$

Table 3.1: Chemical compositions of different phases of hexaferrites

Garnets have the general formula $A_3B_2C_3O_{12}$ with A, B and C being cations [3-3]. The best known magnetic garnet is the yttrium-iron garnet with the chemical composition $Y_3Fe_2(FeO_4)_3$ (the same as $Y_3Fe_5O_{12}$). It crystallizes in the cubic crystal structure with iron occupying the tetrahedral and octahedral sites and the yttrium occupying the dodecahedral

sites. The Fe^{3+} cations on the tetrahedral sites are coupled antiferromagnetically to the Fe^{3+} cations on the octahedral sites. Since the tetrahedral sites have more Fe^{3+} than the octahedral sites (ratio of 3:2), the net moment of the coupling is due to the tetrahedral cations. A weak antiferromagnetic coupling exists for the net moment of the coupling due to Fe^{3+} and the moments of the Y^{3+} [3-1]. Cation substitution for Fe^{3+} by some trivalent cations and for Y^{3+} by the rare earth is possible offering the possibility of tuning the magnetic properties of garnets to match different applications [3-14].

Orthoferrites belong to a large class of materials possessing a distorted perovskite (CaTiO_3) crystal structure. They have a general formula, ABO_3 , which for the orthoferrites is RFeO_3 [3-15]. R stands for a rare earth metal. The cubic crystal structure of perovskites is distorted in orthoferrites to form an orthorhombic crystal structure. In the orthorhombic structure, the O^{2-} anions occupy the face positions; the Fe^{3+} cations (interacting antiferromagnetically) occupy the centre (octahedral cation site) while the R^{3+} occupies the corner positions (dodecahedral cation site). Orthoferrites have a range of tuneable magnetic properties which depend on the magnetic properties of R^{3+} occupying the dodecahedral site. It also depends on temperature and the interaction between R^{3+} and Fe^{3+} .

3.5 Cobalt Ferrite (CoFe_2O_4)

CoFe_2O_4 is ferrimagnetic, with a partial inverse spinel crystal structure and a Curie temperature of about 520°C . Fig. 3.4 shows a typical x-ray diffraction pattern for a spinel structured cobalt ferrite. The strongest diffraction is from the (311) plane. Degrees of inversion $\delta = 0.68, 0.70, 0.80$ and even as high as 0.96 have been reported for CoFe_2O_4 in various studies [3-16, 3-17, 3-18]. This variation in the literature report may be due to different heat treatment processes during fabrication. It was found that fast cooling and slow cooling results in different degrees of inversion in CoFe_2O_4 even for samples prepared the same way [3-18]. Different partial pressures of oxygen during fabrication can even result in the development of a secondary phase [3-19].

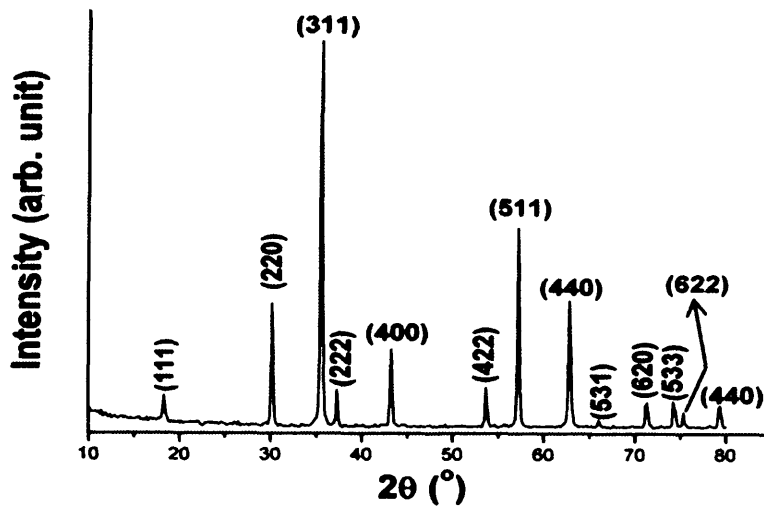


Fig. 3.4: X-ray diffraction pattern for a Co-ferrite spinel structured sample

For completely inverse spinel ferrites, the resultant magnetic moment is that of the divalent cation. Had CoFe_2O_4 been a completely inverse spinel, the net magnetic moment would be $3 \mu_B$ corresponding to the magnetic moment of Co^{2+} . The measured saturation magnetic moment of CoFe_2O_4 at 0 K is $3.7 \mu_B$. The difference between the measured and calculated value could be attributed to the effect of the unquenched orbital moment of Co^{2+} which, when added to the spin moment, would result in higher values of measured magnetic moment [3-1]. It can also be attributed to CoFe_2O_4 being a partially inverse spinel with some Co^{2+} on the A-sites of the spinel structure and the majority on the B-sites.

High anisotropy in CoFe_2O_4 can be explained by the single-ion model of anisotropy considering the contribution of the anisotropy of Co^{2+} in CoFe_2O_4 . This model assumes that the anisotropy of a crystal can be approximated by considering the relative contributions of the constituent ions in the crystal. Though this model ignores the influence of chemical bonding on anisotropy, it is a reasonable approximation in explaining the influence of Co^{2+} on the anisotropy of cobalt containing ferrites. This is easily seen when a small amount of Co^{2+} (Co^{2+} has a positive anisotropy constant) is added to a ferrite with a negative anisotropy constant K_1 . MnFe_2O_4 has a negative anisotropy constant of about $-4 \times 10^3 \text{ J/m}^3$ but substituting a small amount cobalt for manganese to form $\text{Co}_{0.04}\text{Mn}_{0.94}\text{Fe}_2\text{O}_4$ results in K_1 changing from a negative to a positive anisotropy of $0.6 \times 10^3 \text{ J/m}^3$ [3-14]. At all

temperatures shown in Fig. 3.5 [3-20], anisotropy $\text{Co}_x\text{Mn}_{1-x}\text{Fe}_2\text{O}_4$ increases with increase in amount of cobalt.

Moreover, the first cubic anisotropy constant of $\text{FeO}\cdot\text{Fe}_2\text{O}_3$ (Fe_3O_4) is $-1.1 \times 10^4 \text{ J/m}^3$ but on replacing Fe^{2+} with Co^{2+} to form $\text{CoO}\cdot\text{Fe}_2\text{O}_3$ (CoFe_2O_4), the anisotropy increases to $2 \times 10^5 \text{ J/m}^3$. This increase in anisotropy causes the easy axes to change from $\langle 111 \rangle$ (for Fe_3O_4) to $\langle 100 \rangle$ (for CoFe_2O_4). It is therefore apparent that the high anisotropy of cobalt ferrite is due to high anisotropy of Co^{2+} and so, changes in fabrication processes resulting in changes in concentration would result in changes in anisotropy of CoFe_2O_4 . This influence of Co^{2+} on anisotropy of CoFe_2O_4 can also be traced to the unquenched orbital angular momentum of Co^{2+} .

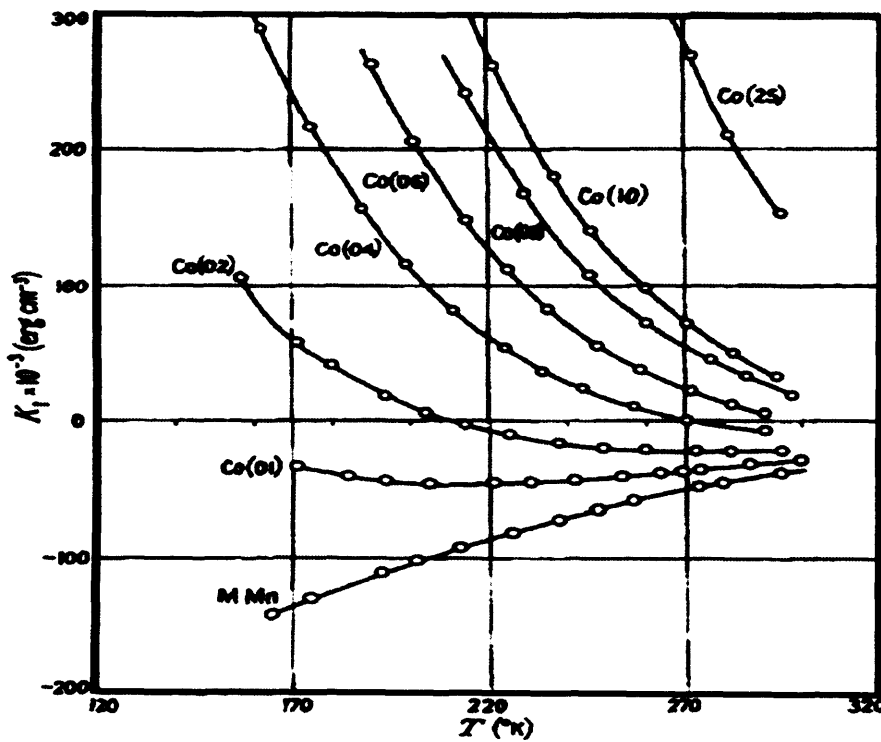


Fig. 3.5: Temperature dependence of first cubic magnetocrystalline anisotropy constant K_1 of $\text{Co}_x\text{Mn}_{1-x}\text{Fe}_2\text{O}_4$ for $x = 0, 0.01, 0.02, 0.04, 0.06, 0.08, 0.1$ and 0.25 . 1 ergcm^{-3} in S.I units is 10 Jm^{-3} . After R. F Pearson [19]

Although coercive field is structure dependent and is affected by other factors such as grain size, shape and the presence of defects which provide pinning sites to domain movement, the presence of Co^{2+} is known to increase coercive field. It has been shown that when Co^{2+} is substituted for Mn^{2+} , the coercive field is increased due to unquenched orbital momentum associated with Co^{2+} [3-21]. The coercive field of CoFe_2O_4 can be as high as 320 kA/m, though this depends on the presence of pinning sites [3-22].

CoFe_2O_4 can be described by two magnetostriction constants, λ_{111} and λ_{100} . λ_{100} is the magnetostriction along the easy directions [100] while λ_{111} is magnetostriction along the hard directions [111]. λ_{100} is negative and is larger in magnitude than the positive λ_{111} . The contribution of Co^{2+} to determining the magnetostriction of CoFe_2O_4 can be observed by comparing to the magnetostriction of Fe_3O_4 . Fe_3O_4 has large positive λ_{111} and smaller negative λ_{100} . On replacement of one Fe^{3+} in Fe_3O_4 with Co^{2+} to form CoFe_2O_4 , the magnetostriction constants change to large negative λ_{100} and a smaller positive λ_{111} .

Fig. 3.6 shows a typical magnetostriction curve of cobalt ferrite. The initial part of the curve (A-B or A-(-B)) represents the region in which the contribution of the negative λ_{100} to the resultant magnetostriction is dominant. This initial high negative slope region continues until all magnetic domains align along the easy axes close to the direction of the applied field. After this, on further application of a magnetic field, the contribution of λ_{111} to the resultant magnetostriction becomes dominant and is observed (B-C or B-(-C)). A-B is steeper than B-C.

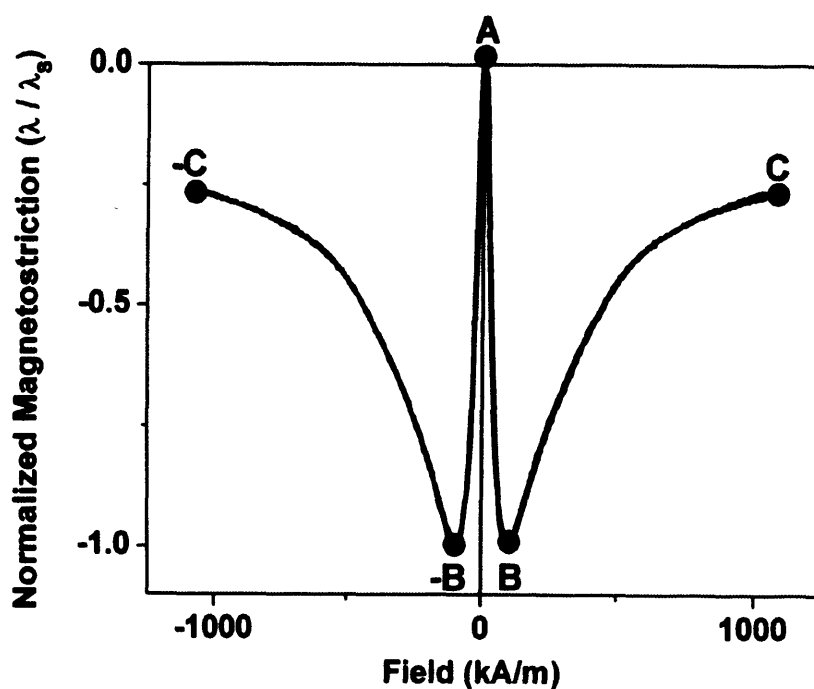


Fig. 3.6: Typical magnetostriction curve of cobalt ferrite measured at 300 K. The hysteresis in this curve has been neglected for clarity of illustration.

Magnetostriction of CoFe_2O_4 is known to depend on temperature. Fig. 3.7 shows that at any magnetic field, magnetostriction amplitude decreases with increase in temperature. Moreover, the magnetic field at which the magnetostriction of CoFe_2O_4 reaches saturation decreases with increase in temperature. This has been shown to be due to decrease in anisotropy of CoFe_2O_4 with increase with temperature [3-23]. Also, magnetomechanical hysteresis increases when magnetostriction is measured at low temperature. This effect is reduced at higher temperatures due to the reduction in magnetocrystalline anisotropy as temperature increases.

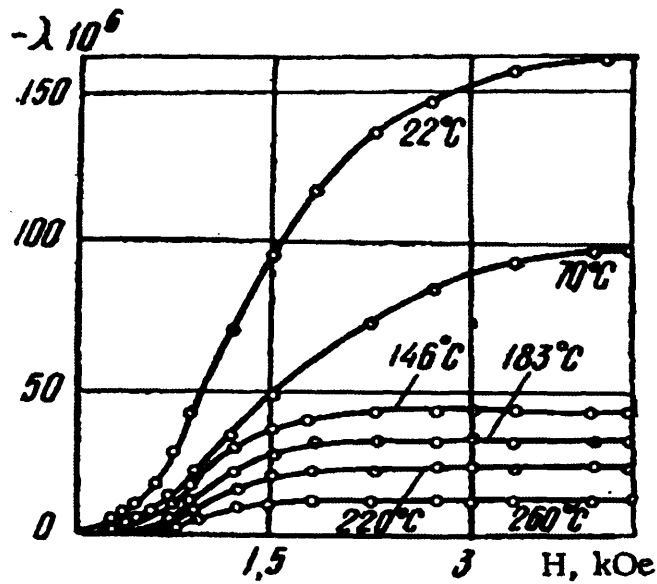


Fig. 3.7: Temperature dependence of magnetostriction of CoFe_2O_4 . 1 kOe = 79.58 kA/m. The figure shows that the amplitude of magnetostriction reduces with increasing measurement temperature [3-22].

Another way of reducing magnetomechanical hysteresis is by substitution of non-magnetic cations into the spinel structure of CoFe_2O_4 resulting in mixed ferrites ($\text{CoM}_x\text{Fe}_{2-x}\text{O}_4$) where M is a non-magnetic cation. Such cation substitution not only reduces the magnetomechanical hysteresis, it also lowers the Curie temperature of CoFe_2O_4 . Lowering of the Curie temperature occurs because substitution of non-magnetic cations into the tetrahedral and/or octahedral sites of the spinel structure of CoFe_2O_4 results in the weakening of the super-exchange coupling that keeps the atomic moments aligned. This makes it easier for thermal energy to disorder the magnetic moments and results in the lowering of Curie temperature.

Also magnetostriction of CoFe_2O_4 can vary due to heat treatment especially when the heat treatment modifies the lattice parameter of CoFe_2O_4 [3-24]. This can be observed as a shift in the 2θ positions of the peaks in the XRD pattern. Shifts to lower 2θ value represent an increase in the lattice parameter while a shift to the higher 2θ values represents a decrease. Strain derivative $d\lambda/dH$ of CoFe_2O_4 represents the rate of change of the output strain with

respect to an applied magnetic field when CoFe_2O_4 is used in application as an actuator. When used as a sensor, stress sensitivity $dB/d\sigma$, represents the rate of change of the output magnetic flux density with respect to an input mechanical stress. Both $d\lambda/dH$ and $dB/d\sigma$ are proportional as shown in equation (2-29). An ideal application for magnetostrictive devices based on CoFe_2O_4 is in non-contact magnetomechanical stress sensor in which it is essential for $dB/d\sigma$ to be high. Compared with Terfenol-D based composites with magnitude of magnetostriction over 1500 ppm, CoFe_2O_4 has lower magnetostriction but higher stress sensitivity and is more suitable for applications where higher sensitivity, chemical stability and robustness are essential. Typical values of $d\lambda/dH$ for cobalt ferrite are in the range 1.13×10^{-9} to $1.5 \times 10^{-9} \text{ Am}^{-1}$ [3-25, 3-26, 3-27]. $d\lambda/dH$ or $dB/d\sigma$ in CoFe_2O_4 can be increased by non magnetic cation substitution.

3.6 Preparation of Bulk Cobalt Ferrite

The method of preparation of CoFe_2O_4 greatly affects the microstructure which in turn affects the magnetic and magnetostrictive properties.

3.6.1 Traditional ceramic method

Fig.3.8 shows the steps for preparing CoFe_2O_4 via the traditional or conventional ceramic method. The aim of the **powder mixing** stage is to ensure that the powder particles are uniformly distributed to help achieve complete solid state reaction. When the volume of powder is small (about 100g or less), manual mixing can be sufficient. Otherwise, commercial shakers/mixers are used to mix the powders. Powders can be mixed wet or dry.

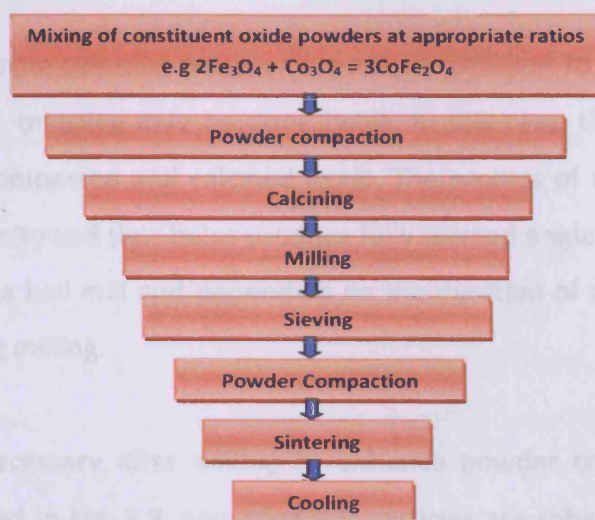
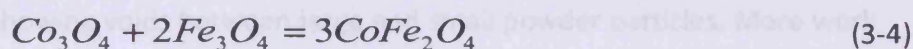


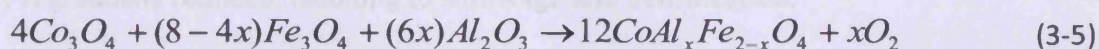
Fig. 3.8: Steps for the preparation of CoFe_2O_4 via the traditional ceramic route

Powder compaction requires the application of pressure to form the powder into the shapes of choice. Powder compaction helps to ensure that the particles which were uniformly distributed make enough contact to encourage bonding during sintering. During this stage, applied pressure deforms the surface of the particles thereby increasing the surface area required for bonding of particles.

Calcining involves heating the compacted sample to a temperature necessary for achieving solid state reaction. It is usually done to allow the powder particles which are already compacted against each other to react and form the required phase. For pure CoFe_2O_4 , the chemical equation for the reaction expected to take place between the constituent oxides is;



For $\text{CoAl}_x\text{Fe}_{2-x}\text{O}_4$ used in this research work (x is the amount of Al^{3+} substituted for Fe^{3+}), the chemical equation is



Since sometimes a single calcining process may not be sufficient to produce a fully reacted, single phase sample, calcining may be done twice. In this case, the calcined samples are milled once more, compacted and calcined again. The process of **milling** the samples also helps achieve uniformity and thus helps produce fully reacted single phased samples. Milling is usually done with a ball mill and depending on the duration of milling, powder particles may also react during milling.

Powder **sieving** is necessary after milling to enhance powder compaction and effective sintering. As illustrated in Fig. 3.9, assuming the particles are spherical, the voids between larger powder particles being larger than voids between smaller particles would require more work to be eliminated by compaction. Well compacted samples enhance the sintering process and the resultant properties of the sample.

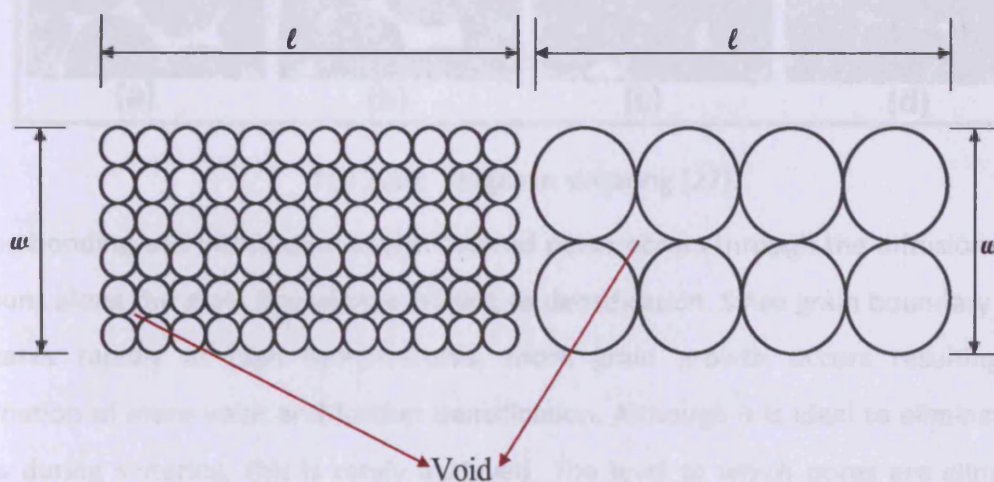


Fig. 3.9: Schematic showing voids between large and small powder particles. More work is required to eliminate voids between larger particles of the same volume.

Sintering is a heat treatment frequently used for processing ceramic powders such as CoFe_2O_4 . The main aim of sintering is to turn loose powders into a consolidated polycrystalline solid. During sintering, powder particles are bonded together and the pore density is gradually reduced, resulting to shrinkage and densification.

The stages in a sintering process are shown in Figure 3.10 [3-28]. Stage (a) represents the state of the powder particles after compaction in which they make stronger contacts than in loose powder particles. As the particles are heated during sintering, stronger bonds are formed between the particles resulting in necking (stage b). Further heating leads to further necking, shrinkage and formation of grain boundaries (stage c). Some grain growth takes place during this stage and the voids which were initially interconnected start to become isolated in pores. In the final stage (d), more heating results in further growth of some grains at the expense of others, stronger bonding, better definition of the grain boundaries and further isolation of voids.

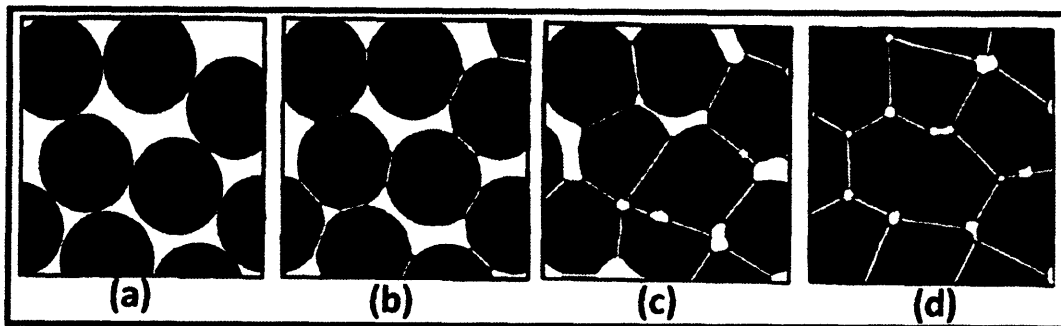


Fig. 3.10: Stages in sintering [27].

Strong bonding and elimination of the isolated pores occurs through the diffusion of atoms and ions along the grain boundaries leading to densification. Since grain boundary diffusion increases rapidly at high temperatures, more grain growth occurs resulting in the elimination of more voids and further densification. Although it is ideal to eliminate all the pores during sintering, this is rarely achieved. The level to which pores are eliminated is determined by the level of the initial porosity in the compacted powder particles, the sintering temperature and the holding time. The sintering temperature is usually higher than the calcining temperature but lower than the melting temperature of the material.

The sintering temperature and holding time should be such that the surface energies of the compacted powder particles are reduced and that bonding is initiated and sustained. This reduction in surface energy is the driving force for sintering operation. Chemical reactions

can also take place, though not in all sintering processes. In solid state sintering in which calcining is insufficient to bring about complete solid state reaction, sintering is usually done both to complete the chemical reaction and for densification. Such is the case of CoFe_2O_4 preparation via solid state chemical reaction between Co_3O_4 and Fe_3O_4 oxide powders. To achieve this, the holding time should be long enough to allow such reactions to take place before cooling sets in. This is because the migration of atoms and ions in solids is comparatively slower than in liquids. Since such migrations are thermally activated, the onset of cooling immobilises atoms and ions and may suspend any on-going reactions resulting in incomplete chemical reactions. Most of the CoFe_2O_4 samples used in this research were held for at least 24 hours both during the sintering and calcining stages.

Controlling the sintering and the cooling processes is important for optimizing the magnetic and magnetostrictive properties of CoFe_2O_4 . The SP^3 paradigm in materials science relates structure, processing, property and performance of a material. It shows that the performance of any materials depends on its properties which depend on the structure and the structure depends on the processing. Thus in processing CoFe_2O_4 via the traditional ceramic method, the sintering and cooling stages should be controlled to obtain microstructures with desirable properties.

Microstructure sensitive properties such as coercive field depend on grain size and grain boundaries available in a material. A sample with small grains has more grain boundaries which serve as pinning sites to domain motion and thus results in high coercive field. If a material is fast cooled, grain growth might not have sufficiently taken place before atoms and ions are immobilized. This would result in the formation of samples with smaller grains and many grain boundaries. Because of domain motion interruption, high pore volume also results in high coercive field. Microstructure also affects mechanical properties which can be controlled during processing. CoFe_2O_4 quenched to room temperature in a medium such water or nitrogen would be brittle and have high residual stress. Since magnetostrictive properties show the interplay between magnetic and mechanical properties, materials with

undesirable mechanical and magnetic properties have undesirable magnetostrictive properties.

It should be noted that when powder particles are sieved, the sieve size represents the maximum particle size allowable through the sieve. This means that when the powder particles of the samples are sieved, the size distribution is inhomogeneous. This affects the microstructure since some grains grow faster than, and at the expense of others. The consequence is that ceramic samples are usually made up of large grains surrounded by smaller ones as shown in Fig. 3.11. It can also be seen from this that just as there large and small grains, there are also very large, intermediate and small pores. These distributions arise due to the initial lack of homogeneity in the powder particles prior to sintering. It thus follows that for materials in which uniformity of grain distribution is crucial for property optimization with respect to targeted performance, control of processing parameters is necessary even from the mixing, grinding and sieving stages. In fact, poor mixing of the sample can result in microstructures with additional phase or phases in the matrix of the parent phase. Fig. 3.12 shows a CoFe_2O_4 with two phases. The parent phase is labelled 1 and the secondary additional phase labelled 2. The formation of a secondary additional phase usually results in large stresses and cracks especially at the interface between the parent phase and the secondary additional phase. Such stresses and cracks have detrimental effect on magnetic and magnetostrictive properties of CoFe_2O_4 .

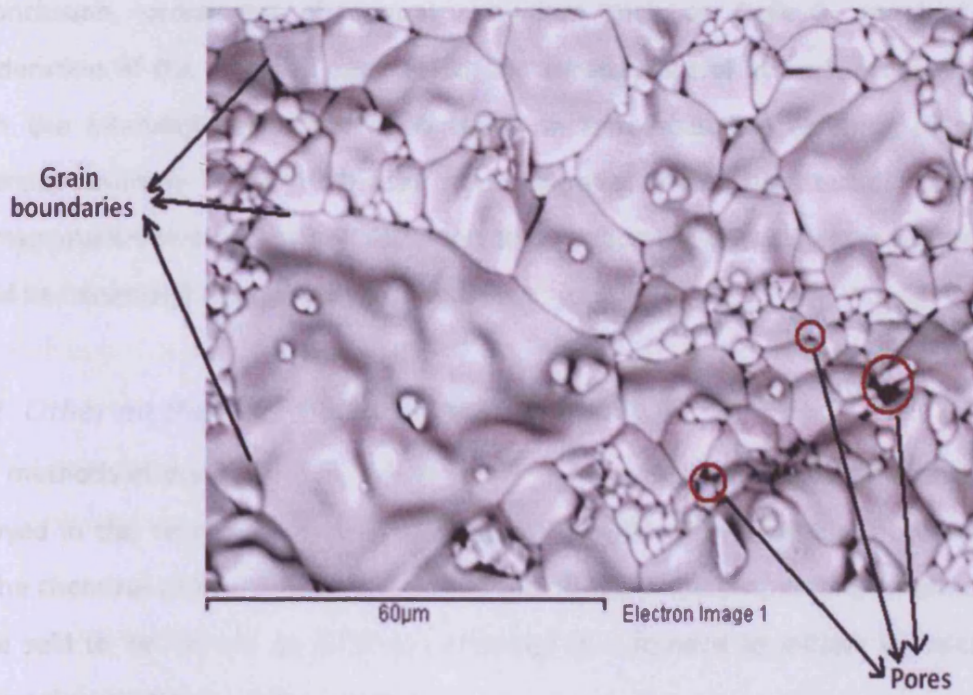


Fig. 3.11: Typical microstructure of ceramic CoFe_2O_4

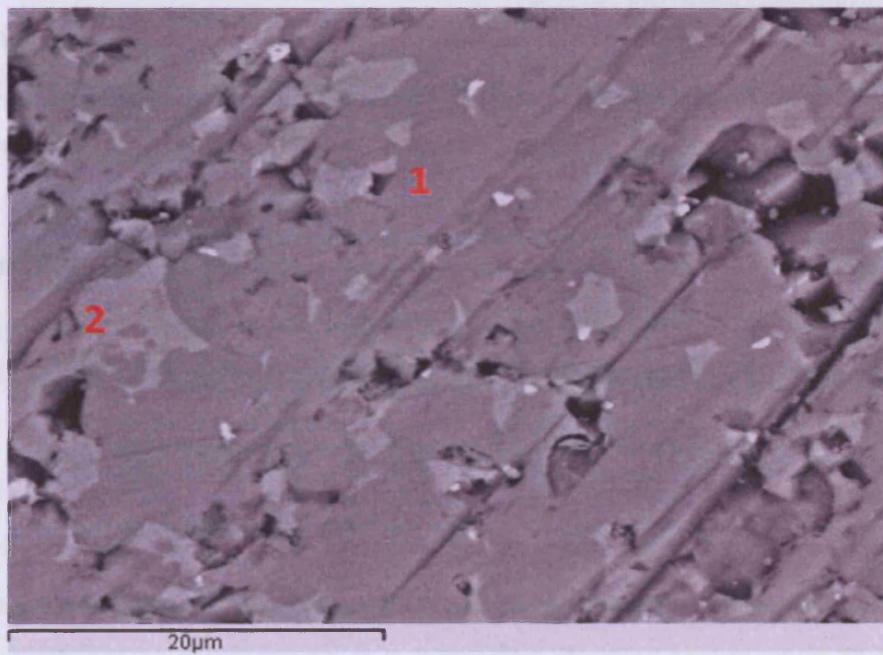


Fig. 3.12: A microstructure of CoFe_2O_4 material with two phases labelled 1 and 2.

In conclusion, processing of ceramic powders such as CoFe_2O_4 requires adequate consideration of the targeted application and careful control at each processing stage to match the intended performance. Variation in microstructure resulting in variation in properties results in samples with the same chemical composition but different magnetic and magnetostrictive properties. Although this variation is in most cases not avoidable, it should be minimised as much as possible.

3.6.2 Other methods of preparing bulk CoFe_2O_4

Other methods of preparing bulk cobalt ferrite are not discussed in detail as they were not employed in this research work. The difference between the methods is usually based on how the chemical compound CoFe_2O_4 is formed. In the traditional ceramic method, CoFe_2O_4 can be said to be formed by heating (calcining) in a furnace to initiate chemical reaction between the constituent oxide powders.

Mechanosynthesis is an advanced method in which the constituent oxides of a ceramic are made to react by mechanical activation. This usually involves days of milling and shaking of the oxides. Once formed, the sample is compacted and sintered as in tradition ceramic method. In the

In the **Self-Propagating-Synthesis** method, an ignitable powder is mixed with the constituent oxide and ignited at elevated temperature resulting in sufficient heat to bring about reaction. This method usually results in poor homogeneity and porosity [3-29].

Co-precipitation method can also be used to produce CoFe_2O_4 , in which case, aqueous solutions of the Fe^{3+} and Co^{2+} are subjected to either oxidative or hydrothermal co-precipitation. In oxidative co-precipitation, CoFe_2O_4 is formed at room temperature [3-30] and in hydrothermal co-precipitation; it is formed at elevated temperature [3-31]. This is a simple process during which the solution is stirred and the powder particle size controlled

by the speed of stirring. The disadvantage is that the process usually results in loss of stoichiometry [3-32].

CoFe₂O₄ can also be synthesized via **complexometric titration** of a mixture of solutions containing Fe³⁺ and Co²⁺ with a chelating (complexing) agent. Such an approach has been used to synthesize CoFe₂O₄ from a mixture of Fe(NO₃)₃ and Co(NO₃)₂ solutions using EDTA (ethylenediaminetetraacetic acid) as the chelating agent [3-32].

In all the preceding methods, after the formation of CoFe₂O₄, the powder particles are usually subjected to compaction and sintering as in the traditional ceramic method.

3.7 Preparation of Thin Film Cobalt Ferrite

Thin film CoFe₂O₄ materials are important having potential applications for the development of noncontact force and torque sensors, magneto-optical devices, spin filters for magnetic tunnel junctions and hybrid data storage devices. Various deposition methods have been used for the preparation of thin film cobalt ferrite samples. One crucial factor is the ability to deposit at temperatures low enough to allow integration with MEMS devices, multilayer hybrid sensors, GMR, TMR, or semiconductor devices. Also, because properties of CoFe₂O₄ can be optimised by cation doping, it is necessary that a chosen method should be applicable in depositing cation substituted CoFe₂O₄ samples.

3.7.1 Pulsed laser deposition (PLD)

A high power pulsed laser beam is used to ablate a substrate in pulsed laser deposition. Although a pulsed laser beam is usually used, it is also possible to ablate a material with a continuous laser beam. As shown in Fig. 3.13 [3-33], in a PLD system, a high energy excimer laser is incident on a rotating target (or targets), which results in the ablation of the target and generation of a plasma plume containing the vaporized target.

The plasma plume is deposited on a substrate at an elevated temperature to form a thin film of the desired material. The route of the excimer laser from the source to the substrate is guided by a combination of lenses. Pulsed laser deposition of CoFe_2O_4 usually starts with a high purity, high density CoFe_2O_4 substrate in oxygen gas environment ablated by laser onto a heated substrate. The substrate temperature contributes to the determination of the final composition, microstructure and magnetic properties of the resultant CoFe_2O_4 film. Lower temperatures may result in the growth of additional phases which tend to vanish with increase in substrate temperature [3-34]. Thermal expansion mismatch between the grown thin film and the substrate and the partial pressure of oxygen during growth can all affect the properties of the film.

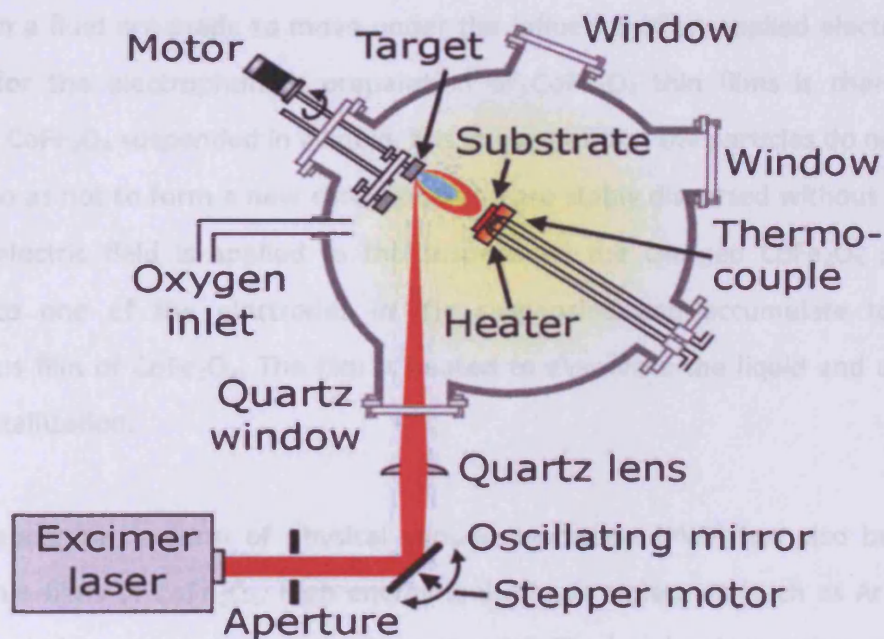


Fig. 3.13: Schematic of a basic pulsed laser deposition system

3.7.2 Other methods of preparing thin films of CoFe_2O_4

The sol-gel method has been employed in the preparation of CoFe_2O_4 samples [3-35, 3-36]. It usually involves dissolving solutions containing Fe^{3+} and Co^{2+} (such as nitrates of the

cations) in solvents (such as an organic acid e.g citric acid) in appropriate proportions. The solution is vigorously heated to bring about a chemical reaction and spin-coated onto thermally oxidized substrates (such as Si wafers). The coated substrates are further heated to a high temperature to remove the organic solvent and to form amorphous thin films of CoFe_2O_4 . The chosen temperature depends on the chosen organic solvent. The amorphous films are then crystallized at higher temperatures. The sol-gel method is useful for preparing cation substituted CoFe_2O_4 thin films. It can also be used for preparing samples at temperature as low as $350\text{ }^\circ\text{C}$ but this usually results in samples with poor homogeneity. To achieve homogeneity, samples should be annealed at and above $450\text{ }^\circ\text{C}$ [3-36].

CoFe_2O_4 thin films can be prepared by **electrophoresis**, a process in which charged particles dispersed in a fluid are made to move under the influence of an applied electric field. The precursor for the electrophoretic preparation of CoFe_2O_4 thin films is charged powder particles of CoFe_2O_4 suspended in a liquid. It is important that the particles do not react with the liquid so as not to form a new compound and are stably dispersed without coagulation. When an electric field is applied to the suspension, the charged CoFe_2O_4 particles are attracted to one of the electrodes in the suspension and accumulate to deposit a homogenous film of CoFe_2O_4 . The film is heated to evaporate the liquid and annealed for proper crystallization.

Sputter deposition, a form of physical vapour deposition (PVD) has also been used to produce thin films of CoFe_2O_4 . High energy ionised gas molecules (such as Ar^+ molecules) are bombarded on a target at a negative potential. The bombardment then results in the ejection of atoms from the surface of the target to a substrate at elevated temperature. The obtained film can be annealed at elevated temperatures (depending on application) to further optimise properties. In order to obtain suitable crystallinity, samples may have to be annealed at higher temperatures. XRD measurement on sputtered CoFe_2O_4 samples show that crystallinity becomes observable at about $900\text{ }^\circ\text{C}$ and increases with increasing annealing temperature [3-37]. Magnetic properties were also found to depend on annealing

temperature. Such a high annealing temperature requirement is detrimental to MEMS and other semiconductor devices and thus sets back integration of thin films of CoFe_2O_4 into such devices.

Highly controllable deposition of CoFe_2O_4 thin film at an atomic scale can be obtained by **atomic layer deposition**. The high controllability of this technique is due to its self-limiting nature. In an atomic layer deposition of CoFe_2O_4 thin film, two precursors containing Fe^{3+} and Co^{2+} are introduced on a substrate in a reaction chamber sequentially. Before the introduction of one precursor, the chamber is purged of the excesses of the previous precursor. One precursor deposited onto the substrate produces a monolayer of the precursor and reacts with a monolayer of the second precursor to produce a monolayer of the thin film. The magnetic properties of atomic layer deposited CoFe_2O_4 films and the effect of magnetic field during the deposition process has been previously studied [3-38].

References to Chapter 3:

- [3-1]. J. Smit and H. P. J. Wijn, *Ferrites: physical properties of ferrimagnetic oxides in relation to their technical application*, Netherlands, Philips Technical Library (1959)
- [3-2]. B. D. Cullity, *Introduction to Magnetic Materials*, USA, Addison-Wisley (1972)
- [3-3]. A. J. Badden Fuller, *Ferrites at Microwave Frequencies*, UK, Cambridge, University Press (1987)
- [3-4]. G. Concas, G. Spano, C. Cannas, A. Musinu, D. Peddis and G. Piccaluga "Inversion degree and saturation magnetization of different nanocrystalline cobalt ferrites" *J Magn Mag Mater* **321** (2009) 1893
- [3-5]. Carta D; Casula M. F.; Faliqi A.; Loched D.; Mountjoy G.; Sangregorio C. and Corrias A. "A Structural and Magnetic Investigation of the Inversion Degree in Ferrite Nanocrystals MFe_2O_4 (M = Mn, Co, Ni)" *J. Phys. Chem.C* **113** (2009) 8606
- [3-6]. Donald R. Askeland, *The Science and Engineering of Materials*, Uk, Chapman and Hall, (1996)
- [3-7]. J. D. Dunitz and L. E. Orgel, "Electronic properties of transition metal oxides II" *J. Phys. Chem. Solids* **3** (1957) 318
- [3-8]. Takashi Yokoyama and Takeshi Meguro, "Relationship between average cation radii and oxygen parameter for various oxides with spinel-type structure" *Jap. J. Appl. Phys.* **44** (2005) 6201-
- [3-9]. Alex Goldman, *Modern Ferrites*, 2nd ed. USA, Springer (2006)
- [3-10]. Relva C. Buchanan, *Ceramic Materials for Electronics*, 3rd ed., USA, Marcel Dekker Inc. (2004)
- [3-11]. Raul Valenzuela, *Magnetic Ceramics*, UK, Cambridge, University Press (1994)
- [3-12]. É. Du Trémolet de Lacheisserie, D. Gignoux, M. Schlenker, *Magnetism, Materials and Applications*, USA, Springer, (2003)
- [3-13]. D.J. Craik, *Magnetic Oxides, -Part 1*, UK: John Wiley & Sons; Ltd, (1975)
- [3-14]. G. Srinivasan, A. N Slavin, *High Frequency Processes in Magnetic Materials*, Singapore, World Scientific (1995)

- [3-15]. D. Carta, M. F. Casula, A. Falqui, D. Loche, G. Mountjoy, C. Sangregorio, and A. Corrias, "A Structural and Magnetic Investigation of the Inversion Degree in Ferrite Nanocrystals MFe_2O_4 ($M = Mn, Co, Ni$)" *J. Phys. Chem.C* **113** (2009) 8606
- [3-16]. D. Carta, G. Mountjoy, G. Navarra, M. F. Casula, D. Loche, S. Marras and A. Corrias "Absorption Investigation of the Formation of Cobalt Ferrite Nanoparticles in an Aerogel Silica Matrix" *J. Phys. Chem. C* **111** (2007) 6308.
- [3-17]. G.A. Sawatzky, F. Van der Woude, A.H. Morrish, "Cation distribution in octahedral and tetrahedral sites of the ferrimagnetic spinel $CoFe_2O_4$ " *J. Appl. Phys.* **39** (1968) 1204
- [3-18]. Shūichi Iida, "Phase diagram of Iron-Cobalt-Oxygen system (1) experimental study" *J. Phys. Soc. Japn.* **11** (1956) 846
- [3-19]. R. F. Pearson "The magnetocrystalline anisotropy of cobalt-substituted manganese ferrite" *Proc. Phys. Soc.* **74** (1959) 505
- [3-20]. Joel S. Miller and Marc Drillon, *Magnetism: Molecules to Materials (IV)*, Germany, Willey-VCH (2003)
- [3-21]. Robert C. O'Handley, *Modern Magnetic Materials, Principle and Applications* USA, John Wiley (2000)
- [3-22]. V. V. Zubov and É. N. Klenov "Temperature dependence of the magnetostriction of cobalt and nickel-cobalt ferrites" *Russ. Phys. Journal.* **14** (1971) 394
- [3-23]. Gumen N. M. "Variation of magnetostriction in heat treated cobalt ferrite" *Sov. Phys. J.E.T.P.*, **22** (1966) 251; as referenced in Etienne. du Trémolet de Lacheisserie, *Magnetostriction, Theory and Application of Magnetoelasticity*, USA, CRC Press, (1993)
- [3-24]. G. S. N. Rao, O. F. Caltun, K. H. Rao, B. Parvatheeswara Rao, H. L. Wamocha and H. H. Hamdeh, "Influence of silicon and cobalt substitutions on magnetostriction coefficient of cobalt ferrite" *Hyperfine Interactions*, **184** (2008) 593
- [3-25]. Y. Chen, J. E. Snyder, C. R. Schwichtenberg, K. W. Dennis, R. W. McCallum, D. C. Jiles "Metal-bonded Co-ferrite composites for magnetostrictive torque sensor applications" *IEEE Trans. on Magn.*, **35** (1999) 3652
- [3-26]. C. C. H. Lo "Compositional Dependence of the Magnetomechanical Effect in Substituted Cobalt Ferrite for Magnetoelastic Stress Sensors" *IEEE Trans. Magn.*, **43** (2007) 2367

- [3-27]. W. E. Lee and W. M. Rainforth, *Ceramic Microstructure*, UK, Kluwer Academic Publishers, (1994)
- [3-28]. Myer Kutz, *Handbook of Materials Selection*, New York, John Wiley (2002)
- [3-29]. M. Rajendran, R.C. Pullar, A.K. Bhattacharya, D. Das, S.N. Chintalapudi, C.K. Majumdar "Magnetic properties of nanocrystalline CoFe_2O_4 powders prepared at room temperature: variation with crystallite size" *J. Magn. Magn. Mater.* **232** (2001) 71
- [3-30]. P.C. Morais, V.K. Garg, A.C. Oliveira, L.P. Silva, R.B. Azevedo, A.M.L. Silva, E.C.D. Lima, "Synthesis and characterization of size-controlled cobalt-ferrite-based ionic ferrofluids" *J. Magn. Magn. Mater.* **225** (2001) 37
- [3-31]. Pham D. Thang, Guus Rijnders, Dave H.A. Blank, "Spinel cobalt ferrite by complexometric synthesis" *J. Magn. Magn. Mater* **295** (2005)251
- [3-32]. http://www.physics.colostate.edu/groups/PattonGroup/systems/pld_desc.html
- [3-33]. C. Araújo, B.G. Almeida, M. Aguiar and J.A. "Mendes Structural and magnetic properties of CoFe_2O_4 thin films deposited by laser ablation on Si (001) substrates" *Vacuum* **82** (2008) 1437
- [3-34]. Fuxiang Cheng, Zuoyan Peng, Zhigang Xu, Chunsheng Liao, Chunhua Yan "The sol-gel preparation and AFM study of spinel CoFe_2O_4 thin film" *Thin Solid Films*, **339** (1999) 109
- [3-35]. Jae-Gwang Lee, Jae Yun Park, Young-Jei Oh and Chul Sung Kim, "Magnetic properties of CoFe_2O_4 thin films prepared by a sol-gel method" *J. Appl. Phys.*, **84** (1998) 2801
- [3-36]. Y. C. Wang, J. Ding, J. B. Yi, B. H. Liu, T. Yu and Z. X. Shen, "High-coercivity Co-ferrite thin films on (100) -SiO_2 substrate" *Appl. Phys. Lett.* **84** (2004) 2596
- [3-37]. Martin Lie, Karina Barnholt Klepper, Ola Nilsen, Helmer Fjellvåg and Arne Kjekshus "Growth of iron cobalt oxides by atomic layer deposition" *Dalton Trans.*, (2008) 253

Chapter 4. Review of Previous Studies on Cobalt Ferrite for Magnetostrictive Applications

4.1 Introduction

The requirement to scale up production has contributed to the need for advanced automated systems in industry. Most automated systems depend heavily on high sensitivity sensors or energy efficient actuator devices. Sensors for mechanical stress measurement or monitoring and actuators can be developed by exploiting the magnetomechanical coupling capability of magnetostrictive materials. This has led to research on magnetostrictive materials and devices for various applications especially where non-contact operation is crucial. Non-contact operation capability is useful because accuracy, repeatability and linearity are degraded over time due to wear and tear in devices operating in contact mode. Suitable magnetostrictive materials for such devices should possess sufficient amplitude of magnetostriction for the intended applications and high sensitivity of magnetostriction to applied magnetic field (strain sensitivity). They should also have good mechanical, thermal and chemical properties of which ferrites are good candidates. Among the ferrites, cobalt ferrites (including the parent material CoFe_2O_4 and derivatives $\text{CoM}_x\text{Fe}_{2-x}\text{O}_4$ (where M stands for a metal ion)) are promising for such device development because of their suitable magnetomechanical properties.

4.2 Previous Researches on Magnetostrictive Application of Cobalt Ferrite

It is important to view the magnetostrictive properties of CoFe_2O_4 considering the well known Terfenol-D. Terfenol-D is a rare earth based material with giant magnetostriction of 1000-2000 ppm [4-1, 4-2]. McCallum et al [4-1] have compared the suitability of materials based on CoFe_2O_4 with those based on Terfenol-D composites for magnetostrictive applications. The authors observed that the magnetostriction and strain derivative (1.3×10^{-9} m/A) of polycrystalline Terfenol-D based composites were sufficiently high for advanced automotive magnetomechanical sensors but the high cost, poor mechanical and corrosion properties are limiting factors. To improve mechanical and corrosion properties, Terfenol-D

based composites was embedded in soda–lime glass, resin, Fe and NaPO_3 glass matrices to form composites. It was reported that though the mechanical and corrosion properties were improved in the composites, the magnetostriction and strain derivative were degraded. In comparison, the strain derivative of CoFe_2O_4 and metal bonded CoFe_2O_4 composites are similar to that of polycrystalline Terfenol-D based composites but the amplitude of magnetostriction (-225 ppm) is much lower. According to the authors, the corrosion properties of CoFe_2O_4 and metal bonded CoFe_2O_4 composites are excellent. The mechanical properties of the metal bonded CoFe_2O_4 composites are the best of all the compositions they studied.

Although the authors preferred metal bonded CoFe_2O_4 composites, it is worth mentioning that the poor magnetostriction and strain derivative observed for Terfenol-D based composites were probably due to the choice of matrix material. The magnetostriction amplitudes obtained for Terfenol-D based composites are less than that reported in a similar study in which another matrix (polyurethane elastomers) was used for the composite [4-3] (It should be noted that this also depends on the volume fraction of Terfenol-D in the composites). In the later study, it was found that application of a magnetic field while the composites were cured (in order to align the magnetic easy axes of the particles) and adjustment of the Terfenol-D/matrix compositions resulted in the ability to improve the strain derivative and mechanical properties. Terfenol-D has higher magnetostriction than, and similar strain derivative to CoFe_2O_4 , and both their mechanical and corrosion properties can be improved by embedding them in matrices. Preference for CoFe_2O_4 and/or its composites to Terfenol-D and/or its composites results from the ability of tuning the magnetostriction and/or strain derivative of CoFe_2O_4 and its composites to a value much more than that of Terfenol-D and its composites.

The possibility of tuning the strain derivative of CoFe_2O_4 by substitution of non-magnetic Cr^{3+} and Mn^{3+} for Fe^{3+} has been demonstrated [4-4]. The author showed that substitution of both cations for Fe^{3+} resulted in an increase of the strain derivative of CoFe_2O_4 from 1.5×10^{-4}

⁹ m/A to a value of 2.5×10^{-9} m/A for $\text{CoCr}_{0.2}\text{Fe}_{1.8}\text{O}_4$ and 2.7×10^{-9} m/A for $\text{CoMn}_{0.2}\text{Fe}_{1.8}\text{O}_4$. The results show an increase in strain sensitivity of over 66% and 80% respectively of that of Terfenol-D. This increase in strain derivative was accompanied by a decrease in the amplitude of magnetostriction from 200 ppm for CoFe_2O_4 to 80 ppm for $\text{CoCr}_{0.2}\text{Fe}_{1.8}\text{O}_4$ and 180 ppm for $\text{CoMn}_{0.2}\text{Fe}_{1.8}\text{O}_4$. Further increase in the amount of non-magnetic cations substituted for Fe^{3+} resulted in lowering magnetostriction amplitude and maximum strain derivative. The author showed that the dependence of stress sensitivity (which is proportional to strain derivative, see [eq. 2-29 in chapter 2](#)) on magnetostriction amplitude and magnetocrystalline anisotropy can be written as

$$\frac{dB}{d\sigma} \propto \frac{d\lambda}{dH} \propto \frac{\lambda_{\max}}{K_1} \quad (4-1)$$

$\frac{dB}{d\sigma}$ is the stress sensitivity; $\frac{d\lambda}{dH}$ is the strain derivative, $\frac{\lambda_{\max}}{K_1}$ is ratio of the maximum magnetostriction amplitude to the first order cubic magnetocrystalline anisotropy coefficient. Thus they argued that the increase in strain derivative found in the study was attributable to the decrease in anisotropy due to substitution of non-magnetic cations. Similar literatures [4-5, 4-6] show that these substitutions also decrease the Curie temperatures. This shows that the temperature dependence of magnetic and magnetostrictive properties of cobalt ferrite can be tuned by cation substitution offering capability of controlling magnetomechanical hysteresis. Depending on site preference, different cations have different effects on the magnetic and magnetostrictive properties of CoFe_2O_4 . This could be seen from the varying influences of Mn^{3+} and Cr^{3+} substituted for Fe^{3+} on the magnetic and magnetostrictive properties of CoFe_2O_4 .

Ga^{3+} substitution for Fe^{3+} resulted in an increase in the strain derivative of CoFe_2O_4 by more than 130 % [4-7]. Similar to other substitutions, it was observed that the magnetostriction amplitude was reduced from 200 ppm for CoFe_2O_4 to 100 ppm for $\text{CoGa}_{0.2}\text{Fe}_{1.8}\text{O}_4$ ($\text{CoGa}_{0.2}\text{Fe}_{1.8}\text{O}_4$ gave the highest amplitude of magnetostriction and strain derivative).

Compared with Terfenol-D, this is a remarkable increase in strain derivative for substituted CoFe_2O_4 sample and seems to endorse the preference of materials based on CoFe_2O_4 for magnetostrictive applications. This is irrespective of the reduction in amplitude of magnetostriction, because magnetostriction amplitude as low as 30 ppm is sufficient for many applications [4-8]. As in the previous studies, substitution of Ga^{3+} also resulted in the lowering of the Curie temperature. Of the substituted cations discussed so far, Ga^{3+} had the strongest effect in lowering the Curie temperature with increase in the cation composition. The authors concluded that the large effect of Ga^{3+} substitution on the Curie temperature is a consequence of strong tetrahedral cation site preference of Ga^{3+} . From substitution of Mn^{3+} , Cr^{3+} and Ga^{3+} for Fe^{3+} , it could be seen that although the strain derivative was improved, the amplitude of magnetostriction was reduced in all cases. Although the magnetostriction amplitudes obtained are still sufficient for device applications, it would be desirable to simultaneously enhance magnetostriction amplitude and strain derivative. If it is impossible to enhance both, it would be at least desirable to maintain either of the properties and enhance the other.

The effect of cation distribution on the magnetic and magnetostrictive properties of CoFe_2O_4 has been studied [4-9]. The authors quenched samples from various temperatures to ambient temperature. The results were discussed as a comparison between quenching and slow cooling. Both magnetostriction and coercive field were lowered with increase in quenching temperature but the saturation magnetization increased. The authors attributed the decrease in coercive field and magnetostriction to the weakening of the magnetic anisotropy due to changes in site occupancy of Co^{2+} following quenching. The results would have been more convincing had the authors measured the variation of anisotropy with quenching heat treatment. Also, the authors presented only the values of the maximum magnetostriction which were very low even for the slowly cooled CoFe_2O_4 (100 ppm). The non availability of the λ -H curve and anisotropy data makes it difficult to estimate the influence of quenching on the strain derivative of CoFe_2O_4 . Considering equation (4-1), the amplitude of magnetostriction is proportional to the product of strain derivative and

magnetocrystalline anisotropy constant. Thus, the low magnetostriction reported in that study might have been due to low magnetocrystalline anisotropy, strain derivative or both. The authors explained their results using the one-ion crystalline-field model in which they described CoFe_2O_4 as a completely inverse spinel structured material. The one-ion crystalline-field model with respect to cobalt ferrite, has been previously studied and reported [4-10].

A previous Mossbauer study showed that CoFe_2O_4 is partially, rather than completely, inverse [4-11]. The study, which investigated the distribution of cations between the tetrahedral and octahedral sites, was made using quenched CoFe_2O_4 samples. The distributions of cations in quenched samples were compared with the distribution in furnace cooled samples and given as; $(\text{Co}_{0.07\pm 0.02}\text{Fe}_{0.93\pm 0.02}) [\text{Co}_{0.93\pm 0.02}\text{Fe}_{1.07\pm 0.02}]\text{O}_4$ for the slowly cooled sample and $(\text{Co}_{0.24\pm 0.02}\text{Fe}_{0.76\pm 0.02}) [\text{Co}_{0.76\pm 0.02}\text{Fe}_{1.24\pm 0.02}]\text{O}_4$ for the quenched sample. The circular bracket represents the tetrahedral site and the square bracket represents the octahedral site. The slowly cooled sample showed a partially inverse structure contrary to the view of Na et al [4-9], but more Co^{2+} migrated from the octahedral to the tetrahedral sites due to annealing at high temperature..

Vaingakar et al studied the cation distribution of CoFe_2O_4 using X-ray spectroscopy and concluded that CoFe_2O_4 is partially inverse structured [4-12]. Their conclusions were based on the comparison between the extended fine structures near the K-edge of Co^{2+} in metal and Co^{2+} in CoFe_2O_4 . Thus, in CoFe_2O_4 , although Co^{2+} prefers the B-sites, there are some Co^{2+} ions also on the A-sites, making CoFe_2O_4 a partially inverse spinel structure. A more recent study performed on nanocrystalline CoFe_2O_4 also agrees that CoFe_2O_4 is a partially inverse crystal structure [4-13].

Magnetic and magnetostrictive properties of CoFe_2O_4 have been shown to depend on sintering parameters [4-14]. The authors prepared CoFe_2O_4 by the conventional ceramic method by sintering the samples at 1100, 1200, 1300 and 1400 °C with dwell times of 4, 8,

16 and 24 hrs. Below 1400 °C, the density of the samples increased with sintering temperature but decreased at 1400 °C. The authors attributed the unexpected decrease in density of the sample sintered at 1400 °C to the effect of increased porosity at 1400 °C. It is not clear whether the authors meant increase in the pore sizes or increase in pore density. If increase in pore sizes was meant, it is understandable how that could decrease the density. If the authors meant increase in pore density, it is not clear why high sintering temperature would increase pore density, it should rather decrease it. The authors also reported changes in saturation magnetization with sintering temperature which they associated with the changes in density. It is also not clear why the saturation magnetization would vary with sintering temperature and holding time because it is known to be both microstructure and processing insensitive. In fact the authors stated that saturation magnetization depends on density (which is a microstructural feature).

The variation of coercive field with processing parameters observed in the study agrees well with the variation in density due to the contribution of grain growth to decreasing the coercive field with increasing sintering temperature and holding time. The result of the study also showed that magnetostriction is more dependent on sintering temperature than holding time. The results presented by the authors on strain derivative seem to be incorrect. The maximum strain derivative obtained by the authors was 102 ppm/Oe (equivalent to 1.28×10^{-6} m/A (1 ppm/Oe = 1.25×10^{-8} m/A)) for the CoFe_2O_4 sample sintered at 1100 °C for 24 hrs. The λ -H curve presented by the authors does not correspond to such a high strain derivative. Strain derivative for CoFe_2O_4 reported in previous studies were in the range of 1.3×10^{-9} to 1.5×10^{-9} A/m [4-1, 4-4].

Fig. 4.1 shows the λ -H plots obtained from the study for samples sintered at 1100 °C. Additional lines have been drawn to help determine the values of the strain derivative by taking slopes of the right angled triangles which are formed. The triangles were obtained around the regions containing data points for the sample sintered at 1100 °C for 24 hrs, which gave the maximum strain derivative. Smaller triangles DEC, GFC and DIG are labelled

within ABC extracted from the figure to help determine the maximum value of the strain derivative.

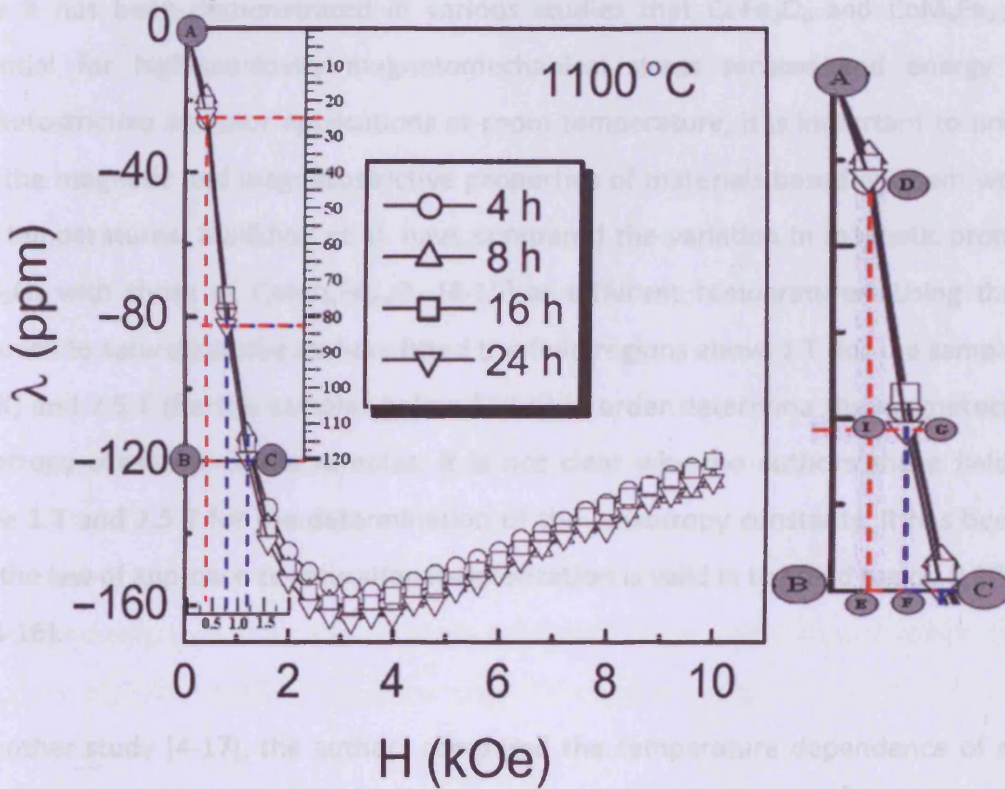


Fig. 4.1: λ - H plots obtained from Fig. 5 of the study by Bhamre et al. [4-14], for samples sintered at 1100 °C. Additional features were drawn to help determine the strain derivative.

The slope obtained from the triangles are as follows; ABC = 0.1 ppm/Oe (1.25×10^{-9} m/A); DEC = 0.12 ppm/Oe (1.5×10^{-9} m/A); GFC = 0.09 ppm/Oe (1.17×10^{-9} m/A) and DIG = 0.14 ppm/Oe (1.75×10^{-9} m/A). The average strain derivative for the sample sintered at 1100 °C for 24 hrs should be about 0.113 ppm/Oe (1.4×10^{-9} m/A). Since DIG is the steepest part of the curve, it is expected that the maximum strain derivative would be between 1.4×10^{-9} m/A and 1.75×10^{-9} m/A. The maximum strain derivative in the study is therefore within the range of or slightly above those of previous literature reports for un-substituted CoFe_2O_4 and less than the values obtained by non-magnetic cation substitution for Fe^{3+} in CoFe_2O_4 .

The authors observed that the strain derivative decreased with increasing sintering temperature.

Since it has been demonstrated in various studies that CoFe_2O_4 and $\text{CoM}_x\text{Fe}_{2-x}\text{O}_4$ have potential for high-sensitivity magnetomechanical stress sensors and energy efficient magnetostrictive actuator applications at room temperature, it is important to understand how the magnetic and magnetostrictive properties of materials based on them would vary with temperatures. Melikhov et al. have compared the variation in magnetic properties of CoFe_2O_4 with those of $\text{CoMn}_x\text{Fe}_{2-x}\text{O}_4$ [4-15] at different temperatures. Using the law of approach to saturation, the authors fitted the field regions above 1 T (for the samples above 150 K) and 2.5 T (for the samples below 150 K) in order to determine the magnetocrystalline anisotropy constants of the samples. It is not clear why the authors chose field regions above 1 T and 2.5 T for the determination of the anisotropy constants. It has been stated that the law of approach to saturation magnetization is valid in the field region $0.97M_s < M < M_s$ [4-16].

In another study [4-17], the authors compared the temperature dependence of magnetic properties of $\text{CoMn}_x\text{Fe}_{2-x}\text{O}_4$ with $\text{CoCr}_x\text{Fe}_{2-x}\text{O}_4$. It was observed that Cr^{3+} -substitution had a greater effect in lowering the magnetocrystalline anisotropy than Mn^{3+} -substitution. Also, Cr^{3+} -substitution resulted in a faster decrease of maximum magnetization than Mn^{3+} -substitution. Similar to the Mn^{3+} -substitution, coercive field varied considerably with temperature. Variation of coercive field with Cr content was more significant than with Mn content. The similarities in trend between Mn^{3+} and Cr^{3+} substitutions for Fe^{3+} is likely due to the fact that both cations have octahedral site preferences. The authors explained that the influence of Cr^{3+} substitution is higher than that of Mn^{3+} because Cr has the stronger octahedral site preference. Both studies were limited to the dependence of magnetic properties on temperature. The authors did not consider the dependence of magnetostrictive properties on temperature variation. Since both Cr^{3+} and Mn^{3+} have

octahedral site preferences, it would be interesting to understand how magnetic properties of cations with tetrahedral site preference vary with temperature.

A study of the temperature dependence of magnetic properties of $\text{CoGa}_x\text{Fe}_{2-x}\text{O}_4$ has been reported [4-18]. Like the case of $\text{CoMn}_x\text{Fe}_{2-x}\text{O}_4$ and $\text{CoCr}_x\text{Fe}_{2-x}\text{O}_4$, the magnetocrystalline anisotropy decreased with increase in temperature for all values of x . Also, it was found to decrease with increasing x at any given temperature. A similar trend was observed for variation in coercive field of $\text{CoMn}_x\text{Fe}_{2-x}\text{O}_4$, $\text{CoCr}_x\text{Fe}_{2-x}\text{O}_4$ and $\text{CoGa}_x\text{Fe}_{2-x}\text{O}_4$ except that at any given temperature, Ga^{3+} had a stronger influence on the coercive field than both Mn^{3+} and Cr^{3+} . The authors also did not report on how magnetostrictive properties of $\text{CoGa}_x\text{Fe}_{2-x}\text{O}_4$ varied with temperature. From the foregoing, it is obvious that magnetic properties of $\text{CoM}_x\text{Fe}_{2-x}\text{O}_4$ (for $0 \leq x \leq 0.8$) are not only composition dependent but also temperature dependent.

Having considered various previous studies related to the magnetic and magnetostrictive properties of $\text{CoM}_x\text{Fe}_{2-x}\text{O}_4$, it could be seen that $\text{CoM}_x\text{Fe}_{2-x}\text{O}_4$ has attracted considerable research interest.

This present study is aimed at investigating the influences of various sample treatments with the purpose of optimizing the properties of $\text{CoM}_x\text{Fe}_{2-x}\text{O}_4$ beyond those obtained from previous studies. This was done focussing on the crystal structure, microstructure, magnetic and magnetostrictive properties of $\text{CoM}_x\text{Fe}_{2-x}\text{O}_4$ subjected to different treatments. The experimental methodology and tools are explained in [chapter 5](#). The results are presented and discussed in subsequent chapters. [Chapter 6](#) includes results of a study of the effect of vacuum sintering, with different sintering temperatures and times, on the microstructure, magnetic and magnetostrictive properties of bulk samples of CoFe_2O_4 . The effect of annealing and quenching heat treatment on the magnetic and magnetostrictive properties of CoFe_2O_4 is presented in [chapter 7](#). The results include the influence of quenching heat

treatment on magnetocrystalline anisotropy and strain derivative which were not reported in a previous study by Na et al [4-9].

The effect of processing parameters including sintering temperatures, holding time at sintering temperatures and powder compaction pressure on crystal structure, microstructure, composition, magnetic and magnetostrictive properties of CoFe_2O_4 is presented and discussed in chapter 8. Bhome and Joy [4-14] investigated the effect of sintering temperature and holding time on structure, magnetic and magnetostrictive properties of CoFe_2O_4 but did not consider the effect of compaction pressure which was studied in this investigation together with the variation of saturation magnetization of CoFe_2O_4 with processing parameters which Bhome and Joy reported. Most studies of the magnetostrictive properties of CoFe_2O_4 have been carried out on samples prepared at a particular temperature in air. It has been said that the oxygen parameter and degree of inversion in CoFe_2O_4 may change depending on temperature and oxygen partial pressure [4-19]. These changes will definitely affect the magnetic and magnetostrictive properties of CoFe_2O_4 but it has not been reported how and to what extent.

It has been shown from various studies that the magnetic and magnetostrictive properties of CoFe_2O_4 can be altered by cation substitution. Mn^{3+} , Cr^{3+} and Ga^{3+} have all been substituted for Fe^{3+} in CoFe_2O_4 in previous studies. In all those studies, cation substitution resulted in an improvement of strain derivative but resulted in lowering of the amplitude of magnetostriction. Chapter 9 includes the results of studies on the dependence of the crystal structure, microstructure, magnetic and magnetostrictive properties of CoFe_2O_4 on cation variation. The results of variation of Al^{3+} substituted for Fe^{3+} and Ga^{3+} substituted for Fe^{3+} at room temperatures are discussed. Also discussed are the temperature dependence of the magnetic and magnetostrictive properties of Al^{3+} and Ga^{3+} substituted cobalt ferrite samples. In addition, the results of room temperature magnetostriction studies on Al^{3+} and Ga^{3+} substituted cobalt ferrite and $\text{Ge}^{4+}/\text{Co}^{2+}$ co-substitution for 2Fe^{3+} in CoFe_2O_4 are compared. The reason for the co-substituting Ge^{4+} and Co^{2+} is that Ge^{4+} is tetravalent and

cannot substitute for trivalent Fe^{3+} . In order to balance the ionic charges, tetravalent Ge^{4+} was co-substituted with a divalent Co^{2+} ion for 2Fe^{3+} .

Due its high coercive field and high anisotropy, thin films of CoFe_2O_4 can be useful for magneto-optical devices and high density magnetic recording media. Also because it has high magnetostriction, tuneable strain derivative, good chemical stability and mechanical properties, thin films of CoFe_2O_4 can be used with piezoelectric materials for magneto-electric applications. Structural and magnetic properties of thin film CoFe_2O_4 made via pulsed laser deposition are presented in chapter 10.

References to Chapter 4:

- [4-1]. R. W. McCallum, K.W. Dennis, D. C. Jiles, J.E Snyder and Y. H. Chen, "Composite magnetostrictive materials for advanced automotive magnetomechanical sensor" *Low Temp.Phys.*, **27** (2001) 266
- [4-2]. N. Galloway, R. D. Greenough, M. P. Schulze and A. G. I. Jenner "The effects of magnetic annealing and compressive stress on the magnetic properties of the rare-earth iron compound Terfenol-D" *J. Magn. Magn, Mater.* **119** (1993) 107
- [4-3]. Cristina Rodríguez, Ainara Barrio, Iñaki Orue, J.L. Vilas, L.M. León, Jose Manuel Barandiarán and M.L. Fdez-Gubieda Ruiz "High magnetostriction polymer-bonded Terfenol-D composites" *Sensors and Actuators A* **142** (2008) 538
- [4-4]. C. C. H. Lo "Compositional Dependence of the Magnetomechanical Effect in Substituted Cobalt Ferrite for Magnetoelastic Stress Sensors" *IEEE Trans. Magn.* **43** (2007) 2367
- [4-5]. S. J. Lee, C. C. H. Lo, P. N. Matlage, S. H. Song, Y. Melikhov, J. E. Snyder, and D. C. Jiles "Magnetic and magnetoelastic properties of Cr-substituted cobalt ferrite" *J. Appl. Phys.* **102** (2007) 073910
- [4-6]. J. A. Paulsen, A. P. Ring, and C. C. H. Lo, J. E. Snyder and D. C. Jiles "Manganese-substituted cobalt ferrite magnetostrictive materials for magnetic stress sensor applications" *J. Appl. Phys.* **97** (2005) 044502
- [4-7]. S. H. Song, C. C. H. Lo and S. J. Lee, S. T. Aldini, J. E. Snyder and D. C. Jiles "Magnetic and magnetoelastic properties of Ga-substituted cobalt ferrite" *J. Appl. Phys.* **101** (2007) 09C517
- [4-8]. A. Affanni, A. Guerra, L. Dallagiovanna and G. Chiorboli, "Design and characterization of magnetostrictive linear displacement sensors" *Proceedings of the 21st IEEE Instrumentation and Measurement Technology Conference, 2004. IMTC 04*, **1** (2004) 206
- [4-9]. J. G. Na, T. D. Lee and S. J. Park "Effects of cation distribution on magnetic properties in cobalt ferrite" *J. Mat. Sci.* **27** (1993) 961
- [4-10]. J. C. Slonczewski "Origin of magnetic anisotropy in cobalt substituted magnetite" *Phys. Rev.* **10** (1958) 1341

- [4-11]. G.A. Sawatzky, F. Van der Woude, A.H. Morrish, "Mossbauer study of several ferrimagnetic spinels" *Phys. Rev.* **187** (1969) 747
- [4-12]. A. S. Vaingankar, B. V. Khasbardar and R. N. Patil "X-ray spectroscopic study of cobalt ferrite" *J. Phys. F: Metal Phys.*, **10** (1980) 1615
- [4-13]. G. Concas, G. Spano, C. Cannas, A. Musinu, D. Peddis and G. Piccaluga "Inversion degree and saturation magnetization of different nanocrystalline cobalt ferrites" *J Magn Mag Mater* **321** (2009) 1893
- [4-14]. S.D Bham and P. A. Joy "Effects of sintering conditions and microstructure on the magnetostrictive properties of cobalt ferrite" *J. Am. Ceram. Soc.* **91** (2008) 1976
- [4-15]. Y. Melikhov, J. E. Snyder, D. C. Jiles A. P. Ring, J. A. Paulsen, C. C. H. Lo and K. W. Dennis "Temperature dependence of magnetic anisotropy in Mn-substituted cobalt ferrite" *J. Appl. Phys.* **99** (2006) 08R102
- [4-16]. E.W. Lee "Magnetostriction and magnetomechanical effects" *Rep. Prog. Phys.* **18** (1955) 184
- [4-17]. Y. Melikhov, J. E. Snyder, C. C. H. Lo, P. N. Matlage, S. H. Song, K. W. Dennis, and D. C. Jiles "The Effect of Cr-Substitution on the Magnetic Anisotropy and Its Temperature Dependence in Cr- Substituted Cobalt Ferrite" *IEEE Trans. Magn.* **42** (2006)2861
- [4-18]. N. Ranvah, Y. Melikhov, D. C. Jiles, J. E. Snyder, A. J. Moses, P. I. Williams, and S. H. Song "Temperature dependence of magnetic anisotropy of Ga-substituted cobalt ferrite" *J. Appl. Physc*, **103** (2008) 07E506
- [4-19]. G. D. Rieck, J. J. M. Thijssen, "The cation distribution in CoFe_2O_4 ", *Acta Cryst. B* **24** (1968) 982

Chapter 5. Experimental Procedure and Measurement Systems

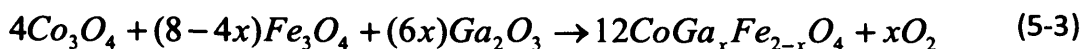
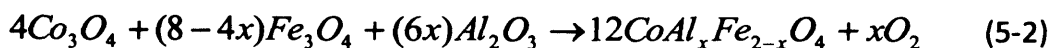
5.1 Introduction

The experimental procedures used in the fabrication and characterization of the bulk and thin film cobalt ferrites are described in this chapter. Also, the measurements systems used for the characterization are described. Bulk cobalt ferrite samples used for this study were fabricated by the traditional ceramic method while the thin film samples were prepared by pulsed laser deposition. Since both methods are discussed in sections 3.6.1 and 3.7.1 respectively, the discussions on preparation of cobalt ferrite in this chapter is restricted to describing the steps taken in sample preparation.

Two types of bulk cobalt ferrite were prepared; un-substituted and substituted cobalt ferrite. While un-substituted cobalt ferrite refers to samples with only Co^{2+} and Fe^{3+} as the cations, substituted cobalt ferrite refers to samples with additional cations such as Al^{3+} , Ga^{3+} and Ge^{4+} . Un-substituted cobalt ferrite is NOT referred to as *pure* cobalt ferrite (as it is sometimes called) because the term pure cobalt ferrite will be used in this thesis to refer to the purity grade of the cobalt ferrite powder used in preparing the samples. Also, the term cobalt ferrite will NOT refer to CoFe_2O_4 in this chapter because actual compositions will be written in the form $\text{Co}_{1+x}\text{Fe}_{2-x}\text{O}_4$ or $\text{Co}_{1-x}\text{Fe}_{2+x}\text{O}_4$.

5.2 Preparation of Bulk Cobalt Ferrite Samples

Un-substituted cobalt ferrite samples were prepared according to equation 5-1 while Al- and Ga-substituted cobalt ferrites were prepared according to equations 5-2 and 5-3.



Ge/Co co-substituted cobalt ferrite samples used in this research were prepared in a previous study [5-1]. In each sample preparation process, care was taken to ensure samples were dense, as defect-free as possible and uniform in composition to avoid degradation of magnetostrictive properties of the samples.

5.2.1 Powder preparation for un-substituted cobalt ferrite

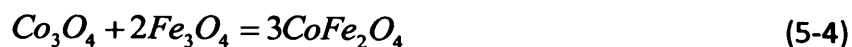
The oxide powders used for sample preparation, their Chemical Abstract Service (CAS) numbers, purity grades and particle sizes are as follows:

Black iron oxide (Fe₃O₄)- CAS #: 1317-61-9; Purity: 99.9%; Particle size: -5μm

Cobalt oxide (Co₃O₄)- CAS #: 1308-06-1; Purity: 99.9%; Particle size: -37 μm

The initial step involves determining the amount of these constituent oxides powders required. This requires deciding the amount of cobalt ferrite powder intended to be produced. During this project, to enable easy handling of powder and ensure uniformity in composition, the maximum amount of powder prepared in a batch was 50 g. The procedure for determining the amount of oxide powders required to produce stoichiometric un-substituted cobalt ferrite (CoFe₂O₄) is as follows:

Chemical Equation for Reaction: Setting $x = 1$ in equation 36;



From equation (5-4), 1 mole of Co₃O₄ and 2 moles of Fe₃O₄ are required to produce 3 moles of CoFe₂O₄.

Amount in grams in y moles = number of moles * formula mass (F.M)

For 1 mole Co₃O₄ (F.M = 240.80 g/mol) = 240.80 g

For 2 moles of Fe_3O_4 (F.M = 231.53 g/mol) = 463.06 g

For 3 moles of CoFe_2O_4 (F.M = 234.62 g/mol) = 703.86g

703.86 g of CoFe_2O_4 requires 240.80 g of Co_3O_4 and 463.06 g of Fe_3O_4

50 g of CoFe_2O_4 requires = $\frac{50 * 240.8}{703.86} = 17.11$ g of Co_3O_4 . Similarly,

50 g of CoFe_2O_4 requires = $\frac{50 * 463.06}{703.86} = 32.89$ g of Fe_3O_4 .

A useful check is to ensure that the sum of the mass of Co_3O_4 and Fe_3O_4 equals the mass of CoFe_2O_4 (law of conservation of mass); $17.11 \text{ g} + 32.89 \text{ g} = 50 \text{ g}$. These masses of Co_3O_4 and Fe_3O_4 were manually mixed by shaking a containing vessel rigorously for 10 to 15 minutes, with intermittent stirring with the tail end of a small plastic scoop.

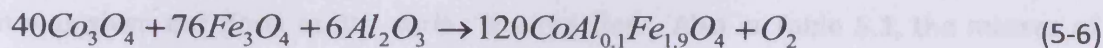
5.2.2 Preparation of substituted cobalt ferrite

The same method was used in preparing Al- and Ga-substituted cobalt ferrite samples. As a result, only Al-substituted cobalt ferrite will be discussed.

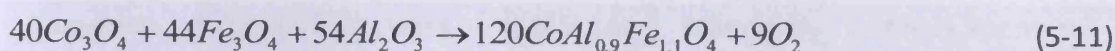
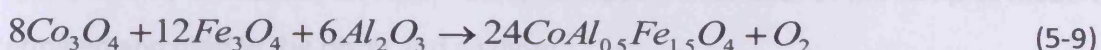
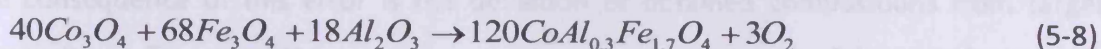
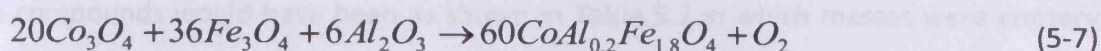
Chemical Equation for Reaction: 15 g of $\text{CoAl}_x\text{Fe}_{2-x}\text{O}_4$ for each of the compositions with $x = 0.0, 0.1, 0.2, 0.3, 0.5, 0.7$ and 0.9 were prepared according to equation (5-2). For $x = 0.0$, the chemical equation for reaction is the same as that of CoFe_2O_4 (equation 5.4). For $x = 0.1$, the chemical reaction equation is



The decimals before some of the chemical compounds are a result of non-stoichiometric nature of the final compound. Because it is conventional to have integers before chemical compounds, equation (5-5) is multiplied by 10 to obtain equation (5-6).



In a similar way, equations (5-6) to (5-10) were used to obtain samples with $x = 0.2, 0.3, 0.5, 0.7$ and 0.9 .



The same oxide powders used in making CoFe_2O_4 were used in addition to following the same procedure as for CoFe_2O_4 . The masses required to make 15 g of the targeted compositions of Al-substituted cobalt ferrite were determined and recorded in Table 4.1.

Targeted Sample Composition	Mass of Co_3O_4 (g)	Mass of Fe_3O_4 (g)	Mass of Al_2O_3 (g)	Mass of O_2 given out (g)	Check for mass conservation (Total) (g)
$\text{CoAl}_{0.1}\text{Fe}_{1.9}\text{O}_4$	5.197	9.496	0.330	-0.017	15.006
$\text{CoAl}_{0.2}\text{Fe}_{1.8}\text{O}_4$	5.265	9.113	0.668	-0.035	15.011
$\text{CoAl}_{0.3}\text{Fe}_{1.7}\text{O}_4$	5.334	8.720	1.016	-0.053	15.017
$\text{CoAl}_{0.5}\text{Fe}_{1.5}\text{O}_4$	5.478	7.901	1.738	-0.091	15.026
$\text{CoAl}_{0.7}\text{Fe}_{1.4}\text{O}_4$	5.630	7.038	2.503	-0.131	15.040
$\text{CoAl}_{0.9}\text{Fe}_{1.1}\text{O}_4$	5.791	6.125	3.310	-0.173	15.053

Table 5.1: Masses of compounds required for producing 15 g of $\text{CoAl}_x\text{Fe}_{2-x}\text{O}_4$. Mass was not conserved due to error in determining the masses of $\text{CoAl}_x\text{Fe}_{2-x}\text{O}_4$.

The masses of oxygen were subtracted from the masses of the other compounds because oxygen was given out (lost) as gas during the reactions. Also in Table 5.1, the masses of $\text{CoAl}_x\text{Fe}_{2-x}\text{O}_4$ produced were not conserved but increased by ~ 0.006 g as x increased. This was a consequence of an error introduced while calculating the formula masses of $\text{CoAl}_x\text{Fe}_{2-x}\text{O}_4$. The mass of aluminium used for calculating the masses of $\text{CoAl}_x\text{Fe}_{2-x}\text{O}_4$ was 26.1895 g instead of 26.9815 g. If the correct formula masses of $\text{CoAl}_x\text{Fe}_{2-x}\text{O}_4$ were used, the masses of the compounds would have been as shown in Table 5.2 in which masses were conserved. The consequence of this error is the deviation of obtained compositions from targeted compositions. To correct the error, the actual composition of each of the samples made was determined and used in the result and analyses.

Targeted Sample Composition	Mass of Co_3O_4 (g)	Mass of Fe_3O_4 (g)	Mass of Al_2O_3 (g)	Mass of O_2 given out (g)	Check for mass conservation (Total) (g)
$\text{CoAl}_{0.1}\text{Fe}_{1.9}\text{O}_4$	5.196	9.492	0.330	-0.017	15.001
$\text{CoAl}_{0.2}\text{Fe}_{1.8}\text{O}_4$	5.262	9.106	0.668	-0.035	15.001
$\text{CoAl}_{0.3}\text{Fe}_{1.7}\text{O}_4$	5.329	8.710	1.015	-0.053	15.001
$\text{CoAl}_{0.5}\text{Fe}_{1.5}\text{O}_4$	5.468	7.887	1.737	-0.091	15.001
$\text{CoAl}_{0.7}\text{Fe}_{1.4}\text{O}_4$	5.615	7.020	2.495	-0.130	15.000
$\text{CoAl}_{0.9}\text{Fe}_{1.1}\text{O}_4$	5.771	6.104	3.299	-0.174	15.000

Table 5.2: Masses of compounds required for producing 15 g of $\text{CoAl}_x\text{Fe}_{2-x}\text{O}_4$ with correction made for mass conservation.

Based on the masses determined, Co_3O_4 , Fe_3O_4 , Al_2O_3 and Ga_2O_3 were weighed using an Ohaus precision balance shown in Fig. 5.1 and mixed as in the case of un-substituted samples. The balance has a maximum capacity of 62 g and accuracy of 0.0001 g. Because the last digit is usually unsettled, masses are reported to the third decimal place. Same balance was used for measuring the masses of powders used in making both substituted and un-substituted samples.



Fig. 5.1: Ohaus precision balance used for measuring masses of the oxide powders

5.2.3 Powder Compaction

After the mixing stage for any sample preparation procedure, the powder was compacted at a pressure of 127 MPa using the Specac hydraulic press shown in Fig. 5.2.

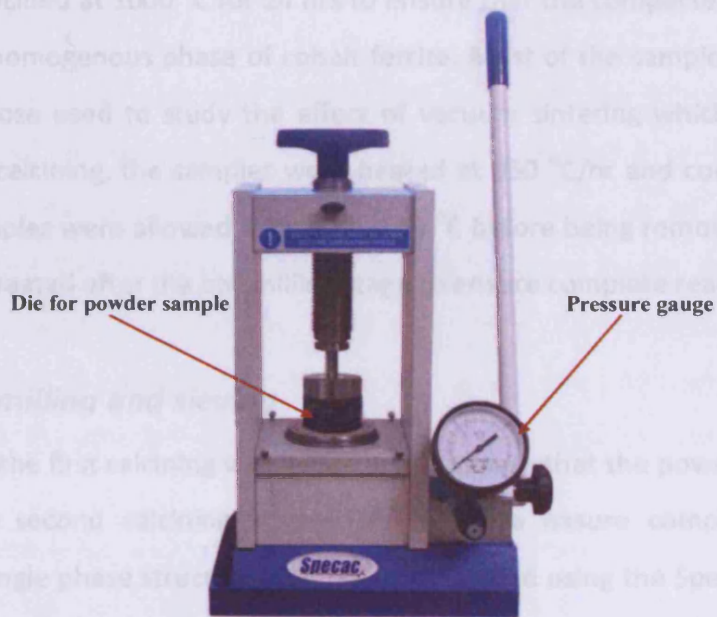


Fig. 5.2: Specac manual hydraulic press used for powder compaction

Samples used for the study of effect of processing parameters on magnetic and magnetostrictive properties of cobalt ferrite were compacted at pressures of 87 and 127 MPa to study the effect of compaction pressure. Because the composition of the samples prepared for aluminium and gallium substituted cobalt ferrite samples were different, the die was cleaned after each compaction to avoid cross contamination of one composition with another. Water was used as a binder to avoid compacted powders disintegrating when being ejected from the die. Organic binder was not used to avoid retaining any residue as impurities in the sample.

The diameter of the samples after compaction was 10 mm (corresponding to the diameter of the die). The height varies depending on the volume of the powder in the die and was usually 10-15 mm. Compacted samples were left in the die for about 15-20 sec before being removed and moved to the furnace for the first calcining step.

5.2.4 Calcining

Samples were calcined at 1000 °C for 24 hrs to ensure that the compacted powder particles react to form a homogenous phase of cobalt ferrite. Most of the samples were calcined in air except for those used to study the effect of vacuum sintering which were sintered in vacuum. During calcining, the samples were heated at 850 °C/hr and cooled by turning off the furnace. Samples were allowed to cool to ≤ 30 °C before being removed for ball milling. Calcining was repeated after the ball milling stage to ensure complete reaction.

5.2.5 Sample milling and sieving

Ball milling after the first calcining was necessary to ensure that the powder particles mixed well before the second calcining stage. This helps to ensure complete reaction and formation of a single phase structure. Samples were milled using the Spectramill ball pestle impact grinder shown in Fig. 5.3. The impact grinder uses five 11 mm stainless steel ball pestles propelled in a figure-8 rotation pattern together with the samples inside a stainless steel vial. About 15 g of material were milled for a minimum of 20 minutes to ensure

samples were well ground and mixed. The balls pestles were cleaned with steel wool before being cleaned with the impact grinder using ethanol in between compositions and at the end of the milling operation.

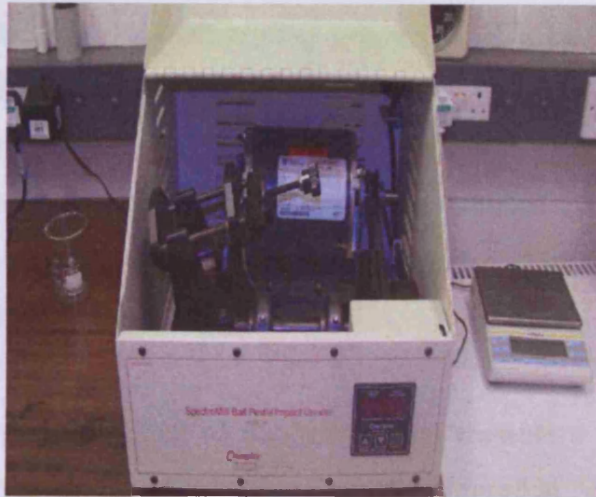


Fig. 5.3: Spetramill ball pestle impact grinder used for sample milling

After grinding, samples were sieved through a 400 mesh size sieve to a particle size of $\leq 37 \mu\text{m}$. This is the first sieving operation which was usually omitted to save time. The second sieving operation was done after the samples have been re-calcined and re-milled. This second sieving operation is more important because it follows the last compaction prior to sintering. Because some of the particles were larger than $37 \mu\text{m}$, ball milling was followed with hand grinding of the powder samples followed by screening through the 400 mesh size sieve. About 8 g of the samples were ground at a time using a mortar and pestle.

Personal protective wear was used while handling fine powder of the samples because cobalt ferrite is potentially carcinogenic. Lab coat, gloves, safety glasses and dust masks were used. Hands were first wiped with napkins dampened with ethanol before washing

with soapy water. Wastes produced during the sample preparation were disposed as hazardous waste according to the University requirement.

5.2.6 Sample sintering

Sample sintering is a very important stage as it determines the final microstructure of the samples which in turn affects other properties. To study the effect of vacuum sintering on microstructure, magnetic and magnetostrictive properties of cobalt ferrite, nine samples were studied, comprising three samples sintered at each of three temperatures, 800°C, 1000°C and 1200°C, and for times of 6, 12 and 24 hrs. All the samples for the vacuum sintering study were heated and cooled at 250°C/hr. The samples used for the study of the effect of processing parameters were sintered in air at 1250, 1350 or 1450 °C and held at temperature for 24 or 36 hrs.

Samples used for studying the effect of quenching heat treatment on the magnetic and magnetoelastic properties of cobalt ferrite were initially sintered at 1350 °C for 24 hrs in air and cooled by turning off the furnace. The air furnace does not have the capability of controlled cooling. Samples heated to 1350 °C and held for 24 hrs typically took about 12 hours to cool to 27 °C. Some samples were reheated (i.e annealed) to 600, 800, 1000, 1200 and 1400 °C in air, held at those temperatures for 24 hours followed by quenching in water to room temperature. To ensure comparative quenching rates samples with similar dimensions were selected, that is, cylindrical samples with a nominal diameter of 9.05 ± 0.02 mm and a height of 10.20 ± 0.02 mm. The rest of the samples were sintered in air at 1350 °C for 24 hrs before furnace cooling to room temperature. They were heated at 250 °C/hr and cooled by turning the furnace off.

The air sintering furnace used was a Carbolite laboratory high temperature chamber furnace with a maximum operating temperature of 1700 °C. The heating elements are made from MoSi₂ which provides efficient high power density at elevated temperatures (20 W/cm² at 1700 °C). These are located on both sides of the furnace chamber thus providing ± 4 °C temperature uniformity over 113 mm of the chamber. The thermocouples are located on

the roof of the chamber for temperature monitoring while using the furnace. For smaller samples such as those used in this research, the thermocouples are too far from the samples and so cannot give the accurate temperature of the sample during sintering. This was taken care of by providing a load monitoring thermocouple located closer to the sample. An 8 segment programmable Eurotherm 2132 controller enabled the heating and cooling process to be set with minimal monitoring. After cooling, samples were cut with a diamond saw for characterization.

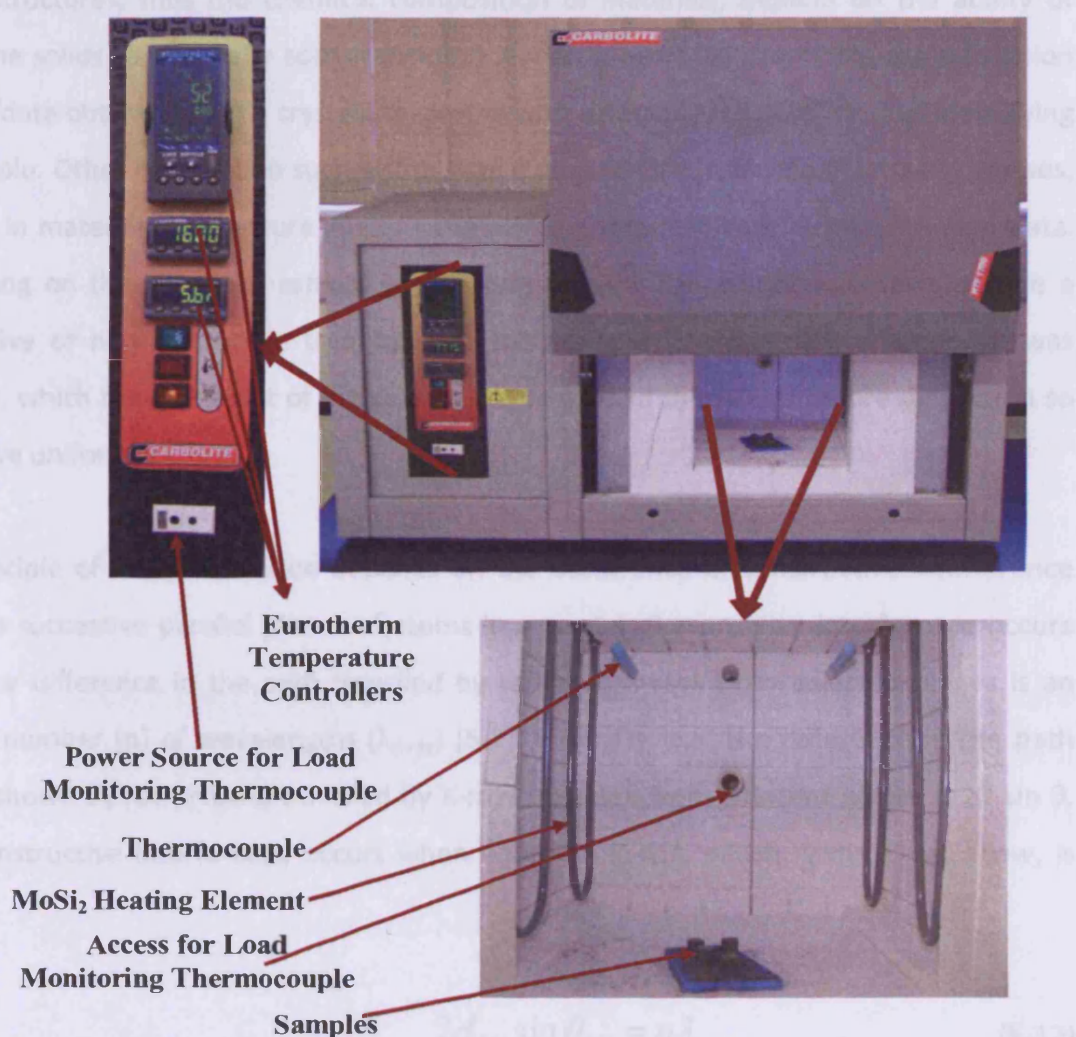


Fig. 5.4: Air furnace used for calcining and sintering of the samples

5.3 Characterization of Bulk Cobalt Ferrite

5.3.1 Crystal structure determination

X-ray powder diffractometry was used to determine the crystal structure of the un-substituted and substituted cobalt ferrite samples produced during this research. After making the samples, it was important to determine their crystal structure because this will both help to understand and analyse the results from subsequent measurements and to save time if the samples were wrongly made. The use of X-ray diffraction in determining the crystal structures, thus the chemical composition of materials, depend on the ability of crystalline solids to elastically scatter incident X-rays. It relies on comparing the diffraction pattern/data obtained from a crystalline sample with a database of patterns thus identifying the sample. Other information such as the lattice parameters, presence of impurity phases, stresses in materials and texture analysis can also be obtained from X-ray diffraction data. Depending on the nature of sample preparation required, X-ray diffractometry can be a destructive or non-destructive technique. In this research the destructive approach was adopted, which requires most of the samples to be ground to powder before diffraction so as to have uniform texture.

The principle of X-ray diffraction depends on the occurrence of constructive interference between successive parallel planes of atoms in a crystal. Constructive interference occurs when the difference in the path travelled by reflected X-rays from adjacent planes is an integral number (n) of wavelengths (λ_{x-ray}) [5-2]. From Fig. 5.5, the difference in the path length (shown by red arrows) travelled by X-rays reflected from adjacent planes is $2d \sin \theta$. Thus constructive interference occurs when equation (5-12), which is the Bragg's law, is fulfilled.

$$2d_{hkl} \sin \theta_{hkl} = n\lambda_{x-ray} \quad (5-12)$$

where θ is the angle between the incident and diffracted X-ray beams. d is inter-planar spacing given for cubic crystal by equation (5-12). a is the lattice parameter while h, k, l are Miller indices.

$$d_{hkl} = \frac{a}{\sqrt{h^2 + k^2 + l^2}} \quad (5-13)$$

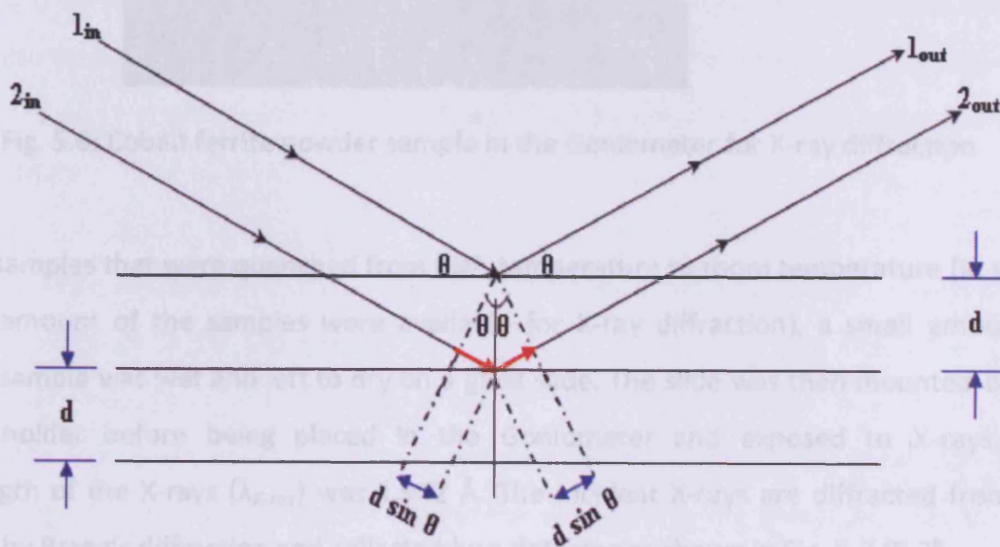


Fig. 5.5: Conditions necessary for Bragg's law for X-ray diffraction

The X-ray diffraction patterns for bulk cobalt ferrite samples used in this research were recorded at a step size of 0.02° on a Philips PW1710 automated powder diffractometer with copper ($\text{CuK}\alpha$) radiation at 35 kV and 40 mA. Cobalt ferrite samples were ground, mounted on an aluminium sample holder and placed in the Goniometer of the diffractometer (as shown in Fig. 5.6) before being exposed to beam of X-rays.



Fig. 5.6: Cobalt ferrite powder sample in the Goniometer for X-ray diffraction

For the samples that were quenched from high temperature to room temperature (in which a small amount of the samples were available for X-ray diffraction), a small amount of powder sample was wet and left to dry on a glass slide. The slide was then mounted on the sample holder before being placed in the Goniometer and exposed to X-rays. The wavelength of the X-rays ($\lambda_{X\text{-ray}}$) was 1.542 Å. The incident X-rays are diffracted from the samples by Bragg's diffraction and collected by a detector as shown in Fig. 5.7 [5-3].

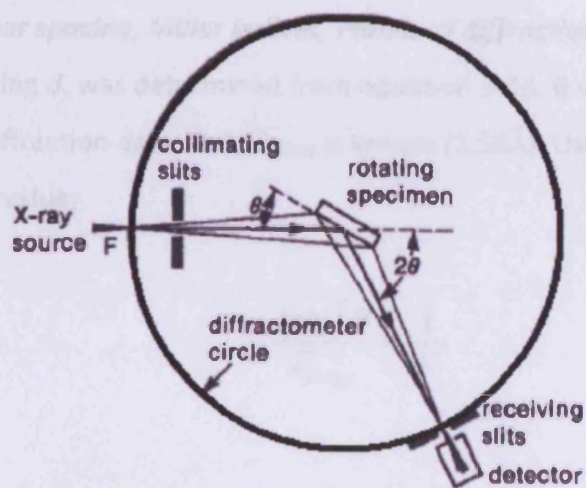


Fig. 5.7: Schematic diagram of an X-ray diffractometer

Extraction of parameters from X-ray diffraction data***i. 2 θ and Intensity Values***

X-ray diffraction results are usually presented as table of 2θ values with corresponding intensities from which lattice parameter of the material and the diffraction planes can be obtained. The data obtained from the Philips PW1710 automated powder diffractometer includes the anode type used, the X-ray wavelength, the Goniometer voltage, the tube current, the scan step size and the data angle range. The software was set to scan 0.16° for each intensity count at a step size of 0.02° to scans 8 times for each intensity count produced. Each scan produces a data point and the average of the 8 data points gives the intensity count.

For a data angle range of 5° to 80° , the first 2θ value recorded was 5° and the subsequent 2θ values were given by the number of scans per count (0.16) plus the value of the preceding 2θ value. Thus for a data angle range of 5° to 80° , the 2θ values is 5° ; 5.16° ; 5.32° ; 5.48° . A plot of intensity counts and the 2θ values gives the diffractogram (X-ray diffraction pattern) which can be compared with the database to identify the peaks and the sample. An example of a diffractogram obtained from a cobalt ferrite sample is shown in Fig. 3.4.

ii. Inter-planar spacing, Miller indices, Planes of diffraction and Lattice parameter

The inter-planar spacing d , was determined from equation 5-13. θ was obtained from the 2θ values of the X-ray diffraction data while $\lambda_{X\text{-ray}}$ is known (1.53\AA). Using the relation, d can be obtained for each 2θ value;

$$\frac{4\sin^2 \theta}{\lambda_{x\text{-ray}}^2} = \frac{1}{d^2} \quad (5-14)$$

The sum of the squares of the miller indices $h^2 + k^2 + l^2$ was determined for each 2θ value by equation 5-15 and rounded off to the nearest integer value. d_1 and d_i are the inter-planar spacing of the first and subsequent peaks respectively.

$$h^2 + k^2 + l^2 = 3 * \left[\frac{d_1^2}{d_i^2} \right] \quad (5-15)$$

Equation 5-14 is multiplied by a factor of three because the cations in the spinel structure of cobalt ferrite form a face centred cubic structure with the oxygen atoms. For face centred cubic structures, diffraction can only come from planes 3, 4, 8, 11, 12, 16, etc. For a body centred cubic structure material, equation 5-14 would have been multiplied by a factor of 2 because for body centred cubic materials, diffractions can only come from planes 2, 4, 6, 8, 10, 12, 14, 16, etc. The method for determining the $h^2+k^2+l^2$ is described in text [5-4]. The diffraction plane (hkl) is given by any three integers which when squared and summed corresponds to the value obtained for $h^2 + k^2 + l^2$. It is possible that two sets of hkl values correspond to the same $h^2 + k^2 + l^2$ value, in which case the diffraction came from two superimposed planes. As an example, $h^2 + k^2 + l^2 = 27$ corresponds to superimposed diffraction coming from planes (333) and (511). Having obtained the inter-planar spacing d from equation 5-14 and $h^2 + k^2 + l^2$ from equation 5-15, the lattice parameters of the samples were determined using equation 5-13.

5.3.2 Microstructure and composition determination

Scanning Electron Microscopy (SEM) and Energy Dispersive X-ray Spectroscopy (EDX) were respectively used to determine sample microstructure and composition. SEM is a powerful tool for subsurface microstructure imaging. Understanding the microstructure of the samples was essential for determining their uniformity if a sample was single or multi-phased. In a typical scanning electron microscope, a beam of electrons generated from an electron gun focused onto a sample generates several signals which are detected by attached detectors.

Fig. 5.8 [5-5] shows the interaction volume of the primary electron beam and the signals generated in the volume. Generated signals relevant to this study are;

- a. Secondary electrons which are generated by inelastic scattering resulting from the interaction between the incident and close-to-the-surface electrons. They are low energy electrons which provide a topographic image of the samples. Image contrasts can reveal phase variations.
- b. Backscattered electrons are high energy electrons generated by interaction of incident electrons with electrons located deeper into the sample. They are reflected from inside the sample and contain both topographic and compositional information about the sample.
- c. Characteristic X-rays are generated when inner shell electrons in the sample are ejected and replaced by outer shell electrons. Because the energy of an outer electron is higher than that of an inner electron, the excess energy is given out as X-rays. The X-rays emitted are characteristics of chemical elements and can be detected by an EDX detector and analysed to determine elemental compositions of the sample.

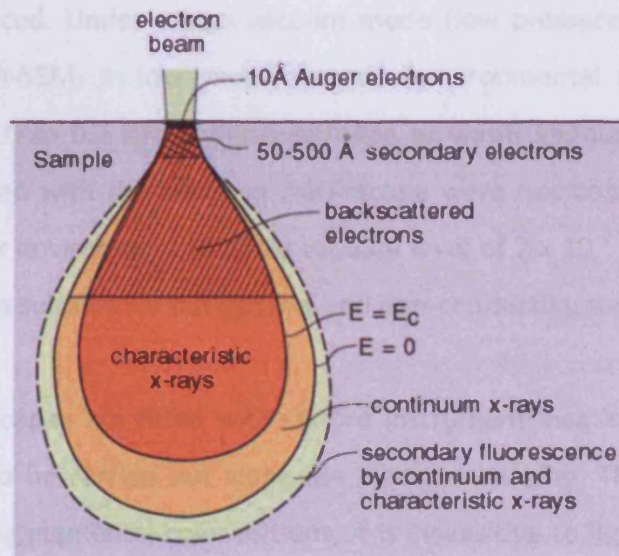


Fig. 5.8: Interaction volume of the primary electron beam in a sample during SEM [5-5]

Two types of scanning electron microscopes were used; the Analytical and Environmental scanning electron microscopes. The Analytical scanning electron microscope (A-SEM) is a Cambridge Instrument (LEO) S360 and can achieve a resolution of up to 5 nm and a magnification, as high as 100,000. The microscope is a traditional SEM which is best suited for conducting materials. Electrons will not be conducted away from the surfaces of non-conducting samples which would result in charge build-up on their surfaces. Charge build-up on sample surfaces results in distorted electron images. Non-conducting samples have to be coated with carbon or gold for imaging. Cobalt ferrite samples imaged with this microscope were coated with carbon to avoid charge build-up. The A-SEM requires a high vacuum of about 7×10^{-7} kPa to allow electrons travel without collision with gases. Backscattered electron images were mostly obtained using the A-SEM. This was to ensure that informative electron images were obtained from the non-conduction sample surfaces.

The Environmental scanning electron microscope (E-SEM) is a Veeco FEI (Philips) XL30 FEG microscope. It can resolve 2 nm details and has magnifications of up to 500,000. A broader range of samples can be imaged using the E-SEM because it can work under variable pressure modes. Depending on the pressure mode chosen, the sample preparation time can be considerably reduced. Under a high vacuum mode (low pressure mode), it works in a similar way to the A-SEM. In low vacuum mode (environmental mode), it works at a pressure range from 0 to 0.2 kPa under a nitrogen or water vapour environment. Cobalt ferrite samples imaged with this electron microscope were not coated and were imaged under a water vapour environment at a low vacuum level of 7×10^{-2} kPa. In this mode, the electron microscope is suitable for out-gassing and non-conducting samples.

Both electron microscopes are fitted with Oxford Instrument Inca X-ray analyzer for EDX, which enables EDX to be carried out alongside electron imaging. Though EDX is a useful technique for studying elemental compositions, it is insensitive to lighter elements such as oxygen. As a result, EDX analyses for cobalt ferrite samples were obtained only for the cations. EDX data were obtained from the atomic percent of the cations at different sites of

interest on a sample surface. If the composition is uniform, data obtained for the cations are averaged and normalized to a ratio of 3 (number of cations in a formula unit of cobalt ferrite) as shown in Table 5.3. If composition varies, data obtained from regions of similar composition for the cations are averaged and normalized to a ratio which depends on the number of cations in a formula unit of the composition.

Sites of Interest	Co = 0.2		Formula = $\text{Co}_{0.2}\text{Fe}_{2.8}\text{O}_4$		
	Fe (atomic %)	Co (atomic %)	Sum of Average		Ratio(Normalized to Fe + Co=3)
1	29.91	1.18	49.16285714	Fe	2.80307433
2	30.44	0.74		Co	0.19692567
3	51.53	9.07		Sum of ratio	3
4	31.83	2.73			
5	83.29	2.88			
6	75.39	4.22			
7	19.16	1.77			
Average	45.93571	3.22714			

Table 5.3: Method of determining cobalt ferrite sample composition using data from EDX result

5.3.3 Measurement of magnetic properties

Magnetic properties of the samples used in this research were measured using a Vibrating Sample Magnetometer (VSM) and a Superconducting Quantum Interference Device (SQUID magnetometer). The VSM is an instrument for measuring the magnetic properties of materials. It works on the basis that an electric voltage induced due to a change in magnetic

field (Faraday's law of induction) contains information about the changing magnetic field. Fig. 5.9 shows the model 7410 VSM used for the purpose of this research.

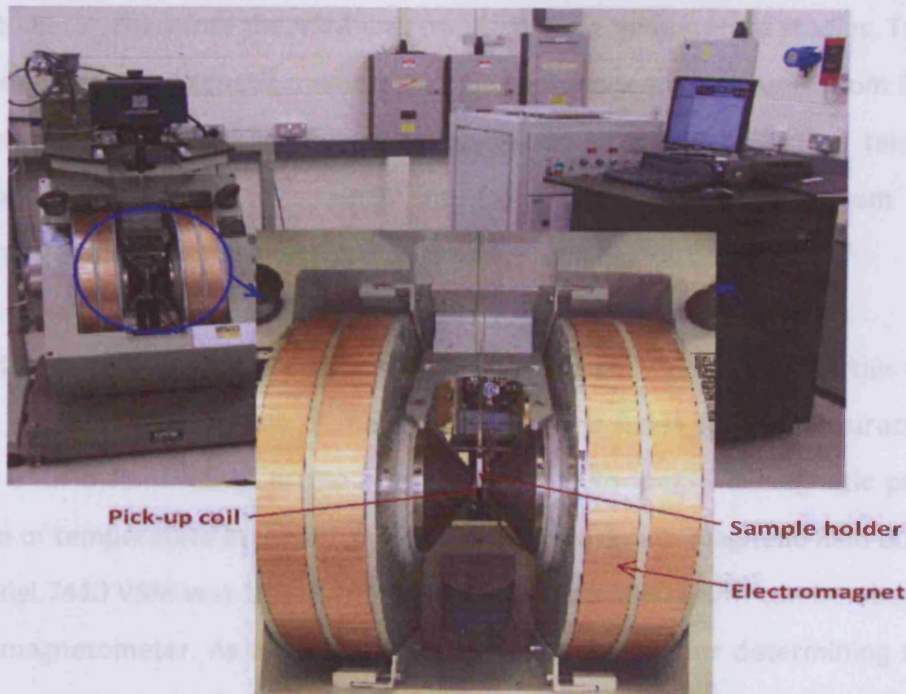


Fig. 5.9: Lakeshore model 7410 VSM with 740-H Head Drive

Cobalt ferrite samples were attached to the sample holder at the tail of a quartz glass rod which was attached to the head drive of the magnetometer. A magnetic field is applied and the VSM is then saddled with a nickel sample to ensure that the sample will be centred between the pole pieces of the electromagnet. The VSM can measure magnetic moment with an accuracy of 10^{-6} emu. When the head drive is turned on and it vibrates in a sinusoidal motion inside a uniform magnetic field, the change in magnetic field results in an electric voltage induced in the pick-up coils located near the sample. The induced electric field is proportional to the magnetic moment of the sample. Magnetization versus applied magnetic field (H) was measured at 300 K with up to a maximum applied field, 1.6 T.

An oven was fitted to the VSM to study the temperature dependence of magnetic properties such as hysteresis loops and the determination of the Curie temperature. The Curie temperature of cobalt ferrite is higher than the upper temperature limit of the SQUID magnetometer, therefore the VSM was used for Curie temperature studies. To measure the Curie temperature, magnetic moments of the samples were measured from 300 K to 873 K in a field of 7.95 kA/m. The plot of the magnetic moment against the temperature was extrapolated by drawing a straight line from the region of maximum slope to the temperature axis.

The SQUID magnetometer used was a Quantum Design Magnetic Properties Measurement System (MPMS). It is capable of measuring magnetic fields with an accuracy of 10^{-8} emu (higher than that of VSM). It also offers the ability to measure magnetic properties as a function of temperature in the range 2-400 K. The maximum magnetic field obtainable from the model 7410 VSM was 1800 kA/m while field up to 3980 kA/m can be obtained with the SQUID magnetometer. As a result, M vs. H measurements for determining the first cubic magnetocrystalline anisotropy constants using equation (2-12) were made with the SQUID magnetometer. M vs. H measurements were made at temperatures of interest under a maximum applied field of 3980 kA/m. Other magnetic properties such as saturation magnetization, coercive field and remanence, were obtained from M vs. H results. Also using the law of approach to saturation magnetization described in chapter 2, first cubic anisotropy constants were determined.

5.3.4 Magnetostriction and strain derivative measurement

Magnetostriction measurement with the PPMS

Non-inductive resistive strain gauges were attached to the samples to measure the magnetostriction under applied magnetic field. Vishay Micro-measurements WK-06-031CF-350 350 Ω strain gauges were used with M-bond 610 adhesive for temperatures above and below 300K and M-bond 200 adhesive for magnetostriction measurements at 300 K. A Quantum Design Physical Properties Measurement System (PPMS) was used for measuring

the temperature dependence of magnetostriction. Using the PPMS, magnetostriction was measured along a direction parallel to the applied field up to a maximum applied field of 1.6 MA/m.

Two half-bridge strain gauge configurations were constructed on a puck for simultaneous measurement of magnetostriction on two samples. A schematic representation of the Wheatstone half-bridge configuration is shown in Fig. 5.10. The samples with attached strain gauges were mounted on the puck with the lead of the strain gauges aligned normal to the puck. This ensured that magnetostriction was measured in a direction parallel to the applied field. The puck was then inserted into the PPMS for magnetostriction measurement. A table of the changes in resistance of the strain gauge due to strain on the sample and corresponding magnetic fields values were obtained from the PPMS. The resistance change was converted to magnetostrictive strain of the samples.

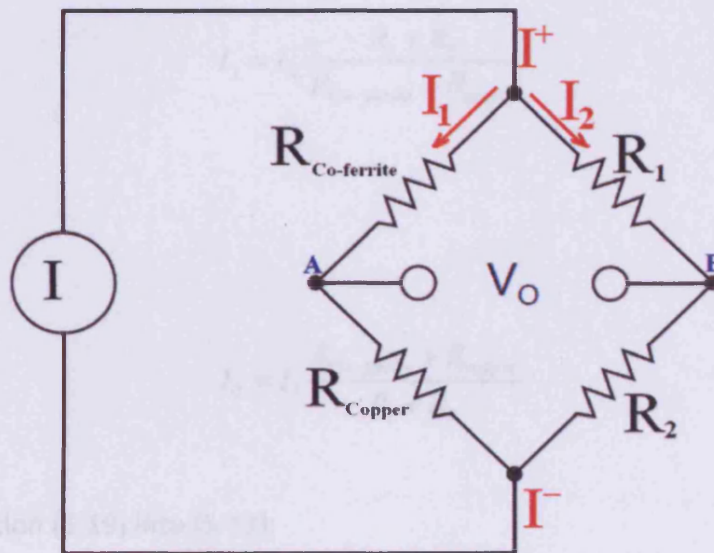


Fig. 5.10: Wheatstone half-bridge configuration for cobalt ferrite magnetostriction measurement using the Quantum Design PPMS. A similar resistive strain that mounted on cobalt ferrite was also mounted on copper and was used as a dummy resistor.

Determination of magnetostriction from changes in resistance of samples

The ratio of the out-of-balance voltage V_o between points A and B, to the constant excitation current I , under no applied field results in a measured resistance ($R_{measured}$);

$$\frac{V_o}{I}(H = 0) = R_{measured} \quad (5-16)$$

From the Wheatstone bridge,

$$I = I_1 + I_2 \quad (5-17)$$

$$\frac{I_1}{I_2} = \frac{R_1 + R_2}{R_{Co-ferrite} + R_{copper}} \quad (5-18)$$

Therefore,

$$I_1 = I_2 \frac{R_1 + R_2}{R_{Co-ferrite} + R_{copper}} \quad (5-19)$$

Also,

$$I_2 = I_1 \frac{R_{Co-ferrite} + R_{copper}}{R_1 + R_2} \quad (5-20)$$

Substituting equation (5-19) into (5-17);

$$I = I_1 + I_1 \frac{R_{Co-ferrite} + R_{copper}}{R_1 + R_2} = I_1 \left(1 + \frac{R_{Co-ferrite} + R_{copper}}{R_1 + R_2} \right) = I_1 \left(\frac{R_1 + R_2 + R_{Co-ferrite} + R_{copper}}{R_1 + R_2} \right) \quad (5-21)$$

Thus, from equation (5-20),

$$I_1 = I \left(\frac{R_1 + R_2}{R_1 + R_2 + R_{Co-ferrite} + R_{copper}} \right) \quad (5-22)$$

Similarly,

$$I_2 = I \left(\frac{R_{Co-ferrite} + R_{copper}}{R_1 + R_2 + R_{Co-ferrite} + R_{copper}} \right) \quad (5-23)$$

From the Wheatstone bridge;

$$V_o = V_A - V_B = I_1 R_{Co-ferrite} - I_2 R_1 \quad (5-24)$$

Substituting the expressions for I_1 and I_2 in equations 5-21 and 5-22 into 5-24,

$$\frac{V_o}{I} = \left(\frac{(R_1 + R_2) R_{Co-ferrite}}{R_1 + R_2 + R_{Co-ferrite} + R_{copper}} - \frac{(R_{Co-ferrite} + R_{copper}) R_1}{R_1 + R_2 + R_{Co-ferrite} + R_{copper}} \right) \quad (5-25)$$

Equation (5-15) becomes;

$$\frac{V_o}{I} (H = 0) = R_{measured} = \frac{R_2 R_{Co-ferrite} - R_{copper} R_1}{R_1 + R_2 + R_{Co-ferrite} + R_{copper}} \quad (5-26)$$

When $R_1 = R_2$, $R_{Co-ferrite} = R_{copper}$ and there is no change in temperature and no magnetic field applied, the bridge is said to be balanced. In such a state the output voltage $V_o = 0$ and no change in resistance ($R_{Measured}$) will be observed. Since R_1 and R_2 are resistors of 350Ω , changes in temperature only, will have similar effect on them, thus the bridge remains balanced. Since both the copper sample and cobalt ferrite samples have a 350Ω resistor attached to them and neglecting the differences in their thermal expansion coefficients, at no applied magnetic field, the bridge will remain balanced. Also, since the strain gauges are

self- temperature compensating, under the above conditions, observed changes in resistance should be due to changes in strain. When magnetic field is applied, $R_{Co-ferrite}$ will increase to $R_{Co-ferrite} + \Delta R_{Co-ferrite}$, and R_{copper} will increase to $R_{copper} + \Delta R_{copper}$. Because $R_1 = R_2 = R_{copper} = R_{Co-ferrite} = R = 350 \Omega$;

$$\frac{V_o}{I}(H = H) = R_{measured} = \frac{R((R + \Delta R_{Co-ferrite}) - (R + \Delta R_{copper}))}{4R} = \frac{\Delta R_{Co-ferrite} - \Delta R_{copper}}{4} \quad (5-27)$$

The magnetostriction of copper can be neglected being non-magnetic; equation (5-27) then reduces to;

$$\frac{V_o}{I}(H = H) = R_{measured} = \frac{\Delta R_{Co-ferrite}}{4} \quad (5-28)$$

The strain due to this change in resistance of cobalt ferrite can be obtained from the expression for the gauge factor, F_G . R is the resistance of the strain gauge, ΔR is the resistance change on the test specimen (in this case cobalt ferrite) and ϵ is the measured strain.

$$F_G = \frac{\Delta R}{R\epsilon} = \frac{\Delta R_{Co-ferrite}}{R\epsilon} = \frac{4R_{measured}}{R\epsilon} \quad (5-29)$$

The measured strain which is the magnetostriction of cobalt ferrite is given by;

$$Magnetostriction = \epsilon = \frac{4R_{measured}}{F_G R} \quad (5-30)$$

F_G and R for the WK-06-031CF-350 strain gauge used were 2.05 and 350 Ω respectively. Therefore magnetostriction for cobalt ferrite samples measured with the PPMS was obtained using;

$$Magnetostriction = \epsilon = R_{measured}(5.58 * 10^{-3}) \quad (5-31)$$

Magnetostriction measurement with the Universal DC Measurement System

When only room temperature magnetostriction measurements were required, the Universal DC Measurement System was used with Vishay Micro-measurement model 3800 wide range strain indicator. The Universal DC Measurement System was modified for room temperature magnetostriction measurements. Because the measurement system provides a traceable calibration route, it offers good flexibility. Through a LabView interface, the following H-coil parameters inputs were made; peak field value (800 kA/m); and H/I ratio (111832 m^{-1}). A schematic of the universal DC measurement system used for magnetostriction measurements at room temperatures is shown in Fig. 5.11.

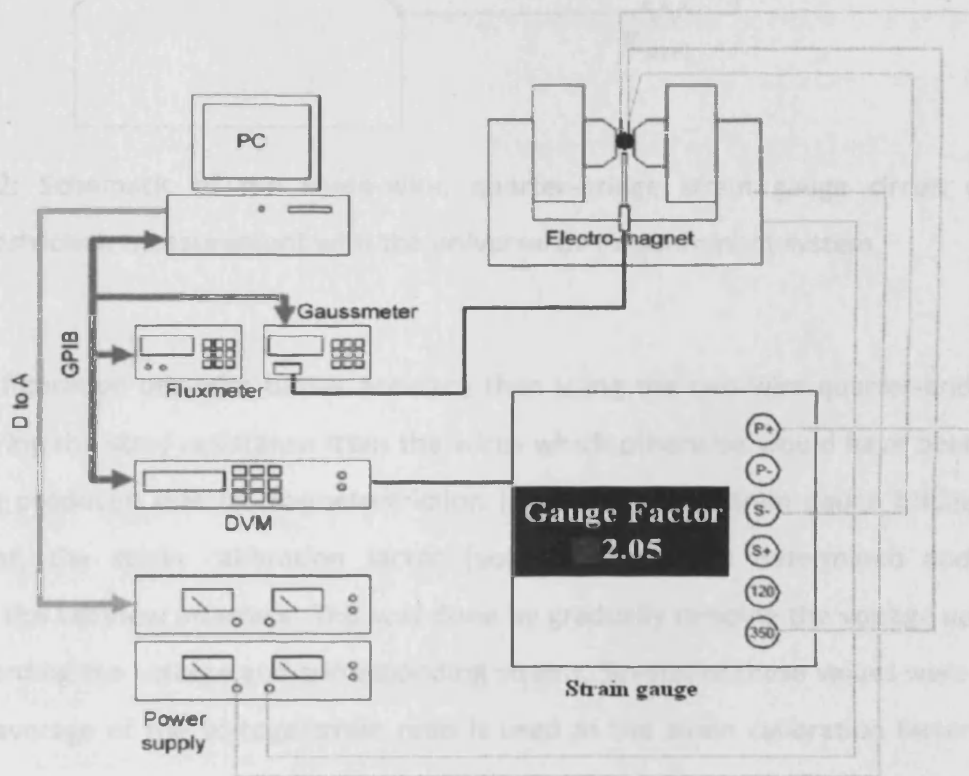


Fig. 5.11: Schematic diagram of the universal dC measurement system used for magnetostriction measurements

The gauge factor (2.05), bridge configuration (three-wire quarter-bridge) and excitation voltage (15 V) required for the measurement were also put in through the wide range strain indicator. The strain indicator was a three-wire, quarter-bridge strain gauge circuit. A schematic diagram of the strain gauge circuit is shown in Fig. 5.12 [5-6].

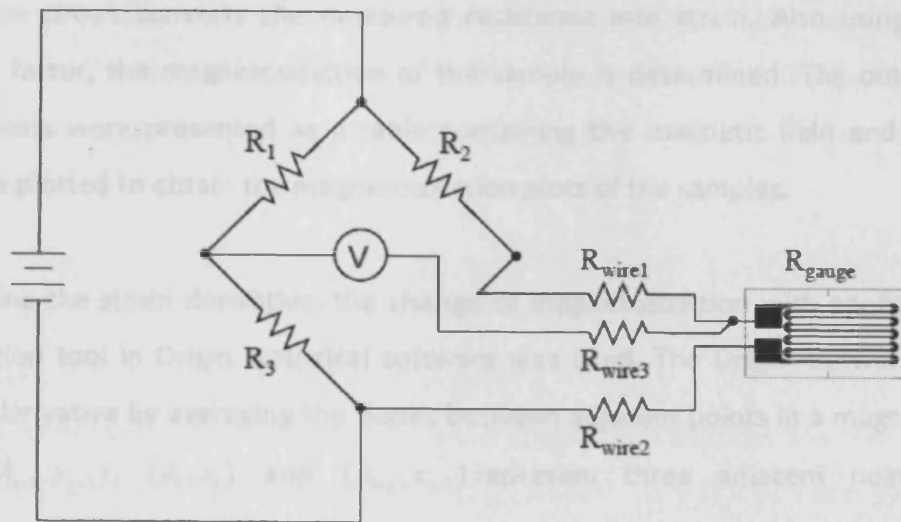


Fig. 5.12: Schematic of the three-wire, quarter-bridge strain gauge circuit used for magnetostriction measurement with the universal dc measurement system

This configuration provides better accuracy than using the two-wire quarter-bridge circuit by lowering the stray resistance from the wires which otherwise would have been misread as being produced due to magnetostriction [5-6]. Using the strain gauge bridge and the voltmeter, the strain calibration factor (voltage/strain) was determined and entered through the LabView interface. This was done by gradually ramping the voltage up or down and recording the voltage and corresponding strains. Several of these values were obtained and an average of the voltage/strain ratio is used as the strain calibration factor for each sample.

The samples were placed between the pole pieces of the electromagnet whose magnetizing current was provided by Kepco bipolar DC power supplies. A 16 bit digital to analogue converter was connected to the programming input of the Kepco power supplies to obtain a resolution of 0.2 mA. Samples were initially demagnetized by applying an AC field at frequency, 0.8 Hz. The AC field was set at a peak field of 800 kA/m, which decayed until the field reached a zero value. After demagnetising, the system prompts for balancing the

quarter-bridge after which measurements were started. Using the parameters entered, the strain gauge circuit converts the measured resistance into strain. Also using the strain calibration factor, the magnetostriction of the sample is determined. The outputs of the measurements were presented as a table containing the magnetic field and strain data which were plotted to obtain the magnetostriction plots of the samples.

To determine the strain derivative, the change of magnetostriction with applied field, the differentiation tool in Origin statistical software was used. The Origin software calculates the strain derivative by averaging the slopes between adjacent points in a magnetostriction curve. If (λ_{i-1}, x_{i-1}) , (λ_i, x_i) and (λ_{i+1}, x_{i+1}) represent three adjacent points on the magnetostriction curve, Origin averages the slopes of points (λ_{i-1}, x_{i-1}) and (λ_i, x_i) ; (λ_i, x_i) and (λ_{i+1}, x_{i+1}) as shown in equation 5-31.

$$\frac{1}{2} * \left[\frac{\lambda_{i+1} - \lambda_i}{x_{i+1} - x_i} + \frac{\lambda_i - \lambda_{i-1}}{x_i - x_{i-1}} \right] \quad (5-32)$$

Data for single loops of the magnetostriction curves were thus plotted and differentiated to obtain the strain derivatives of the cobalt ferrite samples.

5.4 Preparation of Thin Film Cobalt Ferrite Samples

Thin films of cobalt ferrite were prepared using by a PVD Products Inc. PLD2000 Pulsed Laser Deposition (PLD) system with a 6-target manipulator. The vacuum level in the deposition chamber was 1.33×10^{-5} Pa before deposition. Thin films were deposited by ablation of a CoFe_2O_4 target using a KrF (Krypton Fluoride) excimer laser with a wavelength of 248 nm, pulse energy of 210 mJ and repetition rate of 13 Hz. During film growth, the deposition chamber was kept at an oxygen pressure of 2.9 Pa. The CoFe_2O_4 target had a diameter of 5.08 cm and a thickness of 0.6 cm. The substrate was a wafer of 300 nm thermal SiO_2 on Si(100) which was heated by the substrate heater during deposition. The PLD2000

deposition system is capable of ± 3 °C temperature uniformity. Also, the ability to raster the laser beam over a large diameter of the target, and the ability to rotate the targets while rastering ensured the growth of uniform films. The thin films of cobalt ferrite were deposited at substrate temperatures of 523, 623, 723, 823 and 873 K at a constant growth rate of 0.38 Å/s.

5.5 Characterization of Thin Film Cobalt Ferrite Samples

5.5.1 Crystal structure and film orientation

Crystal structures of the thin film samples were determined by XRD. The XRD data of the cobalt ferrite films were recorded at a step size of 0.02° on a Philips PW1710 automated powder diffractometer with copper ($\text{CuK}\alpha$) radiation of wavelength 1.53 Å at 35 kV and 40 mA. The samples were cut and mounted without further preparation into the goniometer of the diffractometer because the sample surfaces were flat enough for X-ray diffractometry. XRD was performed between 2θ values of 2 to 80° .

5.5.2 Film Thickness and Composition

Film thickness was determined using scanning electron microscopy. Samples were measured at magnification of 2×10^5 with acceleration electrons at 20 kV. Sample compositions were determined using EDX by averaging the compositions measured at 15 locations on the films. A similar method to that used for the bulk samples was used to determine sample composition from the EDX data.

5.5.3 Magnetic properties measurements

Magnetization as a function of applied field was measured for the thin film samples with VSM up to a maximum applied field of 1273 kA/m. To understand the nature of anisotropy in the thin film samples, the in-plane and perpendicular magnetization vs. applied field of all samples were measured.

References to Chapter 5:

- [5-1]. S. H. Song, "Magnetic and magnetoelastic properties of M-substituted cobalt ferrites (M= Mn, Cr, Ga, Ge)" *PhD Thesis* submitted to Iowa State University, (2007)
- [5-2]. Charles Kittel, *Introduction to Solid States Physics*, New York: John Wiley & Sons; Ltd, (1996)
- [5-3]. C. Richard Brundle, Charles A. Evans, Jr, Shaun Wilson,, *Encyclopaedia of Materials Characterization*, Butterworth-Heinemann, USA, (1992)
- [5-4]. Donald R. Askeland, *The Science and Engineering of Materials*, UK, Chapman and Hall (1996)
- [5-5]. James H. Wittke, *Detection of signals*, Available: <http://www4.nau.edu/microanalysis/Microprobe-SEM/Signals.html> [Accessed: December 4, 2010]
- [5-6]. Tony R. Kuphaldt, *Lessons in electric circuits, vol. 1- dc*, 5th ed. 2006 [E-book] Available: All about circuits (<http://www.allaboutcircuits.com/>) [Accessed: May 24, 2010]

Chapter 6. Experimental Results and Discussion: Dependence of Properties on Vacuum Sintering Environment

6.1 Introduction

Air and vacuum sintering environments can affect the structural, magnetic and magnetostrictive properties of cobalt ferrite due to the differences in the oxygen partial pressure in both environments. Since most studies on the improvement of magnetostrictive properties of CoFe_2O_4 have concentrated on samples prepared at a particular temperature in air [6-1, 6-2], vacuum sintering conditions were chosen in order to compare and contrast results with those of air sintered samples reported. This can also lead to a better understanding of magnetostrictive properties. Such understanding is particularly important due to the varying levels of magnetostriction reported previously for CoFe_2O_4 in different studies. Values ranging from 100 ppm to 225 ppm have been reported previously [6-1, 6-2, 6-3]. The results of a study on the effect of vacuum sintering, with different sintering temperatures and sintering times, on the structure, magnetic and magnetostrictive properties of bulk samples of CoFe_2O_4 are presented and discussed in this chapter.

6.2 Variation of Density with Sintering Conditions

The variation of the densities of the samples with sintering temperature and time is shown in Fig. 6.1. Densities of the samples were obtained from the masses and volumes of the thick disk shaped samples. Both increase in the sintering temperature or sintering time resulted in increase in the densities of the samples. This is as expected because high sintering temperatures would provide more energy for grain growth and densification than low sintering temperatures. For a similar reason, density also increases with long sintering time and would increase much more with a combination of high sintering temperature and long sintering time. The sample sintered at 800°C for 6 hrs had the lowest density of $4,548 \text{ kg/m}^3$, while the sample sintered at 1200°C for 24 hrs had the highest density of $5,090 \text{ kg/m}^3$. The theoretical density of pure cobalt ferrite is $5,259 \text{ kg/m}^3$. It was also observed that

densification is more sensitive to variations in holding time at higher sintering temperatures than at lower sintering temperatures.

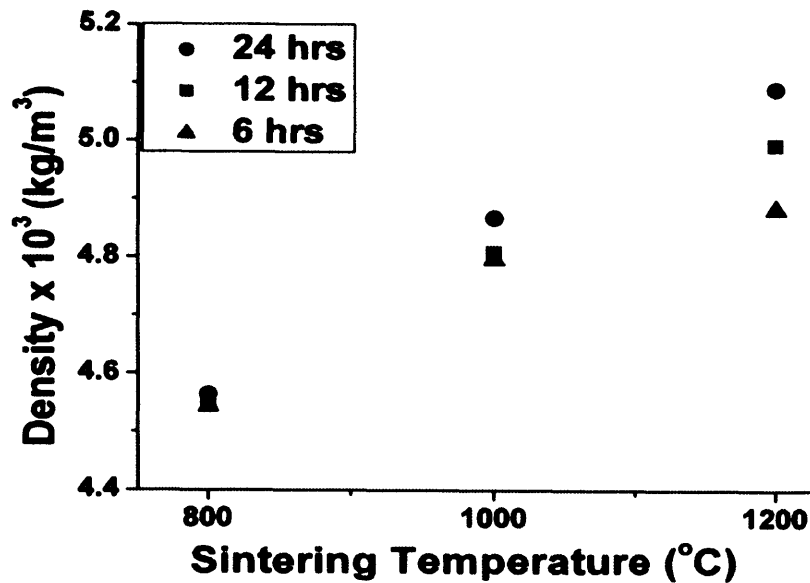


Fig. 6.1: Variation of sample densities with sintering temperature and time

6.3 Crystal Structure Determination

Fig. 6.2 shows the x-ray diffraction patterns of the samples. Comparing the sintered and un-sintered samples, it could be seen that vacuum sintering resulted in the development of additional peaks in the XRD pattern. These peaks, marked with the “▲” symbol were found to match the CoO pattern. Since the additional peaks were consistent in sintered samples but were not found in the un-sintered sample, vacuum sintering thus resulted in changes in both composition and crystal structure. Changes in crystal structure could further be seen by the differences in the 2θ positions of the peaks.

These additional peaks have not been reported in previous studies on magnetostrictive properties of cobalt ferrite samples sintered in air. Spark Plasma Sintering (SPS) of cobalt ferrite in “primary vacuum” was said to have resulted in the development of an additional CoO phase in addition to the parent spinel cobalt ferrite phase [6-4], although it is not clear

what level of vacuum is “primary vacuum”. The authors attributed the formation of the CoO phase either to the nature of the starting material or to incomplete reaction due to short sintering times (5 mins). This present study shows that neither the nature of the starting material nor the sintering conditions were responsible for the formation of the secondary phase. Though the samples used in this study had the same history, the additional phase was still formed irrespective of the sintering temperature or holding time (6, 12 or 24 hrs). In fact, based on this study, the additional phase is possibly not completely a CoO phase but a solid solution. This will be shown from the compositional analyses of the samples.

The formation of the additional phase could be the result of the reducing effect of the vacuum sintering environment. It has been stated by others [6-5], that heat treatment of CoFe_2O_4 in a reducing environment helps the development of an additional phase. To understand the origin of these peaks, SEM and EDX analyses were carried out on selected samples.

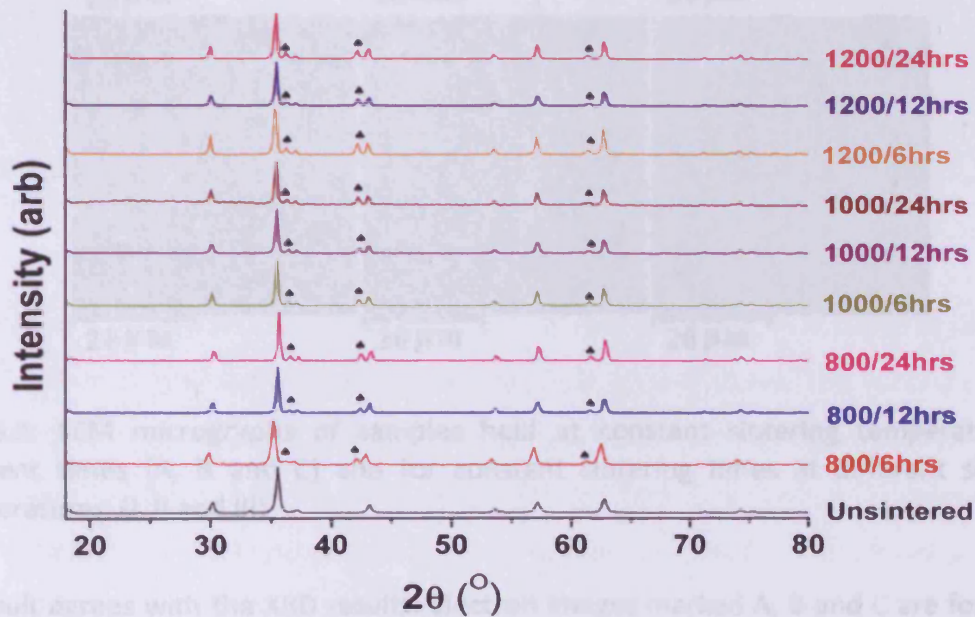


Fig. 6.2: XRD patterns for the samples showing the sintering temperature and holding time at a particular sintering temperature. For each sample, unmarked peaks correspond to the spinel cobalt ferrite pattern. Peaks marked with ♠ correspond to the CoO pattern.

6.4 Microstructure Determination

Samples were selected to reflect the variation in microstructure due to changes in:

- sintering time at constant sintering temperature (micrographs A, B and C)
- sintering temperature at constant sintering time (micrographs I, II and III)

The E-SEM electron images in Fig. 6.3 show that the samples possess two different phases as can be seen from two different contrasts in the electron images.

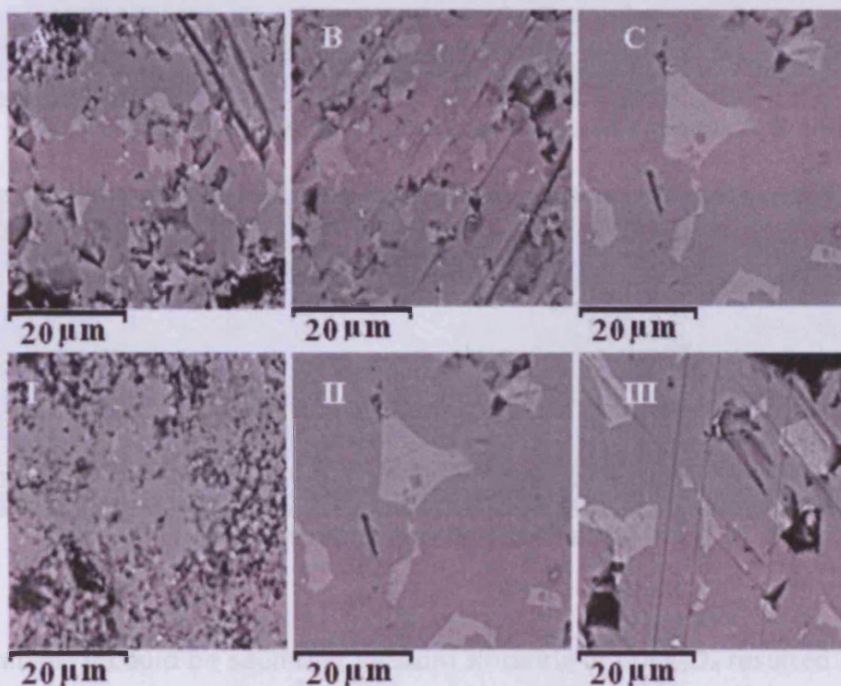


Fig. 6.3: SEM micrographs of samples held at constant sintering temperature for different times (A, B and C) and for constant sintering times at different sintering temperatures. (I, II and III)

The result agrees with the XRD results. Electron images marked A, B and C are for samples sintered at 1000°C for 6, 12 and 24 hrs respectively while those marked I, II and III are for samples sintered for 24 hrs at 800°C, 1000°C and 1200°C respectively. In general, the samples sintered at a lower sintering temperature, or held for a shorter time (or both), showed less of the additional (light coloured) phase.

6.5 Sample Composition

Table 6.1 shows the EDX results for the samples sintered at 1000°C and held for 6, 12 and 24 hrs while Table 6.2 shows those for samples held for 24 hrs at 800, 1000 and 1200°C.

Sample ID	Sintering Temperature/Time	Spinel Phase	Second Phase
A	1000 °C / 6 hrs	Co _{0.92} Fe _{2.08} O ₄	Co _{0.68} Fe _{0.32} O
B	1000 °C / 12 hrs	Co _{0.88} Fe _{2.12} O ₄	Co _{0.67} Fe _{0.33} O
C	1000 °C / 24 hrs	Co _{0.84} Fe _{2.16} O ₄	Co _{0.66} Fe _{0.34} O

Table 6.1: EDX results corresponding to electron images A, B and C

Sample ID	Sintering Temperature/Time	Spinel Phase	Second Phase
I	800 °C / 24 hrs	Co _{0.86} Fe _{2.14} O ₄	Co _{0.67} Fe _{0.33} O
II	1000 °C / 24 hrs	Co _{0.84} Fe _{2.16} O ₄	Co _{0.66} Fe _{0.34} O
III	1200 °C / 24 hrs	Co _{0.83} Fe _{2.17} O ₄	Co _{0.64} Fe _{0.36} O

Table 6.2: EDX results corresponding to electron images I, II and III

From both tables, it could be seen that vacuum sintering of CoFe₂O₄ resulted in two phases; a spinel phase slightly richer in Fe and a Co_{1-x}Fe_xO second phase. The second phase is a single phase of solid solution CoO/FeO in which $x \approx 0.33$; and might have been formed due to the reducing effect of the vacuum environment. Both CoO (Cobalt (II) oxide) and FeO (Iron (II) oxide) have the rocksalt crystal structure. The ionic radii of the cations (Co²⁺ = 0.75 Å, Fe²⁺ = 0.78 Å) and their molar volumes (Co²⁺ = 11.708 cm³/mol, Fe²⁺ = 11.974 cm³/mol) are also similar. Moreover, for all compositions in the temperature range 300 to 2000 K, the CoO/FeO system has a negative free energy and has neither maxima nor minima in its chemical potential versus composition plots over the same temperature range [6-6]. Based on these, it is obvious that CoO and FeO are completely miscible in each other and can form

a single phase solid solution over the range 300 to 2000 K. Analysis of the X-ray diffraction spectra did not show two separate spectra for CoO and FeO because the solid solution CoO/FeO is a single phase with composition $\text{Co}_{1-x}\text{Fe}_x\text{O}$. The X-ray analysis identified the peaks as from only CoO because the solid solution formed is $\sim 67\%$ Co, thus its lattice parameter is closer to CoO than to FeO.

6.6 Effect of Vacuum Sintering on Coercive Field

Fig. 6.4 shows that coercive field decreased with increase in sintering temperature and sintering time. This is in agreement with the increase in density observed in Fig. 6.1. As the grain size increases, it is expected that coercive field would decrease because larger grains provide less pinning sites to impede the movement of the domain walls due to lower volume fraction of grain boundaries. Higher sintering temperature and longer sintering time are expected to result in larger grains and consequently lower coercive field. The maximum coercive field (25.2 kA/m) was observed for the sample sintered at 800°C for 6 hrs and the least (3.7 kA/m) was observed for the sample sintered at 1200°C for 24hrs.

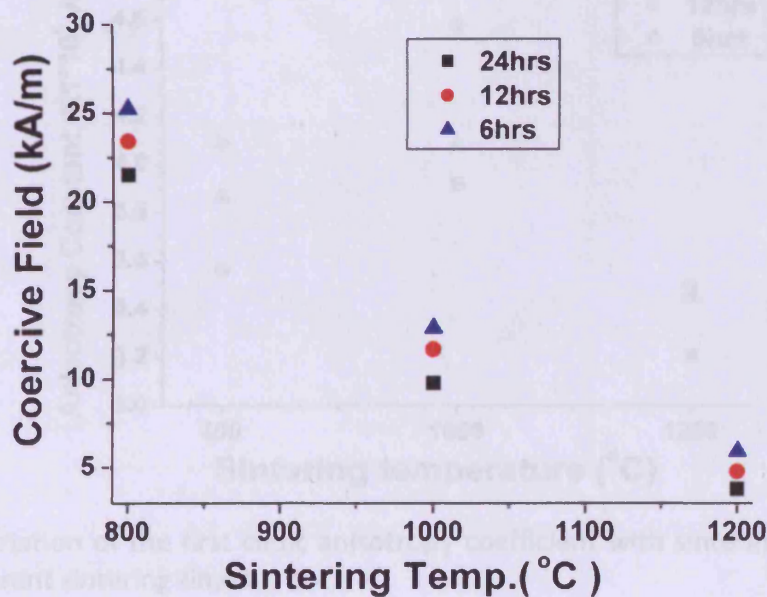


Fig. 6.4: Variation of coercive field with sintering temperature and at different sintering times

6.7 Variation of First Cubic Anisotropy Constant with Vacuum Sintering

The variation of first cubic anisotropy constant (K_1) with sintering temperature is plotted in Fig. 6.5. It could be seen that K_1 initially increased and later decreased with increase in sintering temperature and sintering time. The lowest value of $K_1 = 3.21 \times 10^5 \text{ J/m}^3$, was observed for the sample sintered at 1200°C for 24 hrs whereas the highest value, $4.57 \times 10^5 \text{ J/m}^3$, was observed for the sample sintered at 1000°C for 12 hrs.

The samples sintered at 1200°C showed the lowest anisotropy as expected but the samples sintered at 1000°C showed higher anisotropy than those sintered at 800°C . The high anisotropy obtained for the samples sintered at 1000°C for 12 hrs is not easily explainable from this study. Further study is needed to identify the necessary combination of vacuum level, sintering temperature and time that would result in a combination of high magnetostriction together with a low anisotropy in the absence of the detrimental second phase.

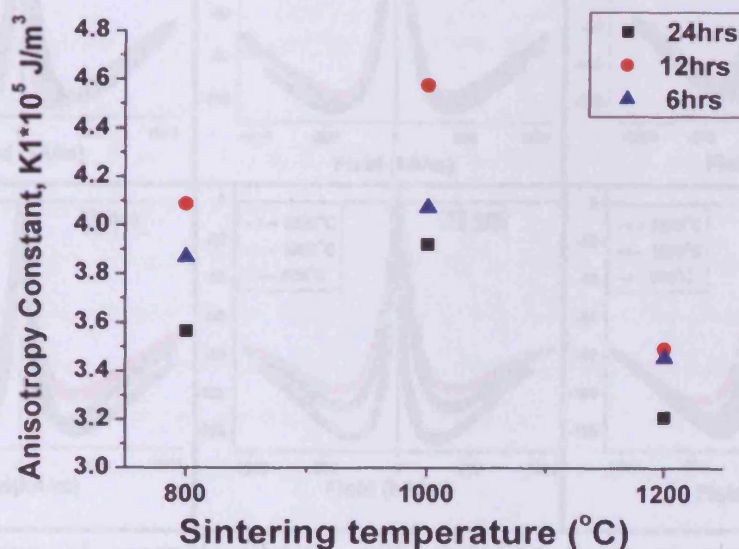


Fig. 6.5: Variation of the first cubic anisotropy coefficient with sintering temperature and at different sintering times

6.8 Influence of Vacuum Sintering on Magnetostriction

In Fig. 6.6, the influence of vacuum sintering on magnetostriction of cobalt ferrite is shown. The variation of magnetostriction with magnetic field is shown for different sintering temperatures at constant sintering time (upper plots) and for different sintering times at constant sintering temperature (lower plots). The upper plots show that varying sintering times at constant sintering temperatures resulted in little variation in peak to peak magnetostriction amplitude. On the other hand, the lower plots show that varying sintering temperatures at constant sintering times resulted in more significant variations in the amplitude of peak to peak magnetostriction. It could thus be said from these results, that the differences in sintering time have less influence on the magnetostriction amplitude of the samples than differences in sintering temperature.

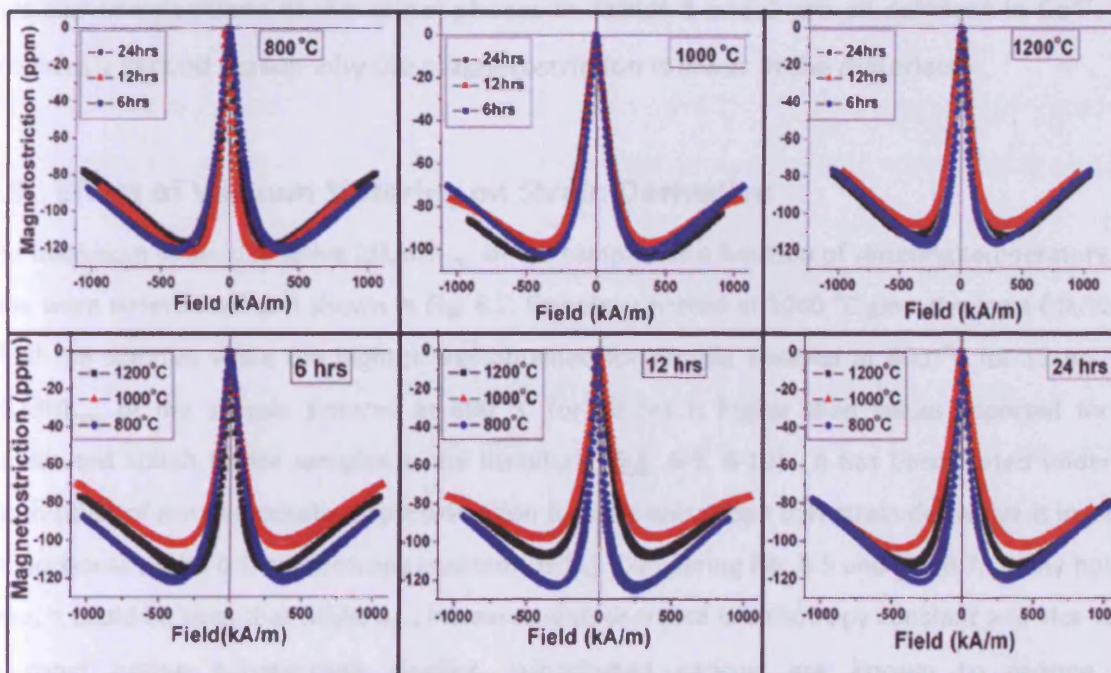


Fig. 6.6: Variation of magnetostriction with sintering times at constant sintering temperatures (upper) and variation of magnetostriction with sintering temperatures at constant sintering times (lower)

It is important to recall that these samples are not single phase samples and so the cumulative magnetostrictive response of both phases may be different from their individual

responses. The highest amplitudes of peak to peak magnetostriction (-125 ppm) obtained were for samples sintered at 800°C. This value falls into the mid range of values reported in the literature for air sintered samples [6-1, 6-3]. $\text{Co}_{1-x}\text{Fe}_x\text{O}$ second phase might have had a detrimental effect on the magnetostriction amplitude. The phase contains more of antiferromagnetic CoO with a Néel temperature at 297 K [6-7]. Magnetostriction of CoO has been reported to be -5.4 ppm at 77 K [6-7, 6-8] and would be expected to be negligible at room temperature. In such a composite magnetostrictive material, it is expected that the effective magnetostriction would decrease with increase in the volume fraction of the $\text{Co}_{1-x}\text{Fe}_x\text{O}$ second phase. Moreover, it has been explained using the single-ion crystalline-field model that magnetostriction in CoFe_2O_4 is due primarily to Co^{2+} located on the B-sites of the spinel crystal structure [6-1]. Any deviation from stoichiometry resulting in a decrease of Co^{2+} on these sites would therefore result in a lower magnetostriction and it can be seen that the compositions of the spinel phases in Tables 1 and 2 are all deficient in Co^{2+} . This provides a second reason why the magnetostriction is lower in the materials.

6.9 Effect of Vacuum Sintering on Strain Derivative

The maximum strain derivative $(d\lambda/dH)_{\text{max}}$ of the samples as a function of sintering temperature and time were determined and shown in Fig. 6.7. Samples sintered at 1000 °C gave the least $(d\lambda/dH)_{\text{max}}$ of all the samples while the highest was obtained for sample sintered at 800 °C for 12 hrs. The $(d\lambda/dH)_{\text{max}}$ of the sample sintered at 800 °C for 12 hrs is higher than values reported for unsubstituted cobalt ferrite samples in the literature [6-3, 6-9, 6-10]. It has been stated under the assumption of the one-constant approximation to cubic anisotropy that strain derivative is inversely proportional to the cubic anisotropy constant [6-11]. Comparing Fig. 6.5 and Fig. 6.7, at any holding time, it could be seen that $(d\lambda/dH)_{\text{max}}$ increases with decrease in anisotropy constant and vice versa. In most cation substitution studies, substituted cations are known to reduce the magnetostriction amplitude but to increase $(d\lambda/dH)_{\text{max}}$ at low concentrations. This same trend is seen in the vacuum sintered samples which thus suggest that the influence of cation substitution and formation of a second phase due to vacuum sintering may be similar.

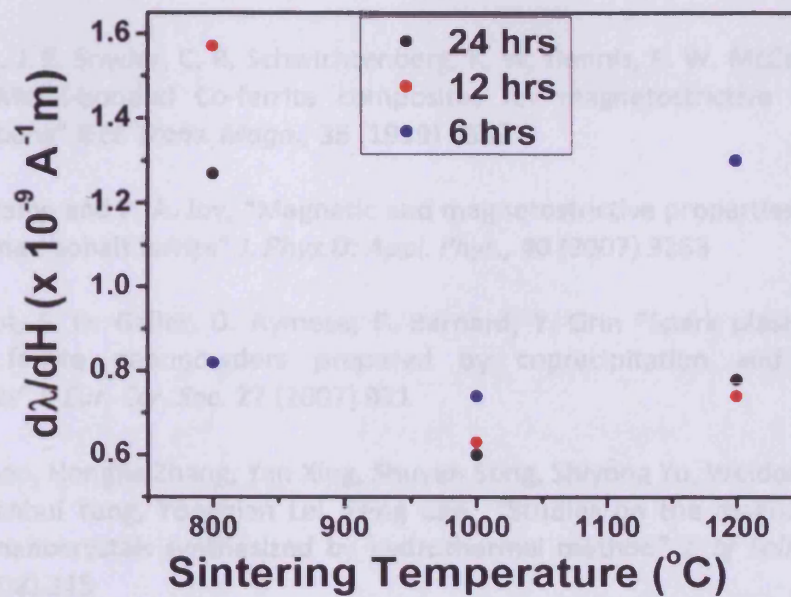


Fig. 6.7: Dependence of strain derivative on sintering temperature and time

In conclusion, it can be seen from the results presented that samples sintered in vacuum at low temperatures and held for longer time; or those sintered at high temperature and held for shorter times, have a combination of the highest values of peak to peak magnetostriction and $(d\lambda/dH)_{max}$. It has also been shown that samples sintered at low vacuum sintering temperature or held for a shorter time or both have less of the second phase. It is then possible to find a combination of vacuum sintering temperature and sintering time which would have an optimum effect on the magnetostrictive properties of cobalt ferrite.

References to Chapter 6:

- [6-1]. J. G. Na, T. D. Lee and S. J. Park, "Effects of cation distribution on magnetic properties in cobalt ferrite" *J. Mat. Sci. Lett.*, **12** (1993) 961

- [6-2]. Y. Chen, J. E. Snyder, C. R. Schwichtenberg, K. W. Dennis, R. W. McCallum and D. C. Jiles, "Metal-bonded Co-ferrite composites for magnetostrictive torque sensor applications" *IEEE Trans. Magn.*, **35** (1999) 3652
- [6-3]. S. D. Bhame and P. A. Joy, "Magnetic and magnetostrictive properties of manganese substituted cobalt ferrite" *J. Phys.D: Appl. Phys.*, **40** (2007) 3263
- [6-4]. N. Millot, S. Le Gallet, D. Aymesa, F. Bernard, Y. Grin "Spark plasma sintering of cobalt ferrite nanopowders prepared by coprecipitation and hydrothermal synthesis" *J. Eur. Cer. Soc.* **27** (2007) 921
- [6-5]. Lijun Zhao, Hongjie Zhang, Yan Xing, Shuyan Song, Shiyong Yu, Weidong Shi, Xianmin Guo, Jianhui Yang, Yongqian Lei, Feng Cao "Studies on the magnetism of cobalt ferrite nanocrystals synthesized by hydrothermal method" *J. of Solid State Chem.*, **181** (2008) 245
- [6-6]. S. B Pongsai "Computational study on thermodynamics of mixing and phase behaviour for CoO/FeO and CoO/MnO solid solutions" *J. Molecular Structure: THEOCHEM* **761** (2006) 171
- [6-7]. T. Nakamichi and M. Yamamoto, "Antiferromagnetic magnetostriction in CoO and NiO single crystals" *J.Phys. Soc. Jpn.*, **16** (1961) 126
- [6-8]. T. R. McGuire and W.A. Crapo, "Magnetic susceptibility and magnetostriction of CoO, MnO and NiO" *J. Appl. Phys.*, **33** (1962) 1291
- [6-9]. S. J. Lee, C. C. H. Lo, P. N. Matlage, S. H. Song, Y. Melikhov, J. E. Snyder, and D. C. Jiles " Magnetic and magnetoelastic properties of Cr-substituted cobalt ferrite" *J. Appl. Phys.* **102** (2007) 073910
- [6-10]. S. H. Song, C. C. H. Lo and S. J. Lee, S. T. Aldini, J. E. Snyder and D. C. Jiles "Magnetic and magnetoelastic properties of Ga-substituted cobalt ferrite" *J. Appl. Phys.* **101** (2007) 09C517
- [6-11]. C. C. H. Lo "Compositional Dependence of the Magnetomechanical Effect in Substituted Cobalt Ferrite for Magnetoelastic Stress Sensors" *IEEE Trans. Magn.* **43** (2007) 2367

Chapter 7. Experimental Results and Discussion: Dependence of Properties on Annealing and Quenching Heat Treatment

7.1 Introduction

It is known that the magnetic and magnetostrictive properties of cobalt ferrite depend on the concentration of Co^{2+} at the B-sites [7-1, 7-2]. Therefore, any change in the site occupancy of the cations will lead to changes in the magnetic and magnetostrictive properties of cobalt ferrite. Heat treatment can result in such changes [7-2] because it has been previously demonstrated that heat treatment can alter the degree of inversion of the spinel structure of CoFe_2O_4 [7-3]. It can result in the migration of Co^{2+} ions from A-sites to their preferred B-sites within the partially inverse spinel structured cobalt ferrite. Such changes can lead to an increase in the amplitude of peak to peak magnetostriction. Similarly if heat treatment results in Co^{2+} moving away from the B-sites, such might result in the lowering of the magnetostriction amplitude. It is therefore important to find a systematic approach to controlling magnetostriction via heat treatment in order to optimize magnetostrictive properties.

A recent heat treatment study shows strong dependence of magnetostrictive properties of cobalt ferrite on sintering conditions and microstructure [7-4]. In that study, the authors allowed the cobalt ferrite samples to cool slowly to room temperature. Therefore, the observed magnetostrictive properties were those of cations at or close to their equilibrium positions at the temperature at which the thermal energy was no longer sufficient to move them. However, it will also be helpful to study the changes in the peak to peak magnetostriction amplitudes and strain derivatives when cations are frozen close to their equilibrium positions at different temperatures. This can be achieved by rapidly cooling the samples from elevated temperatures to room temperature and studying the changes in their magnetostrictive properties. The results presented in this study are for cobalt ferrite samples quenched from different annealing temperatures to room temperature. In

discussing the results, the term heat treatment will be used in referring to the combination of annealing and quenching treatment performed on the samples.

7.2 Influence of Heat Treatment on Crystal Structure and Lattice Parameter

The X-ray diffraction patterns for the samples investigated are shown in Fig. 7.1. It can be seen from the result that all the patterns from the samples are consistent with the presence of spinel phases only. No additional phase was formed following the heat treatment. Using the XRD data and following the procedure explained in section 5.3.1 of chapter 5, the lattice parameters of the samples were determined to be same within experimental uncertainty as shown in Table 7.1. The similarity in the lattice parameters obtained for the samples indicates that the heat treatment performed on the samples did not alter their crystal structures.

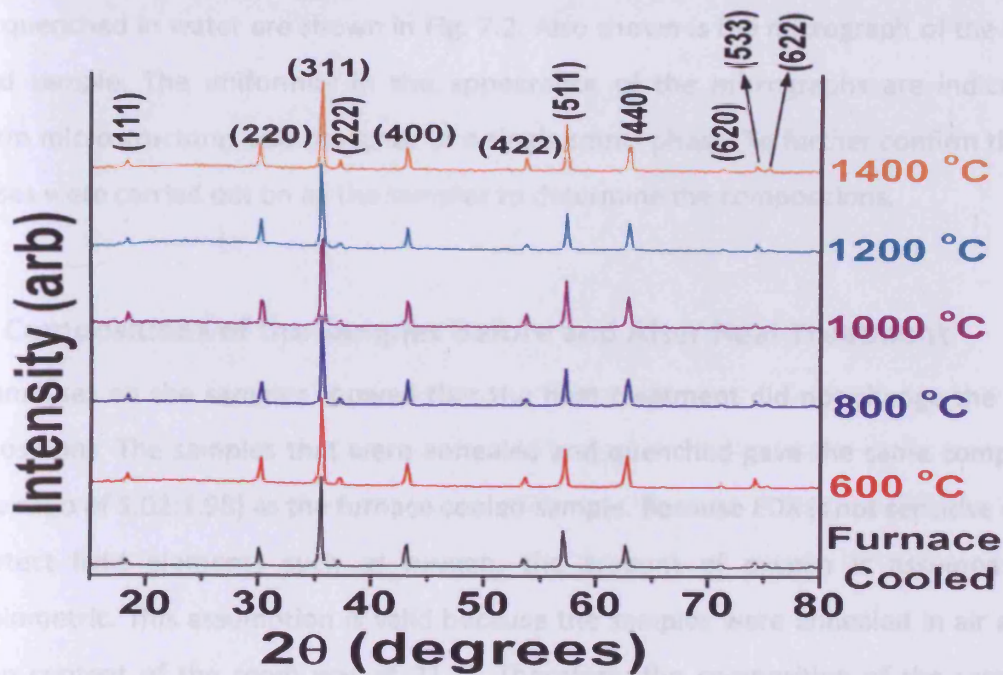


Fig. 7.1: XRD pattern of the quenched and furnace cooled cobalt ferrite samples

Sample	Lattice Parameter (Å)
Furnace Cooled	8.37 ± 0.02
600 °C	8.38 ± 0.01
800 °C	8.38 ± 0.01
1000 °C	8.38 ± 0.01
1200 °C	8.38 ± 0.01
1400 °C	8.37 ± 0.02

Table 7.1: Influence of heat treatment of lattice parameters of the samples

7.3 Influence of Heat Treatment on Microstructure

The E-SEM micrographs of the samples showing their annealing temperatures before they were quenched in water are shown in Fig. 7.2. Also shown is the micrograph of the furnace cooled sample. The uniformity in the appearance of the micrographs are indicative of uniform microstructures and presence of a single spinel phase. To further confirm this, EDX analyses were carried out on all the samples to determine the compositions.

7.4 Compositions of the Samples Before and After Heat Treatment

EDX analyses on the samples showed that the heat treatment did not change the sample compositions. The samples that were annealed and quenched gave the same composition (Co:Fe ratio of 1.02:1.98) as the furnace cooled sample. Because EDX is not sensitive enough to detect light elements such as oxygen, the amount of oxygen is assumed to be stoichiometric. This assumption is valid because the samples were annealed in air and the oxygen content of the room was at 21 %. Therefore, the composition of the samples as determined by EDX was $\text{Co}_{1.02}\text{Fe}_{1.98}\text{O}_4$ which remained constant for the samples.

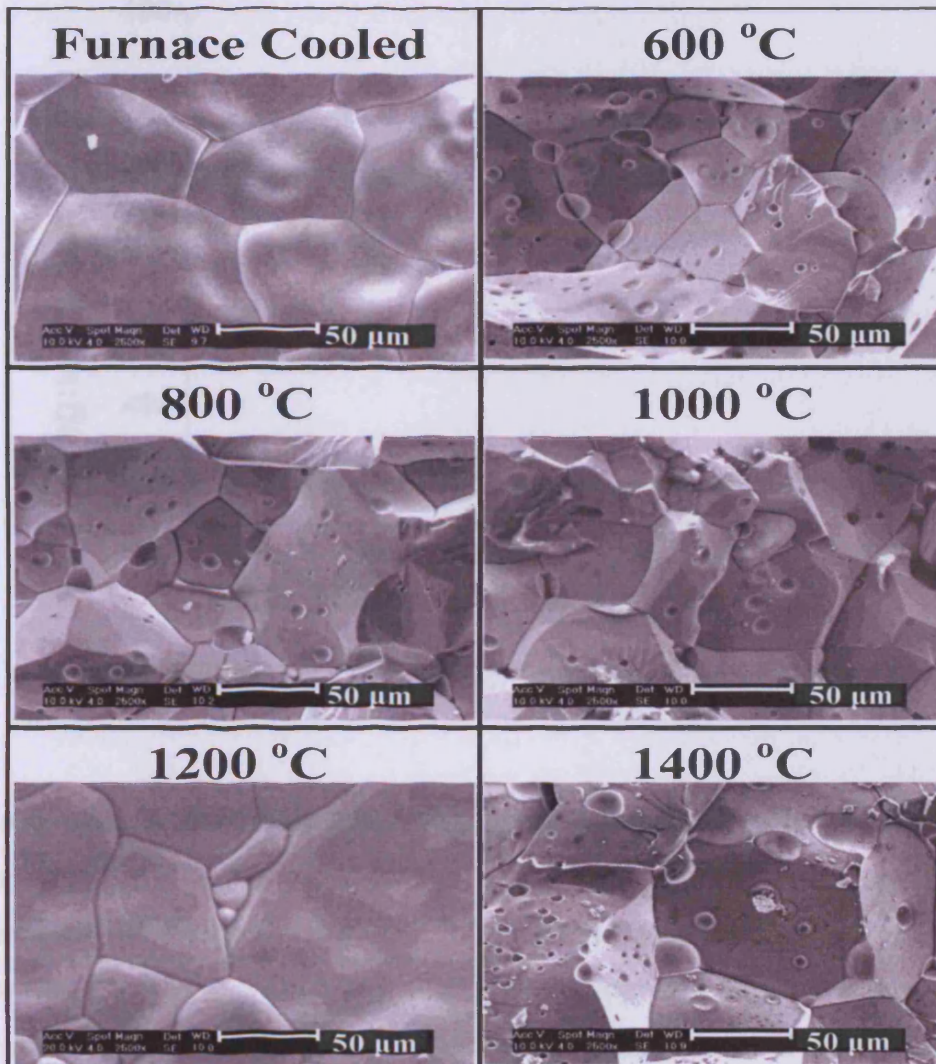


Fig. 7.2: E-SEM micrographs of all the samples. The samples were annealed at temperatures shown before being quenched in water to ambient temperature. Images of the furnace cooled sample and the sample marked 1200 °C were obtained from diamond-sawed sample surfaces. The rest were obtained from fractured surfaces.

7.5 Variation of Saturation Magnetization due to Heat Treatment

The value of the magnetization at 4 MA/m was used for saturation magnetization of the samples. As shown in Fig. 7.3, saturation magnetization increased with increase in heat treatment temperature.

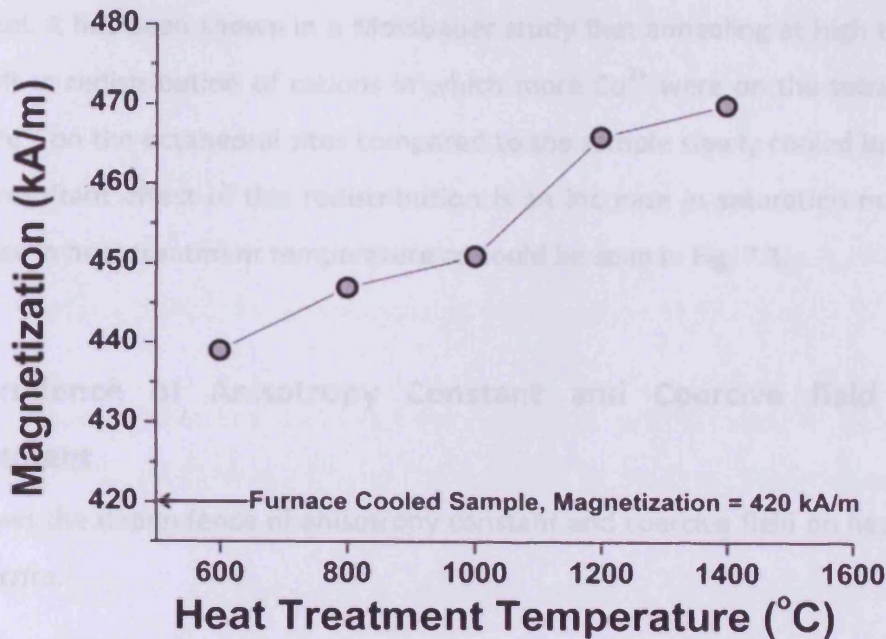


Fig. 7.3: Variation of magnetization at Field (H) = 4 MA/m with heat treatment temperature

The net magnetic moment per formula unit, and hence the magnetization of cobalt ferrite is a function of the super-exchange interaction between Co^{2+} and Fe^{3+} on the tetrahedral and octahedral sites of the spinel structure. Because the coupling between these sites is antiferromagnetic, the net magnetization (M) is the difference between the net magnetic moment of the octahedral sites (M_B) and the net magnetic moment of the tetrahedral sites (M_A);

$$M = \sum M_B - \sum M_A \quad (7-1)$$

Being a partially inverse spinel structured material; cobalt ferrite has a saturation magnetization mostly contributed by Co^{2+} on the octahedral sites. This is because the distribution of Fe^{3+} between the tetrahedral and octahedral sites results in a negligible contribution to the net magnetic moment. This holds more strongly as the degree of inversion tilts towards complete inversion, in which case the moments of Fe^{3+} on both sites

would cancel. It has been shown in a Mossbauer study that annealing at high temperature would result in redistribution of cations in which more Co^{2+} were on the tetrahedral sites and more Fe^{3+} on the octahedral sites compared to the sample slowly cooled in the furnace [7-3]. The resultant effect of this redistribution is an increase in saturation magnetization with increase in heat treatment temperature as could be seen in Fig. 7.3.

7.6 Dependence of Anisotropy Constant and Coercive field on Heat Treatment

Fig. 7.4 shows the dependence of anisotropy constant and coercive field on heat treatment of cobalt ferrite.

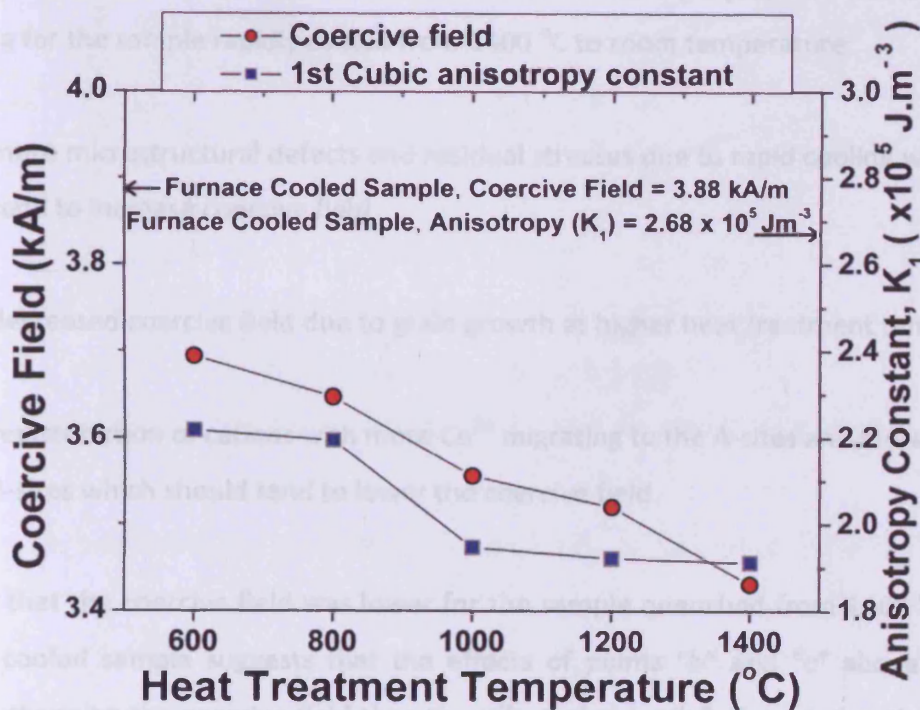


Fig. 7.4: Variation of anisotropy constant and coercive field with heat treatment temperature

As shown in the figure, the first cubic magnetocrystalline anisotropy constant decreased with increase in the heat treatment temperature. It has been reported that the presence

Co^{2+} ions, most of which are on the octahedral sites of the inverse spinel structure of cobalt ferrite, is the main cause of high anisotropy [7-5]. Annealing cobalt ferrite at elevated temperature and rapidly cooling to room temperature leads to cation redistribution in which the composition of the Co^{2+} ions on the octahedral sites decreases. The consequence of this redistribution would be a decrease in the magnetocrystalline anisotropy constant with increase in heat treatment temperature as was observed in this study.

It was also observed that the coercive field decreased with increase in heat treatment temperature. This result follows a similar trend to that of the first cubic magnetocrystalline anisotropy constant, suggesting that magnetocrystalline anisotropy is a major contribution to the coercivity. Because coercive field is structure sensitive, comparing the samples that were rapidly cooled from $1400\text{ }^{\circ}\text{C}$ and the furnace cooled sample, one would expect the following for the sample rapidly cooled from $1400\text{ }^{\circ}\text{C}$ to room temperature:

- a. more microstructural defects and residual stresses due to rapid cooling which should tend to increase coercive field
- b. decreased coercive field due to grain growth at higher heat treatment temperature
- c. redistribution of cations with more Co^{2+} migrating to the A-sites and more Fe^{3+} to the B-sites which should tend to lower the coercive field.

The fact that the coercive field was lower for the sample quenched from $1400\text{ }^{\circ}\text{C}$ than the furnace cooled sample suggests that the effects of points "b" and "c" above contribute more to changing the coercive field than the effect of point "a". Considering that the grain sizes of both samples would be similar due to the small difference in the heat treatment temperature ($50\text{ }^{\circ}\text{C}$), it seems that the major driving force in lowering coercive field in the quenched samples is due to cation redistribution.

7.7 Influence of Heat Treatment on Magnetostriction

Fig. 7.5 shows the variation in the peak to peak magnetostriction amplitude due to the variation in heat treatment temperature. With increasing heat treatment temperature, the amplitude of peak to peak magnetostriction decreased. Magnetostriction in cobalt ferrite also depends on the Co^{2+} on the octahedral sites. It is therefore likely that the migration of Co^{2+} away from the octahedral sites to the tetrahedral sites would have resulted in the lowering of the magnetostriction amplitude in the rapidly cooled samples.

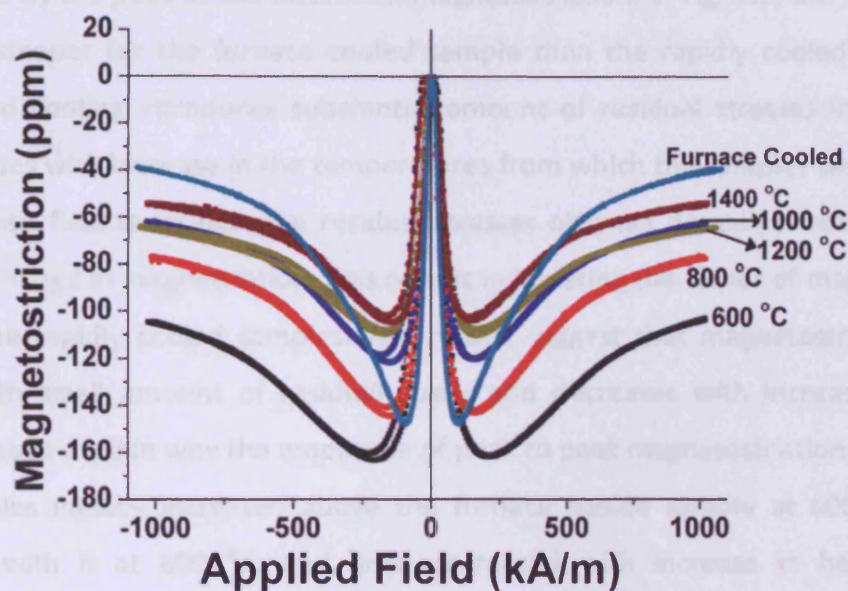


Fig. 7.5: Variation of peak to peak magnetostriction amplitude with applied magnetic field

It can also be seen from the results that the amplitude of magnetostriction for the sample heat treated at 600 °C is highest. Also the furnace cooled sample and the sample heat treated at 800 °C have comparable magnetostriction amplitudes. This does not agree with the proposed explanation of Co^{2+} migrating away from the octahedral to the tetrahedral sites. Migration of Co^{2+} away from the octahedral sites should result in the amplitude of magnetostriction of the furnace cooled sample being the highest of all the samples. It is not clear why this happened but in Fe-Ga alloys, magnetostriction has been found to increase in quenched samples than furnace cooled samples [7-6, 7-7]. A possible explanation might be

the contribution of residual stresses introduced in the samples by rapid cooling, to the magnetomechanical processes.

The effect of residual stresses due to rapid cooling is seen when the low and high field regions of the magnetostriction curves of the rapidly cooled and furnace cooled samples are compared. As shown in Fig. 3.6, the magnetostriction curve of cobalt ferrite is divided into a region in which the contribution of λ_{100} is more pronounced (low field region) and a region in which the contribution of λ_{111} increases and is observed (high field region). Both regions are separated by the peak at the saturation magnetostriction. In Fig. 7.5, the slopes of both regions are steeper for the furnace cooled sample than the rapidly cooled ones. This is because rapid cooling introduces substantial amount of residual stresses in the samples which increases with increase in the temperatures from which the samples were quenched. When magnetic field is applied, the residual stresses obstruct domain processes and thus impede the change in magnetization. This results in lowering the slopes of magnetostriction curves for the rapidly cooled samples. The results suggest that magnetostriction initially increases with small amount of residual stress and decreases with increase in residual stress. This might explain why the amplitude of peak to peak magnetostriction of the rapidly cooled samples initially increased above the furnace cooled sample at 600 °C, became comparable with it at 800 °C, and later decreased with increase in heat treatment temperature.

It was observed that the magnetostriction curves from the samples in this study were remarkably steeper compared with those from previous studies. Fig. 7.6 compares the furnace cooled sample from this study with a furnace cooled sample from a previous study. For the purpose of clarity, the furnace cooled sample used in this study will be referred to as FC1 while that from the previous study will be referred to as FC2 for the rest of this section. This significant difference in steepness suggests improved magnetomechanical response as will be shown in section 7.8.

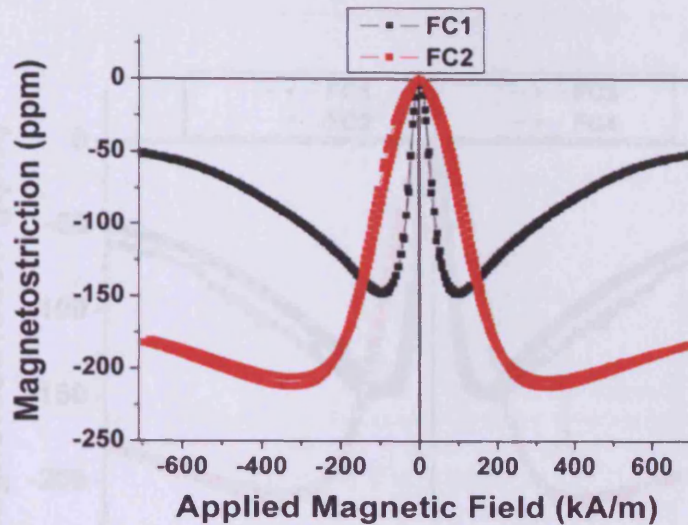


Fig. 7.6: Comparing the magnetostriction curves of furnace cooled samples from this study and previous study.

It was necessary to perform additional measurements to validate the result.

- a. Sample FC1 was glued to the holder with a double sided tape. The result would be affected if the glue had significant constriction on the sample during magnetostriction measurement. As a result, magnetostriction measurement was repeated on sample FC1 without any form of gluing. The result from this second measurement will be referred to as FC3 in this section.
- b. Sample FC1 was measured with the Universal DC measurement system. To ensure that the observed increase in steepness was not associated with the system, magnetostriction measurement was repeated on the sample with the PPMS. The result from this third measurement will be referred to as FC4 in this section.

Fig. 7.7 shows the obtained result. It could be seen that the magnetostriction plots for FC1, FC3 and FC4 are similar especially in the low field region which corresponds to the region of maximum slope. Although the magnetostriction amplitudes obtained for FC1, FC3 and FC4 are less than that for FC2 and some literature values (200 and 194 ppm) [7-8, 7-9], they are higher than some other values previously reported (100, 90 and 105 ppm) [7-10, 7-11, 7-12].

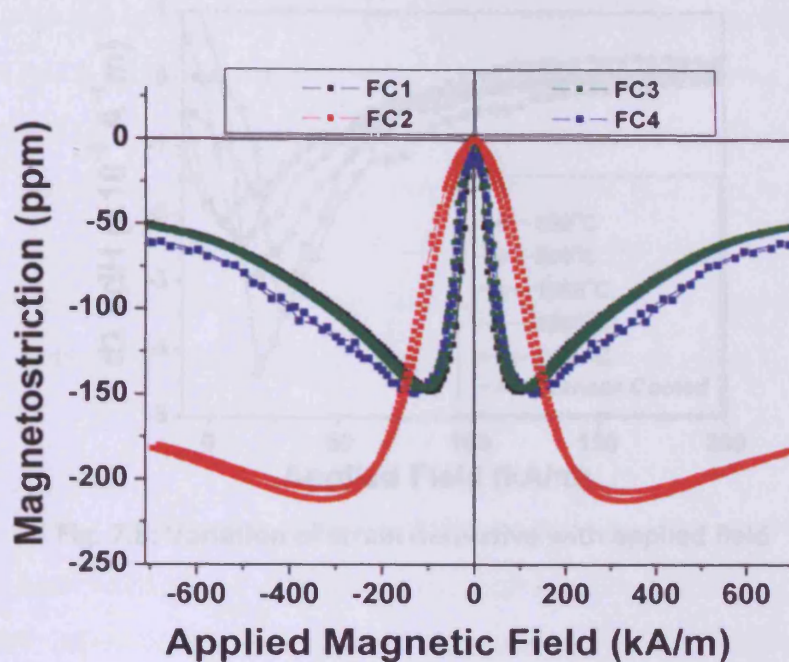


Fig. 7.7: Comparing the magnetostriction curves of furnace cooled samples from this study and previous study.

7.8 Strain Derivative

Fig. 7.8 shows the variation of strain derivative with applied field. The strain derivative was found to decrease with increase in heat treatment temperature as shown in Fig. 7.9. The maximum strain derivative, $(d\lambda/dH)_{\max}$ for the furnace cooled sample ($4.34 \times 10^{-9} \text{ A}^{-1}\text{m}$) is the highest ever reported for both substituted and un-substituted cobalt ferrite samples. Previous reports on the strain derivative of un-substituted cobalt ferrite were between 1.3×10^{-9} and $1.5 \times 10^{-9} \text{ A}^{-1}\text{m}$ [7-13, 7-8]. This result shows that the limit of the sensitivity of cobalt ferrite is higher than previously thought and can be further improved if the underlying mechanism(s) is/are understood. It could also be seen that all the samples in this study showed high $(d\lambda/dH)_{\max}$. For substituted cobalt ferrite samples, the highest $(d\lambda/dH)_{\max}$ previously reported was for $\text{CoGa}_{0.2}\text{Fe}_{1.8}\text{O}_4$ sample ($3.2 \times 10^{-9} \text{ A}^{-1}\text{m}$) [7-9]. Irrespective of the fact that rapid cooling decreases $(d\lambda/dH)_{\max}$ while non magnetic cation substitution improves it, the value for $\text{CoGa}_{0.2}\text{Fe}_{1.8}\text{O}_4$ is less than that obtained for the sample rapidly cooled from 600°C and comparable to that of the sample rapidly cooled from 800°C .

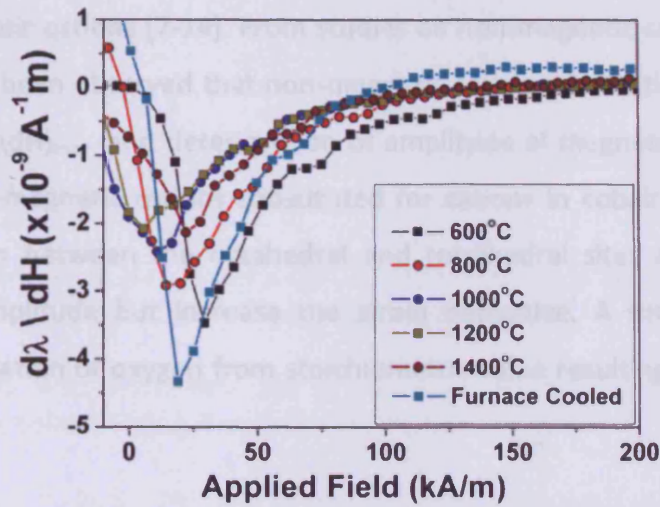


Fig. 7.8: Variation of strain derivative with applied field

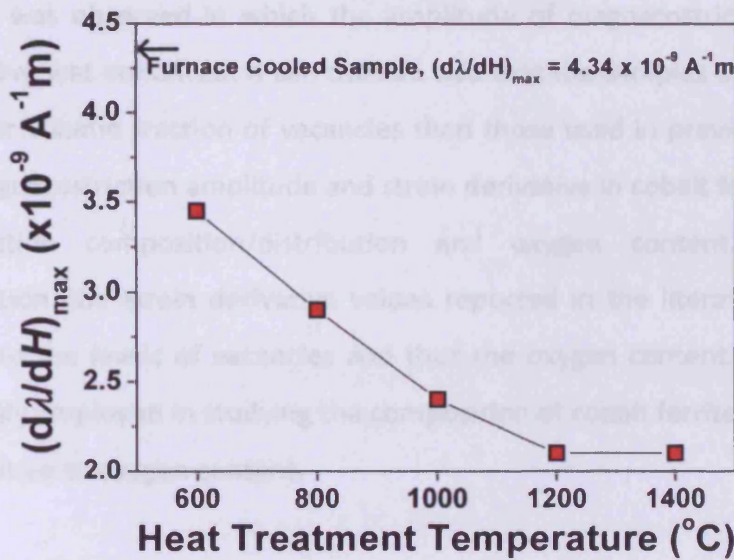


Fig. 7.9: Variation strain derivative with heat treatment

The observed variations in the amplitude of peak to peak magnetostriction and strain derivative of cobalt ferrite samples in the literature may be due to variation in the oxygen content of the samples. Deviation from stoichiometric amounts of oxygen in ferrosinels such as cobalt ferrite can result in vacancies which may have similar effects in the spinel

lattice as non magnetic cations [7-14]. From studies on non-magnetic cation substitution in cobalt ferrite, it has been observed that non-magnetic cation substitution mostly results in improvement of $(d\lambda/dH)_{\max}$ and deterioration of amplitude of magnetostriction [7-8, 7-9]. This is because non-magnetic cations substituted for cations in cobalt ferrite weaken the exchange interaction between the octahedral and tetrahedral sites and thus lower the magnetostriction amplitude but increase the strain derivative. A similar effect may be obtainable with deviation of oxygen from stoichiometric value resulting in vacancies in the spinel lattice.

In a recent study, the variation of magnetostrictive properties due to differences in heat treatments was associated to the variation in the degree of inversion due to the release of oxygen from the cobalt ferrite samples during sintering [7-4]. In this particular study, a similar trend was observed in which the amplitude of magnetostriction was low but the strain derivative was enhanced. It can thus be said that the samples used for this study may contain higher volume fraction of vacancies than those used in previous literature studies. Thus, the magnetostriction amplitude and strain derivative in cobalt ferrite samples depend both on cation composition/distribution and oxygen content. The variations in magnetostriction and strain derivative values reported in the literature for cobalt ferrite may be due to the levels of vacancies and thus the oxygen contents of the samples. EDX analysis usually employed in studying the composition of cobalt ferrite in different studies is not very sensitive to oxygen content.

References to Chapter 7:

- [7-1]. R. D. Greenough and E. W. Lee, "The magnetostriction of cobalt-manganese ferrite" *J. Phys. D* **3** (1970) 1595.
- [7-2]. S. D. Bhame and P. A. Joy "Tuning of the Magnetostrictive Properties of CoFe_2O_4 by Mn Substitution for Co" *J. Appl. Phys.* **100** (2006) 113911.
- [7-3]. G.A Sawatzky, F. Vam der Woude and A.H Morish "Mössbauer Study of Several Ferrimagnetic Spinel" *Phys. Rev.* **187** (1969) 747.
- [7-4]. S.D Bhame and P. A. Joy "Effects of sintering conditions and microstructure on the magnetostrictive properties of cobalt ferrite" *J. Am. Ceram. Soc.* **91** (2008) 1976.
- [7-5]. B. H. Liu, J. Ding, Z. L. Dong, C. B. Boothroyd, J. H. Yin, and J. B. Yi "Microstructural evolution and its influence on the magnetic properties of CoFe_2O_4 powders during mechanical milling" *Phys. Rev. B* **74** (2006) 184427.
- [7-6]. Himalay Basumatary, Mithun Palit, J. Arout Chelvane and S. Pandian, "Disorder trapping in gas quenched magnetostrictive Fe–Ga alloys" *Mat. Sci. Engr.* **167** (2010) 210.
- [7-7]. Arthur E. Clark, Marilyn Wun-Fogle, James B. Restorff, Thomas A. Lograsso, and James R. Cullen, "Effect of Quenching on the Magnetostriction of $\text{Fe}_{1-x}\text{Ga}_x$ (0:13 < x < 0:21)" *IEEE Trans. Mag.* **37** (2001) 2678.
- [7-8]. C. C. H. Lo "Compositional Dependence of the Magnetomechanical Effect in Substituted Cobalt Ferrite for Magnetoelastic Stress Sensors" *IEEE Trans. Magn.*, **43** (2007) 2367.
- [7-9]. S. H. Song, C. C. H. Lo, S. J. Lee, S. T. Aldini, J. E. Snyder and D. C. Jiles "Magnetic and magnetoelastic properties of Ga-substituted cobalt ferrite " *J. Appl. Phys.*, **101** (2007) 09C517.
- [7-10]. J. G. Na, T. D. Lee and S. J. Park "Effects of cation distribution on magnetic properties in cobalt ferrite" *J. Mat. Sci. Let.* **27** (1993) 961
- [7-11]. S. D. Bhame and P. A. Joy "Enhanced magnetostrictive properties of Mn substituted cobalt ferrite $\text{Co}_{1.2}\text{Fe}_{1.8}\text{O}_4$ " *J. Appl. Phys.* **99** (2006) 073901.
- [7-12]. S.D Bhame and P. A. Joy "Magnetic and magnetostrictive properties of manganese substituted cobalt ferrite" *J. Phys. D: Appl. Phys.* **40** (2007) 3263.

- [7-13]. Y. Chen, J. E. Snyder, C. R. Schwichtenberg, K. W. Dennis, R. W. McCallum, D. C. Jiles
"Metal-bonded Co-ferrite composites for magnetostrictive torque sensor applications" *IEEE Trans. on Magn.*, **35** (1999) 3652.
- [7-14]. D. J. Craik, *Magnetic Oxides, Part 1*, John Wiley & Sons; Ltd, (1975).

Chapter 8. Experimental Results and Discussion: Effect of Variation of Processing Parameters on Properties of Cobalt ferrite

8.1 Introduction

Preparation of cobalt ferrite for magnetostrictive applications involves different stages. Because the resultant properties depend on the cumulative contributions from each stage, it is possible to select the properties of cobalt ferrite for magnetoelastic application by altering the processing parameters. This is desirable because it offers the potential of controlling magnetostrictive properties without substitution of non magnetic cations. In this chapter, the results of a study on the dependence of the structural, magnetic and magnetostrictive properties of cobalt ferrite prepared by conventional ceramic methods are presented and discussed. The processing parameters of interest include sintering temperatures, holding times at sintering temperatures and powder compaction pressures. The samples used for this study were pressed at 87 MPa or 127 MPa, sintered in air at 1250, 1350 or 1450 °C and held at those temperatures for 24 or 36 hrs.

8.2 Determination of the Crystal Structure of the Samples

The crystal structures of the samples were studied by XRD. In the XRD pattern presented in Fig. 8.1, samples marked, B, C and D have the same compaction pressure and holding time but different sintering temperatures. Samples marked C and E have the same compaction pressure and sintering temperature but different holding times while samples marked A and C have the same sintering temperature and holding times but different compaction pressure. The peaks in the XRD pattern obtained for all the samples were consistent with that of a single phase spinel structure with no additional phases present. Moreover, the peak positions were not shifted relative to each other. The results indicate that variations in processing parameters did not change the crystal structures of the samples.

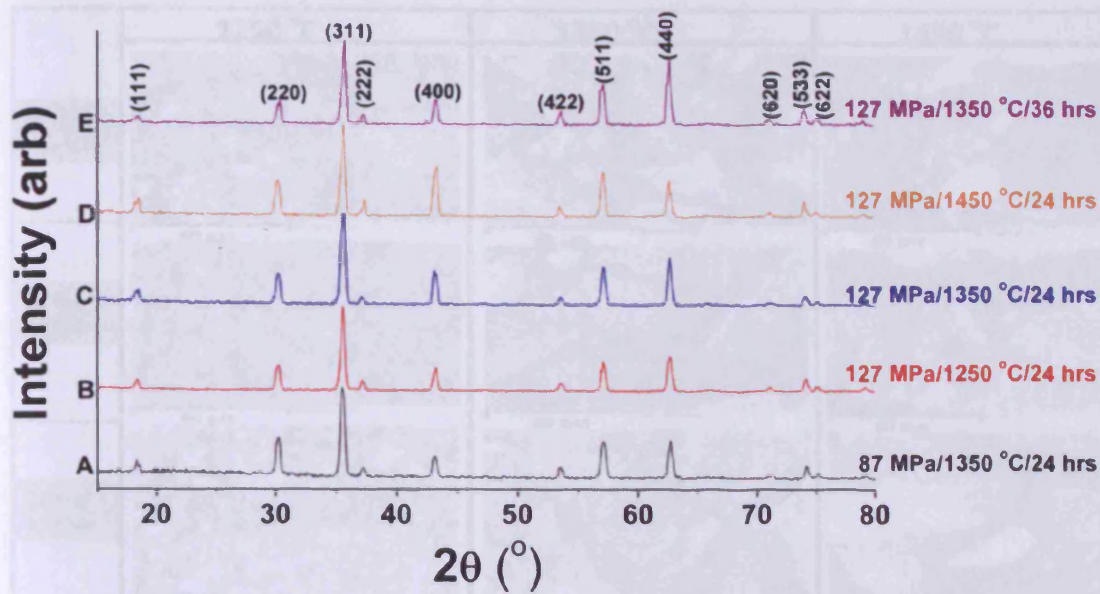


Fig. 8.1: X-ray diffraction patterns for a selected subset of representative samples showing the effect of varying sintering temperature (B, C and D), holding time (C and E) and powder compaction pressure (A and C).

8.3 Effect of Processing Parameters on Microstructure

The backscattered electron images of the samples are shown in the scanning electron micrographs in Fig. 8.2. The micrographs are of uniform appearance which indicates the presence of a single phase. This, together with the XRD results confirms that only a single spinel phase of cobalt ferrite was formed during sample fabrication. It is also seen from the micrographs that at any compaction pressure, an increase in sintering temperature and/or holding time results in an increase in both grain and pore sizes. This is because an increase in temperature and/or holding time provides the required energy for grain growth. Although sintering results in the reduction of pore density, in most sintered bodies especially in ceramics such as cobalt ferrite, pores are not totally eliminated. The consequence is a coalescence of adjacent pores with grain growth. With higher sintering temperatures and/or holding time, pores also acquire sufficient energy to migrate and coalesce.

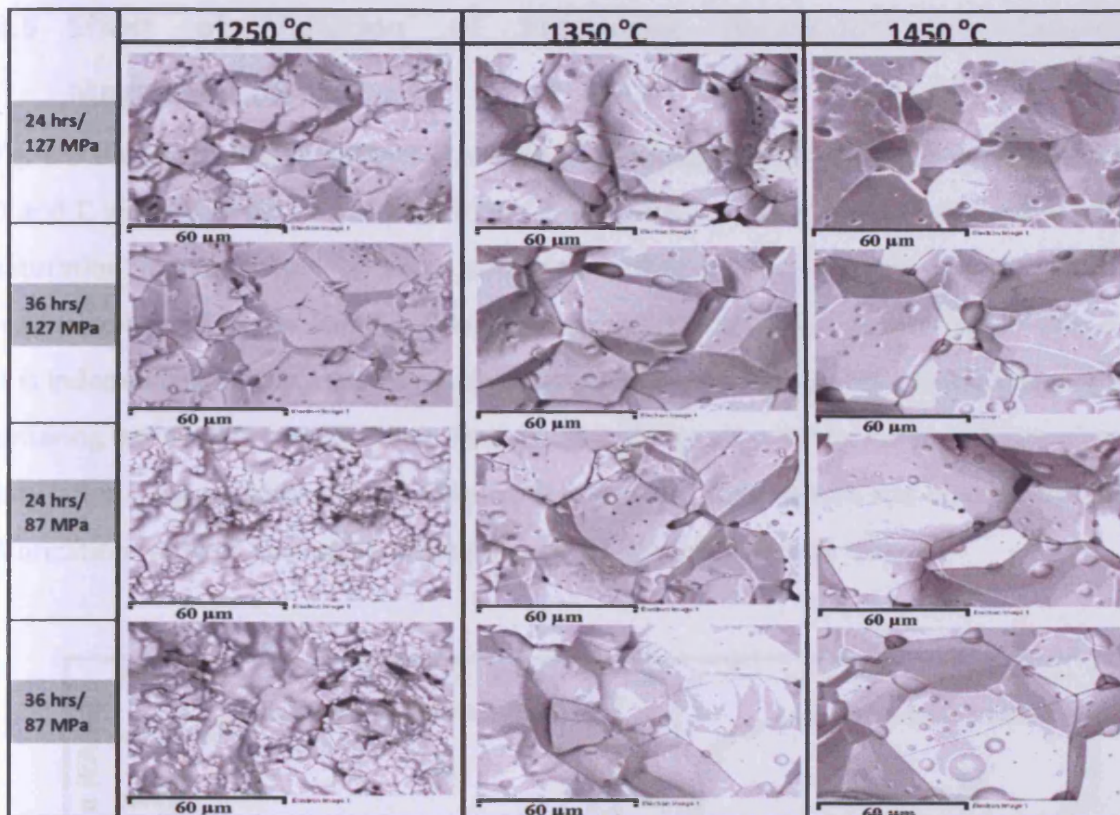


Fig. 8.2: Back scattered electron micrographs of samples after various sintering temperatures, holding times and powder compaction pressures for all the samples. Uniform image contrast indicates the presence of a single phase.

8.4 Composition of the samples

The Co:Fe ratios of the samples were determined by EDX analyses. The oxygen compositions of the samples were not determined by EDX because the sensitivity of EDX is not high enough for oxygen composition determination. Assuming the stoichiometric amount of oxygen (samples were sintered in air environment), the composition of the samples was $\text{Co}_{1.03}\text{Fe}_{1.97}\text{O}_4$ with the variation of cations in the range ± 0.01 . Any changes that were observed in the samples could be attributed to the differences in the microstructure, magnetic and magnetostrictive properties of the samples due to sample processing. This is because the samples are similar both in crystal structure and composition.

8.5 Effect of Variation of Processing Parameters on Saturation Magnetization

Fig. 8.3 shows the first quadrants of the hysteresis loops of the samples. Samples marked A, B and C were sintered at 1250 °C, 1350 °C and 1450 °C respectively. From the result, the saturation magnetization of each sample is within $\pm 1.8\%$ of the average saturation magnetization of all the samples. The similarity in their saturation magnetization shows that it is independent of the processing parameters including the powder compaction pressure, sintering temperature and holding time. This result agrees with the normal observation that saturation magnetization is insensitive to changes in microstructure and is unaffected by the fabrication route or any heat treatment performed on the sample [8-1].

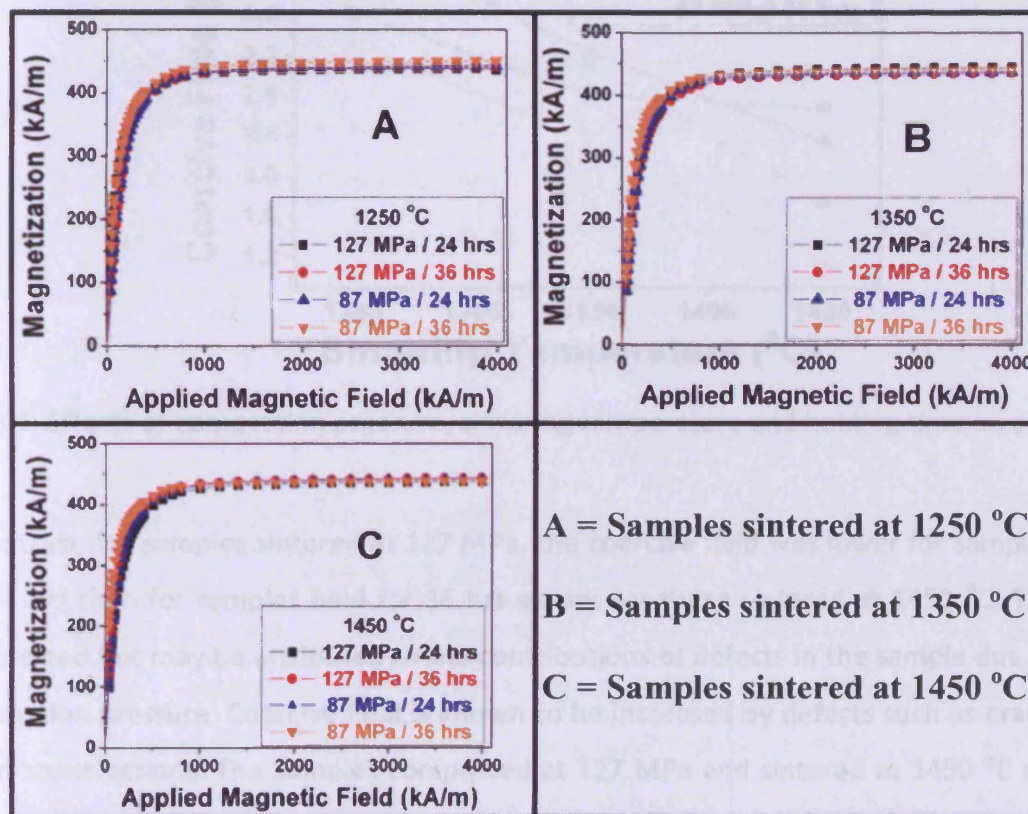


Fig. 8.3: First quadrants of the magnetization vs. hysteresis plots of the samples

8.6 Variation of Coercive Field due to Variation in Processing Parameters

Fig. 8.4 shows the dependence of the coercive field on the processing parameters of the samples. Varying only the sintering temperature and keeping the compaction pressure and holding time constant, the coercive field decreased in all the cases. This agrees with the observation from the backscattered electron micrographs because large grain sizes correspond to smaller coercive fields. For the same reason, samples compacted at 87 MPa showed a decreased coercive field with increase in holding time at any sintering temperature.

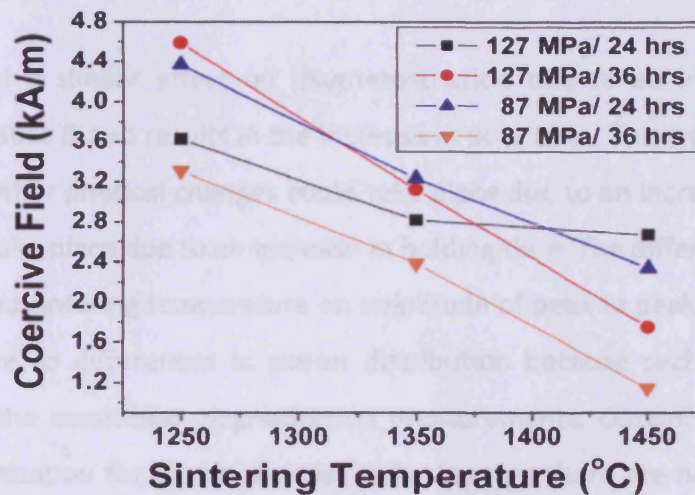


Fig. 8.4: Effects of compaction pressure, sintering temperature and holding time on coercive field

In contrast, for samples sintered at 127 MPa, the coercive field was lower for samples held for 24 hrs than for samples held for 36 hrs except for those sintered at 1450 °C. This was unexpected but may be attributed to the contributions of defects in the sample due to high compaction pressure. Coercive field is known to be increased by defects such as cracks and other imperfections. The samples compacted at 127 MPa and sintered at 1450 °C showed the expected trend because with increase in sintering temperature, the effect of grain growth in lowering coercive field outweighed the effect of defects. From these results, it can be seen that the coercive field was strongly dependent on processing parameter though the saturation magnetization was not.

8.7 Dependence of Magnetostriction on Processing Parameters

In Fig. 8.5, it can be seen that peak to peak magnetostriction amplitudes of the samples decreased with increase in holding time at any compaction pressure and sintering temperature. It is likely that the decrease in magnetostriction with holding time is a result of the increase in pore sizes of the samples with increase in holding time. With the presence of porosities, the measured strain is a contribution from the solid mass of the cobalt ferrite sample and air in the pores. Since the air in the pores would reduce the magnetostriction, it is obvious that with increase in size of the pores, the magnetostriction would decrease and vice versa.

One might expect a similar effect on magnetostriction due to an increase in sintering temperature, because it also results in the increase in pore sizes. This was not observed and is likely because other physical changes could take place due to an increase in temperature which might not take place due to an increase in holding time. The differences in the effects of holding time and sintering temperature on amplitude of peak to peak magnetostriction is unlikely to be due to differences in cation distribution because such would have been observable from the saturation magnetization measurements. Obtaining similar values of saturation magnetization for all the samples indicates that there are no substantial cation distribution differences in the samples.

The considerable variation in peak to peak magnetostriction as opposed to the slight variation in saturation magnetization shows that, although saturation magnetization is independent of processing route, magnetostriction strongly depends on it. This illustrates the facts that saturation magnetization is microstructure insensitive whereas in polycrystalline materials, magnetostriction will depend on the details of microstructure, defects, residual stresses and is also connected to mechanical properties. This may also explain the differences in the amplitudes of peak to peak magnetostriction reported for cobalt ferrite in various literatures [8-2, 8-3].

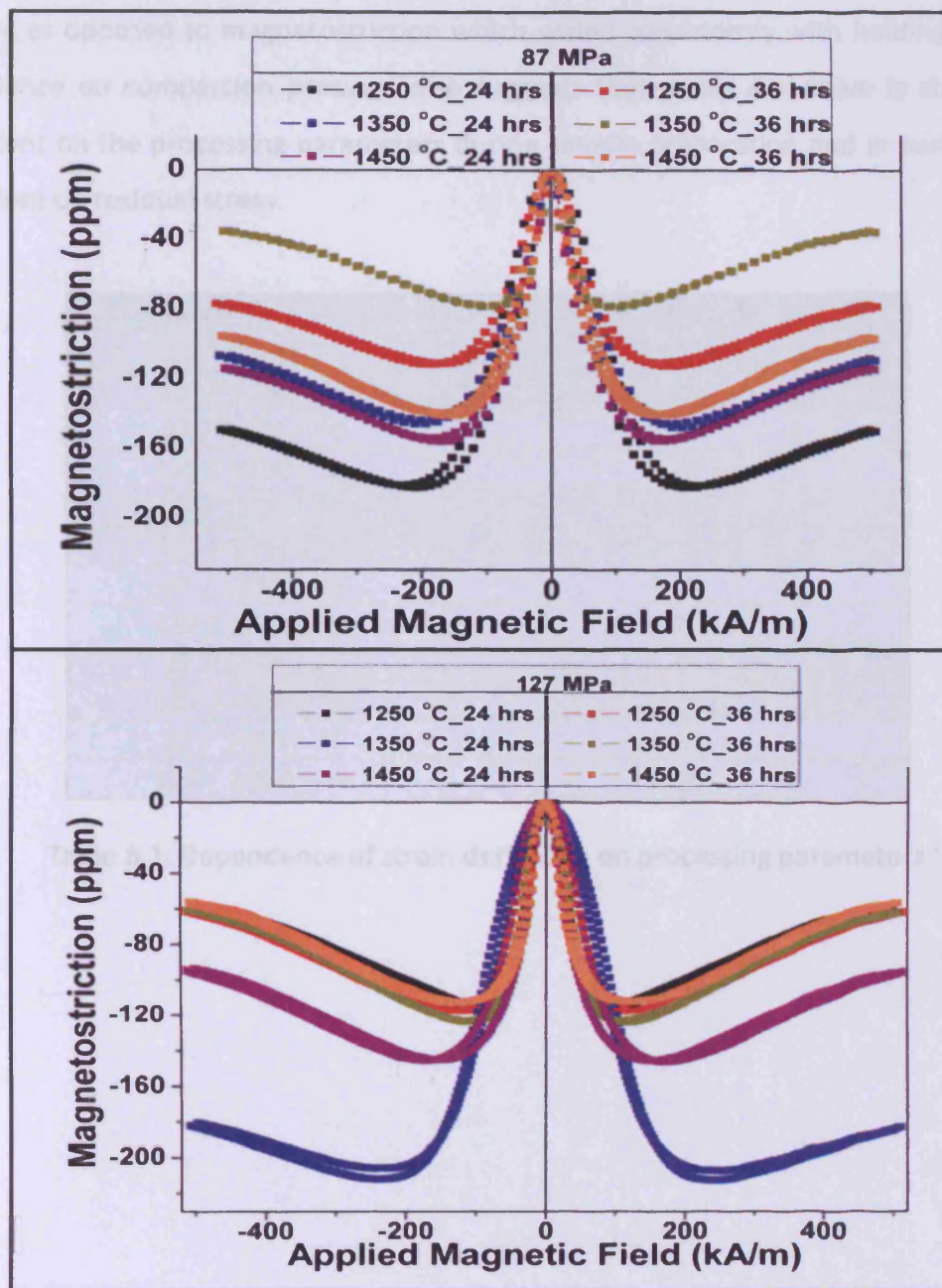


Fig. 8.5: Dependence of magnetostriction on processing parameters

8.8 Dependence of Strain Derivative on Processing Parameters

A summary of the dependence of strain derivative on processing parameters is shown in Table 8.1. It can be seen that the strain derivative varied consistently with compaction

pressure as opposed to magnetostriction which varied consistently with holding time. This dependence on compaction pressure also suggests that strain derivative is also strongly dependent on the processing parameters during sample preparation and in particular, it is dependent on residual stress.

Sample (MPa / °C / hrs)	Strain derivative ($\times 10^{-9} \text{ A}^{-1} \text{ m}$)
87 / 1250 / 24	1.31
127 / 1250 / 24	2.25
87 / 1250 / 36	1.75
127 / 1250 / 36	1.78
87 / 1350 / 24	1.23
127 / 1350 / 24	1.45
87 / 1350 / 36	1.84
127 / 1350 / 36	2.19
87 / 1450 / 24	1.89
127 / 1450 / 24	2.20
87 / 1450 / 36	1.65
127 / 1450 / 36	2.26

Table 8.1: Dependence of strain derivative on processing parameters

References to Chapter 8:

- [8-1]. R. M. Bozorth, *Ferromagnetism*, New York, USA: IEEE Press, (1993)
- [8-2]. J.G. Na, T.D Lee and S.J Park "Effects of cation distribution on magnetic properties of cobalt ferrite" *J. Mat. Sci. Lett.* **12** (1993) 961
- [8-3]. S.D Bham and P.A Joy, "Magnetic and Magnetostrictive Properties of Manganese substituted Cobalt ferrite" *Phys.D: Appl. Phys.* **40** (2007) 3263

Chapter 9. Experimental Results and Discussion: Structure, Magnetic and Magnetostrictive Properties of $\text{CoMe}_x\text{Fe}_{2-x}\text{O}_4$ (Me = Al, Ga and Ge/Co)

9.1 Introduction

Magnetic and magnetostrictive properties of cobalt ferrite can be improved by substitution of non-magnetic cations. Different non-magnetic cations have varying effects on the properties of cobalt ferrite due to their differences in preferences for either the octahedral or tetrahedral site and the strength of such preferences. A non-magnetic cation with strong octahedral site preference such as Mn^{3+} could alter the exchange coupling between both sites and also result in the displacement of some Co^{2+} out of the octahedral sites into the tetrahedral sites. Similarly substitution of a cation with strong tetrahedral site preference such as Ga^{3+} could lead to displacement of Co^{2+} out of the tetrahedral into the octahedral sites. In either case, the magnetocrystalline anisotropy and magnetostrictive properties of cobalt ferrite which are strongly dependent on the concentration and site occupancy of Co^{2+} would be altered. As a result, the desired properties for specific magnetomechanical applications can be tuned by selectively tailoring cation site occupancy via cation substitution.

In this chapter, the results of studies on the structure, magnetic and magnetostrictive properties of $\text{CoAl}_x\text{Fe}_{2-x}\text{O}_4$ and $\text{CoGa}_x\text{Fe}_{2-x}\text{O}_4$ are presented. Unlike most other non-magnetic cations, Al^{3+} has been said to have no defined preference for either the octahedral or tetrahedral sites of a spinel structure [9-1]. Thus, understanding the influence of substituting Al^{3+} compared with other non-magnetic cations such as Mn^{3+} and Ga^{3+} will shed more light on understanding the magnetic and magnetostrictive properties of cobalt ferrite. While Mn^{3+} has octahedral cation site preference, Ga^{3+} has a tetrahedral site preference. Al^{3+} like other non-magnetic (or to be precise, paramagnetic) cations should weaken the exchange interaction in cobalt ferrite which should result in lowering the magnetocrystalline

anisotropy and improving the strain derivative. Results from the studies on $\text{CoAl}_x\text{Fe}_{2-x}\text{O}_4$ and $\text{CoGa}_x\text{Fe}_{2-x}\text{O}_4$ are compared with the results from a study on $\text{Co}_{1+x}\text{Ge}_x\text{Fe}_{2-2x}\text{O}_4$.

9.1.1 Influence of Al^{3+} substitution on the crystal structure of cobalt ferrite

The crystal structures of all the Al-substituted samples were investigated by XRD. The XRD patterns shown in Fig. 9.1 indicate that the samples were of a single phase spinel structure. It can be seen from the patterns that no additional peaks are found although the peaks for the aluminium substituted samples were shifted relative the un-substituted sample indicating a change in the lattice parameter. The XRD pattern for the sample $x = 0.3$ is at the same position as that for $x = 0.0$. For the samples $x = 0.1$ and 0.2 , the XRD patterns were shifted to the lower 2θ while that for the samples $x = 0.5, 0.7$ and 0.9 were shifted to the higher 2θ relative to the sample $x = 0.0$. This shift indicates that substitution of Al^{3+} for Fe^{3+} results in changes in the lattice parameter of the spinel structure.

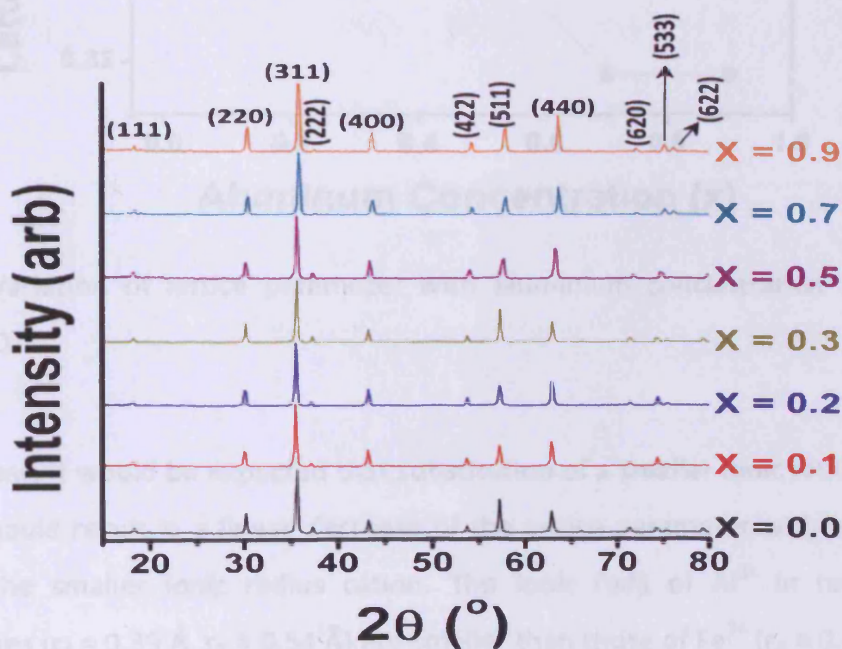


Fig. 9.1: XRD patterns showing the influence of Al^{3+} substitution on the crystal structure of cobalt ferrite. x is the proportion of Al^{3+} in $\text{CoAl}_x\text{Fe}_{2-x}\text{O}_4$

In order to confirm any changes in the lattice parameter of the spinel structure, [equation 5-12](#) was used to determine the lattice parameter. As shown in Fig. 9.2, with reference to the sample $x = 0.0$, the lattice parameters of the substituted samples initially increased from 8.38 \AA to 8.41 \AA and later decreased to 8.31 \AA with increase x . Relating Fig. 9.2 to Fig. 9.1, a shift to the lower 2θ corresponds to increase in lattice parameter while a shift to the higher 2θ corresponds to a decrease.

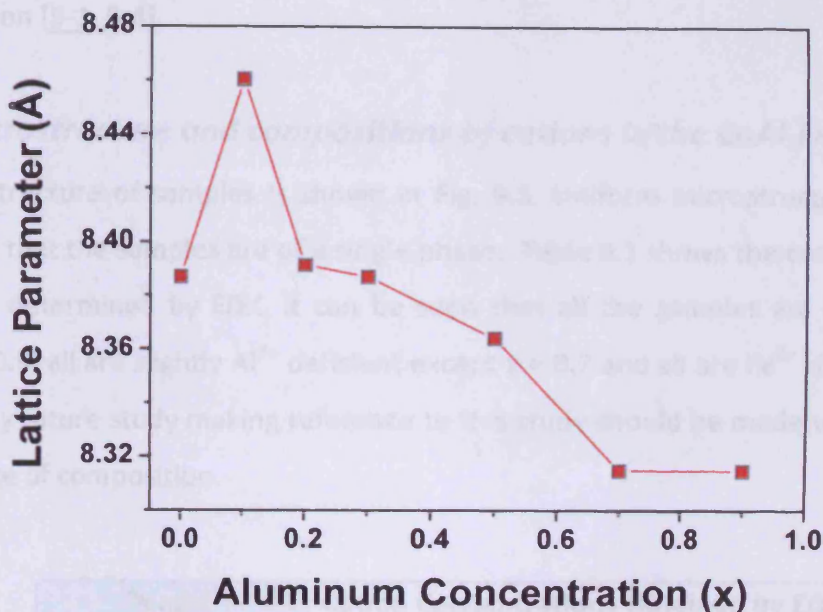


Fig. 9.2: Variation of lattice parameter with aluminium concentration (x) for $\text{CoAl}_x\text{Fe}_{2-x}\text{O}_4$

By Vegard's law, it would be expected that substitution of a smaller ionic radius cation for a larger one should result in a linear decrease of the lattice parameter with increase in the amount of the smaller ionic radius cation. The ionic radii of Al^{3+} in tetrahedral and octahedral sites ($r_A = 0.39 \text{ \AA}$, $r_B = 0.54 \text{ \AA}$) are smaller than those of Fe^{3+} ($r_A = 0.49 \text{ \AA}$, $r_B = 0.65 \text{ \AA}$) and Co^{2+} ($r_A = 0.58 \text{ \AA}$, $r_B = 0.74 \text{ \AA}$) [9-2]. As a result, whether Al^{3+} displaces Fe^{3+} or Co^{2+} from the lattice, by Vegard's law, a linear decrease in the lattice parameter would be expected with increase in Al^{3+} , which was not the case. The initial increase in lattice

parameter and subsequent decrease indicates non-linear changes in lattice parameters with Al^{3+} substitution which contradicts Vegard's law. Such a non-linear trend was reported for $\text{Co}_{1+x}\text{Si}_x\text{Fe}_{2-2x}\text{O}_4$ [9-3]. Similar to Al^{3+} , the ionic radii of Co^{2+} and Fe^{3+} in both cation sites are also larger than that of Si^{4+} . A possible cause of the observed trend might be changes in the rate at which Al^{3+} substitutes into the tetrahedral and octahedral sites with increase in Al^{3+} concentration. Al^{3+} has been reported to substitute into both cation sites, with a ratio that varies with Al^{3+} concentration. However it is not clear how this ratio changes with Al^{3+} concentration [9-1, 9-4].

9.1.2 Microstructure and compositions of cations in the $\text{CoAl}_x\text{Fe}_{2-x}\text{O}_4$ system

The microstructure of samples is shown in Fig. 9.3. Uniform microstructures confirm the XRD results that the samples are of a single phase. Table 9.1 shows the compositions of the samples as determined by EDX. It can be seen that all the samples are slightly Co^{2+} rich except $x = 0.9$, all are slightly Al^{3+} deficient except $x = 0.7$ and all are Fe^{3+} rich except $x = 0.3$ and 0.9 . Any future study making reference to this study should be made with samples of a similar range of composition.

Target Compositions	Cation Concentrations Obtained by EDX		
	Co	Al	Fe
CoFe_2O_4	1.02	-	1.98
$\text{CoAl}_{0.1}\text{Fe}_{1.9}\text{O}_4$	1.03	0.08	1.89
$\text{CoAl}_{0.2}\text{Fe}_{1.8}\text{O}_4$	1.03	0.18	1.79
$\text{CoAl}_{0.3}\text{Fe}_{1.7}\text{O}_4$	1.03	0.25	1.72
$\text{CoAl}_{0.5}\text{Fe}_{1.5}\text{O}_4$	1.03	0.49	1.48
$\text{CoAl}_{0.7}\text{Fe}_{1.3}\text{O}_4$	1.04	0.73	1.23
$\text{CoAl}_{0.9}\text{Fe}_{1.1}\text{O}_4$	0.99	0.87	1.14

Table 9.1: Concentration of cations in the $\text{CoAl}_x\text{Fe}_{2-x}\text{O}_4$ system as determined by EDX

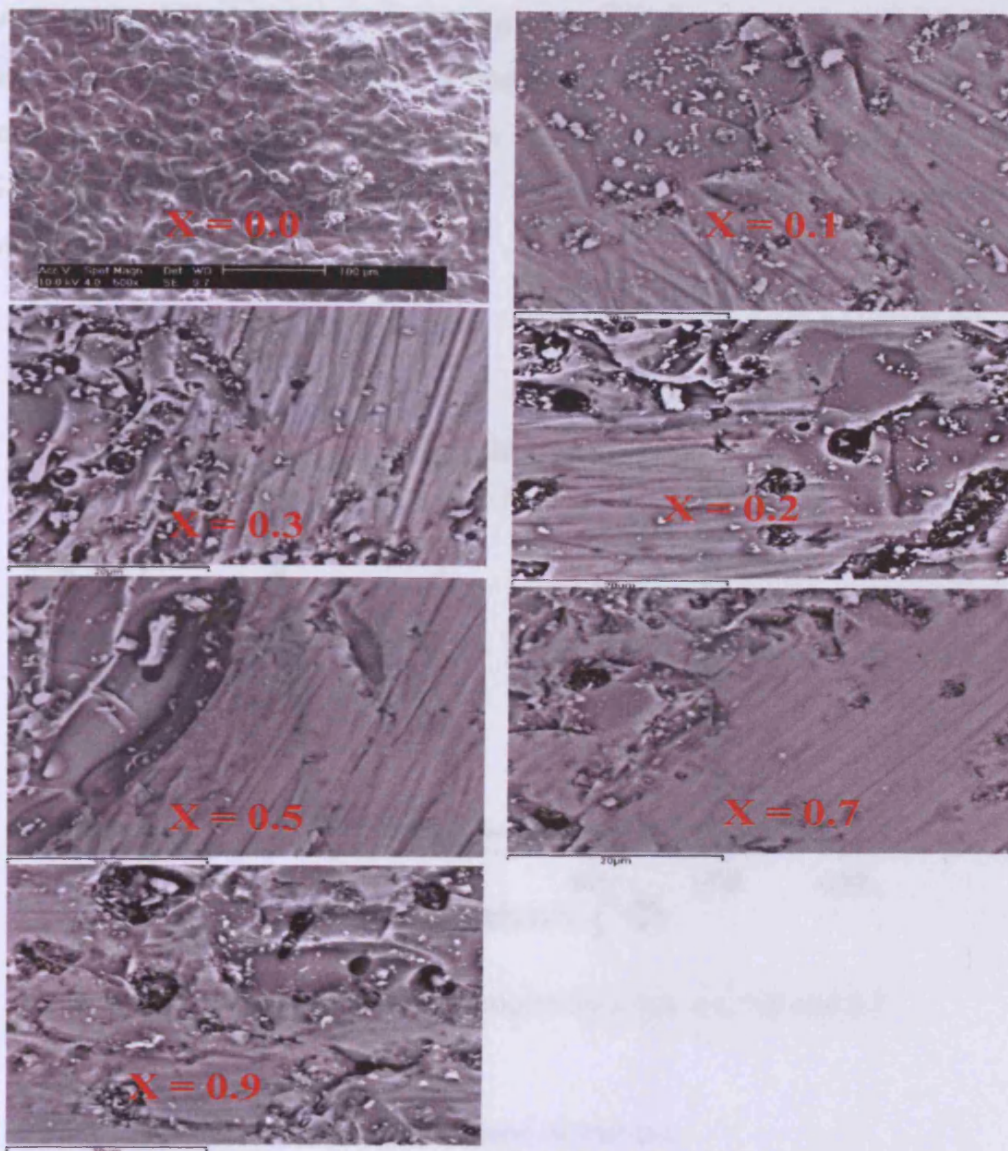


Fig. 9.3: Scanning electron micrographs for different aluminium compositions (x) for the $\text{CoAl}_x\text{Fe}_{2-x}\text{O}_4$ system

9.1.3 Curie temperature of the $\text{CoAl}_x\text{Fe}_{2-x}\text{O}_4$ system

The Curie temperature of the $\text{CoAl}_x\text{Fe}_{2-x}\text{O}_4$ system is shown in Fig. 9.4. As shown, it decreases with increase in the aluminium concentration. Super-exchange interaction keeps the magnetic moments aligned while thermal agitation results in disordering of the moments. Substitution of non-magnetic Al^{3+} for the magnetic Fe^{3+} weakens the super-

exchange interaction, thus lowering the thermal energy required to randomise magnetic moments. The consequence of this is the lowering of the Curie temperature with increase in Al^{3+} concentration, as observed in this study. In previous studies, substitution of Mn^{3+} , Cr^{3+} and Ga^{3+} also resulted in decrease in Curie temperature with increase in concentration of the substituted cation [9-5].

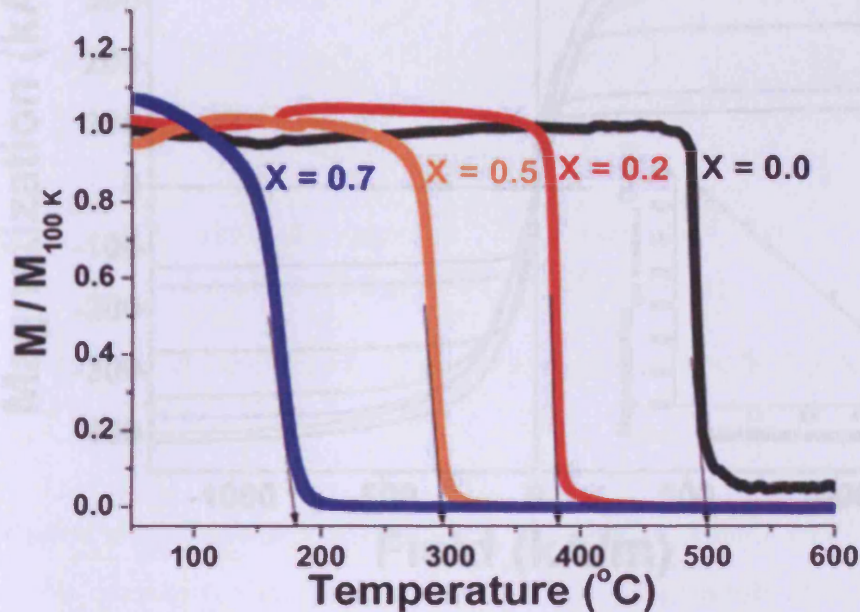


Fig. 9.4: Curie temperature of the samples for $X = 0.0, 0.2, 0.5$ and 0.7

9.1.4 Effect of Al^{3+} substitution on magnetization

Fig. 9.5 shows plots of magnetization against applied magnetic field and an inset of magnetization value at 1250 kA/m (maximum magnetization) measured at 300 K as a function of aluminium concentration. Maximum magnetization decreased approximately linearly with increasing aluminium concentration. Since Al^{3+} is thought to substitute into both cation sites, an equal substitution of Al^{3+} into both sites should result in no significant changes in the net magnetization. The significant change in maximum magnetization observed probably indicates that Al^{3+} substitutes into the cation sites at different rates. An understanding of the site distribution and the rate of substitution into the cation sites can

be obtained by Mossbauer study, which is beyond the scope of the present study. The lowering of the Curie temperature with aluminium substitution will also cause the room temperature magnetization to decrease.

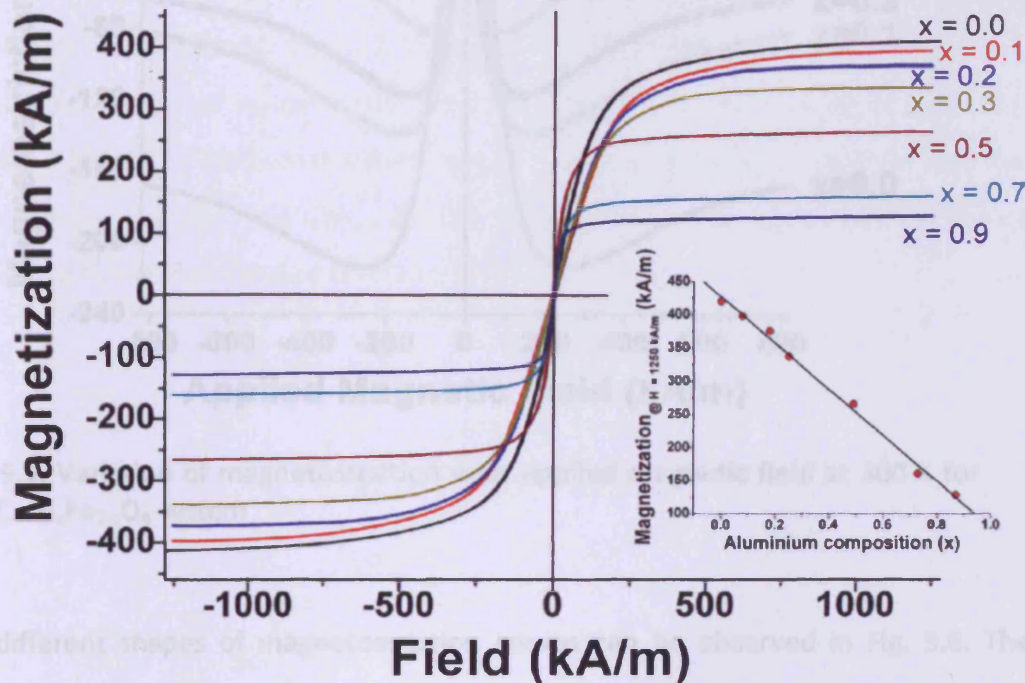


Fig. 9.5: Plots of magnetization against applied magnetic field. The inset is a plot of magnetization at 1250 kA/m as a function of Al^{3+} concentration at 300 K.

9.1.5 Variation of magnetostriction of $\text{CoAl}_x\text{Fe}_{2-x}\text{O}_4$ as a function of Al^{3+} concentration

Peak to peak magnetostriction amplitude decreased with increase in Al^{3+} concentration as shown in Fig. 9.6. The figure also shows that the magnetic field value required for the magnetostriction amplitude also decreased with increase in aluminium concentration. This decrease is likely due to lowering of magnetocrystalline anisotropy with increase in Al^{3+} concentration. Though the magnetostriction amplitude decreased, amplitudes of magnetostriction between 30 ppm and 100 ppm are still sufficient for applications such as linear displacement sensors [9-6].

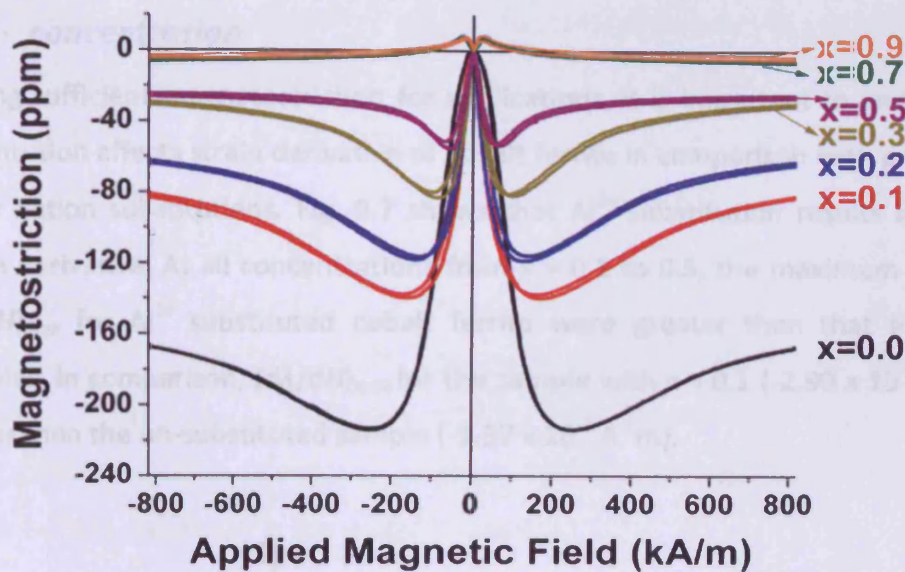


Fig. 9.6: Variation of magnetostriction with applied magnetic field at 300 K for the $\text{CoAl}_x\text{Fe}_{2-x}\text{O}_4$ system

Two different shapes of magnetostriction curves can be observed in Fig. 9.6. The shape observed for aluminium concentrations $x = 0.0$ to 0.5 is one in which the slope of the magnetostriction curve was initially positive and finally negative with increase in the applied field. For aluminium concentration $x = 0.7$ and 0.9 , the shape is one in which the slopes were initially positive and finally negative. This reversal in the sign of the slope indicates either a change in sign of the both magnetostriction constants of cobalt ferrite (λ_{111} and λ_{100}) or a change in sign of the first cubic magnetocrystalline anisotropy constant with increase in aluminium concentration. From these results, it can be seen that the magnetostrictive properties of cobalt ferrite depend strongly on the cations in the lattice and can be tuned by varying the cation concentration.

9.1.6 Variation of strain derivative of $\text{CoAl}_x\text{Fe}_{2-x}\text{O}_4$ as a function of Al^{3+} concentration

Having sufficient magnetostriction for applications, it is important to understand how Al^{3+} substitution affects strain derivative of cobalt ferrite in comparison with previous studies on other cation substitutions. Fig. 9.7 shows that Al^{3+} substitution results in the increase of strain derivative. At all concentrations from $x = 0.1$ to 0.5 , the maximum strain derivatives $(d\lambda/dH)_{\text{max}}$ for Al^{3+} substituted cobalt ferrite were greater than that for un-substituted samples. In comparison, $(d\lambda/dH)_{\text{max}}$ for the sample with $x = 0.1$ ($-2.90 \times 10^{-9} \text{ A}^{-1}\text{m}$) was 110% higher than the un-substituted sample ($-1.37 \times 10^{-9} \text{ A}^{-1}\text{m}$).

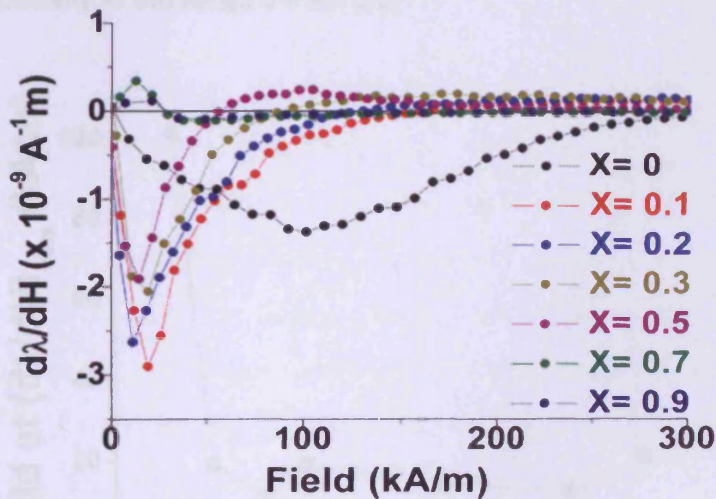


Fig. 9.7: Variation of strain derivative with applied magnetic field at 300 K for the $\text{CoAl}_x\text{Fe}_{2-x}\text{O}_4$ system ($x = 0.0$ to 0.9)

This increase in strain derivative is a demonstration of the application potentials of Al^{3+} substituted cobalt ferrite for magnetomechanical device developments. The increase in strain derivative is because the substitution of non-magnetic Al^{3+} for Fe^{3+} in cobalt ferrite reduces the magnetocrystalline anisotropy by weakening the super-exchange interaction between the tetrahedral and octahedral sites. Previous studies show that a decrease in magnetocrystalline anisotropy in cobalt ferrite was responsible for an increase in strain derivative [9-7].

Fig. 9.8 shows that less magnetic field was required to obtain the maximum value of $d\lambda/dH$ for Al^{3+} substituted cobalt ferrite samples than for the un-substituted sample. The magnetic fields required to obtain the high $(d\lambda/dH)_{\max}$ for $\text{CoAl}_{0.1}\text{Fe}_{1.9}\text{O}_4$ and $\text{CoAl}_{0.2}\text{Fe}_{1.8}\text{O}_4$ were respectively 81% and 89% less than required for un-substituted cobalt ferrite. The response of a magnetomechanical stress sensor to applied stress $dB/d\sigma$ is related to $d\lambda/dH$ [9-8] which shows that $(d\lambda/dH)_{\max}$ is a figure of merit for stress sensor applications. For applications in which $\text{CoAl}_x\text{Fe}_{2-x}\text{O}_4$ has sufficient magnetostriction amplitude, its high $(d\lambda/dH)_{\max}$ value at low applied magnetic field demonstrate that it is more promising for the development of higher sensitivity magnetomechanical stress sensors than un-substituted cobalt ferrites, especially in the range $0 < x \leq 0.2$.

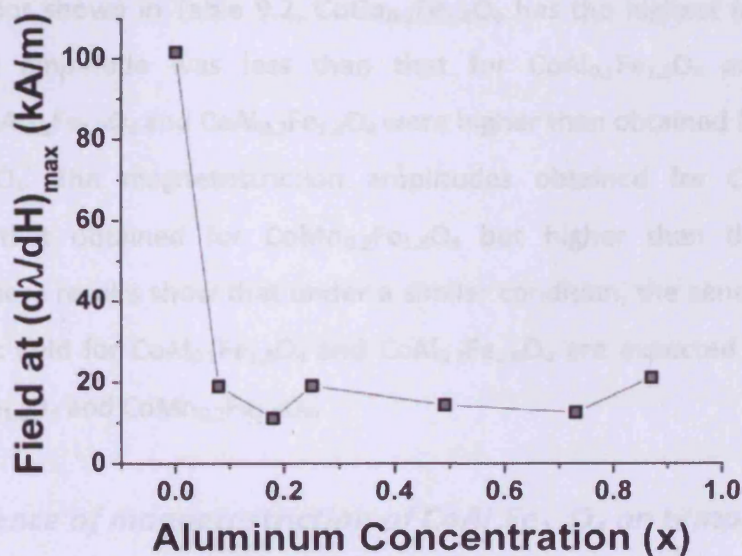


Fig. 9.8: Applied magnetic field at maximum strain derivative $(d\lambda/dH)_{\max}$ as a function of aluminium concentration. The field at $(d\lambda/dH)_{\max}$ are 101 kA/m, 19 kA/m and 11 kA/m for $x = 0.0, 0.1$ and 0.2 respectively.

Table 9.2 is a comparative summary of the magnetostrictive properties of $\text{CoAl}_x\text{Fe}_{2-x}\text{O}_4$ with $\text{CoMn}_x\text{Fe}_{2-x}\text{O}_4$, $\text{CoCr}_x\text{Fe}_{2-x}\text{O}_4$ [9-7] and $\text{CoGa}_x\text{Fe}_{2-x}\text{O}_4$ [9-5]. The highest amplitudes of $(d\lambda/dH)_{\max}$ and their corresponding magnetostriction amplitudes for $\text{CoMn}_x\text{Fe}_{2-x}\text{O}_4$ and $\text{CoGa}_x\text{Fe}_{2-x}\text{O}_4$ were obtained at $x = 0.2$. For $\text{CoCr}_x\text{Fe}_{2-x}\text{O}_4$, the highest $(d\lambda/dH)_{\max}$ at $x = 0.4$.

Sample Composition	Magnetostriction λ (ppm)	Strain-field derivative $(d\lambda/dH)_{\max}$ ($\times 10^{-9} \text{ A}^{-1}\text{m}$)
CoFe_2O_4	-212	-1.37
$\text{CoAl}_{0.1}\text{Fe}_{1.9}\text{O}_4$	-140	-2.9
$\text{CoAl}_{0.2}\text{Fe}_{1.8}\text{O}_4$	-120	-2.63
$\text{CoMn}_{0.2}\text{Fe}_{1.8}\text{O}_4$	-150	-2.5
$\text{CoCr}_{0.4}\text{Fe}_{1.8}\text{O}_4$	-70	-2.0
$\text{CoGa}_{0.2}\text{Fe}_{1.8}\text{O}_4$	-100	-3.2

Table 9.2: Comparison of the magnitude of λ and $(d\lambda/dH)_{\max}$ in $\text{CoAl}_x\text{Fe}_{2-x}\text{O}_4$, $\text{CoMn}_x\text{Fe}_{2-x}\text{O}_4$ [9-7], $\text{CoCr}_x\text{Fe}_{2-x}\text{O}_4$ [9-7] and $\text{CoGa}_x\text{Fe}_{2-x}\text{O}_4$ [9-5].

Of all compositions shown in Table 9.2, $\text{CoGa}_{0.2}\text{Fe}_{1.8}\text{O}_4$ has the highest $(d\lambda/dH)_{\max}$ but the magnetostriction amplitude was less than that for $\text{CoAl}_{0.1}\text{Fe}_{1.8}\text{O}_4$ and $\text{CoAl}_{0.2}\text{Fe}_{1.8}\text{O}_4$. $(d\lambda/dH)_{\max}$ for $\text{CoAl}_{0.1}\text{Fe}_{1.8}\text{O}_4$ and $\text{CoAl}_{0.2}\text{Fe}_{1.8}\text{O}_4$ were higher than obtained for $\text{CoMn}_{0.2}\text{Fe}_{1.8}\text{O}_4$ and $\text{CoCr}_{0.2}\text{Fe}_{1.8}\text{O}_4$. The magnetostriction amplitudes obtained for $\text{CoAl}_{0.1}\text{Fe}_{1.8}\text{O}_4$ was comparable to that obtained for $\text{CoMn}_{0.2}\text{Fe}_{1.8}\text{O}_4$ but higher than that obtained for $\text{CoCr}_{0.2}\text{Fe}_{1.8}\text{O}_4$. These results show that under a similar condition, the sensitivity of strain to applied magnetic field for $\text{CoAl}_{0.1}\text{Fe}_{1.8}\text{O}_4$ and $\text{CoAl}_{0.2}\text{Fe}_{1.8}\text{O}_4$ are expected to be more than that for $\text{CoCr}_{0.2}\text{Fe}_{1.8}\text{O}_4$ and $\text{CoMn}_{0.2}\text{Fe}_{1.8}\text{O}_4$.

9.1.7 Dependence of magnetostriction of $\text{CoAl}_x\text{Fe}_{2-x}\text{O}_4$ on temperature [(x = 0.0, 0.2, 0.5, 0.7) and (T = 50, 150, 250 and 350 K)]

Having shown in comparison with other cation substituted cobalt ferrite samples that $\text{CoAl}_x\text{Fe}_{2-x}\text{O}_4$ is a potential candidate for high sensitivity magnetoelastic applications, it is important to study how the magnetoelastic properties of $\text{CoAl}_x\text{Fe}_{2-x}\text{O}_4$ would vary with temperature. Fig. 9.9 compares the variation of magnetostriction vs. applied field of the aluminium substituted samples with those of the un-substituted samples.

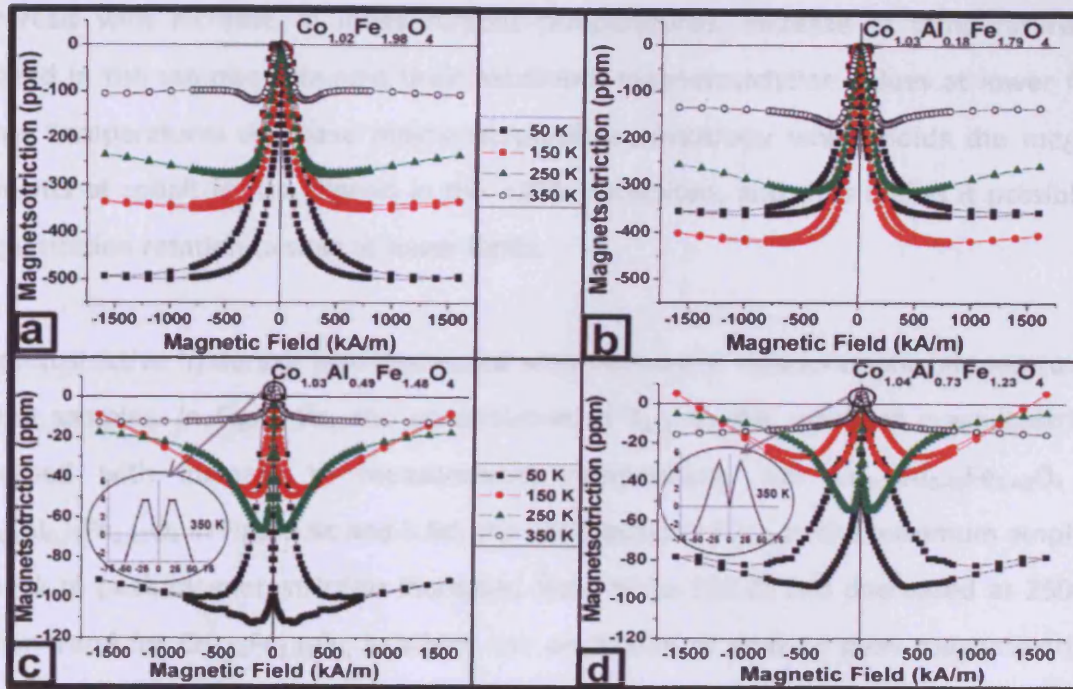


Fig. 9.9 : Magnetostriction vs. field plots for $\text{CoAl}_x\text{Fe}_{2-x}\text{O}_4$ system measure at different temperatures of 50, 150, 250 and 350 K. (a) $\text{Co}_{1.02}\text{Fe}_{1.98}\text{O}_4$ (b) $\text{Co}_{1.03}\text{Al}_{0.18}\text{Fe}_{1.79}\text{O}_4$, (c) $\text{Co}_{1.03}\text{Al}_{0.49}\text{Fe}_{1.48}\text{O}_4$ and (d) $\text{Co}_{1.04}\text{Al}_{0.73}\text{Fe}_{1.23}\text{O}_4$

In Fig. 9.9a, peak to peak magnetostriction amplitude decreases as the temperature approaches the Curie point. This is because during measurement, as the temperature approaches the Curie point, in addition to producing magnetostrictive strain in the samples, the magnetic energy is also used to overcome the contributions from anisotropy and thermal energies. As the measurement temperature deviates from the Curie temperature, the thermal contribution, and hence the energy required for the applied magnetic field to produce magnetostrictive strain reduces. The result is an increase in magnetostriction with a decrease in measurement temperature.

It can also be seen for $\text{Co}_{1.02}\text{Fe}_{1.98}\text{O}_4$ that, as the measurement temperature increased, magnetostrictive hysteresis decreased. Since hysteresis are mainly due to material imperfections, these results suggest that higher temperatures reduce the tendency of imperfections to cause magnetostrictive hysteresis thus resulting in lower magnetostrictive

hysteresis with increase in measurement temperatures. Increase in temperature also resulted in the samples attaining their maximum magnetostriction values at lower fields. Higher temperatures decrease magnetocrystalline anisotropy which holds the magnetic moments of cobalt ferrite aligned in the $\langle 100 \rangle$ directions, and thus makes it possible for magnetization rotation to start at lower fields.

Magnetostrictive hysteresis also decreased with increase in measurement temperature for all the samples. In Fig. 9.9b, the contribution of λ_{111} to the resultant magnetostriction increased with increase in measurement temperature. For $\text{Co}_{1.03}\text{Al}_{0.49}\text{Fe}_{1.48}\text{O}_4$ and $\text{Co}_{1.04}\text{Al}_{0.73}\text{Fe}_{1.23}\text{O}_4$ in Figs. 9.9c and 9.9d, the contribution of λ_{111} to the maximum amplitude of peak to peak magnetostriction increased from 50 to 150 K; and decreased at 250 K. A similar trend for $\text{Co}_{1.02}\text{Fe}_{1.98}\text{O}_4$, in which the amplitude of peak to peak magnetostriction decreased with increasing temperature, was not observed for the substituted samples. Rather, for $\text{Co}_{1.03}\text{Al}_{0.18}\text{Fe}_{1.79}\text{O}_4$, the amplitude of peak to peak magnetostriction initially increased in the range 50 to 150 K and finally decreased in the range 250 to 350 K. For $\text{Co}_{1.03}\text{Al}_{0.49}\text{Fe}_{1.48}\text{O}_4$ and $\text{Co}_{1.04}\text{Al}_{0.73}\text{Fe}_{1.23}\text{O}_4$, it decreased from 50 to 150 K, increased at 250 K and finally decreased at 350 K. The reason for this difference between the substituted and un-substituted samples is not clear but it demonstrates that the magnetostrictive characteristics of cobalt ferrite can be altered by cation substitution.

Also, for $\text{Co}_{1.03}\text{Al}_{0.49}\text{Fe}_{1.48}\text{O}_4$ and $\text{Co}_{1.04}\text{Al}_{0.73}\text{Fe}_{1.23}\text{O}_4$, at or below 250 K, as the applied magnetic field increases from zero, the slope of the magnetostriction curve was initially negative but became positive at high fields. The inset in Figs. 9.9c and 9.9d, shows that at 350 K, as the applied magnetic field increases from zero, the slope was positive at lower field values but negative at higher fields. This trend is opposite below 250 K and shows that at 350 K, λ_{111} is dominant at lower fields. It might be that the anisotropy coefficient changes sign or that both magnetostriction coefficients of cobalt ferrite, λ_{100} and λ_{111} changed sign at 350 K. It was observed that this change in sign of the slopes of magnetostriction curve started at 300 K for $\text{Co}_{1.04}\text{Al}_{0.73}\text{Fe}_{1.23}\text{O}_4$ as shown in Fig. 9.6 and at 350 K for

$\text{Co}_{1.03}\text{Al}_{0.49}\text{Fe}_{1.48}\text{O}_4$. This shows that magnetostriction in cobalt ferrite is both concentration and temperature dependent. It also shows that the slope of magnetostriction can be tuned within the temperature range of interest by adjusting the composition.

9.1.8 Dependence of strain derivative of $\text{CoAl}_x\text{Fe}_{2-x}\text{O}_4$ on temperature [(x = 0.0, 0.2, 0.5, 0.7) and (T = 50, 150, 250 and 350 K)]

The dependence of the maximum strain derivative, $(d\lambda/dH)_{\text{max}}$ of the $\text{CoAl}_x\text{Fe}_{2-x}\text{O}_4$ system on temperature variation is shown in Fig. 9.10.

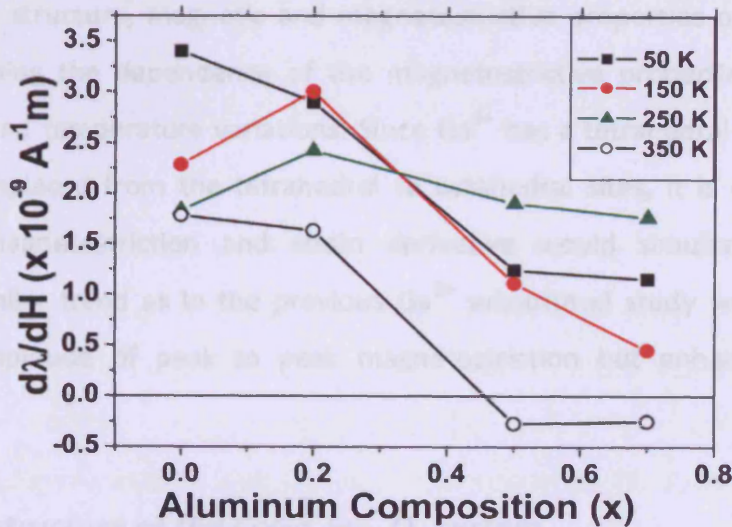


Fig. 9.10: Variation of strain sensitivity with concentration for the $\text{CoAl}_x\text{Fe}_{2-x}\text{O}_4$ system (x = 0, 0.2, 0.5 and 0.7)

At 50 K, $(d\lambda/dH)_{\text{max}}$ decreased with increase in aluminium concentration. At 150 K and 250 K, $(d\lambda/dH)_{\text{max}}$ initially increased from x = 0.0 to 0.2 and decreased at higher values of x. A similar trend was observed in previous studies on cation substituted cobalt ferrite samples in which the $(d\lambda/dH)_{\text{max}}$ initially increased at lower concentrations of the substituted cations (x ≤ 0.2) and finally decreased at higher cation concentrations [9-7, 9-5]. Measurement at 350 K also showed that $(d\lambda/dH)_{\text{max}}$ decreased with increase in aluminium concentration. The results obtained from this study showed that at temperatures of interest, it is possible to

tailor the magnetostrictive properties of cobalt ferrite for different applications by cation substitution.

9.2 Structure, Magnetic and Magnetostrictive Properties of $\text{CoGa}_x\text{Fe}_{2-x}\text{O}_4$

In section 9.1, the results of a study on the structure, magnetic and magnetostrictive properties of $\text{CoAl}_x\text{Fe}_{2-x}\text{O}_4$ were presented and compared with other substituted cobalt ferrite studies including $\text{CoGa}_x\text{Fe}_{2-x}\text{O}_4$. Although the magnetostrictive properties of $\text{CoGa}_x\text{Fe}_{2-x}\text{O}_4$ have been previously studied [9-5], the temperature dependence of magnetostrictive properties of $\text{CoGa}_x\text{Fe}_{2-x}\text{O}_4$ has not been reported. In this section, the variations in the structure, magnetic and magnetostrictive properties of $\text{CoGa}_x\text{Fe}_{2-x}\text{O}_4$ are presented including the dependence of the magnetostrictive properties on both cation concentrations and temperature variations. Since Ga^{3+} has a tetrahedral site preference, if Co^{2+} ions are displaced from the tetrahedral to octahedral sites, it is expected that the amplitude of magnetostriction and strain derivative would simultaneously increase. Otherwise, a similar trend as in the previous Ga^{3+} substituted study would be obtained: reduction in amplitude of peak to peak magnetostriction but enhancement in strain derivative.

9.2.1 Crystal structure of the $\text{CoGa}_x\text{Fe}_{2-x}\text{O}_4$ system

X-ray diffraction patterns of the samples are shown in Fig. 9.11. The patterns only have peaks which are consistent with the cubic spinel phase. The patterns for the Ga^{3+} substituted samples are not shifted relative to the un-substituted sample as was the case of $\text{CoAl}_x\text{Fe}_{2-x}\text{O}_4$. This indicates that the lattice parameters of the samples were similar. The lattice parameter was found to be 8.38 Å for all the samples. The preservation of the lattice parameter for $\text{CoGa}_x\text{Fe}_{2-x}\text{O}_4$ in contrast with the $\text{CoAl}_x\text{Fe}_{2-x}\text{O}_4$ system is because the ionic radii of Ga^{3+} in tetrahedral and octahedral positions ($r_A = 0.47$ Å, $r_B = 0.62$ Å) are similar to those of Fe^{3+} ($r_A = 0.49$ Å, $r_B = 0.65$ Å). Therefore, substituting Ga^{3+} for Fe^{3+} is expected to have a less significant effect on the lattice parameter than the substitution of the Al^{3+} with much smaller ionic radii ($r_A = 0.39$ Å, $r_B = 0.54$ Å).

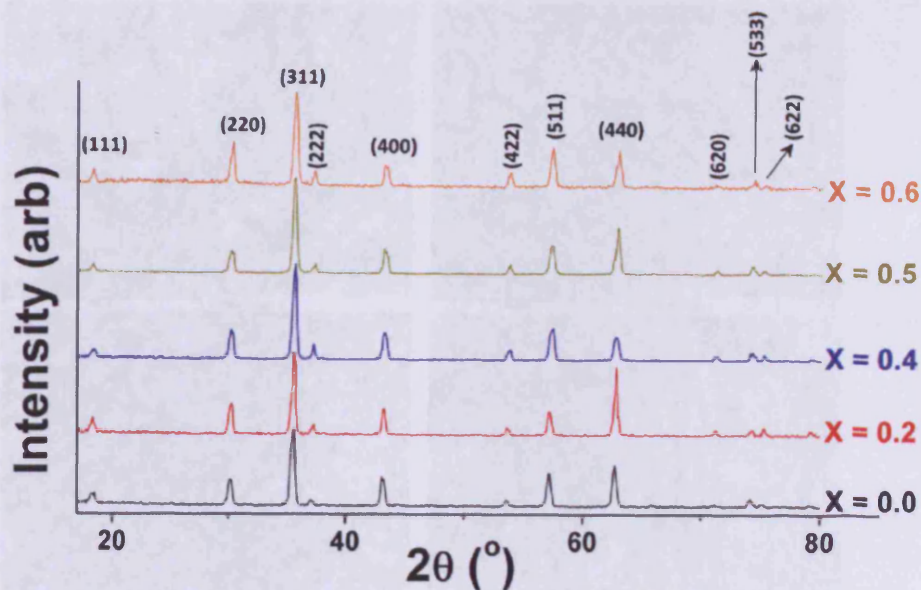


Fig. 9.11: XRD patterns of the $\text{CoGa}_x\text{Fe}_{2-x}\text{O}_4$ samples ($x = 0.0, 0.2, 0.4, 0.5$ and 0.6)

9.2.2 Composition of cations and microstructure of the $\text{CoGa}_x\text{Fe}_{2-x}\text{O}_4$ system

Table 9.3 shows the concentration of the samples determined by EDX. As shown, the obtained concentrations are cobalt rich but they are close to those targeted. Fig. 9.12 shows the backscattered electron images of the samples. The uniformity in contrast observed for all the samples further confirms that all have single phase crystal structure. It also shows that they are of uniform compositions because the image contrast in a backscattered electron image is a function of composition.

Target Compositions	Cation Concentrations as Determined by EDX		
	Co	Ga	Fe
CoFe_2O_4	1.02	-	1.98
$\text{CoGa}_{0.2}\text{Fe}_{1.8}\text{O}_4$	1.04	0.2	1.76
$\text{CoGa}_{0.4}\text{Fe}_{1.6}\text{O}_4$	1.03	0.39	1.58
$\text{CoGa}_{0.5}\text{Fe}_{1.5}\text{O}_4$	1.04	0.47	1.49
$\text{CoGa}_{0.6}\text{Fe}_{1.4}\text{O}_4$	1.03	0.58	1.39

Table 9.3: Concentrations of the cations in $\text{CoGa}_x\text{Fe}_{2-x}\text{O}_4$ system as determined by EDX

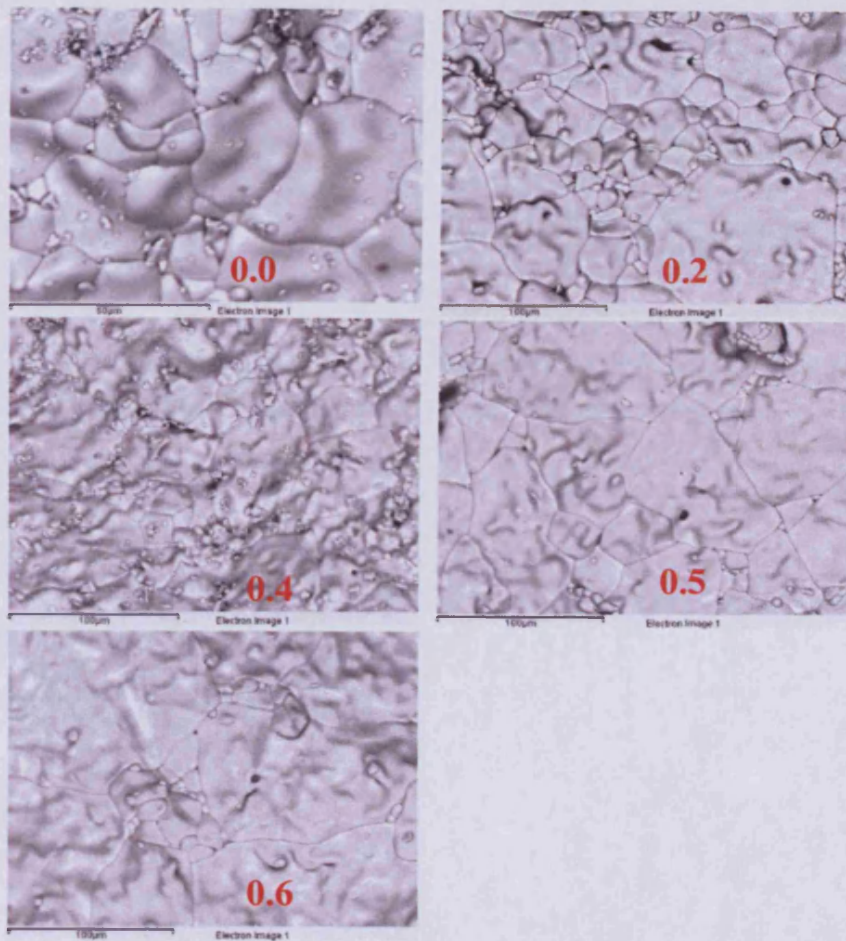


Fig. 9.12: Backscattered electron images of the $\text{CoGa}_x\text{Fe}_{2-x}\text{O}_4$

9.2.3 Variation of magnetization at 300 K as a function of Ga^{3+} substitution

The variation of magnetization with applied magnetic field is shown in Fig. 9.13. The inset shows the influence of Ga^{3+} substitution on saturation magnetization. In contrast with Al^{3+} substitution, the saturation magnetization of the Ga^{3+} substituted cobalt ferrite initially increases at $x = 0.2$ and later decreases at higher values of x . The saturation magnetization at $x = 0.4$ is also higher than that at $x = 0.0$. The increase in saturation magnetization with Ga^{3+} substitution is in agreement with Ga^{3+} having tetrahedral site preference. Since the moments of the tetrahedral sites (A-sites) and octahedral sites (B-sites) couple antiferromagnetically in cobalt ferrite, the net magnetization will be $M_B - M_A$. Substituting non-magnetic Ga^{2+} into the tetrahedral sites for Fe^{3+} reduces the moment of the tetrahedral

sites (M_A), thus the net magnetization of the substituted cobalt ferrite increases. The consequence will be the increase in saturation magnetization as observed.

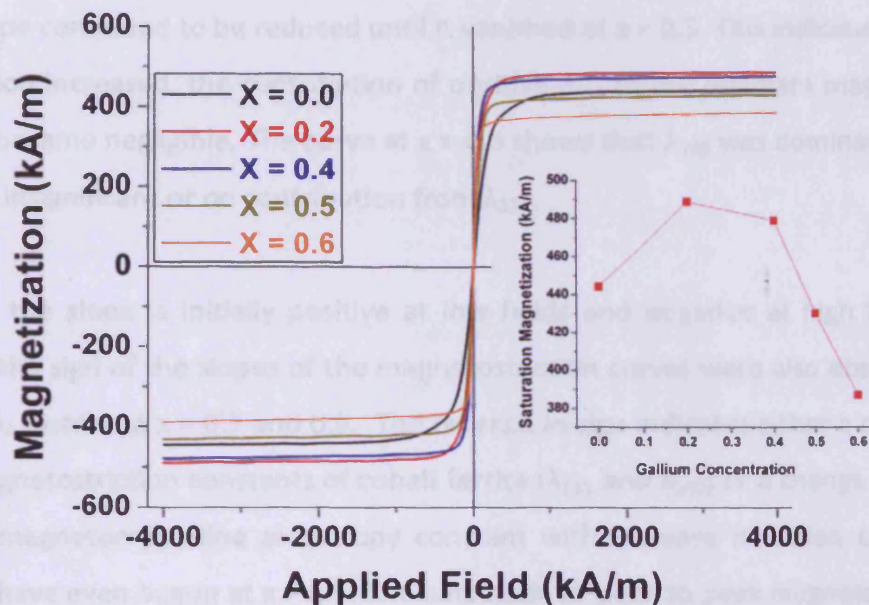


Fig. 9.13: Variation of magnetization at 300 K as a function of applied field for Ga^{3+} concentrations $x = 0.0$ to 0.6 . The inset shows the variation of saturation magnetization at 300 K with gallium concentration.

One would expect the saturation magnetization to increase further at higher Ga^{3+} substitution, which is not the case. It is important to state that although Ga^{3+} has tetrahedral site preference, some The higher the concentration of the substituted Ga^{3+} , the lower the Curie temperature becomes such that at higher Ga^{3+} concentrations, the room temperature significantly compares to the Curie temperature. The resultant effect would be a reduction in the saturation magnetization.

9.2.4 Room temperature magnetostriction studies on $\text{CoGa}_x\text{Fe}_{2-x}\text{O}_4$

Fig. 9.14 shows the dependence of magnetostriction on variation of Ga^{3+} concentration. It can be seen that for samples with concentration $x = 0.0$ (a typical magnetostriction curve of un-substituted cobalt ferrite samples), the slope of the magnetostriction curve is initially negative at low fields, peaked at intermediate fields and then became positive at high

magnetic field values. With Ga^{3+} substitution, the slopes of the curves changed indicating a strong influence of Ga^{3+} substitution for Fe^{3+} on magnetoelastic properties of cobalt ferrite. As Ga^{3+} concentration increased from $x = 0.2$ to 0.5 , the high field regions of the curves with positive slope continued to be reduced until it vanished at $x = 0.5$. This indicates that as Ga^{3+} concentration increased, the contribution of positive λ_{111} to the resultant magnetostriction amplitude became negligible. The curve at $x = 0.5$ shows that λ_{100} was dominant at all fields with either insignificant or no contribution from λ_{111} .

At $x = 0.6$, the slope is initially positive at low fields and negative at high fields. Similar reversal in the sign of the slopes of the magnetostriction curves were also observed for the $\text{CoAl}_x\text{Fe}_{2-x}\text{O}_4$ system at $x = 0.7$ and 0.9 . The reversal in sign indicates either a change in sign of both magnetostriction constants of cobalt ferrite (λ_{111} and λ_{100}) or a change in sign of the first cubic magnetocrystalline anisotropy constant with increase in cation concentration. This might have even begun at $x = 0.5$. The amplitude of peak to peak magnetostriction also decreased with increase in Ga^{3+} substitution.

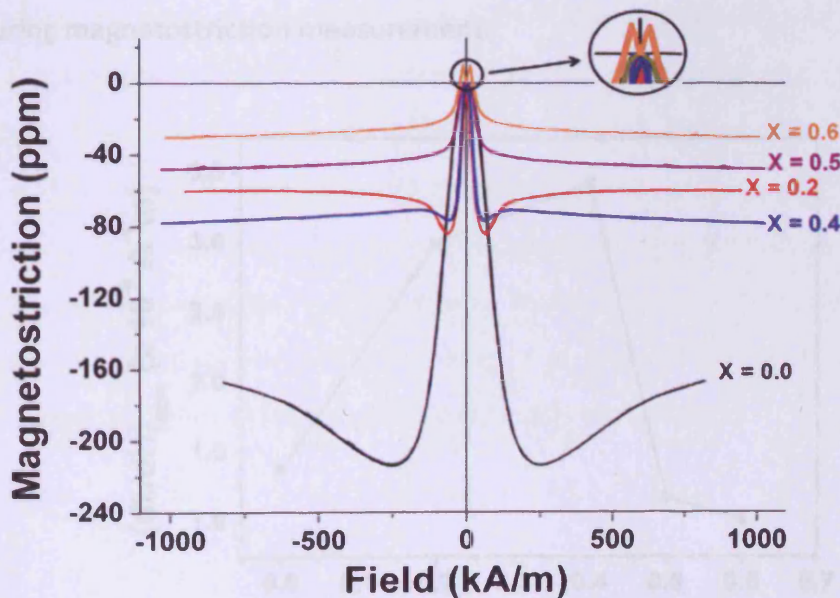


Fig. 9.14: Variation of magnetostriction as a function of applied field for $\text{CoGa}_x\text{Fe}_{2-x}\text{O}_4$

9.2.5 Dependence of maximum strain derivative of $\text{CoGa}_x\text{Fe}_{2-x}\text{O}_4$ on Ga^{3+} concentration

Ga^{3+} substitution for Fe^{3+} significantly improved the strain derivative of cobalt ferrite beyond that observed for the $\text{CoAl}_x\text{Fe}_{2-x}\text{O}_4$ system. The $(d\lambda/dH)_{\text{max}}$ for the $\text{CoAl}_x\text{Fe}_{2-x}\text{O}_4$ system ($2.9 \times 10^{-9} \text{ m}^{-1}\text{A}$) was obtained for the concentration $x = 0.2$ but Fig. 9.15 shows that $(d\lambda/dH)_{\text{max}}$ of $3.4 \times 10^{-9} \text{ m}^{-1}\text{A}$ was obtained for $\text{CoGa}_x\text{Fe}_{2-x}\text{O}_4$ system at $x = 0.4$. Compared to un-substituted sample, Ga^{3+} substitution at $x = 0.4$ resulted in more than 150 % increase in strain derivative.

As shown in Table 9.4, the increase in strain derivative with Ga^{3+} substitution was 18 % greater than Al^{3+} , 37 % greater than Mn^{3+} and 71 % greater than Cr^{3+} [9-7] cation substitution studies, respectively. The maximum $(d\lambda/dH)_{\text{max}}$ in this study was obtained at $x = 0.4$ in contrast to a previous study on the $\text{CoGa}_x\text{Fe}_{2-x}\text{O}_4$ system in which the maximum $(d\lambda/dH)_{\text{max}}$ of $3.2 \times 10^{-9} \text{ m}^{-1}\text{A}$ was obtained at $x = 0.2$. Maximum $(d\lambda/dH)_{\text{max}}$ for the $\text{CoCr}_x\text{Fe}_{2-x}\text{O}_4$ system was also obtained at $x = 0.4$. The observed increase in strain derivative might be due to decrease in magnetocrystalline anisotropy following Ga^{3+} substitution. Lower anisotropy makes it easier to rotate the magnetization when a magnetic field is applied during magnetostriction measurement.

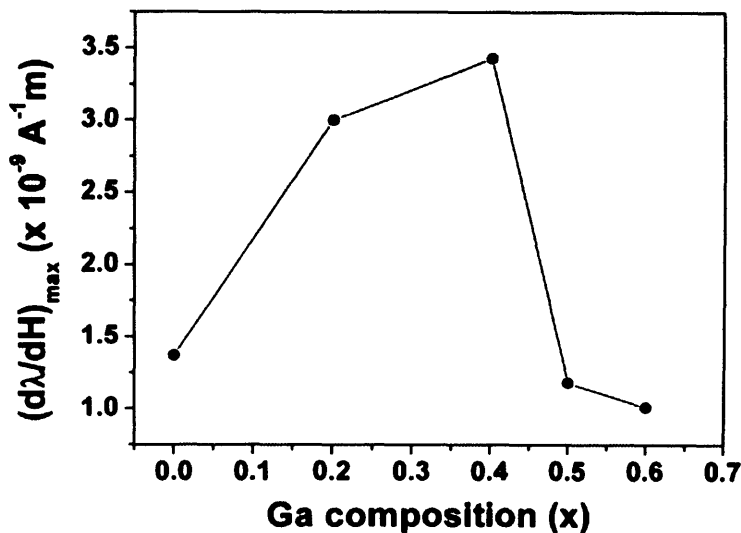


Fig. 9.15: Variation of maximum strain derivative as a function of applied field for

Concentration	Strain-field derivative $(d\lambda/dH)_{\max}$ ($\times 10^{-9} \text{ A}^{-1}\text{m}$)
$\text{CoAl}_{0.1}\text{Fe}_{1.9}\text{O}_4$ (Present Study)	-2.9
$\text{CoMn}_{0.2}\text{Fe}_{1.8}\text{O}_4$ (Previous Study)	-2.5
$\text{CoCr}_{0.4}\text{Fe}_{1.6}\text{O}_4$ (Previous Study)	-2
$\text{CoGa}_{0.2}\text{Fe}_{1.8}\text{O}_4$ (Previous Study)	-3.2
$\text{CoGa}_{0.4}\text{Fe}_{1.6}\text{O}_4$ (Present Study)	-3.4

Table 9.4: Comparison of the $(d\lambda/dH)_{\max}$ in $\text{CoAl}_x\text{Fe}_{2-x}\text{O}_4$, $\text{CoMn}_x\text{Fe}_{2-x}\text{O}_4$ [7], $\text{CoCr}_x\text{Fe}_{2-x}\text{O}_4$ [7] and $\text{CoGa}_x\text{Fe}_{2-x}\text{O}_4$ [9]. Sample from this study is shown in red font while those from previous studies are in black font.

9.2.6 Temperature dependence of magnetostriction in $\text{CoGa}_x\text{Fe}_{2-x}\text{O}_4$ system

[(x = 0.0, 0.2, 0.4) and (T = 50, 150, 250 and 350 K)]

As shown in Fig. 9.16a for un-substituted cobalt ferrite samples, peak to peak magnetostriction amplitude increased with decrease in the measurement temperature. In all the samples, the slope of the high field region of the magnetostriction curve was initially low at 50 K, increased at 150 K and decreased at higher measurement temperatures. Also, in Fig. 9.16a, it is seen that the contribution of λ_{111} to the resultant magnetostriction increased with increase in measurement temperature. It can be seen from all the results that increase in temperature reduces the magnetostrictive hysteresis. Magnetostrictive hysteresis is mainly caused by the difficulty to rotate magnetization past imperfections in the samples. This difficulty reduces with increase in thermal energy, making it possible to have less magnetostrictive hysteresis with increase in temperature.

9.2.7 Temperature dependence of strain derivative of $\text{CoGa}_x\text{Fe}_{2-x}\text{O}_4$ system

[(x = 0.0, 0.2, 0.4) and (T = 50, 150, 250 and 350 K)]

Fig. 9.17 shows the variation of $(d\lambda/dH)_{\max}$ of $\text{CoGa}_x\text{Fe}_{2-x}\text{O}_4$ with temperature. At all temperatures studied except 250 K, $(d\lambda/dH)_{\max}$ decreased with increase in temperature.

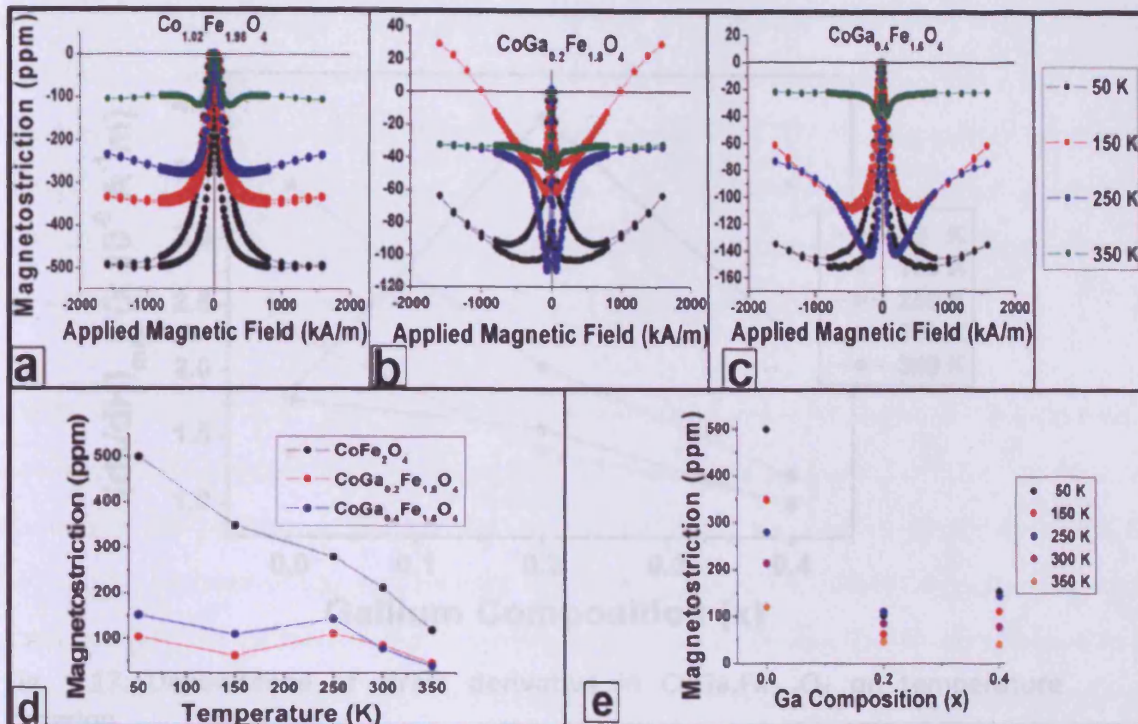


Fig. 9.16: Dependence of magnetostriction in $\text{CoGa}_x\text{Fe}_{2-x}\text{O}_4$ on temperature variation

In both $\text{CoGa}_{0.2}\text{Fe}_{1.8}\text{O}_4$ (Fig. 9.16b) and $\text{CoGa}_{0.4}\text{Fe}_{1.6}\text{O}_4$ (Fig. 9.16c), magnetostriction measured at 250 K is higher than when measured at 150 K. A similar result was obtained for the magnetostriction of $\text{CoAl}_x\text{Fe}_{2-x}\text{O}_4$ at $x = 0.5$ and 0.7 . This result shows that the substitution of Ga^{3+} for Fe^{3+} alters the magnetostrictive behaviour of cobalt ferrite even at different temperatures as shown in Fig. 9.16d. It could also be seen in Fig. 4d that under temperature variations, the magnetostriction of $\text{CoGa}_x\text{Fe}_{2-x}\text{O}_4$ is more stable than CoFe_2O_4 which could be essential for sensor applications. In Fig. 4e, it appears that $\text{CoGa}_{0.2}\text{Fe}_{1.8}\text{O}_4$ is more stable with temperature variation than $\text{CoGa}_{0.4}\text{Fe}_{1.6}\text{O}_4$.

9.2.7 Temperature dependence of strain derivative of $\text{CoGa}_x\text{Fe}_{2-x}\text{O}_4$ system

$[(x = 0.0, 0.2, 0.4) \text{ and } (T = 50, 150, 250 \text{ and } 350 \text{ K})]$

Fig. 9.17 shows the variation of $(d\lambda/dH)_{\text{max}}$ of $\text{CoGa}_x\text{Fe}_{2-x}\text{O}_4$ with temperature. At all temperatures studied except 250 K, $(d\lambda/dH)_{\text{max}}$ decreased with increase in gallium concentration.

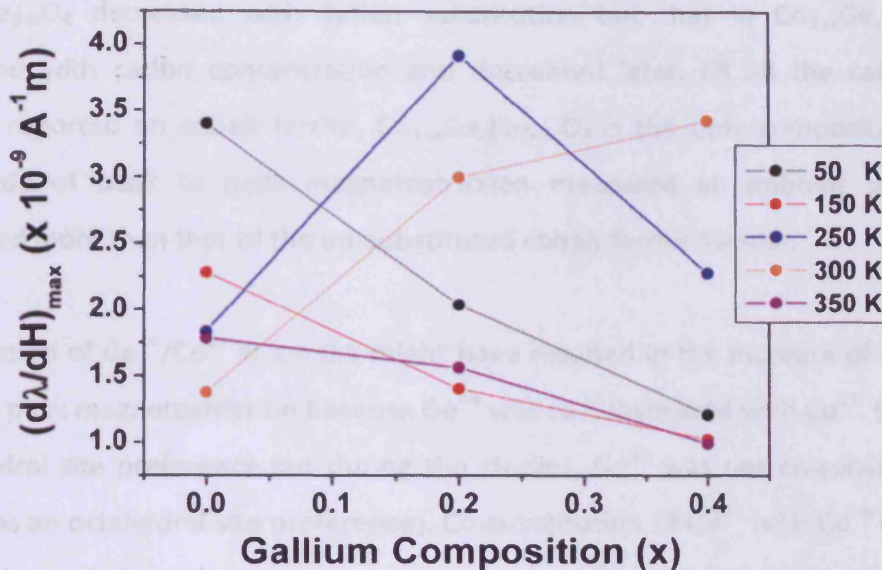


Fig. 9.17: Dependence of strain derivative in $\text{CoGa}_x\text{Fe}_{2-x}\text{O}_4$ on temperature variation

As in the case of Al^{3+} substituted cobalt ferrite, at 250 K, $(d\lambda/dH)_{\text{max}}$ initially increased from $x = 0.0$ to 0.2 and decreased after. This is similar to the observation at 300 K except that the maximum $(d\lambda/dH)_{\text{max}}$ was at $x = 0.4$ rather than 0.2. A similar trend was observed in previous studies on cation substituted cobalt ferrite samples in which the $(d\lambda/dH)_{\text{max}}$ initially increased at lower concentrations of the substituted cations ($x \leq 0.2$) and finally decreased at higher cation concentrations. The figure also shows that with cation substitution, the maximum strain derivative is in the temperature range, 250 to 300 K. These results demonstrate the capability to alter the magnetomechanical performance to suit intended applications by adjusting composition at different temperatures.

9.3 Comparison of 300 K Magnetostrictive Properties of $\text{CoAl}_x\text{Fe}_{2-x}\text{O}_4$, $\text{CoGa}_x\text{Fe}_{2-x}\text{O}_4$ and $\text{Co}_{1+x}\text{Ge}_x\text{Fe}_{2-2x}\text{O}_4$

Fig. 9.18 summarizes the variation of magnetostriction of $\text{Co}_{1+x}\text{Ge}_x\text{Fe}_{2-2x}\text{O}_4$, $\text{CoAl}_x\text{Fe}_{2-x}\text{O}_4$ and $\text{CoGa}_x\text{Fe}_{2-x}\text{O}_4$ with cation variation at ambient temperature. The highest magnetostriction of all the substituted samples was obtained for $\text{Co}_{1+x}\text{Ge}_x\text{Fe}_{2-2x}\text{O}_4$ at $x = 0.1$ as shown in Fig.

9.18A. Fig. 9.18B shows that the maximum magnetostriction in $\text{CoAl}_x\text{Fe}_{2-x}\text{O}_4$ and $\text{CoGa}_x\text{Fe}_{2-x}\text{O}_4$ decreased with cation substitution but that in $\text{Co}_{1+x}\text{Ge}_x\text{Fe}_{2-2x}\text{O}_4$ initially increased with cation concentration and decreased later. Of all the cation substitution studies reported on cobalt ferrite, $\text{Co}_{1+x}\text{Ge}_x\text{Fe}_{2-2x}\text{O}_4$ is the only composition in which the amplitude of peak to peak magnetostriction measured at ambient temperature was increased more than that of the un-substituted cobalt ferrite sample.

Substitution of $\text{Ge}^{4+}/\text{Co}^{2+}$ at $x = 0.1$ might have resulted in the increase of the amplitude of peak to peak magnetostriction because Ge^{4+} was co-substituted with Co^{2+} . Ge^{4+} like Ga^{3+} has tetrahedral site preference but during the studies, Ga^{3+} was not co-substituted with Co^{2+} (Co^{2+} has an octahedral site preference). Co-substitution of Ge^{4+} with Co^{2+} was necessary to attain charge balance between the cations and might have resulted in an increase in the concentration of Co^{2+} on the octahedral sites; which is known to be responsible for the high magnetostriction amplitude in cobalt ferrite. Increase in the concentration of the substituted Ge^{4+} might have significantly weakened the exchange coupling and thus resulted in decreased amplitude of peak to peak magnetostriction.

For all the compositions, it was observed that as the amount of the substituted cation increased, the field at which the maximum magnetostriction amplitude was obtained reduced as can be seen in Fig. 9.18A. Also, in Fig. 9.18B, it can be seen that the rate of decrease in magnetostriction amplitude with increase in substitution was least for $\text{CoAl}_x\text{Fe}_{2-x}\text{O}_4$ and $\text{CoGa}_x\text{Fe}_{2-x}\text{O}_4$ compared to $\text{Co}_{1+x}\text{Ge}_x\text{Fe}_{2-2x}\text{O}_4$ which shows that $\text{Ge}^{4+}/\text{Co}^{2+}$ co-substitution has a stronger effect on the amplitude of peak to peak magnetostriction than Al^{3+} or Ga^{3+} substitution.

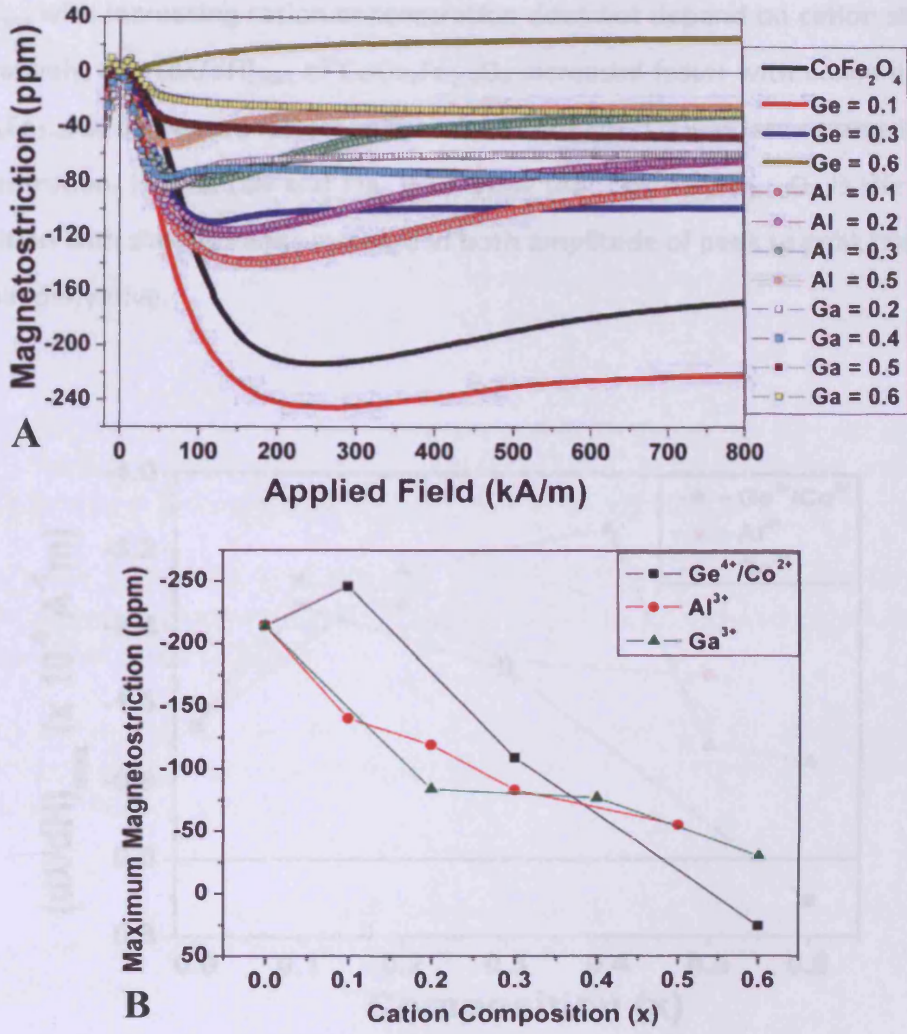


Fig. 9.18: Comparison of ambient temperature magnetostriction of $\text{Co}_{1+x}\text{Ge}_x\text{Fe}_{2-2x}\text{O}_4$, $\text{CoAl}_x\text{Fe}_{2-x}\text{O}_4$ and $\text{CoGa}_x\text{Fe}_{2-x}\text{O}_4$

The $(d\lambda/dH)_{\text{max}}$ of $\text{CoAl}_x\text{Fe}_{2-x}\text{O}_4$, $\text{CoGa}_x\text{Fe}_{2-x}\text{O}_4$ and $\text{Co}_{1+x}\text{Ge}_x\text{Fe}_{2-2x}\text{O}_4$ are plotted against composition in Fig. 9.19. Compared with un-substituted cobalt ferrite, all the samples showed an initial increase in $(d\lambda/dH)_{\text{max}}$ which afterwards decreased with cation substitution. A similar result was obtained for $\text{CoMn}_x\text{Fe}_{2-x}\text{O}_4$ and $\text{CoCr}_x\text{Fe}_{2-x}\text{O}_4$ [9-9]. The similarity in the trend with which $(d\lambda/dH)_{\text{max}}$ varies with concentration for Ga^{3+} and Ge^{4+} (cations with tetrahedral site preference); Mn^{3+} and Ga^{3+} (cations with octahedral site preference); and Al^{3+} (cation with no defined site preference) indicates that the variation of

$(d\lambda/dH)_{\max}$ with increasing cation concentration does not depend on cation site preference. Comparatively, the $(d\lambda/dH)_{\max}$ of $\text{CoGa}_x\text{Fe}_{2-x}\text{O}_4$ increased faster with concentration, that of $\text{Co}_{1-x}\text{Ge}_x\text{Fe}_{2-2x}\text{O}_4$ decreased faster while that of $\text{CoAl}_x\text{Fe}_{2-x}\text{O}_4$ was less responsive to variation in concentration. Figs. 9.18B and Fig. 9.19 show that $\text{Co}_{1-x}\text{Ge}_x\text{Fe}_{2-2x}\text{O}_4$ is the only reported composition with simultaneous increase in both amplitude of peak to peak magnetostriction and strain derivative.

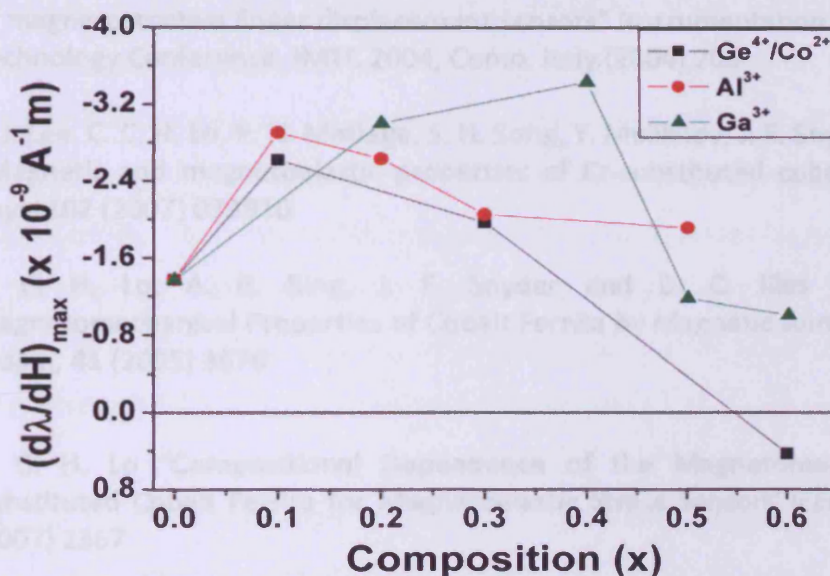


Fig. 9.19: Dependence of $(d\lambda/dH)_{\max}$ of $\text{Ge}^{4+}/\text{Co}^{2+}$, Al^{3+} and Ga^{3+} on concentrations

References to Chapter 9:

- [9-1]. A. A. Yousif; M. E Elzain; H.H Sutherland and S.H Salah, "Mossbauer studies on Al-ferrites" *Hyperfine Interactions*, **68** (1991) 323

- [9-2]. R. D Shannon "Revised effective ionic radii and systematic studies of interatomic distances in halides and chalcogenides" *Acta Crystallographica A*, **32** (1976) 751
- [9-3]. S. S. Shinde and K. M. Jadhav, *J. Mat. Sci. Lett.*, **17** (1998) 849
- [9-4]. B. S Trivedi and R.G Kulkarni, *Sol. State Comm.*, **86** (1993) 327
- [9-5]. S. H. Song, C. C. H. Lo, S. J. Lee, S. T. Aldini, J. E. Snyder, and D. C. Jiles "Magnetic and magnetoelastic properties of Ga-substituted cobalt ferrite" *J. Appl. Phys.* **101**(2007) 09C517
- [9-6]. A. Affanni, A. Guerra, L. Dallagiovanna and G. Chiorboli, "Design and characterization of magnetostrictive linear displacement sensors" Instrumentation and Measurement Technology Conference, IMTC 2004, Como, Italy (2004) 206
- [9-7]. S. J. Lee, C. C. H. Lo, P. N. Matlage, S. H. Song, Y. Melikhov, J. E. Snyder, and D. C. Jiles "Magnetic and magnetoelastic properties of Cr-substituted cobalt ferrite" *J. Appl. Phys.* **102** (2007) 073910
- [9-8]. C. C. H. Lo, A. P. Ring, J. E. Snyder and D. C. Jiles "Improvement of Magnetomechanical Properties of Cobalt Ferrite by Magnetic Annealing" *IEEE Trans. Magn.*, **41** (2005) 3676
- [9-9]. C. C. H. Lo "Compositional Dependence of the Magnetomechanical Effect in Substituted Cobalt Ferrite for Magnetoelastic Stress Sensors" *IEEE Trans. Magn.* **43** (2007) 2367

Chapter 10. Experimental Results and Discussion: Dependence of Crystal Structure and Magnetic Properties of Thin Film Cobalt Ferrite on Deposition Temperature (T = 523, 623, 723, 823 and 873 K)

10.1 Introduction

The magnetic, magnetostrictive, magneto-optic and magneto-transport properties of cobalt ferrite can be exploited for the development of force and torque sensors, high frequency devices, hybrid data storage systems and magneto-optic devices. In some applications especially for miniature devices, cobalt ferrite needs to be produced in thin film rather than bulk form. Exploiting these properties for such applications would require crystalline thin films of cobalt ferrite. This is challenging because it has been shown in previous studies that cobalt ferrite thin films were deposited in the range of 723 to 1173 K for crystallinity and homogeneity [10-1, 10-2, 10-3]. Such high temperatures limit the integration of thin films of cobalt ferrite into MEMS and other semiconductor devices.

This study reports on the variation of crystal structure and magnetic properties of cobalt ferrite thin films made by pulsed laser deposition. Although cobalt ferrite has been previously deposited by pulsed laser deposition, the lowest deposition temperature in that study was 623 K [10-4]. In this study, thin film cobalt ferrite has been deposited over the range 523 to 873 K.

10.2 Variation of Crystal Structure with Deposition Temperature

Crystal structures of the thin film cobalt ferrite samples studied by XRD are shown in Fig. 10.1. All the samples were crystalline at all deposition temperature including at 523 K. The ability to deposit crystalline cobalt ferrite thin films at 523 K demonstrates the potential for integration of the films into MEMs and semiconductor devices. Also the ability to deposit at higher temperatures offers an opportunity to exploit the good thermal stability of cobalt

ferrite. Comparatively, it could be seen that the intensities of the peaks from (111), (222) and (333) planes increased in moving from sample $T_{\text{Dep}} = 873 \text{ K}$ to 523 K . This indicates that deposition at lower temperatures results in a (111) textured cobalt ferrite films. Similarly, deposition at higher temperatures produced films with a (100) texture. The variation in texture with deposition temperature is indicative of the possibility of growing thin films of cobalt ferrite with suitable textures to match specific applications.

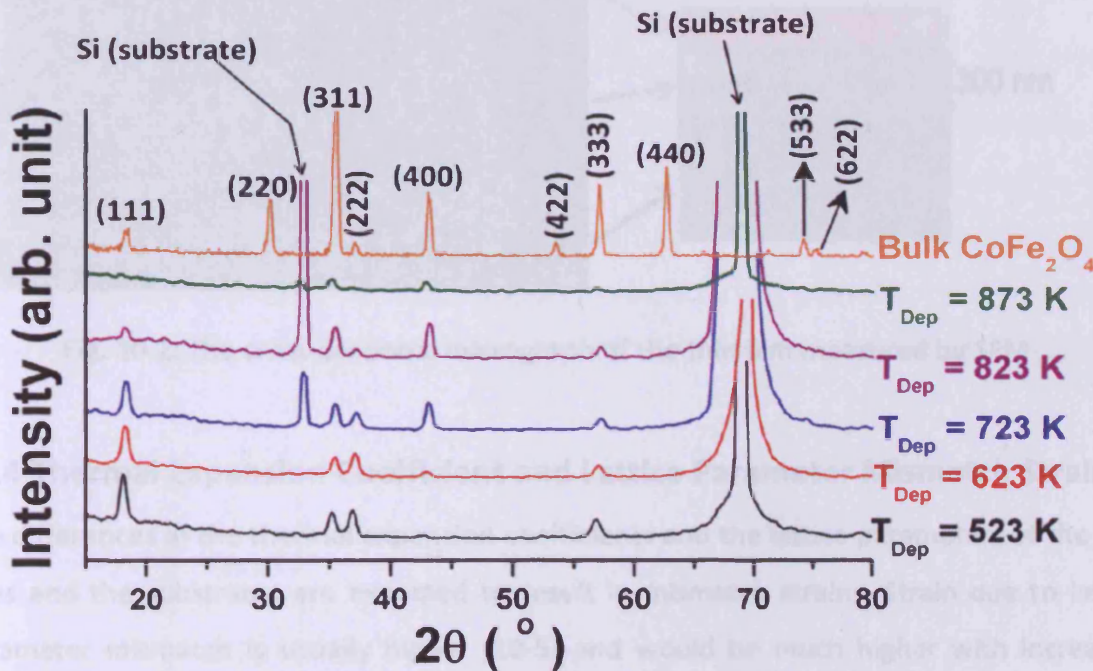


Fig. 10.1: XRD pattern of the thin film cobalt ferrite deposited from 523 to 873 K. The pattern plotted in orange line is for a bulk sample fabricated by the traditional ceramic method. The peaks marked Si (substrate) are peaks from Si/SiO₂ substrate.

10.3 Film Composition and Thickness

The thickness and compositions of the films were measured using an SEM as shown in Fig. 10.2. Variation in deposition temperature did not result in significant variation in film thickness. The thicknesses of all the films were $135 \pm 5 \text{ nm}$. The compositions of the films were determined by EDX as $\text{Co}_{1.1}\text{Fe}_{1.9}\text{O}_4$ with ± 0.05 variation in cation composition. The uniformity in the composition between the films at different deposition temperatures is an

indication of high repeatability in depositing cobalt ferrite thin films by PLD. It also demonstrates the suitability of PLD for large scale production of cobalt ferrite thin films.

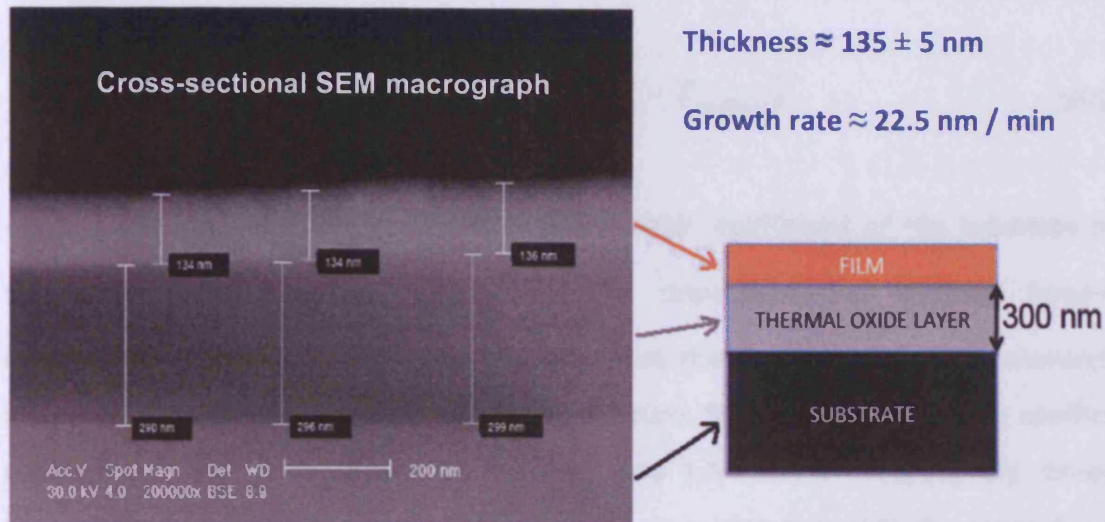


Fig. 10.2: The cross-sectional micrograph of the thin film measured by SEM

10.4 Thermal Expansion Coefficient and Lattice Parameter Mismatch Strains

The differences in the thermal expansion coefficients and the lattice parameters of the thin films and the substrates are expected to result in mismatch strains. Strain due to lattice parameter mismatch is usually higher [10-5] and would be much higher with increasing differences between the lattice parameters of the films and substrates. Although there is significant difference in the lattice parameters of cobalt ferrite (8.38 \AA) and Si (5.43 \AA), the lattice mismatch strain can be ignored for the cobalt ferrite thin film samples. This is because, the Si substrate was coated with 300 nm amorphous SiO_2 buffer and so lattice mismatch strain was eliminated [10-6]. Consequentially, the only thermal expansion mismatch strain need be considered.

The Si substrate is much thicker than the SiO_2 buffer and the cobalt ferrite thin film, and so would be expected to expand according to its own thermal expansion coefficient. The thin film being much thinner is also expected to strain according to the thermal expansion

coefficient of the Si substrate. Thus thermal expansion mismatch strain was calculated as the difference between the strain when the film is free and when it is attached to the Si substrate as shown in equation 10-1.

$$\epsilon = (\alpha_{film} - \alpha_{substrate})(T_{Dep} - T_{Ambient}) \tag{10-1}$$

$\alpha_{substrate}$ and α_{film} are the linear thermal expansion coefficient of the substrate and film respectively while T_{Dep} and $T_{Ambient}$ are the deposition and ambient temperatures respectively. It could be seen from Fig. 10.3 that the thermal expansion mismatch strain increased linearly with the deposition temperature. The thermal expansion coefficients of cobalt ferrite and Si are about $10 \times 10^{-6} \text{ K}^{-1}$ and $3.5 \times 10^{-6} \text{ K}^{-1}$ respectively. Because the thermal expansion coefficient of cobalt ferrite is more than that of Si, the cobalt ferrite films are subjected to planar stress during cooling which results in an in-plane isotropic tension.

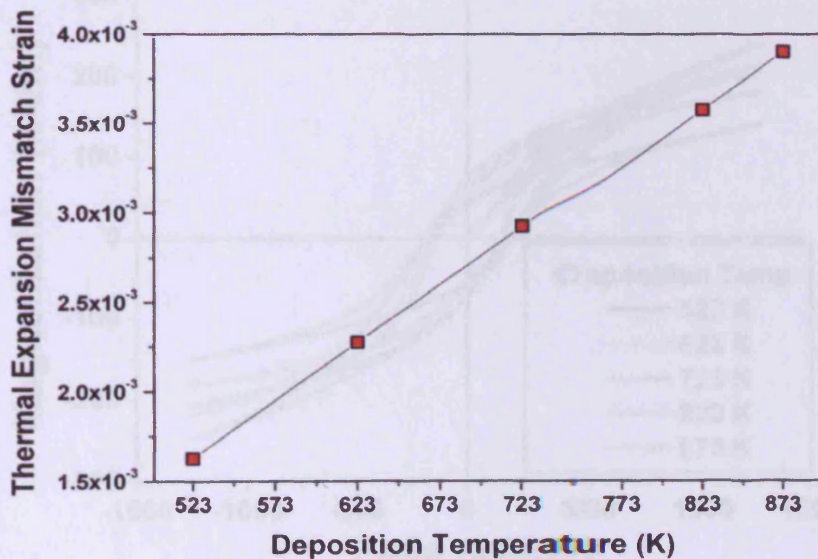


Fig. 10.3: Dependence of thermal expansion mismatch strain on deposition temperature

10.5 Magnetic Properties of the Thin Film Cobalt Ferrite Samples

10.5.1 Variation of magnetization with deposition temperature

Figs. 10.4 and 10.5 show the variation of magnetization with applied magnetic field measured at different deposition temperatures. The measurements were performed both in-plane and perpendicular to the thin film surfaces using a VSM. The samples used were thin films of dimension, 5 mm x 5 mm. The figures show that maximum magnetization (M_{\max}) of the thin film samples increased with increase in deposition temperature. The term maximum magnetization is used instead of saturation magnetization because, as can be seen, the samples were not saturating at the maximum applied field value of 1270 kA/m. Since the net magnetization in cobalt ferrite depends on the net moments from the antiferromagnetic coupled cation sites, the observed variation in magnetization might have resulted from the differences in the cation compositions between the sites with changes in deposition temperature.

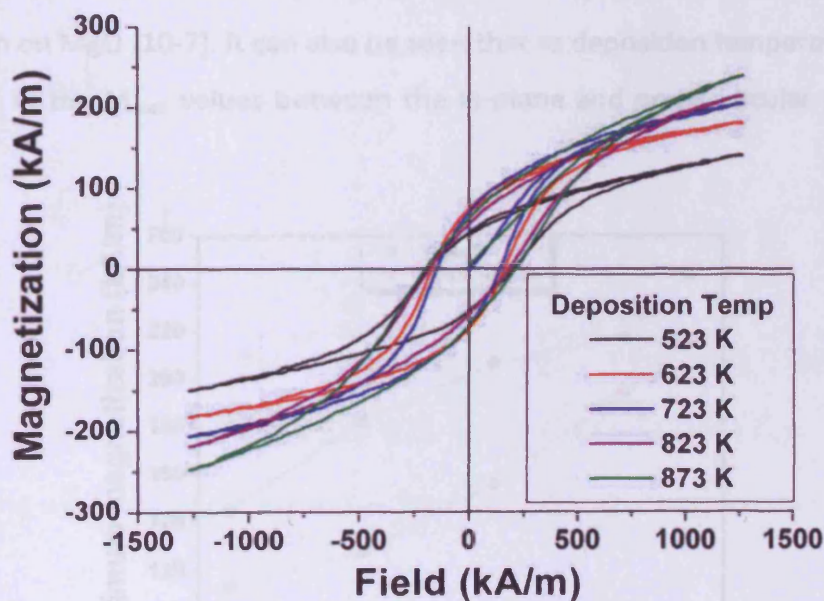


Fig. 10.4: In-plane magnetization vs. field plots measured on the thin film samples at different deposition temperatures.

Fig. 10.5: Variation of maximum magnetization with deposition temperature of the thin film cobalt ferrite samples.

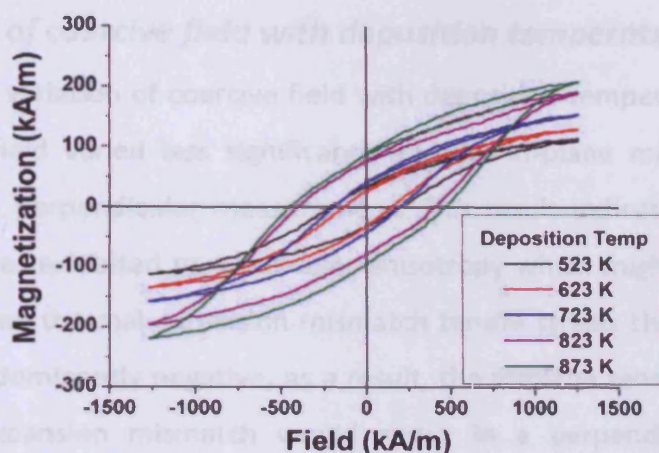


Fig. 10.5: Perpendicular magnetization vs. field plots measured on the thin film samples at different deposition temperatures.

As shown in Fig. 10.6, the increase in M_{\max} with deposition temperature was fairly linear for both in-plane and perpendicular measurements although higher M_{\max} values were obtained for in-plane measurements than perpendicular measurements. A similar result, in which M_{\max} increased with deposition temperature, has been reported for thin film cobalt ferrite samples grown on MgO [10-7]. It can also be seen that as deposition temperature increased, the difference in the M_{\max} values between the in-plane and perpendicular measurements decreased.

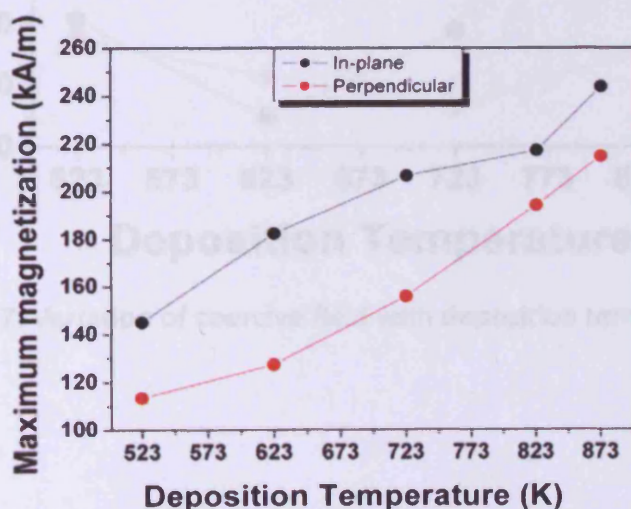


Fig. 10.6: Variation of maximum magnetization with deposition temperature of the thin film cobalt ferrite samples

10.5.2 Variation of coercive field with deposition temperature

Fig. 10.7 shows the variation of coercive field with deposition temperature. It can be seen that the coercive field varied less significantly for the in-plane measurement but very significantly for the perpendicular measurement. This result indicates that the thin film cobalt ferrite samples exhibited perpendicular anisotropy which might have resulted from the observed in-plane thermal expansion mismatch tensile strain. The magnetostriction in cobalt ferrite is predominantly negative, as a result, the in-plane tensile strain on the films due to thermal expansion mismatch would result in a perpendicular anisotropy, as observed.

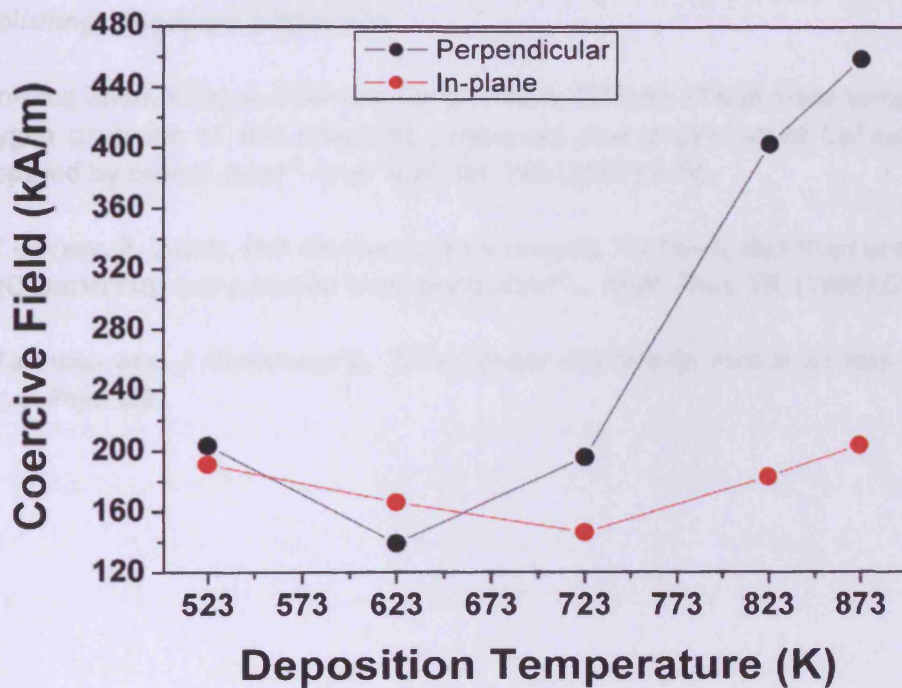


Fig. 10.7: Variation of coercive field with deposition temperature

References to Chapter 10:

- [10-1]. C. Araújo, B.G. Almeida, M. Aguiar and J.A. Mendes "Structural and magnetic properties of CoFe_2O_4 thin films deposited by laser ablation on Si (001) substrates" *Vacuum* **82** (2008) 1437
- [10-2]. Jae-Gwang Lee, Jae Yun Park, Young-Jei Oh and Chul Sung Kim, "Magnetic properties of CoFe_2O_4 thin films prepared by a sol-gel method" *J. Appl. Phys.*, **84** (1998) 2801
- [10-3]. Y. C. Wang, J. Ding, J. B. Yi, B. H. Liu, T. Yu and Z. X. Shen, "High-coercivity Co-ferrite thin films on (100) - SiO_2 substrate" *Appl. Phys. Lett.* **84** (2004) 2596
- [10-4]. J. Zhou, H. He, and C. Nan, "Effects of substrate temperature and oxygen pressure on the magnetic properties and structures of CoFe_2O_4 thin films prepared by pulsed-laser deposition" *Appl. Surf. Sci.* **253** (2007) 7456
- [10-5]. W. K. Liu, M. B. Santos "Thin film heteroepitaxial systems" *World Scientific Publishing, Singapore* (1999) 300
- [10-6]. Jian-ping Zhou, Hong-cai He and Ce-Wen Nan, "Effects of substrate temperature and oxygen pressure on the magnetic properties and structures of CoFe_2O_4 thin films prepared by pulsed-laser" *Appl. Surf. Sci.* **253** (2007) 7456
- [10-7]. P.C Dorsey, P. Lubitz, D.B Chrisey and J.S Horwitz "CoFe₂O₄ thin films grown on (100) MgO substrates using pulsed laser deposition" *J. Appl. Phys.* **79** (1996) 6338
- [10-8]. C Tannous and J Gieraltowski, "The Stoner–Wohlfarth model of ferromagnetism" *Eur. J. Phys.* **29**

Chapter 11. Conclusions and Recommended Future Research

11.1 Conclusions

The variation in structural, magnetic and magnetostrictive properties of cobalt ferrite due to changes in processing, heat treatment and composition (cation constitution) have been investigated and reported in this thesis. Results were also published in leading international journals and/or presented in major international magnetism and magnetic materials conferences. The results obtained have provided more insight into the properties of cobalt ferrite and its derivative materials, and will be useful for optimizing the properties. The following conclusions can be drawn from this research;

- a. Sintering cobalt ferrite for magnetostrictive applications in air is preferable to sintering in vacuum due to the formation of a deleterious second phase of $\text{Co}_{1-x}\text{Fe}_x\text{O}$ solid solution system ($x \approx 0.33$) when vacuum sintering is used. Variation in the sintering conditions, including sintering temperature and holding time affects the distribution of the $\text{Co}_{1-x}\text{Fe}_x\text{O}$ phase. This suggests that a combination of holding time, sintering temperature and oxygen partial pressure could be found which would result in desirable properties. The formation of the $\text{Co}_{1-x}\text{Fe}_x\text{O}$ phase is detrimental to the structural, magnetic and magnetostrictive properties of cobalt ferrite. If cobalt ferrite samples are prepared in vacuum, the measured properties will represent that of a composite ($\text{CoFe}_2\text{O}_4 + \text{Co}_{1-x}\text{Fe}_x\text{O}$) which makes it difficult to selectively tune properties for intended applications.
- b. This research shows that annealing and quenching heat treatments result in cation redistribution which in turn results in changes in the magnetic and magnetostrictive properties. Annealing at $600\text{ }^\circ\text{C}$ prior to quenching can lead to higher magnetostriction amplitudes than furnace cooling. These variations in properties observed with annealing and quenching can be exploited for tailoring the magnetostrictive properties of cobalt ferrite for the development of stress sensors and actuators. This research also shows that the limit of the strain sensitivity of un-substituted cobalt ferrite is higher than

previously thought. The $(d\lambda/dH)_{max}$ for furnace cooled sample is the highest ever reported for both substituted and un-substituted due to deviations from the stoichiometric amount of oxygen in the samples. This indicates that higher strain derivatives can be obtained by both cation substitution and controlling the variation in the oxygen content.

- c. It was also found that variation in processing parameters does not affect the cation distribution although it affects the magnetostrictive properties. Magnetostriction amplitude and strain derivative depend more on holding time and compaction pressure respectively. While coercive field is dependent on processing parameters, saturation magnetization is insensitive.
- d. $Co_{1+x}Ge_xFe_{2-2x}O_4$, $CoGa_xFe_{2-x}O_4$ and $CoAl_xFe_{2-x}O_4$ are materials with potential for application in high-sensitivity magnetomechanical stress sensor and energy efficient magnetostrictive actuator devices. The highest reported strain derivative for substituted cobalt ferrite samples was obtained for $CoGa_xFe_{2-x}O_4$. Simultaneous improvement in magnetostriction and strain derivative was obtained for $Co_{1+x}Ge_xFe_{2-2x}O_4$, which also resulted in the highest magnetostriction amplitude of all reported magnetostrictive studies on substituted and un-substituted cobalt ferrite materials. $CoAl_xFe_{2-x}O_4$ showed a compromise with strain derivative higher than $Co_{1+x}Ge_xFe_{2-2x}O_4$ but lower than $CoGa_xFe_{2-x}O_4$ and amplitude of magnetostriction higher than $CoGa_xFe_{2-x}O_4$ but lower than $Co_{1+x}Ge_xFe_{2-2x}O_4$.
- e. It has been demonstrated that thin films of cobalt ferrite with (111) orientation can be grown at temperatures as low as 523 K by PLD. The ability to deposit crystalline cobalt ferrite at such a low temperature offers the potential for integration of thin films based on cobalt ferrite into MEMS and other semiconductor devices. Perpendicular anisotropy can be induced and tuned by controlling the substrate temperature during deposition.

11.2 Recommended Future Works

From the findings of this research the following future works on structure magnetic and magnetostrictive properties of cobalt ferrite are suggested;

11.2.1 Mechanical properties of cobalt ferrite

A drawback of Terfenol-D for magnetomechanical applications is its poor mechanical properties. It is known from the literature that cobalt ferrite is mechanically robust [11-1]. Despite this claim and various studies on cobalt ferrite for magnetomechanical applications, there are no reports on studies of mechanical properties of cobalt ferrite. The mechanical properties of cobalt ferrite such as elastic modulus can be determined by ultrasonic methods. The procedure for determining the mechanical properties by an ultrasonic method is shown in Appendix I. Although this was beyond the scope of this research, it was attempted. For this research, the mechanical properties of cobalt ferrite were evaluated at the Centre for Non-destructive Evaluation (CNDE) in Iowa State University, USA. The results obtained were not reliable because the samples were transported by courier services and were severely cracked. Such a study is thus recommended as a future work.

11.2.2 Distribution of cations between the tetrahedral and octahedral sites

Understanding how cations are distributed between the tetrahedral and octahedral sites is useful for determining how magnetic and magnetoelastic properties would change with cation substitution. Mossbauer spectroscopy has been used to study the cation distribution in $\text{CoGa}_x\text{Fe}_{2-x}\text{O}_4$ [11-2] and $\text{CoAl}_x\text{Fe}_{2-x}\text{O}_4$ [11-3] but not $\text{Co}_{1+x}\text{Ge}_x\text{Fe}_{2-2x}\text{O}_4$. $\text{Co}_{1+x}\text{Ge}_x\text{Fe}_{2-2x}\text{O}_4$ has been shown in this research to be the only cation substituted cobalt ferrite series capable of simultaneous magnetostriction amplitude and strain derivative improvement. Therefore understanding the distribution of Ge^{4+} , Co^{2+} and Fe^{3+} among the cation sites can be useful for further improving the magnetostrictive properties and is thus suggested.

11.2.3 Oxygen content determination

It has been proposed in this study that variation in the oxygen content can alter the magnetomechanical performance of cobalt ferrite samples. The highest strain derivative for cobalt ferrite samples was obtained in this study for un-substituted cobalt ferrite. This high strain derivative was proposed to be due to deviation of oxygen contents of the sample from the stoichiometric value. It is not known how close to or far from stoichiometry the oxygen contents of the samples are due to the insensitivity of EDX to light elements such as oxygen. A suitable method for determining accurately the elemental composition of the samples studied is needed. This will not only help in accurate comparison of different composition but also in systematic tailoring of properties.

11.2.4 Domain studies

Understanding the connection between domain processes and magnetostrictive properties of cobalt ferrite can result in fundamental capability of optimizing magnetostrictive properties. Domain study on cobalt ferrite was attempted but was not progressed due to non availability of suitable samples. Samples prepared via the traditional ceramic method are unsuitable for domain studies due the large content of external effects such as residual stresses and pinning sites. Domain images of cobalt ferrite obtained in this research and the instrumentation for sample preparation for the imaging are shown in Appendix II. Preparation route for producing samples with minimal pinning sites is required to make samples more suitable for domain studies. It is important to note that preparation following another route is likely to result in different properties from samples made via the ceramic method.

11.2.5 Modelling the magnetostrictive properties of cobalt ferrite

To model magnetostriction accurately, strong magnetomechanical coupling is essential. For cobalt ferrite, a magnetostriction model capable of capturing the properties of cobalt ferrite

especially with cation substitution is needed. This was also attempted in this research and the results are presented in Appendix III.

11.2.6 Measuring the magnetostriction of thin film cobalt ferrite samples

The ability to measure the magnetostriction amplitude and thus determine the strain derivative of thin films of cobalt ferrite is necessary for optimizing the magnetostrictive properties for applications. The magnetostrictive properties of thin films cobalt ferrite used in this study were not studied because, the substrate being much thicker, it was difficult to measure the magnetostriction of the thin film cobalt ferrite.. In the absence of a suitable way for direct magnetostrictive effect, a possibility is to study the inverse magnetostrictive effect (Villary effect).

References to Chapter 11:

- [11-1]. Y. Chen, J. E. Snyder, C. R. Schwichtenberg, K. W. Dennis, R. W. McCallum, D. C. Jiles "Metal-bonded Co-ferrite composites for magnetostrictive torque sensor applications" *IEEE Trans. on Magn.*, **35**, (1999) 3652

- [11-2]. K. Kriebel, M. Devlin, J. Lee, T. Aldini and J. E. Snyder "Investigation of Ga substitution in cobalt ferrite (Co_{1-x}Ga_xFe₂O₄) using Mossbauer spectroscopy" *J. Appl. Phys.* **103** (2008) 07E508

- [11-3]. Sam Jin Kim, Kwang-Deog Jung and Chul Sung Kim "Mossbauer and Neutron Diffraction Studies on Co-Al Ferrite" *Hyperfine Interactions* **156-157** (2004) 113

Appendix I Determination of Mechanical Properties of Cobalt Ferrite by an Ultrasonic Method

Fig. A.1 shows the principle of measuring the mechanical properties cobalt ferrite via the single probe ultrasonic method.

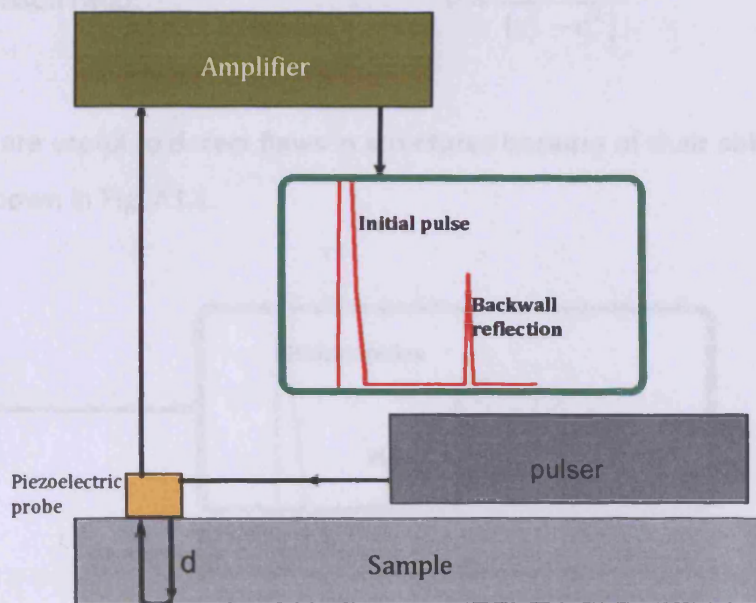


Fig. A1.1: Principle of measuring the mechanical properties of cobalt ferrite using the single probe ultrasonic method.

The velocity of the ultrasonic wave can be determined and used for determining the mechanical properties as follows;

$$c = \frac{2d}{t} \quad \text{A- 1}$$

c , d and t are velocity of the wave, thickness of the medium and time of wave propagation respectively. If the longitudinal velocity c_l , shear velocity c_s and density are known, the following mechanical properties can be determined;

Young's Modulus:
$$E = \rho c_s^2 \frac{[3c_l^2 - 4c_s^2]}{[c_l^2 - c_s^2]} \quad \text{A- 2}$$

Bulk Modulus:
$$B = \rho \left[c_l^2 - \frac{4}{3} c_s^2 \right] \quad A-3$$

Shear Modulus:
$$G = \rho c_s^2 \quad A-4$$

Poisson ratio:
$$\nu = \frac{[c_l^2 - 2c_s^2]}{[c_l^2 - c_s^2]} \quad A-5$$

Ultrasonic waves are useful to detect flaws in structures because of their ability to deflect off the flaws as shown in Fig. A1.2.

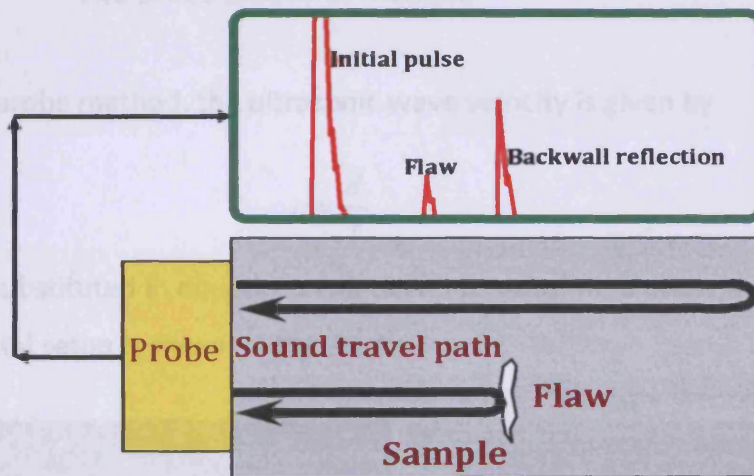


Fig. A1.2: Using the ultrasonic wave method for flaw detection

This ability of the ultrasonic waves to reflect off the flaws makes the single probe method unsuitable for materials which are prone to imperfections such as ceramic cobalt ferrite. Using a single piezoelectric probe to measure the mechanical properties of cobalt ferrite with defects, will result in the waves reflecting off the defects thus giving an inaccurate value of d for use in equation A-1. The solution is to use the two probe method; a transmitting probe on one side of the test specimen and a receiving probe on the other.

Thus only the waves that successfully pass through the samples are detected by the receiving probe; giving an accurate value of d . This is illustrated in Fig. A1.3.

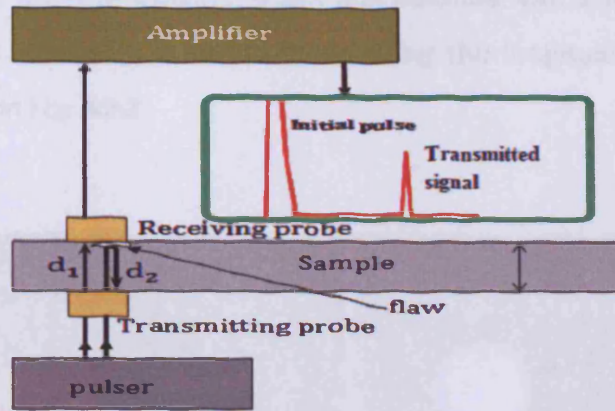


Fig. A1.3: Measuring the mechanical properties of cobalt ferrite using the two probe ultrasonic method.

Using the two probe method, the ultrasonic wave velocity is given by

$$c = \frac{d}{t} \quad \text{A- 6}$$

c can then be substituted in equations A-2 to A-5 to determine other mechanical properties.

The experimental setup is shown in Fig. A1.4.

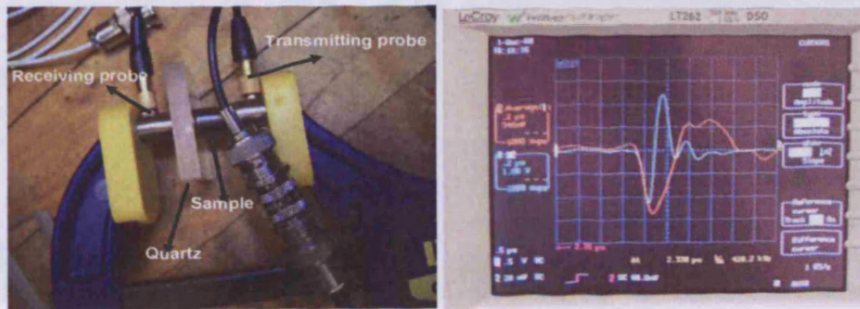


Fig. A1.4: Experimental setup for determining the mechanical properties of cobalt ferrite via the ultrasonic method.

Appendix II Domain Studies in Cobalt Ferrite Samples

Domain images were obtained from cobalt ferrite samples prepared according to [equation 5-4](#). The samples were cut with a diamond saw and polished with a Struers Polishing System as shown in Fig. A2.1. Domains were observed using the longitudinal Kerr effect in Kerr microscope as shown in Fig. A2.2.

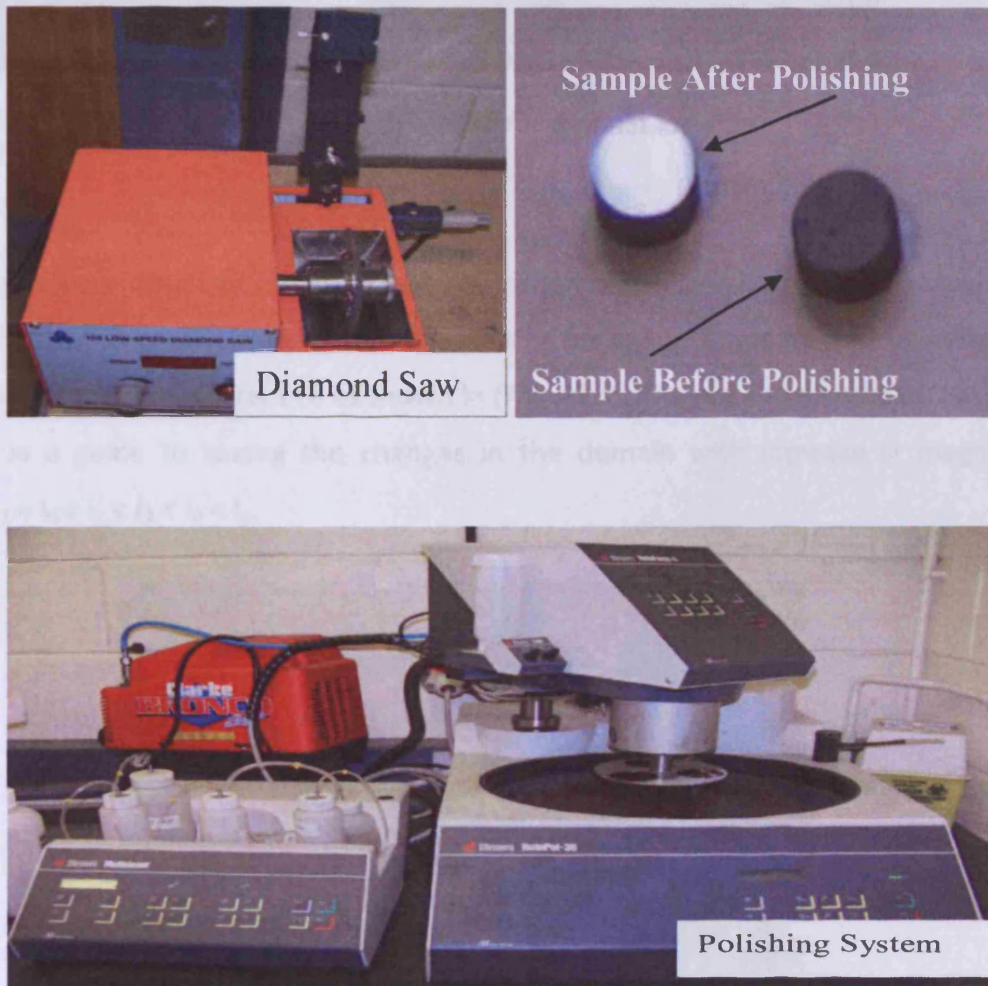


Fig. All. 1: Sample preparation instrumentation for domain imaging

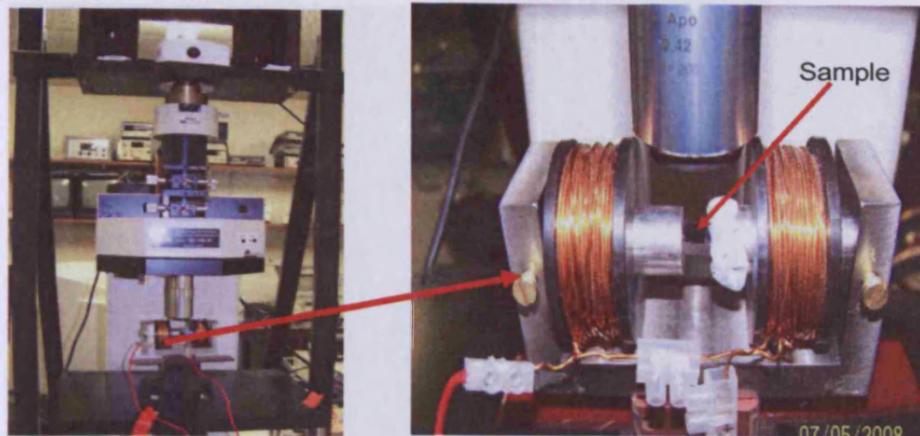


Fig. All. 2: Kerr microscope used for domain imaging

Bar domains were obtained for the cobalt ferrite samples (Fig. A2.3). The red arrows show the direction of magnetization in the domains. Changes in domain were observed with increase in magnetizing current (I) as shown in (Fig. A2.4). The red and blue boxes have been inserted as a guide to seeing the changes in the domain with increase in magnetizing current. $I_1 = I_6 < I_2 < I_3 < I_4 < I_5$.

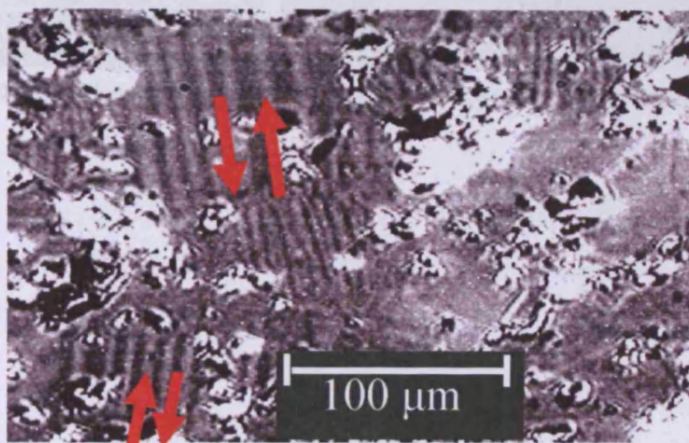


Fig. All. 3: Bar domains of cobalt ferrite obtained using Kerr microscopy

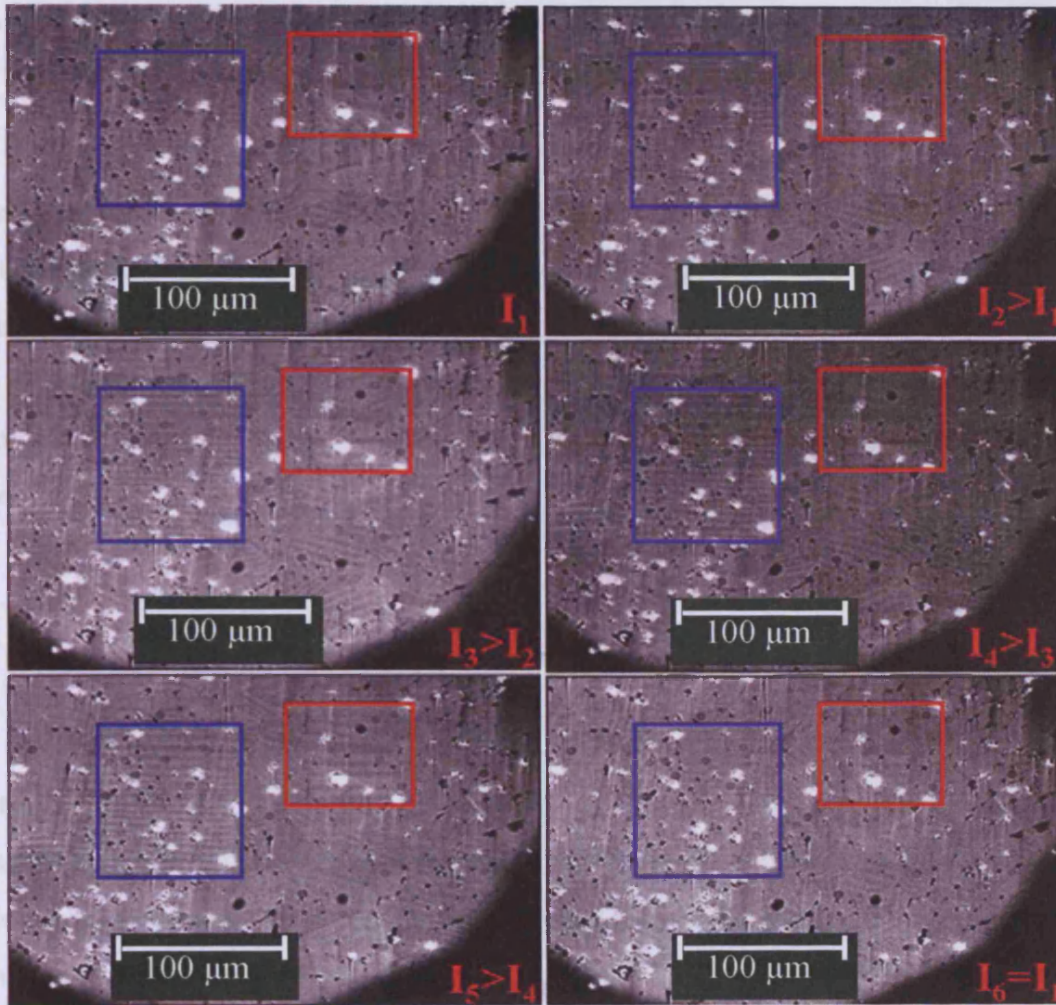


Fig. All. 4: Changes in domain with changes in magnetizing current

Appendix III Modelling the Magnetic and Magnetostrictive Properties of Cobalt Ferrite

The mechanical and magnetic properties were coupled by the non-linear constitutive equation shown in [equation 2-18](#). The 1/3 term in the equation was omitted in this model because it was assumed that the sample was sufficiently pre-stressed such that the domains were aligned 90° to the direction of magnetization and so magnetization takes place entirely by domain rotation. Therefore setting $\cos\theta$ as (M/M_s) [[AIII-11-1](#)] [equation 2-18](#) can be re-written as;

$$\lambda_s(\theta) = \frac{3}{2} \lambda_s \left(\frac{M}{M_s} \right)^2 \quad \text{AIII- 1}$$

Equation AIII-1 was incorporated into Comsol Multiphysics to couple the magnetomechanical behaviour of cobalt ferrite. The M vs. H curve measured for a cobalt ferrite sample was used to model the non-linear magnetic properties of cobalt ferrite. The mechanical properties of cobalt ferrite were defined by inputting Young's modulus = 168 GPa, Poisson's ratio = 0.28 and density = 5290 kg/m³. Since the mechanical properties of cobalt ferrite used in this research were not measured, these values were obtained from a study on Co_xZn_{1-x}Fe₂O₄ [[AIII-2](#)], for x = 1. It is preferable that both mechanical and magnetic properties be obtained from the same material as the properties can significantly depend on processing route. The results obtained from the modelling are shown in this appendix.

Fig. AIII.1 shows the geometry of the model comprising of a steel casing, copper wire, air and the magnetostrictive rod. The model was meshed as shown in Fig. AIII. 2 with finer meshes around the magnetostrictive rod and steel casing. As shown in Fig. AIII.3, the magnetic field did not increase noticeably at current density 1 to 1 x 10⁴ A/m². Further increase in the current density resulted to noticeable increase in magnetic field strength (Fig. AIII.4).

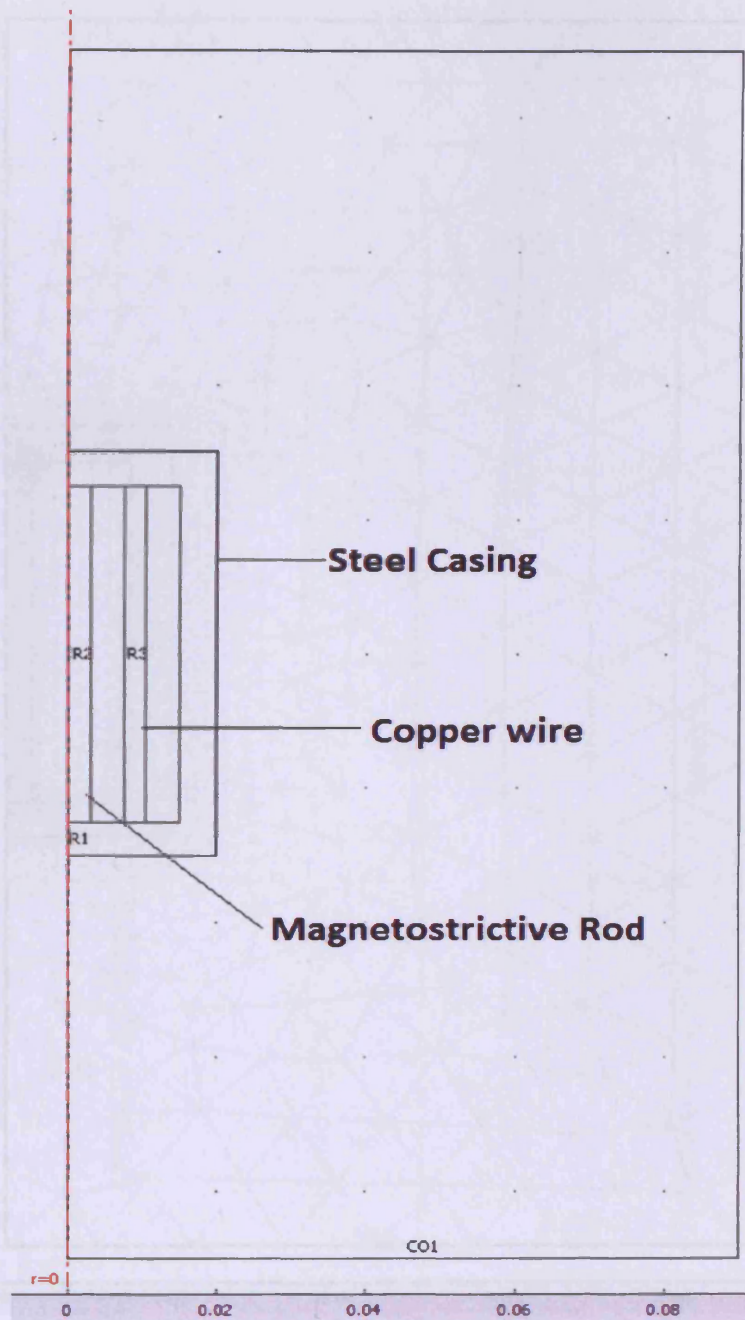


Fig. AIII. 2: Mesh

Fig. AIII. 1: Model geometry

Magnetic field strength increased with increase in current density as shown in Fig. AIII.3.

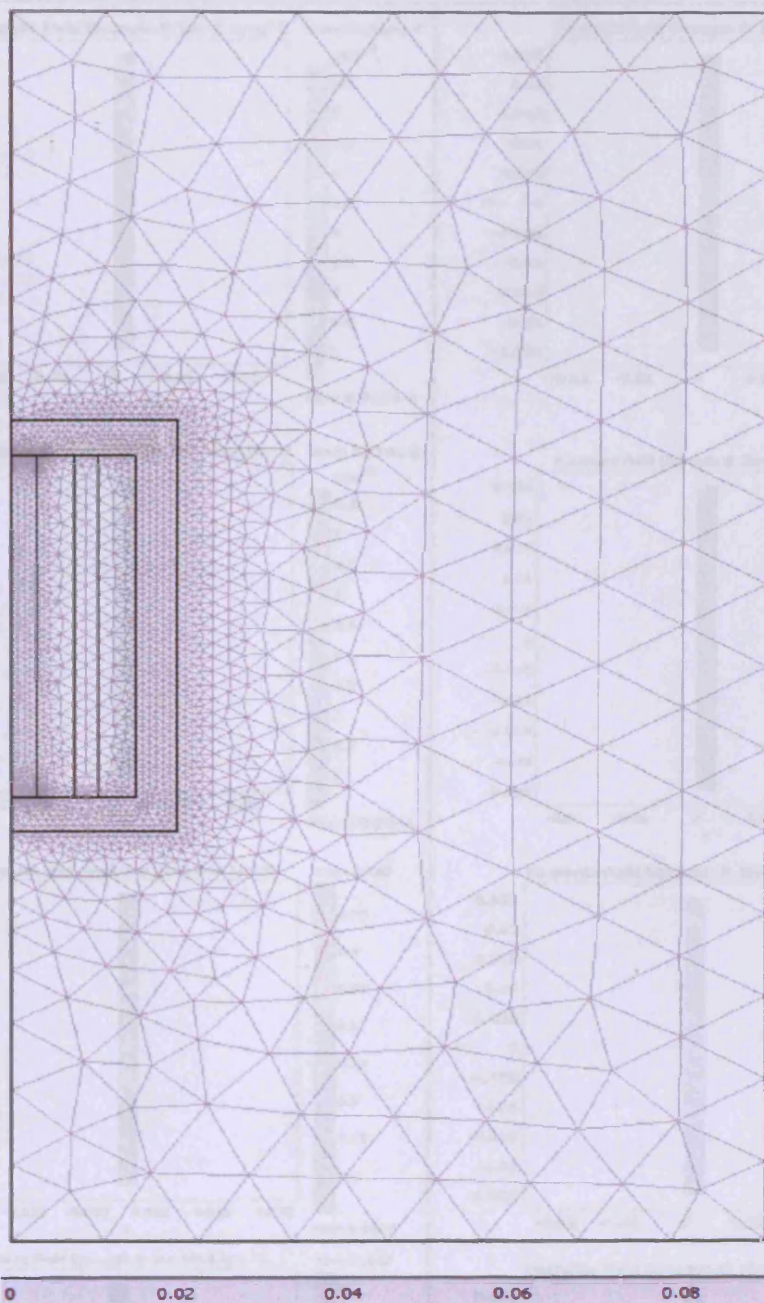


Fig. AIII. 2: Model mesh

Magnetic field strength increased with increase in current density as shown in Fig. AIII.3.

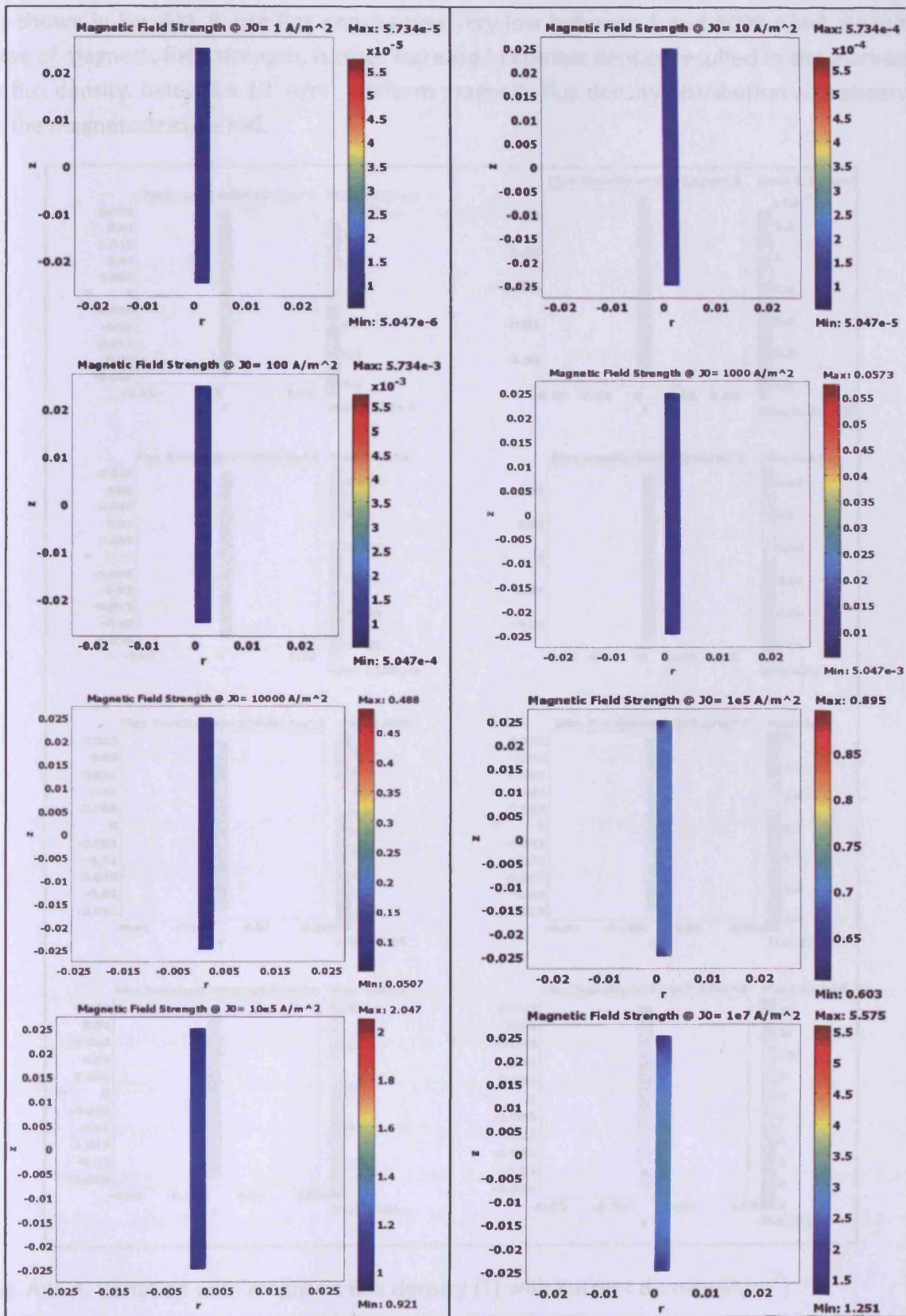


Fig. AIII. 3: Variation with magnetic field strength (A/m) with current density (A/m^2)

As shown in Fig. AIII. 5, the flux density was very low between 1 and 1000 A/m². As in the case of magnetic field strength, further increase in current density resulted in the increasing in flux density. Below 1 x 10⁷ A/m², uniform magnetic flux density distribution was observed in the magnetostrictive rod.

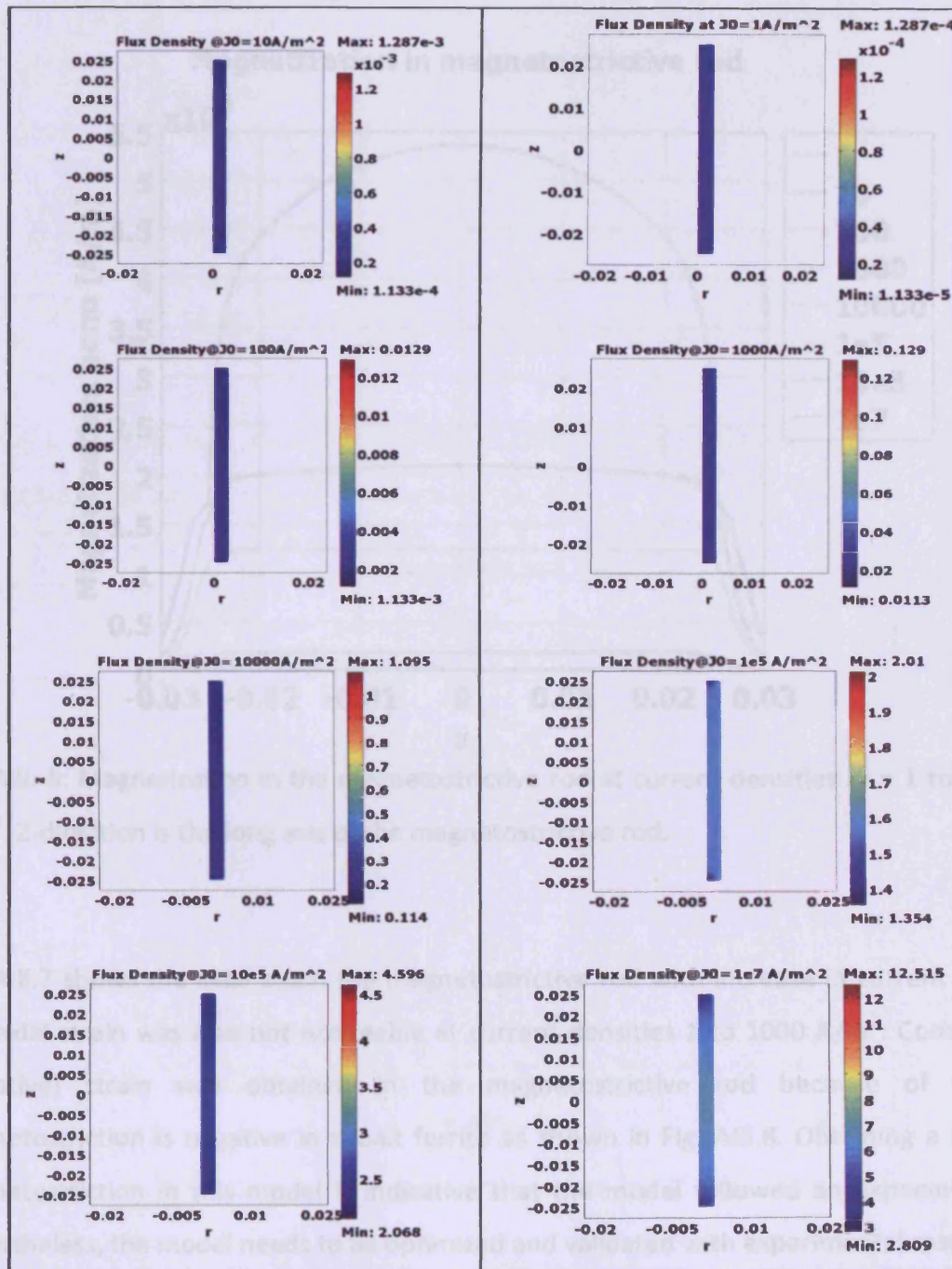


Fig. AIII. 4: Variation with magnetic flux density (T) with current density (A/m²)

In Fig. AIII. 6, the magnetization the magnetostrictive rod was also very low between 1 and 1000 A/m² but increased afterwards. Also, the magnetization was less uniform in the magnetostrictive rod at 1 x 10⁷ A/m² than at lower values of current density.

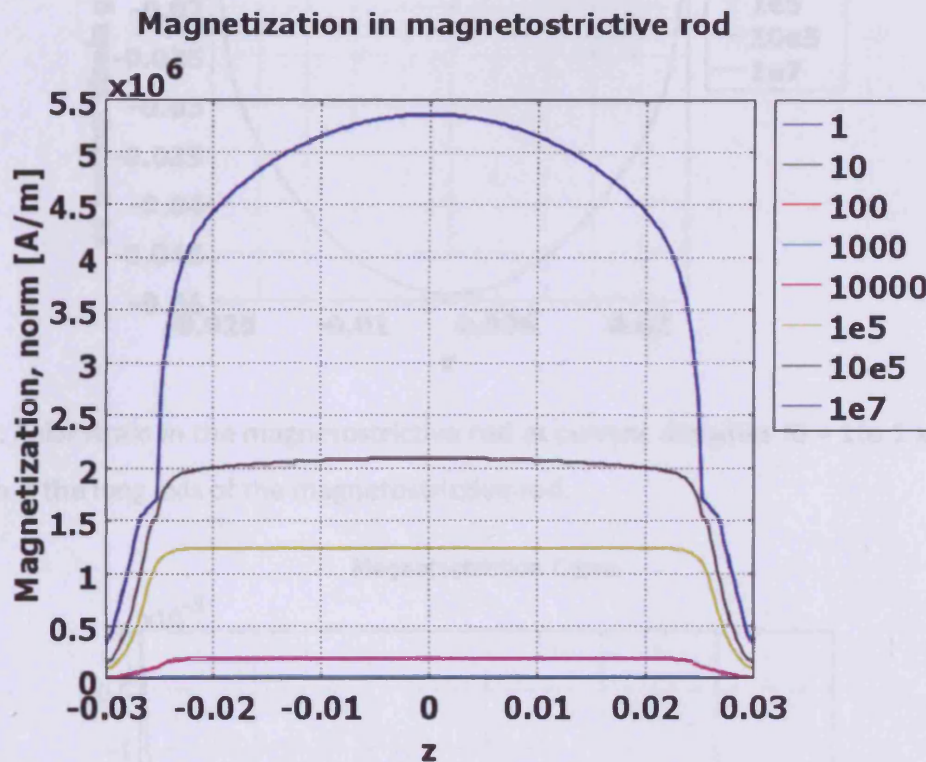


Fig. AIII. 5: Magnetization in the magnetostrictive rod at current densities $J_0 = 1$ to 1×10^7 A/m². Z-direction is the long axis of the magnetostrictive rod.

Fig. AIII.7 shows the axial strain the magnetostrictive rod with increase in current density. The axial strain was also not noticeable at current densities 1 to 1000 A/m². Compressive (negative) strain was obtained in the magnetostrictive rod because of because magnetostriction is negative in cobalt ferrite as shown in Fig. AIII.8. Obtaining a negative magnetostriction in this model is indicative that the model followed an expected trend. Nevertheless, the model needs to be optimized and validated with experimental results.

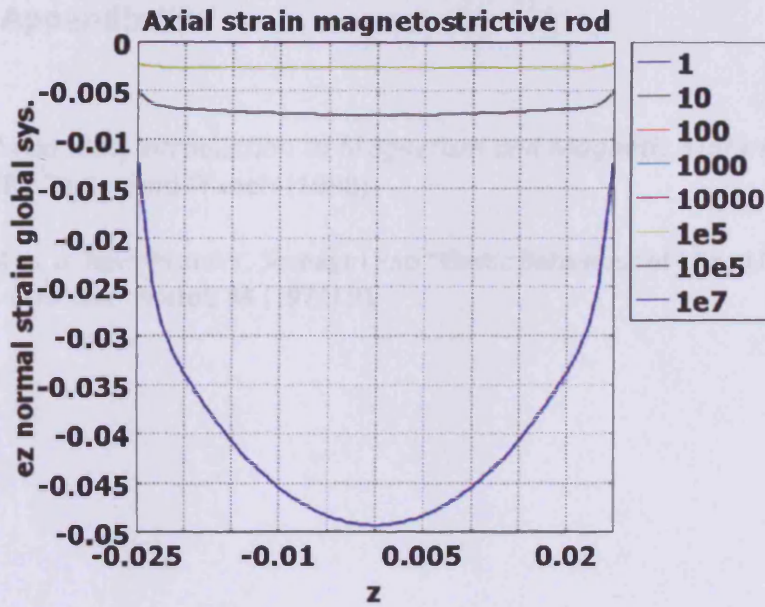


Fig. AIII. 6: Axial strain in the magnetostrictive rod at current densities $J_0 = 1$ to 1×10^7 A/m². Z-direction is the long axis of the magnetostrictive rod.

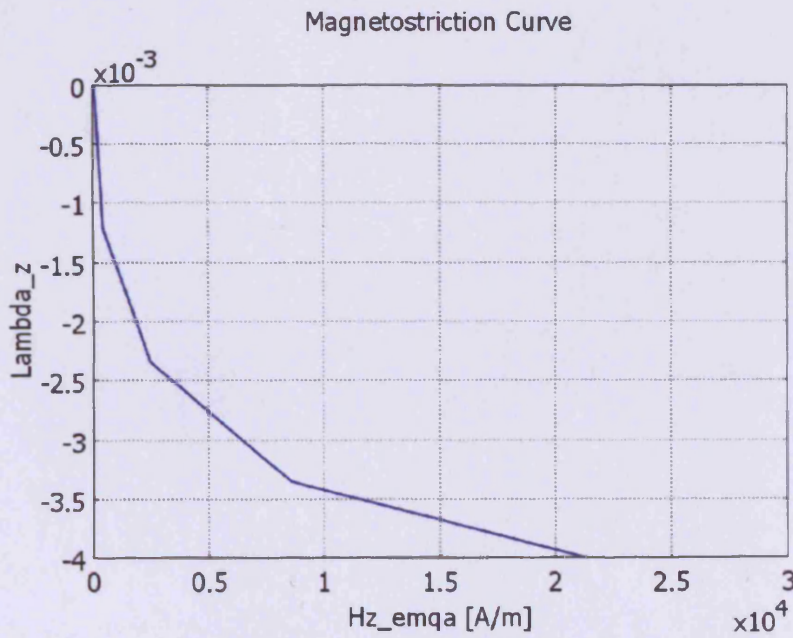


Fig. AIII. 7: Variation of magnetostriction with applied field along the magnetostrictive rod.

Reference to Appendix III:

- [AIII-1]. David Jiles, *Introduction to Magnetism and Magnetic Materials, 2nd ed.* USA, CRC Taylor and Francis (1998)
- [AIII-2]. Miss. B. Revathi and T. Seshagiri Rao "Elastic Behaviour of Mixed Cobalt-Zinc Ferrite"
J. Less. Com. Metals **34** (1974) 91

Appendix IV Journal Publications and Conference Presentations Based on this Research

Journal Publications:

1. I. C. Nlebedim, N. Ranvah, Y. Melikhov, P. I. Williams, J. E. Snyder, A. J. Moses, and D. C. Jiles "Effect of Temperature Variation on the Magnetoelastic Properties of $\text{CoAl}_x\text{Fe}_{2-x}\text{O}_4$ " *J. Appl. Phys.* **107** (2010) 09A936
2. I. C. Nlebedim, N. Ranvah, P. I. Williams, Y. Melikhov, J. E. Snyder, A. J. Moses, and D. C. Jiles "Effect of Heat Treatment on the Cation Distribution in Magnetostrictive CoFe_2O_4 " *J. Magn. Mater.* **322** (2010) 1929
3. I. C. Nlebedim, J. E. Snyder, A. J. Moses, D. C. Jiles "Dependence of magnetic and magnetostrictive properties of cobalt ferrite on processing parameters" Accepted: *J. Magn. Mater.* (DOI:10.1016/j.jmmm.2010.08.026)
4. A. Raghunathan, I. C. Nlebedim, D. C. Jiles, and J. E. Snyder "Growth of Crystalline Cobalt ferrite Thin Films at Lower Temperatures using Pulsed-laser Deposition Technique" *J. Appl. Phys.* **107** (2010) 09A516
5. N. Ranvah, I. C. Nlebedim, Y. Melikhov, J. E. Snyder, P. I. Williams, A. J. Moses, and D. C. Jiles "Temperature dependence of magnetic properties of $\text{CoAl}_x\text{Fe}_{2-x}\text{O}_4$ " *IEEE Trans. Mag.* **45** (2009) 4261
6. I. C. Nlebedim, N. Ranvah, Y. Melikhov, P. I. Williams, J. E. Snyder, A. J. Moses, and D. C. Jiles, "Magnetic and Magnetomechanical Properties of $\text{CoAl}_x\text{Fe}_{2-x}\text{O}_4$ for Stress Sensor and Actuator Applications" *IEEE Trans Mag.* **45** (2009) 4120

7. I.C. Nlebedim, N Ranvah, P.I. Williams, Y Melikhov, F Anayi, J.E. Snyder, A.J. Moses, D.C. Jiles "Influence of Vacuum Sintering on Microstructure and Magnetic Properties of Magnetostrictive Cobalt Ferrite" *J. Magn. and Mag. Mater.* **321** (2009) 2528

8. Naresh Ranvah, I. C. Nlebedim, Y. Melikhov, J. E. Snyder, D. C. Jiles, A. J. Moses, P. I. Williams, F. Anayi, and Sang-Hoon Song "Temperature dependence of magnetostriction of $\text{Co}_{1-x}\text{Ge}_x\text{Fe}_{2-2x}\text{O}_4$ for magnetostrictive sensor and actuator applications" *IEEE Trans. Mag.*, **44** (2008) 3013

9. N. Ranvah, Y. Melikhov, I. C. Nlebedim, D. C. Jiles, J. E. Snyder, A. J. Moses, and P. I. Williams "Temperature dependence of magnetic anisotropy of germanium/cobalt co-substituted cobalt ferrite" *J. Appl. Phys.*, **105** (2009) 07A518

10. I. C. Nlebedim, Y. Melikhov, J. E. Snyder, A. J. Moses, D. C. Jiles "Dependence of Magnetomechanical Performance of $\text{CoGa}_x\text{Fe}_{2-x}\text{O}_4$ on Temperature Variation" Submitted to *J. Appl. Phys.*

Effect of temperature variation on the magnetostrictive properties of $\text{CoAl}_x\text{Fe}_{2-x}\text{O}_4$

I. C. Nlebedim,^{*)} N. Ravvah, Y. Melikhov, P. I. Williams, J. E. Snyder, A. J. Moses, and D. C. Jiles
 Wolfson Centre for Magnetics, School of Engineering, Cardiff University, CF24 3AA, Cardiff, United Kingdom

(Presented 19 January 2010; received 31 October 2009; accepted 9 December 2009; published online 3 May 2010)

The effect of temperature variation on the magnetoelastic properties of the $\text{CoAl}_x\text{Fe}_{2-x}\text{O}_4$ system (for $x=0.0, 0.2, 0.5$, and 0.7) has been studied. Substitution of Al^{3+} for Fe^{3+} was found to lower the Curie temperature of the samples and to change the lattice parameter. The magnitude of peak to peak magnetostriction, strain sensitivity, magnetomechanical hysteresis, and relative contributions of λ_{111} and λ_{100} to the resultant magnetostriction were found to vary with temperature. The results show the possibility of tailoring the magnetoelastic properties of highly magnetostrictive cobalt ferrite at temperatures of interest by cation substitution. © 2010 American Institute of Physics. [doi:10.1063/1.3357404]

I. INTRODUCTION

The present study investigates the temperature dependence of the magnetoelastic properties of $\text{CoAl}_x\text{Fe}_{2-x}\text{O}_4$ for applications in order to enable optimization of these materials for particular temperature ranges of interest. The increased interest in CoFe_2O_4 - and CoFe_2O_4 -based materials is mainly due to their strong magnetoelastic effects and their potential usefulness in developing robust magnetoelastic stress sensors and energy efficient actuators. Pure cobalt ferrite (Co-ferrite) without cation substitution has high enough magnetostriction (λ) for advanced magnetomechanical stress sensor and actuator applications but is limited by the magnetomechanical hysteresis. Substitutions of nonmagnetic cations for Fe^{3+} in Co-ferrite can lead to lower magnetomechanical hysteresis and an increase in the strain sensitivity ($d\lambda/dH$).¹

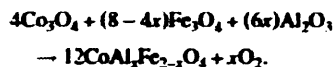
Cations such as Mn^{2+} , Ge^{4+} , and Al^{3+} have been substituted into Co-ferrite in different studies.¹⁻³ Because these cations have different site preferences between the tetrahedral sites (A-sites) and octahedral sites (B-sites), their degrees of influence on the magnetostrictive properties of Co-ferrite vary. Mn^{2+} for instance which has a B-site preference tends to displace some of the Co^{2+} from B-sites to A-sites,⁴ and has been shown to improve $d\lambda/dH$ though it lowers the magnitude of λ when substituted for Fe^{3+} in Co-ferrite at room temperature.¹ Ge^{4+} on the other hand has an A-site preference while Co^{2+} has a B-site preference and in a $\text{Ge}^{4+}/\text{Co}^{2+}$ cosubstitution for 2Fe^{3+} has been reported to result in the increase of both magnitude of λ and $d\lambda/dH$ at room temperature.² Unlike Mn^{2+} and Ge^{4+} with defined cation site preferences, Al^{3+} has been reported to have no particular preference for either the A-site or B-site of the spinel structured Co-ferrite.⁵ Like Mn^{2+} , Al^{3+} substitution at $x \leq 0.2$ resulted in an increased $d\lambda/dH$ but lower magnitude of λ at room temperature. Though $\text{Ge}^{4+}/\text{Co}^{2+}$ cosubstitution re-

sulted in higher magnitude of λ compared to Al^{3+} substitution, the enhancement of $d\lambda/dH$ was greater with Al^{3+} .³ It is important to study how magnetostrictive properties of cation substituted Co-ferrite vary with temperature in order to understand how to adjust those properties with suitable cation substitutions.

A study of the temperature dependence of the magnetostrictive properties of $\text{Co}_{1-x}\text{Ge}_x\text{Fe}_{2-2x}\text{O}_4$ (for $x=0, 0.1$, and 0.6) from 250 to 400 K showed that both the magnitude of λ and $d\lambda/dH$ decreased with increasing temperature.² The study also showed that the slopes of the λ -H plots changed both with composition and temperature. The influence of temperature on the magnitude of λ and $d\lambda/dH$ for $\text{CoAl}_x\text{Fe}_{2-x}\text{O}_4$ is not well understood. Since it has been demonstrated in comparison with other substitutions that $\text{CoAl}_x\text{Fe}_{2-x}\text{O}_4$ has potential for high-sensitivity magnetomechanical stress sensor and energy efficient magnetostrictive actuator applications at room temperature,³ it is important to understand how this material perform at different temperatures. This study extends the investigation of the magnetoelastic properties of magnetostrictive $\text{CoAl}_x\text{Fe}_{2-x}\text{O}_4$ over a wider temperature range of 50–350 K.

II. EXPERIMENTAL DETAILS

Co_3O_4 , Fe_2O_3 , and Al_2O_3 were mixed in appropriate proportions and calcined twice at 1000 °C for 24 h in air to obtain $\text{CoAl}_x\text{Fe}_{2-x}\text{O}_4$ following the chemical equation:



After calcining, the samples were finally sintered at 1350 °C for 24 h also in air. X-ray diffractometry (XRD) was used to study the crystal structure of the samples. The microstructures and final compositions were studied using a scanning electron microscope (SEM) equipped with an x-ray analyzer for energy dispersive x-ray (EDX) spectroscopy. The

*Electronic mail: nlebedimci@cardiff.ac.uk

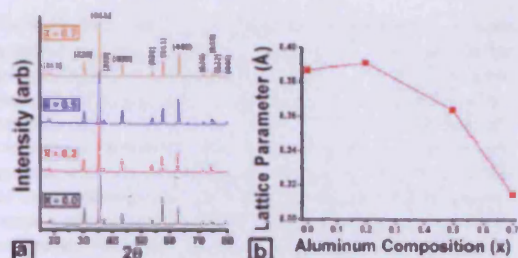


FIG. 1. (Color online) (a) XRD patterns for $\text{CoAl}_x\text{Fe}_{2-x}\text{O}_4$ system, and (b) variation of lattice parameter determined from the XRD result for $\text{CoAl}_x\text{Fe}_{2-x}\text{O}_4$ system ($x=0, 0.2, 0.5,$ and 0.7).

compositions of the samples as determined by EDX are $\text{Co}_{1.00}\text{Fe}_{1.00}\text{O}_4$, $\text{Co}_{1.03}\text{Al}_{0.18}\text{Fe}_{1.79}\text{O}_4$, $\text{Co}_{1.03}\text{Al}_{0.40}\text{Fe}_{1.57}\text{O}_4$, and $\text{Co}_{1.04}\text{Al}_{0.73}\text{Fe}_{1.27}\text{O}_4$.

Curie temperatures of the samples were measured in a vibrating sample magnetometer. Magnetostriction (λ) was measured parallel to the applied field with strain gauges attached on the samples, over a temperature range of 50–350 K using a physical property measurement system. The λ -H curve was differentiated with respect to field to obtain the strain sensitivity ($d\lambda/dH$).

III. RESULTS AND DISCUSSIONS

The XRD results for the $\text{CoAl}_x\text{Fe}_{2-x}\text{O}_4$ in Fig. 1(a) showed a single phase cubic spinel structure. The sample with $x=0.2$ shifted slightly to lower 2θ while samples with $x=0.5$ and 0.7 shifted to higher 2θ relative to the sample with $x=0.0$.

Figure 1(b) shows that at $x=0.2$, the lattice parameter initially increased slightly but later decreased with increase in x . If Vegard's law was obeyed and because Al^{3+} has smaller ionic radii on A-sites and B-sites compared to Fe^{3+} and Co^{2+} , a linear decrease of x with the lattice parameter would have been obtained. The samples showed deviation from Vegard's law at $x=0.2$ and a compliance at higher concentrations of $x=0.5$ and 0.7 indicating non linear changes in lattice parameter with Al^{3+} substitution. One possible expla-

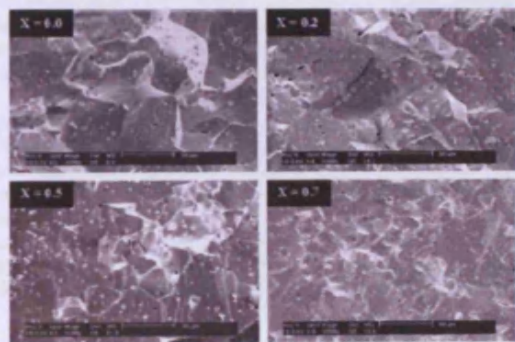


FIG. 2. Scanning electron micrographs for the $\text{CoAl}_x\text{Fe}_{2-x}\text{O}_4$ system. The dimension bar represents 50 μm .

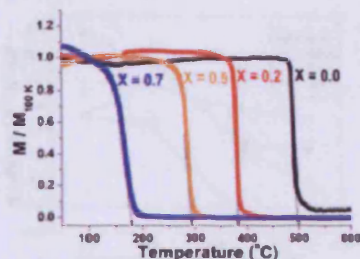


FIG. 3. (Color online) Variation of the magnetization with temperature for the $\text{CoAl}_x\text{Fe}_{2-x}\text{O}_4$ samples ($x=0.0, 0.2, 0.5,$ and 0.7).

nation of this trend is the variation in the ratio with which Al^{3+} substitutes into the two different sublattices as Al^{3+} concentration (x) increases. Al^{3+} has been reported to substitute into both A- and B-sites, with a ratio that changes with x , however different groups report different trends of how that ratio changes with x .^{5,6} Such nonlinear trend has been reported for $\text{Co}_{1+x}\text{Si}_x\text{Fe}_{2-2x}\text{O}_4$ system.⁷ The ionic radii of Si^{4+} for both the A- and B-sites are also smaller than those of Co^{2+} and Fe^{3+} .

Scanning electron micrographs in Fig. 2 show that the samples are single phase. This confirms the XRD result as the presence of additional phases would have been seen by additional peaks in the XRD diffractogram and varying contrast in the SEM micrographs.

As shown in Fig. 3, Curie temperatures of the samples decreased linearly with increase in Al concentration x . Since Al^{3+} is nonmagnetic, its substitution weakens the superexchange coupling that keeps the atomic moments aligned thus making it easier for thermal energy to disorder the moments. This results in lower Curie temperatures with increase in Al^{3+} content. A similar trend was reported for other cation substituted Co-ferrite studies.⁸

Figure 4(a) shows the λ -H curves for $\text{Co}_{1.00}\text{Fe}_{1.00}\text{O}_4$ from 50 to 350 K. In a typical room temperature λ -H curve for Co-ferrite,³ λ initially decreases steeply to a maximum negative value at low field, reaches a peak, and then saturates at a smaller negative value at high field. This is because

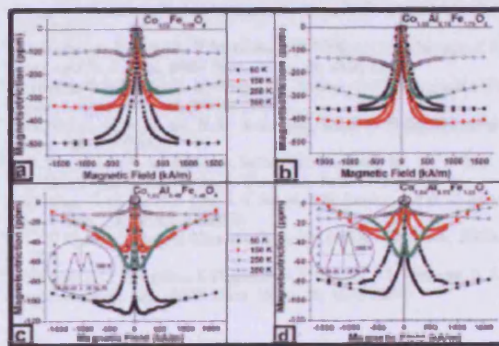


FIG. 4. (Color online) Magnetostriction curves for (a) $\text{Co}_{1.00}\text{Fe}_{1.00}\text{O}_4$, (b) $\text{Co}_{1.03}\text{Al}_{0.18}\text{Fe}_{1.79}\text{O}_4$, (c) $\text{Co}_{1.03}\text{Al}_{0.40}\text{Fe}_{1.57}\text{O}_4$, and (d) $\text{Co}_{1.04}\text{Al}_{0.73}\text{Fe}_{1.27}\text{O}_4$.

CoFe_2O_4 has (100) easy magnetization directions, a large negative λ_{100} and a smaller positive λ_{111} .⁹ The result in the present study shows that peak to peak λ increased as temperature decreased away from the Curie temperature of the samples which resulted in lower magnitudes of λ with increasing temperature. Also, magnetostrictive hysteresis decreased with increase in temperature. It can also be seen that as the temperature increased, the samples reached their maximum λ at smaller fields. This is because magnetocrystalline anisotropy decreases¹⁰ and as a result, the process of rotation of magnetization away from the (100) easy directions starts at smaller fields.

For $\text{Co}_{1.03}\text{Al}_{0.15}\text{Fe}_{1.79}\text{O}_4$ [Fig. 4(b)], the magnetostrictive hysteresis decreased while the contribution of λ_{111} to the resultant λ increased with increase in temperature. Unlike $\text{Co}_{1.02}\text{Fe}_{1.98}\text{O}_4$, the magnitude of peak to peak λ initially increased from 50 to 150 K and decreased afterwards from 250 to 350 K.

Figure 4(c) shows the λ -H curves for $\text{Co}_{1.03}\text{Al}_{0.49}\text{Fe}_{1.48}\text{O}_4$. Similar to previous results, magnetostrictive hysteresis decreased, while the contribution of λ_{111} to the maximum λ increased in going from 50 to 150 K, and decreased at 250 K. This is also true of the $\text{Co}_{1.04}\text{Al}_{0.73}\text{Fe}_{1.23}\text{O}_4$ [Fig. 4(d)]. Also for $\text{Co}_{1.03}\text{Al}_{0.49}\text{Fe}_{1.48}\text{O}_4$, it was observed that the magnitude of peak to peak λ decreased from 50 to 150 K, increased at 250 K, and afterwards decreased at 350 K. It is unclear why this happens but a similar trend was obtained for $\text{Co}_{1.04}\text{Al}_{0.73}\text{Fe}_{1.23}\text{O}_4$ shown in Fig. 4(d). These results indicate the possibility of altering the magnetostrictive characteristics of CoFe_2O_4 at temperatures of interest by cation substitution.

Also, for $\text{Co}_{1.03}\text{Al}_{0.49}\text{Fe}_{1.48}\text{O}_4$ in Fig. 4(c), at or below 250 K, from $H=0$, the slope of the λ -H curve was negative, and it was positive at high fields. The inset shows that at 350 K, from $H=0$, the slope was positive at low fields and negative at higher fields, until λ saturated at a negative value. This is opposite to the observation at or below 250 K, and signifies either λ_{111} being dominant at lower fields due to change in sign of the anisotropy coefficient, or a change in sign of both λ_{100} and λ_{111} . Interestingly, this characteristic which is observed for $\text{Co}_{1.03}\text{Al}_{0.49}\text{Fe}_{1.48}\text{O}_4$ at 350 K was observed for $\text{Co}_{1.04}\text{Al}_{0.73}\text{Fe}_{1.23}\text{O}_4$ at 300 K (Ref. 3) indicating the dependence of the slopes of the λ -H curve in CoFe_2O_4 and CoFe_2O_4 -based materials on composition and temperature. Thus it is possible to adjust composition to obtain desired λ and slope of λ within a temperature range of interest.

Figure 5 shows the variation of $(d\lambda/dH)_{\text{max}}$ with composition of the samples at temperature range of 50–350 K. At 50 K, all the samples showed a continuous decrease in $(d\lambda/dH)_{\text{max}}$ as a function of Al content x . $(d\lambda/dH)_{\text{max}}$ at 150 and 250 K increased from $x=0.0$ to 0.2 and decreased at higher values of x . This result is in agreement with previous studies on cation substituted Co-ferrite samples in which $(d\lambda/dH)_{\text{max}}$ improved at substitution levels of $x \leq 0.2$ and deteriorated at higher values of x .

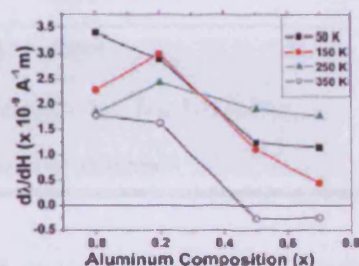


FIG. 5. (Color online) Variation of strain sensitivity with composition for the $\text{CoAl}_x\text{Fe}_{2-x}\text{O}_4$ system ($x=0, 0.2, 0.5$, and 0.7).

IV. CONCLUSIONS

Magnetic and magnetoelastic properties of $\text{CoAl}_x\text{Fe}_{2-x}\text{O}_4$ ($x=0, 0.2, 0.5$, and 0.7) have been observed to show substantial temperature dependence over the range 50–350 K, which can be adjusted by varying composition. Curie temperature was lowered as Al^{3+} substitution for Fe^{3+} was increased. For $x=0$, a monotonic dependence was found for the magnitude of peak to peak λ , $(d\lambda/dH)_{\text{max}}$, relative contribution of λ_{100} and λ_{111} to the resultant λ and magnetostrictive hysteresis. For $x=0.2, 0.5$, and 0.7 , a monotonic dependence was also found for the magnetostrictive hysteresis but not for relative contribution of λ_{100} and λ_{111} to the resultant λ nor for the magnitude of peak to peak λ and $(d\lambda/dH)_{\text{max}}$. Depending on intended application, this study shows that at temperatures of interest, magnetostrictive properties of Co-ferrite can be tailored by cation substitution.

ACKNOWLEDGMENTS

This research was supported by the UK EPSRC (Grant No. EP/057094) and by the U.S. NSF (Grant No. DMR-0402716).

- J. A. Pauthen, A. P. Ring, C. C. H. Lo, J. E. Snyder, and D. C. Jiles, *J. Appl. Phys.* **97**, 044502 (2005).
- N. Ranvah, I. C. Niebedim, Y. Melikhov, J. E. Snyder, D. C. Jiles, A. J. Moses, P. I. Williams, F. Anayi, and S. H. Song, *IEEE Trans. Magn.* **44**, 3013 (2008).
- I. C. Niebedim, N. Ranvah, Y. Melikhov, P. I. Williams, J. E. Snyder, A. J. Moses, and D. C. Jiles, *IEEE Trans. Magn.* **45**, 4120 (2009).
- K. Krichle, T. Schaeffer, J. A. Pauthen, A. P. Ring, C. C. H. Lo, and J. E. Snyder, *J. Appl. Phys.* **97**, 10F101 (2005).
- A. A. Younis, M. E. Elzain, H. H. Sutherland, and S. H. Salah, *Hyperfine Interact.* **68**, 323 (1992).
- B. S. Trivedi and R. G. Kulkarni, *Solid State Commun.* **96**, 327 (1993).
- S. S. Shinde and K. M. Jadhav, *J. Mater. Sci. Lett.* **17**, 849 (1998).
- S. H. Song, C. C. Lo, S. J. Lee, S. T. Adami, J. E. Snyder, and D. C. Jiles, *J. Appl. Phys.* **101**, 09C517 (2007).
- R. C. O'Handley, *Modern Magnetic Materials* (Wiley, New York, 2000), pp. 225.
- N. Ranvah, I. C. Niebedim, Y. Melikhov, J. E. Snyder, P. I. Williams, A. J. Moses, and D. C. Jiles, *IEEE Trans. Magn.* **45**, 4261 (2009).



Contents lists available at ScienceDirect

Journal of Magnetism and Magnetic Materials

journal homepage: www.elsevier.com/locate/jmmm

Effect of heat treatment on the magnetic and magnetoelastic properties of cobalt ferrite

I.C. Nlebedim^{*}, N. Ranvah, P.J. Williams, Y. Melikhov, J.E. Snyder, A.J. Moses, D.C. Jiles

Wolfson Centre for Magnetism, School of Engineering, Cardiff University, Cardiff CF24 3AA, UK

ARTICLE INFO

Article history:

Received 15 July 2009

Received in revised form

8 December 2009

Available online 13 January 2010

Keywords:

Anisotropy coefficient

Cobalt ferrite

Magnetostriction

Annealing temperature

Quenching

Strain sensitivity

ABSTRACT

The influence of different heat treatments on the magnetic and magnetoelastic properties of highly magnetostrictive CoFe_2O_4 has been investigated. The first order cubic anisotropy coefficient, coercive field, magnetostriction and high strain sensitivity were observed to decrease as the heat treatment temperature increased. The saturation magnetization of the samples on the other hand increased with increase in heat treatment temperature. These changes were not accompanied by any observable changes in crystal structure or composition and are indicative of migration of Co^{2+} from the octahedral sites (B-sites) to the tetrahedral sites (A-sites) and Fe^{3+} from the A-sites to the B-sites of the spinel structure. Different distributions of the cations at the two distinct lattice sites can strongly affect the magnetic and magnetoelastic properties of these materials.

© 2010 Elsevier B.V. All rights reserved.

1. Introduction

Cobalt ferrite (CoFe_2O_4) and its derivatives $\text{CoM}_2\text{Fe}_{2-x}\text{O}_4$ (where M stands for a metal ion) are promising materials for use in devices such as transducers, vibration controllers and sound generators because of their high magnetostriction and high rate of change of strain with magnetic field. Their technological potential as an alternative to the rare earth based magnetostrictive materials has recently attracted much interest. Apart from good mechanical and chemical properties, it has been shown that composites based on CoFe_2O_4 have a higher sensitivity of strain to applied field (corresponding to higher signal to background noise ratio) compared to Terfenol based composites [1].

CoFe_2O_4 is a spinel structured material and depending upon the positions of the cations, can be either a normal or an inverse spinel. For normal spinel materials such as ZnFe_2O_4 , all the divalent cations are on the tetrahedral sites (A-sites) and all the trivalent cations are on the octahedral sites (B-sites). By contrast, inverse spinel materials such as MgFe_2O_4 have half of their trivalent cations on the A-sites and the other half of the trivalent cations plus all of the divalent cations on the B-sites. Inverse spinel materials can be completely inverse or partially inverse depending on the distribution of the cations among the two types of lattice sites. Previously there has been some disagreement on the degree of inversion in CoFe_2O_4 [2–4] but it is known that the

Co^{2+} ions in CoFe_2O_4 have a preference for the B-sites. Also, it is known that the magnetic and magnetostrictive properties of CoFe_2O_4 depend on the concentration of Co^{2+} at the B-sites [5,6]. As a result, changes in the site occupancy of the cations will affect the magnetic and magnetostrictive properties. Such changes can be brought about by cation substitution [7,8] or heat treatment [2]. If initially all the Co^{2+} ions were on the B-sites (complete inversion), any heat treatment or cation substitution resulting in the movement of the Co^{2+} ions out of the B-sites will reduce the level of anisotropy and magnetostriction. On the other hand, if initially some Co^{2+} were on the A-sites (partial inversion), heat treatment or cation substitution may lead to some being moved to the B-sites resulting in an increase in the level of magnetostriction.

Until now, most of the studies on the magnetostrictive properties of CoFe_2O_4 have concentrated on understanding the effect of cation substitution. However, it has been reported that the degree of inversion in CoFe_2O_4 can be altered by heat treatment [9]. Since cation site occupancy is crucial in determining magnetostrictive properties, and this can be altered depending on heat treatment conditions, there is a need for a systematic study of the variation of heat treatment to produce desired magnetostrictive properties. Also, since the mechanical properties of magnetostrictive materials depend on the heat treatment, it is important to find a suitable compromise between magnetostrictive and mechanical properties when optimizing materials for specific types of applications. A recent study by Bhame and Joy [10] has shown that sintering conditions and microstructure can strongly influence the magnitude of the magnetostriction and

^{*} Corresponding author.

E-mail address: nlebedimc@Cardiff.ac.uk (I.C. Nlebedim).

strain sensitivity of CoFe_2O_4 . The cooling rate in that study was slow enough to allow the cations enough time to migrate close to their room temperature equilibrium positions. However, it is important to understand how the magnetostrictive properties of CoFe_2O_4 vary if the cations were frozen close to their equilibrium positions at different temperatures by rapidly cooling the samples from elevated temperatures.

This present study reports on the effect of heat treatment on the magnetic and magnetostrictive properties of CoFe_2O_4 samples quenched from different annealing temperatures. The crystal structure, microstructure and compositions of the annealed and quenched samples were studied and compared with those of a furnace cooled sample. Saturation magnetization (M_s), coercive field (H_c), first order cubic anisotropy constant (K_1), magnetostriction (λ), and strain sensitivity ($d\lambda/dH$) were measured for the samples quenched from different annealing temperatures and compared to a furnace cooled sample. Hereafter, the combination of annealing and quenching treatment will be referred to as heat treatment.

2. Experimental details

Cobalt ferrite (Co-ferrite) was prepared by mixing Fe_2O_3 and Co_2O_3 in the appropriate ratios and calcining twice at 1000°C for 24 h and then sintering at 1350°C for 24 h and finally furnace cooling to room temperature. The crystal structures of the samples were determined using X-ray diffractometry. The patterns were recorded at a step size of 0.02° on a Philips PW1710 automated powder diffractometer with copper (Cu K α) radiation at 35 kV and 40 mA. Scanning electron microscopy (SEM) analysis and energy dispersive X-ray spectroscopy (EDX) were carried out to ascertain the microstructure and chemical composition of the samples respectively. The EDX analysis could determine the compositions of cobalt and iron in the samples but not that of oxygen.

Some of the samples were reheated (i.e. annealed) to 600 , 800 , 1000 , 1200 and 1400°C in air, held at those temperatures for 24 h followed by quenching in water at room temperature. To ensure comparative quenching rates samples were selected with similar size and shape; that is, cylindrical samples with a nominal diameter of 9.05 ± 0.02 mm and a height of 10.20 ± 0.02 mm. Magnetic properties were measured using a SQUID magnetometer up to a maximum applied field of $H=4$ MA/m. Magnetostriction was measured at room temperature in the direction parallel to the applied field using resistive strain gauges bonded onto the samples. From the magnetostriction results, the sensitivity of magnetostriction to applied field was determined.

The first cubic anisotropy coefficients (K_1) of the samples were determined using the Law of Approach to saturation magnetization experimentally obtained [11] as

$$M = M_s \left(1 - \frac{a}{H} - \frac{b}{H^2} - \dots \right) + \kappa H \quad (1)$$

M_s and H are the saturation magnetization and applied field respectively, and κH is the forced magnetization term [12]. In using this law, it was assumed that in the region where the magnetization approaches saturation, all the magnetization processes were due to reversible rotation against the magnetic anisotropy. The coefficient $a \approx 0$ in the higher field region as it is related to domain wall pinning. For cubic structured randomly oriented polycrystalline samples, the coefficient b is given by Eq. (2) [13] in which μ_0 is the permeability of free space.

$$b = \frac{8}{105} \frac{K_1^2}{\mu_0 M_s^2} \quad (2)$$

The Law of Approach is said to be valid in the range $0.97 M_s < M < M_s$ [14] therefore, the high field region of the magnetization curve corresponding to this range was used to determine K_1 .

3. Results and discussion

Fig. 1 shows the X-ray diffraction patterns for all the samples investigated in this work. All the patterns were consistent with the presence of only spinel phases with no additional peaks present. The lattice parameters for the samples obtained from the X-ray diffraction results were found to be the same within experimental uncertainty ($8.37 \pm 0.02 \text{ \AA}$). Since the starting materials were also spinels, X-ray diffractometry was not sufficient to completely identify the samples as single phase Co-ferrite, hence, SEM and EDX analyses were also carried out.

The scanning electron micrographs of all the samples are shown in Fig. 2. The dimension bars on the micrographs represent $50 \mu\text{m}$. This showed uniform image contrast which is indicative of the presence of a single phase and confirms the results from the XRD patterns above.

Compositional analysis of the samples, as determined by EDX, showed that heat treatment did not change the composition of the samples. All the quenched and furnace cooled samples have a Co:Fe ratio of 1.02:1.98. These XRD, and EDX results signify that observed differences in magnetic and magnetostrictive properties in the quenched samples did not arise from changes in crystal structure or compositions following the heat treatment.

Fig. 3 shows the variation of magnetization value at an applied field of 4 MA/m for different heat treatment temperatures. Our results show an increase in magnetization with an increase in heat treatment temperature. The overall magnetization in spinel materials such as Co-ferrite depends on the super-exchange interaction between the cations on the A-sites and those on the B-sites. The coupling between the A-site and B-site moments is generally anti-parallel, with each type of site forming a parallel aligned sub-lattice. The resulting moment (M) is thus the

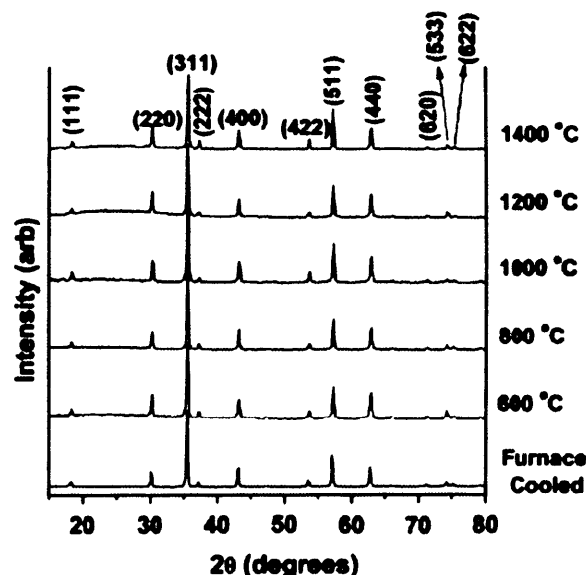


Fig. 1. X-ray diffraction patterns of the quenched and furnace cooled Co-ferrite samples.

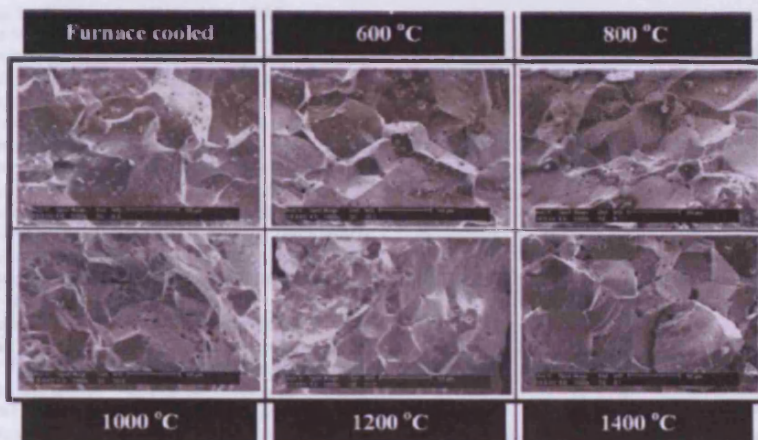


Fig. 2. SEM images of the samples. The dimension bar represents 50 μm.

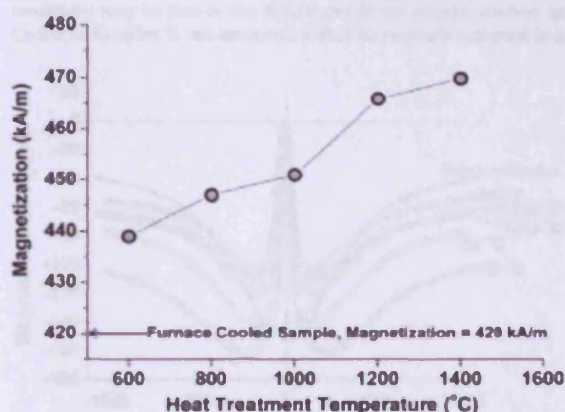


Fig. 3. Variation of magnetization at field (H)=4 MA/m with heat treatment temperature.

difference of the sum of the B-site moments (M_B) and the sum of the A-site moments (M_A)

$$M = \sum M_B - \sum M_A \quad (3)$$

If Co-ferrite was a complete inverse spinel, there would be equal amounts of Fe^{3+} on the A-sites and B-sites and their moments would cancel. The overall magnetization would then be the sum of the Co^{2+} moments on the B-sites. Annealing at elevated temperatures results in the redistribution of Co^{2+} and Fe^{3+} between the A-sites and B-sites. Higher temperatures favour arrangements which tend more towards random distribution, that is, more Co^{2+} on the A-sites and more Fe^{3+} on the B-sites compared with the furnace cooled state. This effect has been observed in a Mössbauer study [9]. The effect on magnetization would be to cause an increase with increasing heat treatment temperature, which is indeed our observation.

The variation of anisotropy with heat treatment temperature is shown in Fig. 4. The anisotropy decreased with increase in heat treatment temperature. High anisotropy in Co-ferrite is mainly due to the Co^{2+} on the B-sites of the spinel structure [15]. Again, according to the proposed explanation, since high temperature

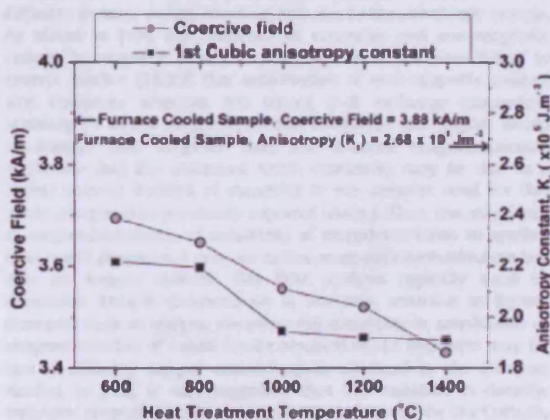


Fig. 4. Variation of coercive field and first cubic anisotropy constant with heat treatment temperature.

annealing followed by quenching results in cation distribution with more Co^{2+} on the A-sites and more Fe^{3+} on the B-sites than furnace cooling, this redistribution resulted in lower anisotropy as the heat treatment temperature increased.

As shown in Fig. 4, H_c decreased with increase in heat treatment temperature. This can be explained in terms of the change in the anisotropy energy required to rotate the magnetization away from easy directions into the direction of the applied field. The decrease in coercive field observed in our results is largely a consequence of a decrease in anisotropy of the samples due to the cation redistribution with increasing heat treatment temperature.

Magnetostriction amplitude was found to decrease with increasing heat treatment temperature as shown in Fig. 5. This can also be a consequence of the migration of Co^{2+} away from the B-sites into the A-sites. Like the anisotropy, the magnetostriction in Co-ferrite is also mainly due to the Co^{2+} on the B-sites of the spinel structure. Hence, migration of Co^{2+} away from the B-sites would lower the magnetostriction amplitude. The magnetostriction curve of Co-ferrite contains two regions; the low field region in which the

contribution from λ_{100} is dominant and the high field region in which the contribution from λ_{111} is also observed. The contribution from the low field region continues until all magnetic domains align parallel to the direction of easy magnetization $\langle 100 \rangle$. Fig. 5 also shows that the slopes of the low and high field regions of the curves are steeper for the furnace cooled sample compared to the annealed and quenched samples. This is because the annealed and quenched samples have a substantial amount of stress due to the quenching process that will impede the change of magnetization at those field regions causing lower slope of magnetostriction and leading to lower λ_{111} contribution. Further studies are required to determine any correlations between stress, quenching temperature and magnetostrictive properties and how these could be controlled to systematically tune the desired properties.

Fig. 6 shows the variation of strain sensitivity ($d\lambda/dH$) with applied field. The furnace cooled sample gave the highest value of $(d\lambda/dH)_{\max} = 4.34 \times 10^{-9} \text{ A}^{-1} \text{ m}$ which is higher than the previously reported values for un-doped Co-ferrite (1.3×10^{-9} and $1.5 \times 10^{-9} \text{ A}^{-1} \text{ m}$) [1,16]. On the other hand, the amplitude of magnetostriction in this study is lower than the value we previously reported for undoped Co-ferrite (225 ppm) [17] but higher than that reported by other investigators (100 and 90 ppm) [2,18]. The reason for this variation in the amplitude of magnetostriction and strain sensitivity may be due to the differences in the oxygen content in Co-ferrite samples. It has been stated that ferrosipinels can exist in a

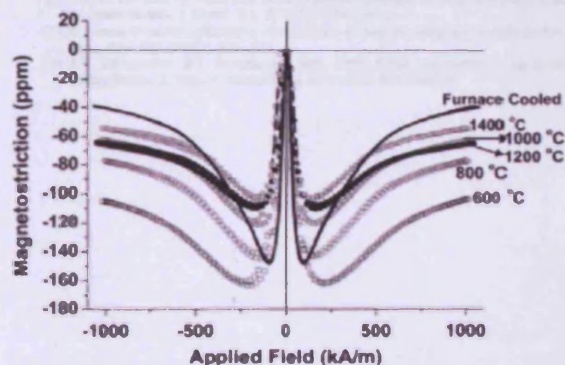


Fig. 5. Variation of magnetostriction amplitude with applied field.

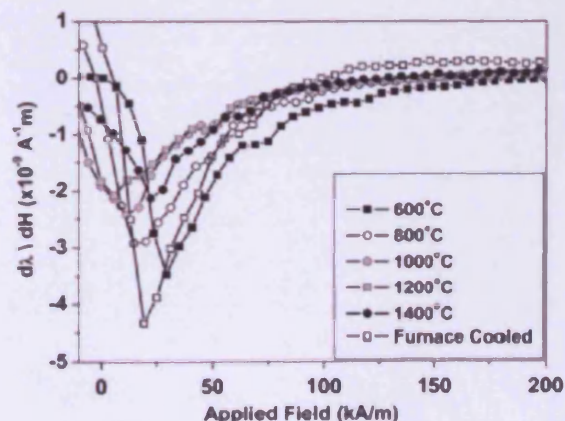


Fig. 6. Strain sensitivity of the furnace cooled and quenched Co-ferrite samples.

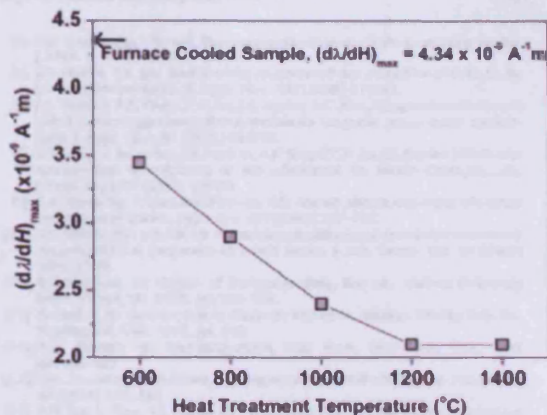


Fig. 7. Variation of maximum $d\lambda/dH$ at different heat treatment temperatures.

state with non-stoichiometric amounts of oxygen which can result in vacancies in the lattice [19]. These vacancies contribute to the diffusion process during sintering and also to the anisotropy energy. As stated in [19], the influence of vacancies and non-magnetic cations in magnetic oxides may be similar. It has been found in several studies [16,20] that substitution of non-magnetic cations into Co-ferrite weakens the strong A–B exchange interaction resulting in lower magnetostriction amplitude and higher strain sensitivity. This suggests that the reduced magnetostriction amplitude and the enhanced strain sensitivity may be due to a higher volume fraction of vacancies in the samples used for this study compared to previously reported studies. Thus, the amplitude of magnetostriction and sensitivity of magnetostriction to applied field could depend not only on cation composition/distribution but also on oxygen content. The EDX analysis typically used to determine sample compositions is not very sensitive to lighter elements such as oxygen, therefore the variability in amplitudes of magnetostriction of cobalt ferrite reported in the literature may be due to differing oxygen concentrations obtained in the different studies. In [10], it was suggested that the variation in density, magnetic properties and magnetostriction observed for the CoFe_2O_4 samples studied might be attributed to changes in the degree of inversion due to the release of oxygen from the samples during sintering.

From Fig. 7, it can be seen that as the heat treatment temperature increased from 600 to 1400 °C, the maximum strain sensitivity $(d\lambda/dH)_{\max}$ decreased. In previous studies [16,20], anisotropy and magnetostriction were decreased by substitution of other trivalent cations for some of the Fe^{3+} , thus disrupting the exchange coupling (and in some cases, displacing some of the Co from the B-sites to the A-sites). It was thought that the anisotropy decreased at a relatively fast rate compared to the magnetostriction, thus giving higher slopes. In this study, no cations were substituted, but as proposed, the Fe and Co distribution has been altered. This could be expected to give different relative decreases thus different resultant change in slope or strain sensitivity. Moreover, quenching also increases the stress in the samples which in turn could impede domain processes, thus lowering the sensitivity.

4. Conclusions

The results of a study of the effect of heat treatment on magnetoelastic and magnetic properties of highly magnetostrictive

Co-ferrite have been presented. XRD, SEM and EDX results showed that no crystal structure or compositional changes occurred in the samples as a result of the heat treatment. Magnetization increased with increasing heat treatment temperature which implies that there is a Co^{2+} migration from the B-sites to the A-sites and a corresponding Fe^{3+} migration from the A-sites to the B-sites of the spinel structure. This cation redistribution resulted in a decrease of the first order cubic anisotropy coefficient and the coercive field of the samples. The magnitude of magnetostriction of the samples also decreased which is also due to cation redistribution. The samples showed high maximum strain sensitivity but this reduced as the heat treatment temperatures increased.

Acknowledgments

This research was supported by the UK Engineering and Physical Science Research Council under Grant number EP057094 and by the US National Science Foundation under Grant number DMR-0402716.

References

- [1] Y. Chen, J.E. Snyder, C.R. Schwabach, K.W. Dennis, R.W. McCallum, D.C. Jiles, Metal-bonded Co-ferrite composites for magnetostrictive torque sensor applications, *IEEE Trans. Magn.* 35 (1999) 3652–3654.
- [2] J.G. Na, T.D. Lee, S.J. Park, Effects of cation distribution on magnetic properties in cobalt ferrite, *J. Mater. Sci.* 27 (1993) 961–962.
- [3] E. Prince, Neutron diffraction observation of heat treatment in cobalt ferrite, *Phys. Rev.* 102 (1956) 674–676.
- [4] A.S. Vaingankar, B.V. Khashtarkar, R.N. Patel, X-ray spectroscopic study of cobalt ferrite, *J. Phys. F: Metal Phys.* 10 (1980) 1615–1619.
- [5] R.D. Gansough, E.W. Lee, The magnetostriction of cobalt–manganese ferrite, *J. Phys. D.* 3 (1970) 1595–1604.
- [6] S.D. Bhame, P.A. Joy, Tuning of the magnetostrictive properties of CoFe_2O_4 by Mn substitution for Co, *J. Appl. Phys.* 100 (2006) 113011.
- [7] J.A. Paulsen, A.P. Ring, C.C.H. Lo, J.E. Snyder, D.C. Jiles, Manganese-substituted cobalt ferrite magnetostrictive materials for magnetic stress sensor applications, *J. Appl. Phys.* 97 (2005) 044502.
- [8] K. Kriebitz, T. Scharfner, J.A. Paulsen, A.P. Ring, C.C.H. Lo, J.E. Snyder, Mössbauer spectroscopy investigation of Mn-substituted Co ferrite $\text{Co}_{1-x}\text{Fe}_x\text{O}_4$, *J. Appl. Phys.* 97 (2005) 10F101.
- [9] G.A. Sawatzky, F. Van der Woude, A.H. Moort, Mössbauer study of several ferromagnetic spinels, *Phys. Rev.* 187 (1969) 747–757.
- [10] S.D. Bhame, P.A. Joy, Effects of sintering conditions and microstructure on the magnetostrictive properties of cobalt ferrite, *J. Am. Ceram. Soc.* 91 (2008) 1976–1980.
- [11] S. Chikazumi, in: *Physics of Ferromagnetism*, 2nd ed., Oxford University Press, Oxford, UK, 1987, pp. 503–508.
- [12] D. Cullity, in: *Introduction to Magnetic Materials*, Addison-Wesley Pub. Co., Reading MA, USA, 1972, pp. 347.
- [13] R.M. Bozorth, in: *Ferromagnetism*, IEEE Press, New York, USA, 1993, pp. 486–487.
- [14] E.W. Lee, Magnetostriction and magnetoelastic effects, *Rep. Prog. Phys.* 18 (1955) 184–229.
- [15] R.H. Liu, J. Ding, Z.L. Dong, C.B. Boothroyd, J.H. Yin, J.R. Yi, Microstructural evolution and its influence on the magnetic properties of CoFe_2O_4 powders during mechanical milling, *Phys. Rev. B* 74 (2006) 180427.
- [16] C.C.H. Lo, Compositional dependence of the magnetoelastic effect in substituted cobalt ferrite for magnetoelastic stress sensors, *IEEE Trans. Magn.* 43 (2007) 2367–2368.
- [17] N. Ravva, I.C. Nlebedim, Y. Melikhov, J.E. Snyder, D.C. Jiles, A.J. Moses, P.J. Williams, E. Anayi, Sang-Hoon Song, Temperature dependence of magnetostriction of $\text{Co}_{1-x}\text{Fe}_x\text{O}_4$ for magnetostrictive sensor and actuator applications, *IEEE Trans. Magn.* 44 (2008) 3013–3016.
- [18] S.D. Bhame, P.A. Joy, Enhanced magnetostrictive properties of Mn substituted cobalt ferrite $\text{Co}_{1-x}\text{Fe}_x\text{O}_4$, *J. Appl. Phys.* 99 (2006) 093901.
- [19] D.J. Craik, in: *Magnetic Oxides*, Part 1, John Wiley & Sons, Ltd., 1975, pp. 266–268.
- [20] I.C. Nlebedim, N. Ravva, Y. Melikhov, P.J. Williams, J.E. Snyder, A.J. Moses, D.C. Jiles, Magnetic and magnetoelastic properties of $\text{CoAlFe}_{1-x}\text{O}_4$ for stress sensor and actuator applications, *IEEE Trans. Magn.* 45 (2009) 4120.



Dependence of the magnetic and magnetoelastic properties of cobalt ferrite on processing parameters

I.C. Nlebedim^{*}, J.E. Snyder, A.J. Moses, D.C. Jiles

School of Engineering, Cardiff University, Cardiff CF24 3AA, UK

ARTICLE INFO

Article history:

Received 24 March 2010
Received in revised form
29 July 2010

Keywords:

Cobalt ferrite
Processing parameter
Sintering temperature
Holding time
Powder compaction pressure
Magnetostriction
Strain derivative

ABSTRACT

The dependence of the magnetic and magnetoelastic properties of highly magnetostrictive cobalt ferrite on processing parameters has been investigated. The cobalt ferrite samples used in this study were prepared via conventional ceramic processing methods. The processing parameters of interest were sintering temperature, holding time at the sintering temperature and powder compaction pressure. It was observed that the crystal structure, composition and saturation magnetization of the samples studied did not vary with changes in processing parameters but coercive field decreased with increasing sintering temperature. The amplitude of peak to peak magnetostriction was dependent on the holding time and powder compaction pressure. The strain derivative on the other hand was found to depend on powder compaction pressure at any given sintering temperature or holding time. The results show how the magnetoelastic properties of cobalt ferrite can be varied by changing the processing parameters.

© 2010 Elsevier B.V. All rights reserved.

1. Introduction

The need for advanced automated systems in industries is increasing due to the requirement to scale up production. Most automated systems depend heavily on high sensitivity sensor or energy efficient actuator devices. Stress sensors and actuators can be developed by exploiting the magnetomechanical coupling capability in magnetostrictive materials. It is important to optimize the properties of these materials for such applications. This has sparked considerable research interest in magnetostrictive materials in developing devices for different applications, especially where non-contact operation is crucial. Non-contact operation capability is very useful for devices because accuracy, repeatability and linearity are degraded over time due to wear and tear in devices operating in contact mode. Suitable magnetostrictive materials for such devices should possess sufficient amplitude of magnetostriction for the intended applications and high sensitivity of magnetostriction to applied magnetic field (strain derivative). Materials based on cobalt ferrite are candidates for such device development because of their desirable magnetostrictive properties [1].

Cobalt ferrite (CoFe_2O_4) and its derivatives $\text{CoM}_x\text{Fe}_{2-x}\text{O}_4$ (where M stands for a metal ion) have high strain derivative, good chemical stability and are suitable for developing robust magnetomechanical devices. Moreover, since it has been shown that magnetostriction amplitude of as low as 30 ppm is sufficient

for several applications [2], the typical amplitudes of magnetostriction, 100–225 ppm, reported for cobalt ferrite in various studies [3–5] are high enough for many applications. As a result, sensor and actuator designs based on cobalt ferrite are expected to be durable, chemically stable and exhibit good response to stimulus in application.

Cobalt ferrite has a partially inverse spinel crystal structure. Fig. 1 [6] shows the cation and oxygen distribution around the tetrahedral and octahedral sites of a spinel crystal structure. For cobalt ferrite, it is generally accepted that a large fraction of Co^{2+} are on the octahedral sites (B-sites) and the rest are on the tetrahedral sites (A-sites) [7]. In comparison with other ferrite materials, the high amplitude of magnetostriction in cobalt ferrite is thought to be due to the Co^{2+} on the B-sites of the spinel structure. This suggests that changes in site occupancy of Co^{2+} and deviation of targeted composition from stoichiometry (CoFe_2O_4) affect the amplitude of magnetostriction and strain derivative of cobalt ferrite. With two different cation sites, Co-ferrite offers the potential for tailoring its magnetostrictive properties by influencing the site occupancy of the cations. Substitution of cations such as Mn^{3+} , Ga^{3+} , Cr^{3+} , Ge^{4+} , Co^{2+} and Al^{3+} have been shown to affect the magnetostrictive properties of Co-ferrite in different ways depending on the site into which they substitute [3]. Since magnetostrictive properties also depend on heat treatment and other processing parameters, the capability to optimize magnetostrictive properties without cation substitution is desirable.

The effect of quenching heat treatments and the influence of vacuum sintering on the magnetostrictive properties of Co-ferrite have been studied [8,9]. Both studies showed degradation of magnetostriction and strain derivative due to cation redistribution

^{*} Corresponding author.

E-mail address: nlebedimc@Cardiff.ac.uk (I.C. Nlebedim).



ARTICLE IN PRESS

2

I.C. Nlebedim et al. / Journal of Magnetism and Magnetic Materials 4 (2010) 1–11

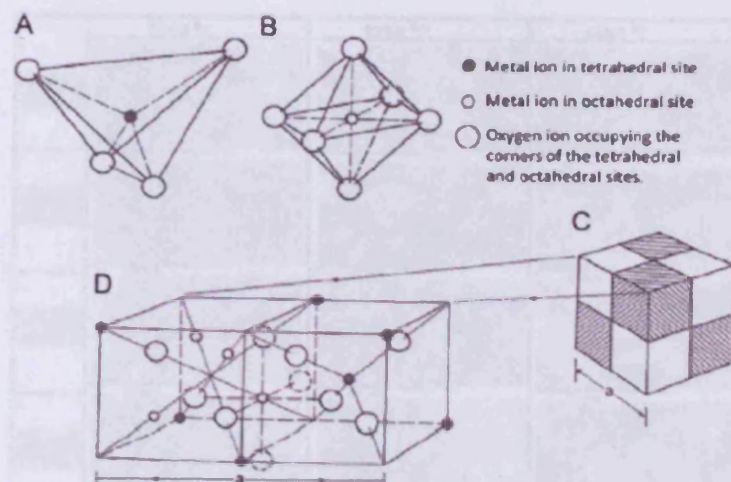


Fig. 1. (a) Tetrahedral site surrounded by four oxygen ions. (b) Octahedral site bounded by six oxygen ions. (c) Spinel crystal structure. Shaded and non-shaded parts represent octants of similar cation occupancy. (d) Two octants showing cation and oxygen distribution. After Cullity [6].

and development of additional phase, respectively. Since it is possible to alter magnetostrictive properties by altering the processing parameters, this study aims at investigating in detail the dependence of the magnetic and magnetostrictive properties of Co-ferrite prepared via conventional ceramic methods on compaction pressure, sintering temperature and holding time during the preparation of Co-ferrite.

2. Experimental details

Co_2O_3 and Fe_2O_3 were mixed in their appropriate proportions and calcined twice for 24 hrs at 1000 °C in air following the chemical equation:



Calcining the samples twice was necessary to ensure complete solid state reaction of the oxides. After calcining, the powder samples were pressed at 87 or 127 MPa, sintered in air at 1250, 1350 or 1450 °C and held at those temperatures for 24 or 36 h. To confirm a complete formation of the spinel phase, X-ray diffractometry (XRD) was used to study the crystal structure of the samples. The spectra were measured at increments of 0.02° on a Philips PW1710 automated powder diffractometer with copper ($\text{CuK}\alpha$) radiation at 35 kV and 40 mA. The microstructures and final compositions of the samples were studied using an FEI XL30 FEG environmental scanning electron microscope (ESEM) equipped with an Oxford Instrument Inca X-ray analyzer for energy dispersive X-ray spectroscopy (EDX).

Magnetic properties were studied with a SQUID magnetometer up to a maximum applied field of 50 kOe. Room temperature magnetostriction (λ) was measured parallel to the applied field using strain gauges attached to the samples. The sensitivity of magnetostriction to applied magnetic field ($d\lambda/dH$) was determined by differentiating the magnetostriction curve with respect to the magnetic field.

3. Results and discussion

The X-ray diffraction patterns shown in Fig. 2 are representative of all samples investigated. Five of the twelve patterns were

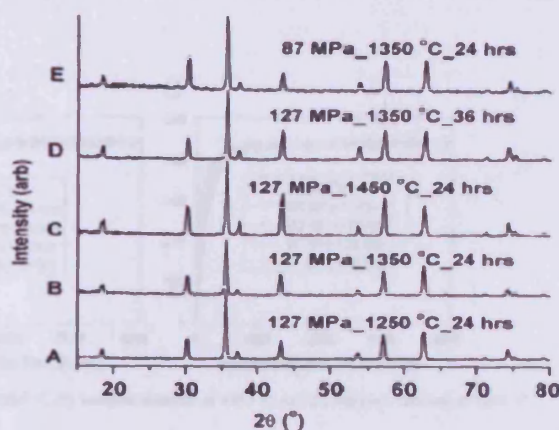


Fig. 2. X-ray diffraction patterns for a selected subset of representative samples showing the effect of varying sintering temperature (A–C), holding time (B and D) and powder compaction pressure (B and E).

selected to show different effects of the processing parameters studied on the crystal structure of cobalt ferrite. Samples A, B and C have different sintering temperatures, samples B and D have different holding times at a sintering temperature while samples B and E have different powder compaction pressures. All XRD spectra showed only the peaks of the single spinel phase crystal structure. Furthermore, no shifts in the peak positions were observed indicating that no observable changes in lattice constants took place due to the variation of the processing parameters. SEM and EDX analyses were also carried out to further confirm the presence of a single phase by investigating the microstructure and determining the final compositions of the samples studied.

Fig. 3 shows backscattered electron micrographs of the samples. Backscattered electron imaging is used because unlike the secondary electron imaging, the image contrast is a function of the elemental composition of the sample studied.

Please cite this article as: I.C. Nlebedim, et al., J. Magn. Magn. Mater. (2010), doi:10.1016/j.jmmm.2010.08.026



ARTICLE IN PRESS

I.C. Nlebedim et al. / Journal of Magnetism and Magnetic Materials 310 (2010) 200–208

3

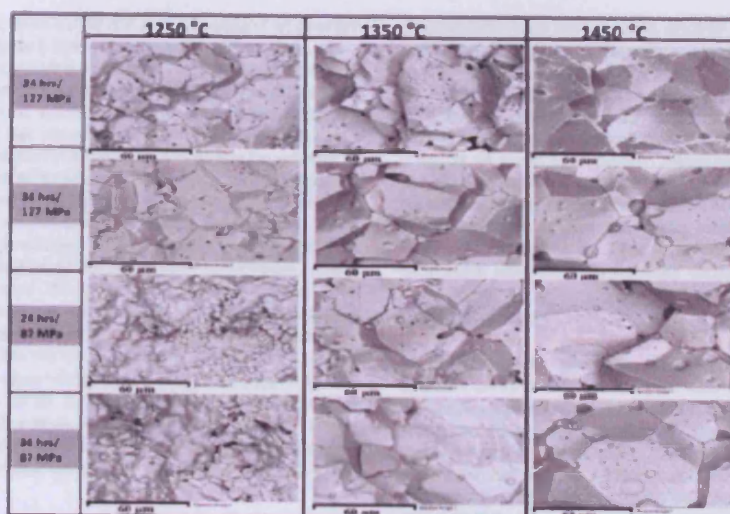


Fig. 3. Backscattered electron micrographs of samples after various sintering temperatures, holding times and powder compaction pressures for all the samples. Uniform image contrast indicates the presence of a single phase.

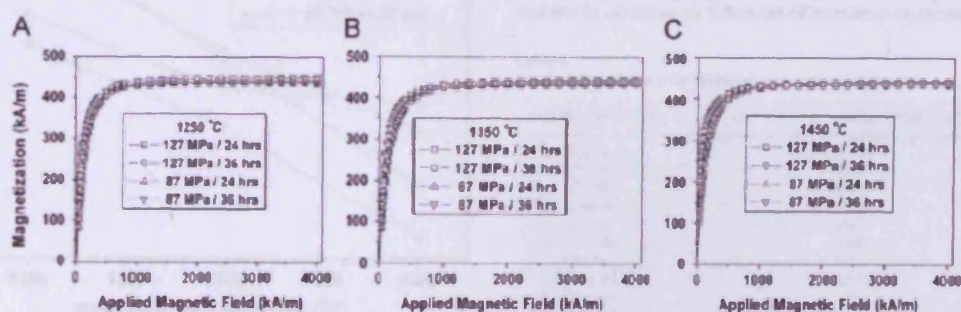


Fig. 4. First quadrant of the hysteresis loop showing: (A) samples sintered at 1250 °C, (B) samples sintered at 1350 °C and (C) samples sintered at 1450 °C.

The micrographs showed uniform image contrast indicating that the samples have a single phase, which is in agreement with the XRD patterns. The SEM results also showed that both the pore sizes and grain sizes of the samples increased with both increase in sintering temperature and holding time.

The final composition of the samples was determined by EDX analysis as $\text{Co}_{1.03}\text{Fe}_{1.97}\text{O}_4$ with ± 0.01 variation in cation composition between the samples. The uniformity in composition and crystal structure of the samples indicates that changes from one sample to the next could be attributed to changes in microstructure, magnetic and magnetostrictive properties following processing.

The first quadrants of the hysteresis loop of the samples sintered at 1250, 1350 and 1450 °C are shown in Fig. 4A–C, respectively. The saturation magnetization (M_s) is within $\pm 1.8\%$ of the average M_s for all the samples. The results show that varying the powder compaction pressure, sintering temperature or holding time does not affect M_s . This is in agreement with the normal observation that for samples of the same chemical composition, M_s is microstructure insensitive; being unaffected by fabrication or heat treatment [10].

The coercive field on the other hand varied with processing parameters as shown in Fig. 5. For the same compaction pressure, the coercive field of all the samples decreased with increase in sintering temperature. This result is consistent with the SEM result because increase in sintering temperature resulted in an increase in grain size and hence a decrease in coercive field.

For the samples compacted at 87 MPa and sintered at any sintering temperature, a holding time of 36 h resulted in lower coercive field than a holding time of 24 h. This is because longer holding time at the sintering temperatures resulted in larger grains and thus lower coercive field. However, for samples pressed at 127 MPa, a holding time of 24 h resulted in lower coercive field than a holding time of 36 h at all sintering temperatures except at 1450 °C. It is not clear why a shorter holding time would produce lower coercive field than a longer holding time at 127 MPa. It may represent the contribution of defects to increasing the coercive field due to such a high compaction pressure. At 1450 °C, a holding time of 36 h resulted in lower coercive field instead, which may be because at such a high temperature, the tendency of grain growth to decrease the coercive field outweighed that of defects to increase it.

Please cite this article as: I.C. Nlebedim, et al., J. Magn. Magn. Mater. (2010), doi:10.1016/j.jmmm.2010.08.026

ARTICLE IN PRESS

4

I.C. Nlebedim et al. / Journal of Magnetism and Magnetic Materials 3 (2010) 00–00

These results indicate that coercive field is also dependent on powder compaction pressure, sintering temperature and holding time.

Fig. 6 shows the magnetostriction curves of various samples. The results show that peak to peak magnetostriction amplitude decreased with increase in holding time at any given sintering temperature for any of the powder compaction pressures. This decrease in magnetostriction with holding time may be related to the increase in pore sizes with holding time. One might expect a similar effect on magnetostriction due to increase in sintering temperature, because it also results in the increase in pore sizes. This was not observed however, likely because other physical changes could take place due to increase in temperature, which might not take place due to increase in holding time. The differences in the influences of holding time and sintering temperature on amplitude of peak to peak magnetostriction is unlikely to be due to differences in cation distribution because such would have been observable from the M_s measurements. Obtaining similar values of M_s for all the samples indicates that there are no substantial cation distribution differences in the samples. A previous study has related the variation in M_s to the differences in cation distribution [8]. In summary, peak to peak

magnetostriction varied considerably indicating a strong dependence on processing parameters. This may explain the reason for the different peak to peak magnetostriction amplitude reported for cobalt ferrite in the literature [3–5].

Table 1 summarises the dependence of strain derivative of cobalt ferrite on processing parameters. Strain derivative $d\lambda/dH$ is a figure of merit of a magnetostrictive material, which indicates the strain response of the material to an applied magnetic field. As shown in the table, strain derivative of cobalt ferrite increases with increase in powder compaction pressure at any given sintering temperature. Like the magnetostriction result, strain derivative also depends strongly on processing parameters.

4. Conclusions

Backscattered electron imaging of cobalt ferrite samples showed uniform microstructure and changes in grain size with variation in processing parameters. Crystal structure, composition and saturation magnetization of the samples were insensitive to the processing parameters. Peak to peak magnetostriction and strain derivative on the other hand showed strong dependence on the variation of the processing parameters. The results from this study indicate that the reported differences in literature of the magnetostrictive properties of cobalt ferrite are likely due to different processing routes adopted by different authors. It thus suggests that optimizing the magnetostrictive properties of cobalt ferrite requires appropriate consideration of processing parameters in addition to selection of chemical compositions.

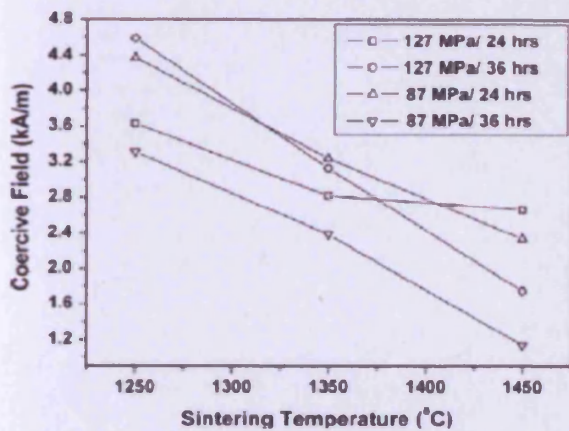


Fig. 5. Variation of coercive field with sintering temperature at different holding times and powder compaction pressures.

Table 1

Dependence of strain derivative on processing parameters.

Sample (MPa/°C/h)	Strain derivative ($\times 10^{-9} \text{ A}^{-1} \text{ m}$)
87/1250/24	1.31
127/1250/24	2.25
87/1250/36	1.75
127/1250/36	1.78
87/1350/24	1.23
127/1350/24	1.45
87/1350/36	1.84
127/1350/36	2.19
87/1450/24	1.89
127/1450/24	2.20
87/1450/36	1.65
127/1450/36	2.26

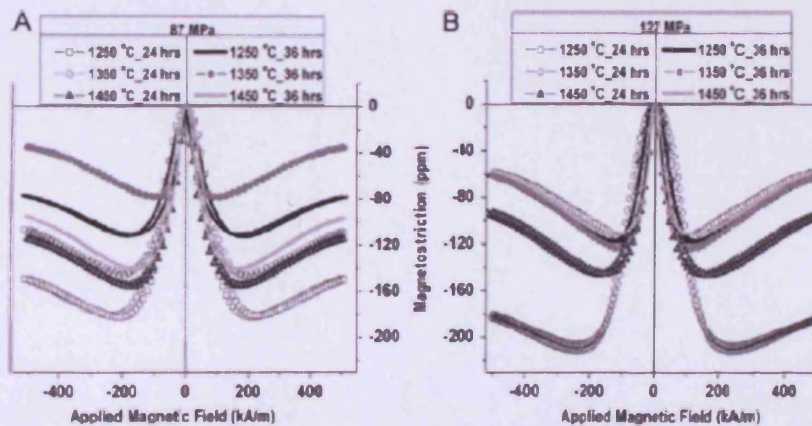


Fig. 6. Magnetostriction plots for samples compacted at (A) 87 MPa and (B) 127 MPa.

Please cite this article as: I.C. Nlebedim, et al., J. Magn. Magn. Mater. [2010], doi:10.1016/j.jmmm.2010.08.026

ARTICLE IN PRESS

I.C. Nlebedim et al. / Journal of Magnetism and Magnetic Materials 310 (2010) 14–15

5

Acknowledgments

This research was supported by the UK Engineering and Physical Science Research Council under Grant no. EP/057094.

References

[1] Y. Chen, J.E. Snyder, C.R. Schlichtenberg, K.W. Dennis, R.W. McCallum, D.C. Jiles, Metal-bonded Co ferrite composites for magnetostrictive torque sensor applications, *IEEE Trans. Magn.* 35 (1999) 3652–3654.

[2] A. Alfanni, A. Guerra, L. Dall’Agiovanna, G. Chiorboli, Design and characterization of magnetostrictive linear displacement sensors, in: *Proceedings of the 21st IEEE Instrumentation and Measurement Technology Conference, 2004, IMTC 04*, vol. 1, 2004, pp. 206–209.

[3] I.C. Nlebedim, N. Ravvah, Y. Melikhov, P.I. Williams, J.E. Snyder, A.J. Moses, D.C. Jiles, Magnetic and magnetoelastic properties of $\text{CoAl}_2\text{Fe}_{1-x}\text{D}_x$ for stress sensor and actuator applications, *IEEE Trans. Magn.* 45 (2009) 4120–4123.

[4] J.C. Na, T.D. Lee, S.J. Park, Effects of cation distribution on magnetic properties in cobalt ferrite, *J. Mater. Sci. Lett.* 12 (1993) 961–962.

[5] S.D. Bhamu, P.A. Jay, Magnetic and magnetostrictive properties of manganese substituted cobalt ferrite, *J. Phys. D: Appl. Phys.* 40 (2007) 3263–3267.

[6] B.D. Culity, *Int. Introduction to Magnetic Materials*, Addison-Wiley, USA, 1972 185.

[7] A.S. Vaingankar, B.V. Khabardar, R.N. Patil, *J. Phys. F: Metal Phys.* 101 (2007) 05C517.

[8] A.S. Vaingankar, B.V. Khabardar, R.N. Patil, *J. Phys. F: Metal Phys.* 10 (1980) 1615.

[9] I.C. Nlebedim, N. Ravvah, P.I. Williams, Y. Melikhov, J.E. Snyder, A.J. Moses, D.C. Jiles, Effect of Heat Treatment on the Magnetic and Magnetoelastic Properties of Cobalt Ferrite, *J. Magn. Magn. Mater.* 322 (2010) 1929–1933.

[10] I.C. Nlebedim, N. Ravvah, P.I. Williams, Y. Melikhov, F. Anayi, J.E. Snyder, A.J. Moses, D.C. Jiles, Influence of vacuum sintering on microstructure and magnetic properties of magnetostrictive cobalt ferrite, *J. Magn. Magn. Mater.* 321 (2009) 2528–2532.

[11] R.M. Bozorth, in: *Ferromagnetism*, IEEE Press, New York, USA, 1993 pp.14–15.

1. INTRODUCTION

The study of magnetostrictive materials has been a subject of interest for many years. Magnetostriction is the change in length of a material when it is subjected to a magnetic field. This phenomenon is observed in all ferromagnetic materials, but it is particularly pronounced in certain materials such as iron, nickel, and cobalt. The study of magnetostriction is important for many applications, including the design of sensors, actuators, and transducers. In this paper, we will discuss the magnetostrictive properties of cobalt ferrite, a material that has been widely studied in the literature. We will first review the basic principles of magnetostriction and then discuss the specific properties of cobalt ferrite. Finally, we will discuss the applications of cobalt ferrite in various fields of science and technology.

2. THEORETICAL BACKGROUND

The magnetostrictive effect is a result of the interaction between the magnetic field and the lattice structure of the material. In a ferromagnetic material, the magnetic moments are aligned in the same direction, and this alignment causes the lattice to expand or contract. The magnetostrictive coefficient, λ , is defined as the change in length per unit length per unit magnetic field. The magnetostrictive coefficient is a function of the magnetic field and the temperature. In this paper, we will discuss the magnetostrictive properties of cobalt ferrite, a material that has been widely studied in the literature. We will first review the basic principles of magnetostriction and then discuss the specific properties of cobalt ferrite. Finally, we will discuss the applications of cobalt ferrite in various fields of science and technology.

3. EXPERIMENTAL PROCEDURE

The magnetostrictive properties of cobalt ferrite were measured using a magnetostrictive torque sensor. The sensor was calibrated using a known weight and a known magnetic field. The magnetostrictive torque was measured as a function of the magnetic field and the temperature. The magnetostrictive coefficient was calculated from the slope of the magnetostrictive torque versus magnetic field curve. The magnetostrictive coefficient was found to be a function of the magnetic field and the temperature. In this paper, we will discuss the magnetostrictive properties of cobalt ferrite, a material that has been widely studied in the literature. We will first review the basic principles of magnetostriction and then discuss the specific properties of cobalt ferrite. Finally, we will discuss the applications of cobalt ferrite in various fields of science and technology.

Please cite this article as: I.C. Nlebedim, et al., *J. Magn. Magn. Mater.* (2010), doi:10.1016/j.jmmm.2010.08.026



Growth of crystalline cobalt ferrite thin films at lower temperatures using pulsed-laser deposition technique

A. Raghunathan,^{a)} I. C. Nlebedim, D. C. Jiles, and J. E. Snyder
Wolfson Centre for Magnetism, Cardiff University, Cardiff, CF24 3AA, United Kingdom

(Presented 20 January 2010; received 29 October 2009; accepted 5 December 2009; published online 4 May 2010)

Cobalt ferrite thin films were grown on SiO₂/Si(100) substrates using pulsed-laser deposition technique at substrate temperatures ranging from 250 to 600 °C. Thermal expansion mismatch between the film and substrate appears to have a substantial effect on the magnetic properties of the cobalt ferrite films, due to the large magnetoelastic coupling of cobalt ferrite. It was shown in this study, that polycrystalline films with (111)-preferred orientation could be prepared at substrate temperatures as low as 250 °C. The growth of crystalline cobalt ferrite films at such low temperatures indicates the potential to use cobalt ferrite for microelectromechanical systems devices and sensor applications including integration with a wider range of multilayer device structures.

© 2010 American Institute of Physics. [doi:10.1063/1.3357315]

I. INTRODUCTION

Due to exceptional magnetoelastic, magnetotransport, magneto-optical, photomagnetic, electronic, and magnetic properties, cobalt ferrite (CFO) has been proposed for applications in noncontact force and torque sensors,¹ as spin filters for magnetic tunnel junctions,² for hybrid data storage,³ for magneto-optical media,⁴ and as anode materials for advanced Li-ion batteries.⁵ Depending on the requirements of application, magnetic and magnetoelastic properties of CFO can be fine-tuned by appropriate cation substitution^{1,6–8} and magnetic annealing.⁹

The optimum substrate temperature for thin film growth has been reported to be 600 °C,¹⁰ in order to produce crystalline CFO. However, such high substrate temperatures limit the potential use of CFO in microelectromechanical systems (MEMS) devices, multilayer hybrid sensors, or integration with giant magnetoresistance, tunneling magnetoresistance, or semiconductor devices. Hence, it is necessary to investigate the optimum growth conditions for CFOs, which would enable pulsed-laser deposition (PLD) of crystalline CFO films at lower substrate temperatures.

II. THIN FILM GROWTH

The films for this study were deposited from a CoFe₂O₄ target using a 248 nm KrF excimer laser at 210 mJ and 13 Hz repetition rate. The laser spot size was 9 × 1.5 mm². The target-to-substrate distance was maintained at 5 cm. Substrates were Si(100) wafers with 300 nm thermal SiO₂ on top. The chamber was pumped down to 1 × 10⁻⁷ Torr before deposition. A series of five different substrate temperatures (T_{DEP}) were investigated: 250, 350, 450, 550, and 600 °C. All films were deposited in 22 mTorr of oxygen, and cooled to room temperature under the same oxygen pressure. This process gave film growth rates of 2.25 nm/min, which did not vary with deposition temperature in this study.

^{a)}Electronic mail: arunkumar@cardiff.ac.uk

III. EXPERIMENTAL

Film thicknesses were measured from cross-sections in the scanning electron microscope (SEM), and were 135 ± 5 nm for all samples. Crystal structure and orientation were investigated by θ -2 θ x-ray diffraction (XRD) scans. Composition was determined by energy-dispersive x-ray spectroscopy (EDX) in the SEM, averaging over 15 locations. Magnetic hysteresis loops were measured at room temperature using a vibrating sample magnetometer (VSM) with maximum applied field of 16 kOe.

Surface morphology and roughness of the deposited films were determined by atomic force microscopy (AFM). The imaging of magnetic domains in the films was carried out using magnetic force microscopy (MFM) with the phase detection technique.

IV. RESULTS AND DISCUSSION

A. Crystallography

The XRD patterns of the deposited CFO films are shown in Fig. 1. All of the films were crystalline and single-phase with the cubic spinel structure. From EDX, compositions were found to be Co_{0.9}Fe_{1.9}O₄ (with the oxygen content assumed, since EDX cannot determine it accurately). The films grown at low T_{DEP} showed preferred (111)-texture with some (311) whereas, at higher temperatures, films prefer to grow in (100) and (311) orientation. This represents a considerably different trend from that observed by Zhou *et al.*¹⁰ The growth of crystalline CFO films with (111)-texture at lower temperatures (T_{DEP}=250 °C) show potential for hybrid multilayer sensor applications and integration with multilayer structures that require lower processing temperatures.

B. Magnetic properties

Hysteresis loops of the CFO films, measured by VSM at room temperature are shown in Figs. 2(a)–2(e). The films deposited at 600 °C and 550 °C show a large perpendicular

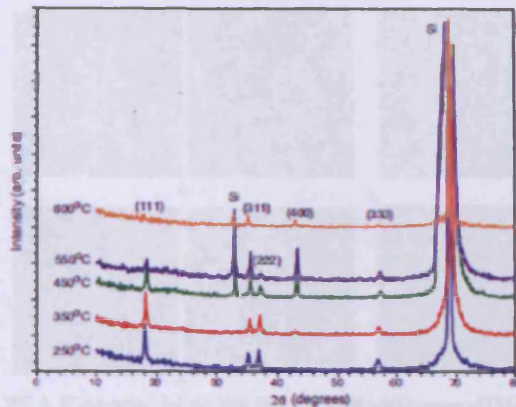


FIG. 1. (Color online) XRD patterns of films deposited at different substrate temperatures. At lower temperatures, the films were crystalline with predominantly (111)-texture and some (311) whereas, at higher temperatures, preferred orientation is (100) and (311).

anisotropy contribution [see Figs. 2(a) and 2(b)]. For decreasing T_{DEP} , the hysteresis loops show the perpendicular anisotropy contribution decreasing, and the in-plane anisotropy contribution increasing [Figs. 2(c)–2(e)]. However, although the effect of perpendicular anisotropy contribution is less significant at lower temperatures, it is still high enough to produce substantial out-of-plane magnetization [Figs. 3(a)–3(e)], and contribute to the high coercivity of the films.

It is evident from Fig. 2(f) that in-plane coercivity is almost constant with temperature whereas the coercivity measured from perpendicular loops increases with temperature indicating also that the perpendicular magnetic anisotropy increases with T_{DEP} .

The thermal expansion coefficients of silicon substrate and CFO are reported to be $3.5 \times 10^{-6} \text{ K}^{-1}$ and $1 \times 10^{-5} \text{ K}^{-1}$, respectively.¹⁰ Due to the mismatch, when the substrate-film combination is cooled down to room temperature, an in-plane isotropic tension will be induced in the film. The amount of strain induced due to thermal expansion mismatch can be predicted from¹¹

$$\varepsilon = (\alpha_s - \alpha_f)\Delta T, \quad (1)$$

where α_s and α_f are thermal expansion coefficients of substrate and film, respectively, and ΔT is the difference between the deposition temperature and measuring temperature (usually room temperature). Figure 2(g) shows the predicted induced strain due to thermal expansion mismatch versus substrate temperature. As the T_{DEP} increases, strain induced on the film becomes larger showing a linear relationship. Since CFO has predominantly negative magnetostriction,⁹ in-plane tension is expected to give rise to perpendicular magnetic anisotropy, which increases with increasing T_{DEP} .

Crystallographic texture together with magnetocrystalline anisotropy can also contribute to perpendicular anisotropy. To the extent that the high T_{DEP} films show some preferred (100)-texture, that would be expected to contribute some in-plane anisotropy (since K_1 is reported to be positive for CFO¹²) and to the extent that the lower T_{DEP} films show some preferred (111)-texture, that would be expected to contribute some perpendicular anisotropy.¹³ However for the films of this study, it is apparent that the magnetoelastic contribution predominates, since the perpendicular anisotropy shows the reverse trend (highest for highest T_{DEP} and lowest for lower T_{DEP}).

The variation in magnetization (measured at 16 kOe applied field) with T_{DEP} is shown in Fig. 2(h). As the T_{DEP} increases, magnetization increases probably due to varying amounts of oxygen vacancies and varying cation site occupancies of Co and Fe. At 600 °C, the magnetization decreases by 10% from its peak value. As can be seen from Fig. 2(h), the room temperature magnetization values (measured at 16 kOe) lie in the range of 130–270 emu/cm^2 whereas the saturation magnetization value of bulk CFO is $\sim 400 \text{ emu}/\text{cm}^2$.¹⁴

C. Surface morphology and domain imaging

Figures 3(a)–3(e) show surface morphology seen in AFM (on the left) and magnetic domain patterns seen in MFM (on the right) of CFO thin films deposited at different temperatures. The rms surface roughness was found to be

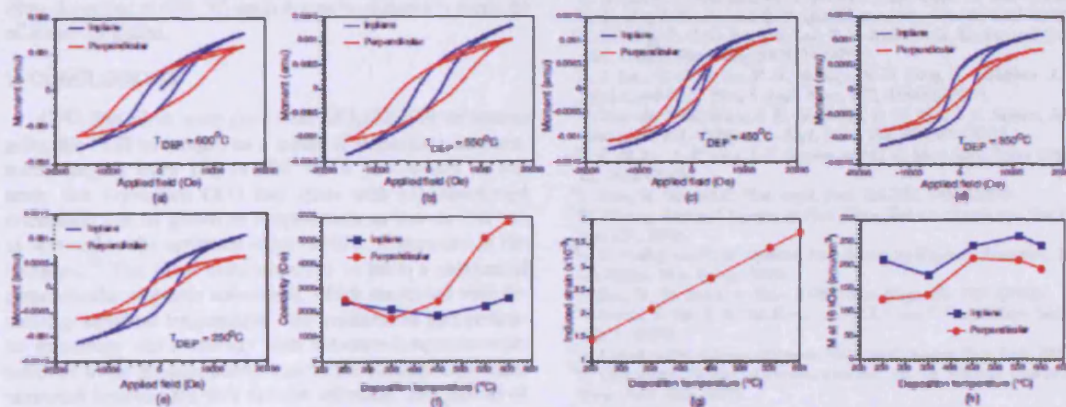


FIG. 2. (Color online) (a)–(e) M-H hysteresis loops of CFO thin films deposited at 600 °C, 550 °C, 450 °C, 350 °C, and 250 °C, respectively. (f) Coercivity as a function of substrate temperature. (g) Calculated variation in thermal expansion mismatch-induced strain with deposition temperature. (h) Variation in measured magnetization (at 16 kOe) with deposition temperature.

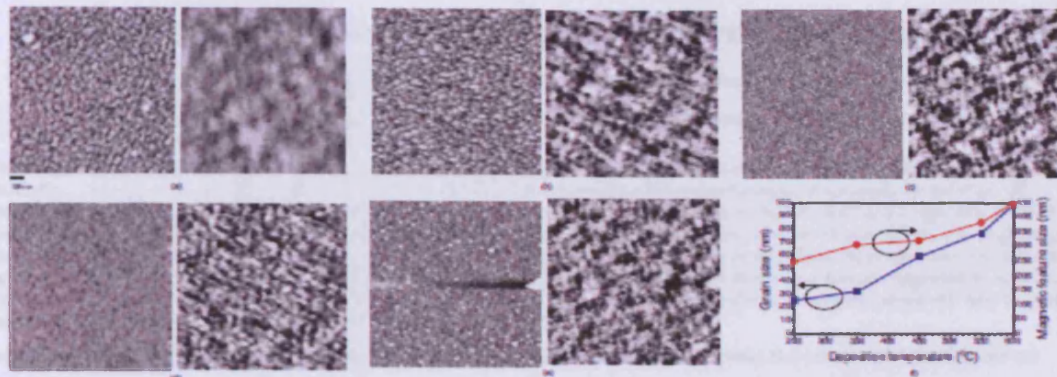


FIG. 3. (Color online) (a)–(e) AFM (left) and MFM (right) images of CFO samples deposited at 600 °C, 550 °C, 450 °C, 350 °C, and 250 °C, respectively. The grain size and magnetic feature size increase with deposition temperature and are plotted in (f). Magnetic domains are irregular in shape but reflect a feature size similar to the equilibrium period of maze type domains. This type of behavior is typical for magnetic thin films with high perpendicular anisotropy and high domain wall coercivity Ref. 15.

around 3 nm for all samples. The grain size increases with T_{DEP} as shown in Fig. 3(f) from about 25 nm for $T_{\text{DEP}}=250$ °C, to about 100 nm for $T_{\text{DEP}}=600$ °C.

Irregular domain patterns with global nonequilibrium character observed in these films are commonly observed in materials with strong perpendicular anisotropy and high domain wall coercivity. Though these domains are at global nonequilibrium, they nonetheless reflect a typical feature size similar to the equilibrium period of maze-type domains.¹⁵ As shown in Fig. 3(f), the magnetic feature size increases with increasing T_{DEP} . According to a simple stripe domain model, for materials with easy axis perpendicular to the crystal surface, the domain width (or magnetic feature size) increases with increasing perpendicular anisotropy constant K_u (as $K_u^{1/4}$).¹⁶ Hence the observed increase in magnetic domain size is consistent with the magnetic property measurements discussed in Sec. IV B, where perpendicular anisotropy was also observed to increase with increasing T_{DEP} .

Grain size and magnetic feature size increase with T_{DEP} at different rates. In films deposited at 250 °C each magnetic domain is made up of approximately 100 grains, whereas for films deposited at 600 °C, each magnetic domain is made up of about 25 grains.

V. CONCLUSIONS

CFO thin films were grown on SiO₂/Si(100) substrates using the PLD technique, at a series of deposition temperatures, ranging from 250 to 600 °C. It was shown in this study that crystalline CFO thin films with (111)-preferred orientation can be grown at temperatures as low as 250 °C, as opposed to the optimum value of 600 °C reported in the literature.¹⁰ The films were observed to have a substantial perpendicular magnetic anisotropy, which decreased with decreasing substrate temperature. The variation in perpendicular anisotropy and coercivity with substrate temperature are believed to be predominantly due to the thermal expansion mismatch between the film and the substrate. The growth of

CFO thin films at lower temperatures indicates their potential to be integrated with a wider range of multilayer device structures and MEMS devices.

The saturation magnetization in such CFO thin films could be further improved by optimizing deposition oxygen pressure or by postdeposition annealing in an oxygen-containing atmosphere, in order to decrease oxygen vacancies.

ACKNOWLEDGMENTS

This research was supported by the UK Engineering and Physical Sciences Research Council under Grant No. EP/D057094 and the U.S. National Science Foundation under Grant No. DMR-0402716, and by Cardiff University School of Engineering.

- ¹J. A. Paulsen, A. P. Ring, C. C. H. Lo, J. E. Snyder, and D. C. Jiles, *J. Appl. Phys.* **97**, 044502 (2005).
- ²A. V. Ramos, T. S. Santos, G. X. Miao, M.-J. Guinet, J.-B. Morisson, and J. S. Moodera, *Phys. Rev. B* **78**, 180402 (2008).
- ³A. K. Giri, E. M. Kirkpatrick, P. Moeckharnklang, S. A. Majetich, and V. G. Harris, *Appl. Phys. Lett.* **80**, 2341 (2002).
- ⁴L. Stichauer, G. Gavolille, and Z. Simsa, *J. Appl. Phys.* **79**, 3645 (1996).
- ⁵Y.-Q. Chu, Z.-W. Fu, and Q.-Z. Qin, *Electrochim. Acta* **49**, 4915 (2004).
- ⁶S. H. Song, C. C. H. Lo, S. J. Lee, S. T. Aldini, J. E. Snyder, and D. C. Jiles, *J. Appl. Phys.* **101**, 09C517 (2007).
- ⁷S. J. Lee, C. C. H. Lo, P. N. Maitage, S. H. Song, Y. Melikhov, J. E. Snyder, and D. C. Jiles, *J. Appl. Phys.* **102**, 073910 (2007).
- ⁸N. Ravva, Y. Melikhov, I. C. Nebedim, D. C. Jiles, J. E. Snyder, A. J. Moses, and P. I. Williams, *J. Appl. Phys.* **105**, 07A518 (2009).
- ⁹C. C. H. Lo, A. P. Ring, J. E. Snyder, and D. C. Jiles, *IEEE Trans. Magn.* **41**, 3676 (2005).
- ¹⁰J. Zhou, H. He, and C. Nan, *Appl. Surf. Sci.* **253**, 7456 (2007).
- ¹¹M. Ohtani, *Material Science of Thin Films*, 2nd ed. (Academic, San Diego, CA, 2001).
- ¹²B. D. Cullity and C. D. Graham, *Introduction to Magnetic Materials*, 2nd ed. (Wiley, New Jersey, 2009).
- ¹³P. Zou, W. Yu, and J. A. Rain, *IEEE Trans. Magn.* **38**, 3501 (2002).
- ¹⁴Y. Suzuki, G. Hu, R. B. Van Dover, and R. J. Cava, *J. Magn. Magn. Mater.* **191**, 1 (1999).
- ¹⁵A. Hubert and R. Schafer, *Magnetic Domains* (Springer, New York, 1998).
- ¹⁶S. Chikazumi, *Physics of Ferromagnetism*, 2nd ed. (Oxford University Press, New York, 1997).

Temperature Dependence of Magnetic Properties of $\text{CoAl}_x\text{Fe}_{2-x}\text{O}_4$

N. Ravvah, I. C. Nlebedim, Y. Melikhov, J. E. Snyder, P. I. Williams, A. J. Moses, and D. C. Jiles

Wolfson Centre for Magnetism, School of Engineering, Cardiff University, Cardiff CF24 3AA, U.K.

The temperature dependence of magnetic properties of a series of aluminium-substituted cobalt ferrite, with the general composition of $\text{CoAl}_x\text{Fe}_{2-x}\text{O}_4$ ($x = 0, 0.1, 0.2, 0.5$), has been studied. It was observed that the magnetization, at an applied field of $\mu_0 H = 5$ T and a temperature of 10 K, does not change significantly for small amounts of Al, then reduces sharply for larger amounts of Al. Magnetic hysteresis loops were measured over a field range of $-5 \text{ T} \leq \mu_0 H \leq 5 \text{ T}$ at temperatures between 10 and 400 K. The high field regions of these loops were modelled using the Law of Approach to saturation, which can be used to calculate the magnetocrystalline anisotropy using its description of the processes of rotation of domain magnetizations against anisotropy and forced magnetization. It was found that the first-order cubic anisotropy of these materials decreased with increasing temperature. It was also observed that the anisotropy of these materials decreased with increasing Al-content at a given temperature.

Index Terms—Aluminium substitution, cobalt ferrite, magnetic anisotropy, magnetization, site occupancy, spinel structure.

I. INTRODUCTION

HIGHLY magnetostrictive cobalt ferrite materials have generated recent interest as candidate materials for torque/stress sensor and actuator applications [1]–[4]. The materials have attractive properties of high magnetostriction (λ), low hysteresis, high chemical stability, mechanical strength and above all high magnetostrictive strain sensitivity ($d\lambda/dH$). The high magnetostrictive strain sensitivity implies that these materials can produce high magnetostriction at low fields, which points towards a lower magnetizing current requirement in actuator applications [5]. The magnetoelastic properties of these materials are related to their magnetic properties. It has been found that a lower anisotropy leads to higher magnetostrictive strain sensitivity. In the past, several substitutions of Mn^{3+} [3], Cr^{3+} [4], Ga^{3+} [6] and $\text{Ge}^{4+}/\text{Co}^{2+}$ [7] for some of the Fe^{3+} have been found to improve their magnetic and consequently magnetoelastic properties.

In the present work, we have investigated a new Al^{3+} substitution in the place of some of the Fe^{3+} in cobalt ferrite.

II. SAMPLE PREPARATION AND EXPERIMENTAL DETAILS

A series of randomly oriented polycrystalline Al-substituted cobalt ferrite samples with the general formula of $\text{CoAl}_x\text{Fe}_{2-x}\text{O}_4$ were prepared using standard powder ceramic techniques with a final sintering of 1300°C for 24 hours, followed by furnace cooling to room temperature [1], [2]. The target compositions were $x = 0.0, 0.1, 0.2$ and 0.5 . The actual compositions were determined using energy dispersive X-ray spectroscopy (EDS) in a scanning electron microscope (SEM), and were found to be close to the target compositions (see Table I).

The temperature dependence of magnetization was measured at an applied field of $\mu_0 H = 5$ T within a temperature range of 10 K to 400 K. The magnetic hysteresis loops were measured

Manuscript received March 06, 2009; revised May 24, 2009. Current version published September 18, 2009. Corresponding author: N. Ravvah (e-mail: nravvah@gmail.com).

Color versions of one or more of the figures in this paper are available online at <http://ieeexplore.ieee.org>.

Digital Object Identifier 10.1109/TMAG.2009.2024767

TABLE I
COMPOSITION OF $\text{CoAl}_x\text{Fe}_{2-x}\text{O}_4$ DETERMINED BY EDS

Target compositions	Composition by EDS		
	Co	Al	Fe
CoFe_2O_4	1.02	-	1.98
$\text{CoAl}_{0.1}\text{Fe}_{1.9}\text{O}_4$	1.03	0.08	1.89
$\text{CoAl}_{0.2}\text{Fe}_{1.8}\text{O}_4$	1.03	0.18	1.79
$\text{CoAl}_{0.5}\text{Fe}_{1.5}\text{O}_4$	1.03	0.49	1.48

over a field range of -5 T to $+5$ T at several temperatures between 10 K and 400 K. The high field regions of these loops were modelled using the Law of Approach (LA) to saturation to extract anisotropy information. The LA method accounts for the two dominant processes at high fields—rotation of domain magnetizations against anisotropy and the linearly increasing forced magnetization. These two processes have been described in the LA as [8]

$$M = M_s \left[1 - \frac{8}{105} \frac{K_1^2}{\mu_0^2 M_s^2 H^2} \right] + \kappa H \quad (1)$$

where M is the magnetization, H is the magnetic field, M_s is the saturation magnetization, K_1 is the first-order cubic anisotropy constant and the term κ is the forced magnetization coefficient that describes the linear increase in spontaneous magnetization at high fields. The constant $8/105$ is relevant to the calculations for randomly oriented polycrystalline cubic materials. At temperatures above 150 K, the M - H data above $\mu_0 H = 1$ T was fitted to the LA method as described in (1) to calculate K_1 . Close to 150 K, the anisotropy fields rise rapidly and hence a higher field is needed to cause rotation against anisotropy. Therefore, at these temperatures, only M - H data above $\mu_0 H = 2$ T was fitted to (1) to calculate K_1 .

III. RESULTS AND DISCUSSIONS

The study of the temperature dependence of magnetic properties of aluminium-substituted cobalt ferrite can be broken down into two temperature ranges:—above and below 150 K.

Fig. 1 shows the variation of magnetization (measured at $\mu_0 H = 5$ T) with temperature. Above 150 K, the magnetization increases monotonically with decreasing temperature for all compositions. Below 150 K, the applied field of $\mu_0 H = 5$

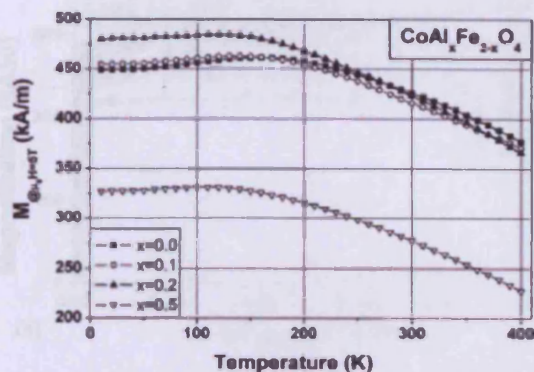


Fig. 1. Variation of magnetization of $\text{CoAl}_x\text{Fe}_{2-x}\text{O}_4$ at an applied field of $\mu_0H = 5$ T. There is a 5% error bar on all points on this graph.

T was not enough to saturate the domain magnetization and its rotation against high anisotropy fields at low temperatures. Thus, the slight decrease observed in magnetization below 150 K was not indicative of saturation magnetization. However, the magnetization at these low temperatures is still a good indicator of the trends in near zero Kelvin saturation magnetization.

The magnetic properties of cobalt ferrite based materials are heavily dependent on the site occupancy of different ions in its lattice. The spinel structure of cobalt ferrite based materials has half the number of tetrahedral sites (A) in comparison to octahedral sites (B). In a pure inverse spinel, all the divalent M^{2+} cations and half of the Fe^{3+} go into the B-sites. In reality, cobalt ferrite has Co^{2+} residing in both A and B sites and the structure is a mixed spinel.

The strongest exchange coupling is the antiparallel coupling between the A and B sites keeping the moments in them aligned antiparallel to each other. The net magnetization comes from subtracting the net moment on A-sites from the net moment on B-sites. The study of near zero Kelvin saturation magnetization is useful in this case because the magnetic moments are predominantly aligned either parallel or antiparallel to each other due to the lack of thermal disorder. Since the change in near zero Kelvin magnetization due to change in composition depends on the site occupancy and the magnetic moment contribution of the dopant ion, its analysis can be used to deduce trends in site occupancy with substitution.

It has been reported that aluminium does not have a strong preference for either of the sites in the cobalt ferrite lattice [9]. The observation that with low amounts of aluminium ($x = 0.1$ and 0.2), the saturation magnetization does not change significantly in comparison to cobalt ferrite, leads us to believe that initially aluminium ions substitute into both the sites in approximately equal numbers reducing their moments in approximately equal amounts and hence keeping the net moment at the same level as pure cobalt ferrite ($x = 0$). With higher amounts of Al, the net magnetization decreases. This could be due to the additional Al substituting increasingly into B-sites or it could be due to non-collinear spin arrangement caused by greatly decreased tetrahedral-octahedral exchange coupling.

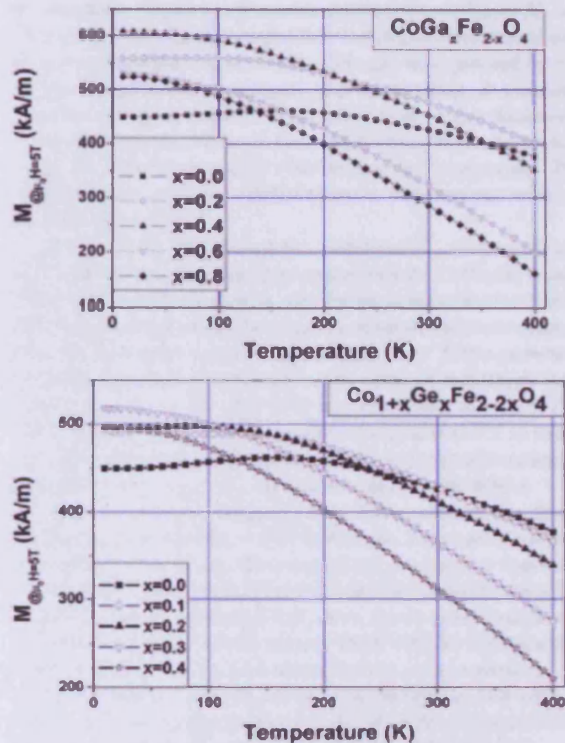


Fig. 2. Variation of magnetization of Ga-substituted [6] and Ge/Co-cosubstituted [7] cobalt ferrite at an applied field of $\mu_0H = 5$ T.

The model outlined above can be supported by analysing the near zero Kelvin saturation magnetization in Ga-substituted and Ge/Co-cosubstituted cobalt ferrite materials (see Fig. 2). Ga^{3+} ions have a preference for A-sites [10]. Therefore, initially, for low amounts of gallium, Ga^{3+} ions substitute into the A-sites in place of Fe^{2+} . Since the Ga^{3+} ions do not contribute to the magnetic moment, the net moment in A-sites decreases, leading to an increase in the net magnetization of the material. However, for higher amounts of gallium, the net magnetization decreases. This could be due to the additional Ga substituting increasingly into B-sites, or it could be due to non-collinear spin arrangements brought on by the decreased A-B exchange coupling.

In the case of germanium substitution, Ge^{4+} ions have a very strong A-site (tetrahedral) preference because of their valence state and tendency to form four bonds with tetrahedral coordination. Therefore, for almost all compositions, the Ge^{4+} ions go into the A-sites reducing their moment and hence increasing the net magnetization [7]. The near zero Kelvin saturation magnetization observations for all the three substitutions are in agreement with the hypothesised site occupancy predictions.

An example of the M - H loops measured for calculation of the anisotropy coefficient and coercive field is shown in Fig. 3. The temperature dependence of anisotropy coefficient K_1 is shown in Fig. 4. Like the analysis of magnetization of aluminium-substituted cobalt ferrite, the analysis of anisotropy

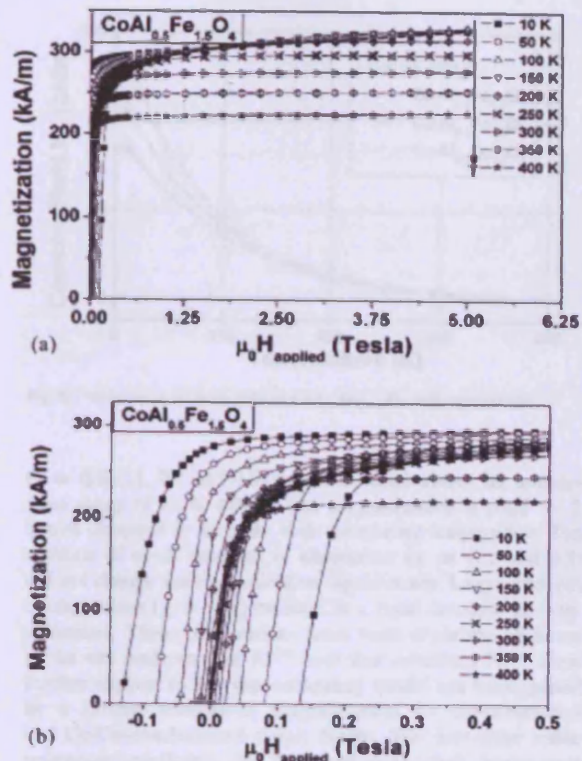


Fig. 3. First quadrant of hysteresis loop of $\text{CoAl}_{0.5}\text{Fe}_{1.5}\text{O}_4$. (a) Shows the high field regions that were used for the calculation of anisotropy. (b) Low field regions of these loops, which were used for calculation of coercive field.

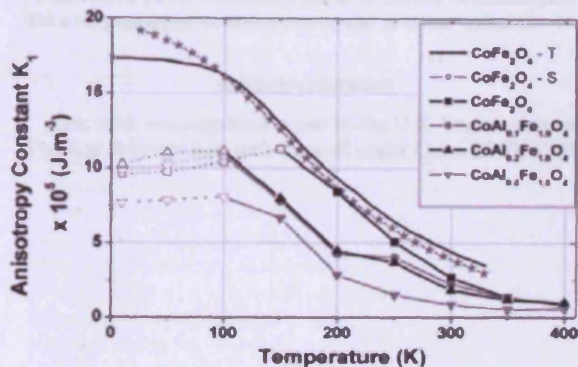


Fig. 4. First order cubic anisotropy constant of Al-substituted cobalt ferrite. The hollow markers indicate temperatures at which the anisotropy field value is more than the maximum applied field in the experiment ($\mu_0 H = 5$ T). The data is in agreement with the theoretical calculations of Tachiki [13] and experimental observations of Shenker [12], shown here as CoFe_2O_4 -T and CoFe_2O_4 -S respectively.

of these materials can also be broken down into two regions: below and above 150 K.

Above 150 K, the applied fields were high enough to overcome anisotropy, and cause the rotation of the domain magnetizations against anisotropy, hence causing a complete approach

to saturation. The first-order cubic anisotropy coefficient K_1 increased with decreasing temperature for all compositions of aluminium-substituted cobalt ferrite. This can be explained by exchange interactions, unchanged with temperature, dominating over thermal agitations that reduce when temperature decreases. It was also observed that, as we cooled down, beyond a certain point, K_1 increased rapidly with decreasing temperature. The region of steep increase shifted to lower temperatures with increasing Al-content.

Below 150 K, the anisotropy coefficient K_1 showed an apparent decrease with reducing temperature for CoFe_2O_4 below 150 K, and for all aluminium-substituted samples below 100 K. This can be explained by the presence of anisotropy fields higher than the maximum applied field of $\mu_0 H = 5$ T that prevent a complete approach to saturation. The value of anisotropy field given by $\mu_0 H_k = 2K_1/M$ [11] was calculated to be 4.8 T at 150 K for CoFe_2O_4 and is expected to rise above 5 T at lower temperatures. For these cases, the forced magnetization constant was set to zero, i.e., the calculations were made with $\kappa = 0$ and with M_s and K_1 being the only fitting parameters. These points are shown in Fig. 4 with hollow markers and are joined with dotted lines. Since, the assumption of complete approach to saturation of the LA method is not fulfilled in these cases, the calculation of K_1 , although indicative, is not considered accurate. The anisotropy results are consistent with the experimental work of Shenker [12], who measured the cubic anisotropy of single crystals of CoFe_2O_4 using torque measurements near an easy axis. The calculated values of K_1 for CoFe_2O_4 are also in agreement with the theoretical predictions of Tachiki [13].

Magneto-crystalline anisotropy is an important metric of performance in evaluating magnetoelastic materials for use in stress sensor and actuator applications. The magnetoelastic properties of magnetic materials are coupled to their magnetic properties. An understanding of how chemical substitution changes magnetic properties helps in understanding its effect on the magnetoelastic properties which are crucial to the potential stress sensor and actuator applications. It has been observed in the case of Mn, Cr, Ga and Ge/Co substitution that with lower cubic anisotropy, the magnetostrictive strain sensitivity increases. Although the magnetostriction amplitude was seen to reduce by a small amount, the magnetostrictive strain sensitivity was observed to increase by 112% for Al-substituted cobalt ferrite [14].

Another important metric of performance for a sensor or actuator material is hysteresis. While the magnetostrictive strain sensitivity improved with addition of aluminium, the coercivity was seen to not change significantly with aluminium addition at temperatures in the potential operational range around 300 K for the proposed devices. Two important factors determining the coercivity are the anisotropy field and domain wall pinning. Although anisotropy reduced with increasing Al content, a seemingly insignificant change in coercivity points towards the fact that the anisotropy is not the dominating factor deciding coercivity in these materials. The temperature dependence of the coercive field is shown in Fig. 5.

IV. CONCLUSION

The magnetic properties of aluminium-substituted cobalt ferrite with the general composition of $\text{CoAl}_x\text{Fe}_{2-x}\text{O}_4$

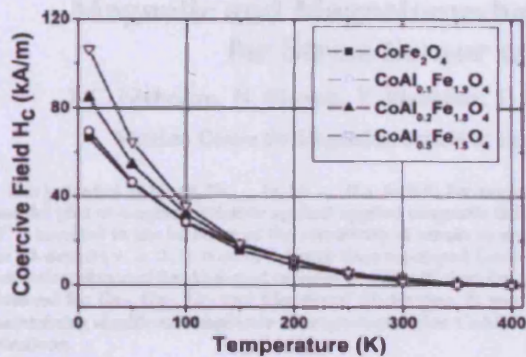


Fig. 5. Variation of coercive field of $\text{CoAl}_x\text{Fe}_{2-x}\text{O}_4$ with temperature.

($x = 0, 0.1, 0.2$ and 0.5) were measured within the temperature range of 10 to 400 K. The magnetization at $\mu_0 H = 5$ T was observed to increase with decreasing temperature. The addition of small amounts of aluminium ($x = 0.1$ and 0.2) did not change the magnetization significantly. Large amounts of aluminium ($x = 0.5$) resulted in a rapid decrease in magnetization. These observations have been explained in terms of the site preference of Al^{3+} ions that substitute Fe^{3+} ions. Further support to this site occupancy model has been gained by a similar analysis of magnetization for Ga-substituted and Ge/Co-cosubstituted cobalt ferrite. The first-order cubic anisotropy coefficient for Al-substituted cobalt ferrite was calculated using the LA method. The cubic anisotropy of cobalt ferrite was seen to decrease with substitution of aluminium in place of some of the iron. This caused an increase in the magnetostrictive strain sensitivity, a crucial metric of performance for a magnetostrictive stress sensor and actuator material.

ACKNOWLEDGMENT

This work was supported in part by the U.K. Engineering and Physical Sciences Research Council under Grant EP/D057094

and by the US National Science Foundation under Grant DMR-0402716.

REFERENCES

- [1] Y. Chen, J. E. Snyder, C. R. Schwichtenberg, K. W. Cullum, and D. C. Jiles, "Metal-bonded Co-ferrite composites for magnetostrictive torque sensor applications," *IEEE Trans. Magn.*, vol. 35, no. 5, p. 3652, Oct. 1999.
- [2] J. A. Paulsen, A. P. Ring, C. C. H. Lo, J. E. Snyder, and D. C. Jiles, "Manganese-substituted cobalt ferrite magnetostrictive materials for magnetic stress sensor applications," *J. Appl. Phys.*, vol. 97, p. 044502, 1999.
- [3] Y. Melikhov *et al.*, "Temperature dependence of magnetic anisotropy in Mn-substituted cobalt ferrite," *J. Appl. Phys.*, vol. 99, p. 08R102, 2006.
- [4] Y. Melikhov *et al.*, "The effect of Cr-substitution on the magnetic anisotropy and its temperature dependence in Cr-substituted cobalt ferrite," *IEEE Trans. Magn.*, vol. 42, no. 10, pp. 2861–2863, 2006.
- [5] N. Ravva, L. C. Nlebedim, Y. Melikhov, J. E. Snyder, D. C. Jiles, A. J. Moses, and P. I. Williams, "Temperature dependence of magnetostriction of $\text{Co}_{1-x}\text{Ge}_x\text{Fe}_{2-2x}\text{O}_4$ for magnetostrictive sensor and actuator applications," *IEEE Trans. Magn.*, vol. 44, no. 11, pp. 3013–3016, 2008.
- [6] N. Ravva, Y. Melikhov, D. C. Jiles, J. E. Snyder, A. J. Moses, P. I. Williams, and S. H. Song, "Temperature dependence of magnetic anisotropy of Ga-substituted cobalt ferrite," *J. Appl. Phys.*, vol. 103, no. 7, p. 07E506, 2008.
- [7] N. Ravva, Y. Melikhov, L. C. Nlebedim, D. C. Jiles, J. E. Snyder, A. J. Moses, and P. I. Williams, "Temperature dependence of magnetic anisotropy of germanium/cobalt co-substituted cobalt ferrite," in *53rd MMM Conf.*, Austin, Nov. 10–14, 2009.
- [8] S. Chikazumi, *Physics of Ferromagnetism*. Oxford, U.K.: Oxford University Press, 1997, pp. 502–504.
- [9] A. Sattar, H. El-Sayed, K. El-Shokrofy, and M. El-Tahy, "Improvement of the magnetic properties of Mn-Ni-Zn ferrite by the non-magnetic Al^{3+} -ion substitution," *J. Appl. Sci.*, vol. 5, no. 1, pp. 162–168, 2005.
- [10] K. Kriebel, M. Devlin, S. J. Lee, S. T. Aldini, and J. E. Snyder, "Investigation of gas-substitution in cobalt ferrite ($\text{CoGa}_x\text{Fe}_{2-x}\text{O}_4$) using Mossbauer spectroscopy," *J. Appl. Phys.*, vol. 103, p. 07E508, 2008.
- [11] B. D. Cullity, *Introduction to Magnetic Materials*. Reading, MA: Addison-Wesley, 1972, p. 233.
- [12] H. Shenker, "Magnetic anisotropy of cobalt ferrite ($\text{Co}_{0.91}\text{Fe}_{1.09}\text{O}_{3.92}$) and nickel cobalt ferrite ($\text{Ni}_{0.72}\text{Fe}_{0.28}\text{Co}_{0.09}\text{Fe}_{1.91}\text{O}_4$)," *Phys. Rev.*, vol. 107, p. 1246, 1957.
- [13] M. Tachiki, "Origin of the magnetic anisotropy energy of cobalt ferrite," *Prog. Theor. Phys.*, vol. 23, p. 1055, 1960.
- [14] C. I. Nlebedim, N. Ravva, Y. Melikhov, P. I. Williams, J. E. Snyder, A. J. Moses, and D. C. Jiles, "Magnetic and magnetostrictive properties of $\text{CoAl}_x\text{Fe}_{2-x}\text{O}_4$ for stress sensor application," in *INTERMAG*, Sacramento, CA, May 4–8, 2009, Digest ID: 606241.

Magnetic and Magnetomechanical Properties of $\text{CoAl}_x\text{Fe}_{2-x}\text{O}_4$ for Stress Sensor and Actuator Applications

I. C. Nlebedim, N. Ravvah, Y. Melikhov, P. I. Williams, J. E. Snyder, A. J. Moses, and D. C. Jiles

Wolfson Centre for Magnetics, School of Engineering, Cardiff University, Cardiff CF24 3AA, U.K.

The potential of $\text{CoAl}_x\text{Fe}_{2-x}\text{O}_4$ ($x = 0.1$ to 0.9) for magnetomechanical stress sensor applications has been studied. It was found that the plot of magnetostriction against applied magnetic field changed shape as Al content increased. Furthermore, substituting with Al^{3+} resulted in the increase of the sensitivity of strain to applied magnetic field $(d\lambda/dH)_{\text{max}}$. The maximum magnetostriction for the Al-doped ($x = 0.1$) was 34% lower than un-doped Co-ferrite but the $(d\lambda/dH)_{\text{max}}$ was 112% higher. The magnitude of magnetostriction obtained for Al-doped samples is still sufficient for stress sensor and actuator applications. Results were compared with those obtained for Ge-, Ga-, Cr- and Mn-doped Co-ferrites. It was found that in terms of improving strain response to applied field whilst maintaining significant amplitude of magnetostriction $\text{CoAl}_x\text{Fe}_{2-x}\text{O}_4$ has promising potential for magnetomechanical stress sensor applications.

Index Terms—Cobalt ferrite, magnetomechanical properties, magnetostriction, strain sensitivity, stress sensor.

I. INTRODUCTION

MAGNETOELASTIC materials suitable for high sensitivity strain sensor development have been the subject of much interest recently, especially due to their non-contact sensing capabilities and possibility for use at high temperatures. The limitations of highly magnetostrictive alloys such as Terfenol-D include poor mechanical properties and high cost of production. This suggests the need for alternatives of which cobalt ferrite (Co-ferrite) is a very good candidate. Though Co-ferrite has a lower saturation magnetostriction (λ) than Terfenol based composites, it has a higher sensitivity of strain to applied magnetic field $(d\lambda/dH)$ which makes it attractive for sensor applications [1].

The tunability of the Curie temperature, magnetostriction (λ) and the response of strain to applied magnetic field $(d\lambda/dH)$ of Co-ferrite by magnetic annealing and cation substitution indicate capability for control and systematic improvement of its magnetomechanical properties. It has been demonstrated that substituting Mn^{3+} for Fe^{3+} enables control of the Curie temperature, which could be used to minimize the magnetomechanical hysteresis [2]. Other trivalent cations such as Ga^{3+} and Cr^{3+} have been found to improve strain sensitivity, $d\lambda/dH$ of Co-ferrite [3], [4]. Tetravalent Ge^{4+} has been co-substituted with additional Co^{2+} in a previous study in which both λ and $d\lambda/dH$ were found to increase [5]. Also, magnetic annealing of Co-ferrite has been shown to improve its magnetomechanical properties leading to an increase of both λ and $d\lambda/dH$ [6].

Co-ferrite has a partially inverse spinel structure in which a larger fraction of Co^{2+} is located on octahedral-sites (B-sites), and the remainder on the tetrahedral-sites (A-sites) [7]. This indicates that Co^{2+} ions in Co-ferrite have a B-site preference. The magnetic anisotropy and magnetostriction of Co-ferrite are thought to depend mainly on the proportion of Co^{2+} on the B-sites and the strong A-B exchange interaction. Doping with

cations with a strong A-site preference such Ge^{4+} [5], in addition to changing the exchange coupling, could displace some of the Co^{2+} from the A-sites to the B-sites. Likewise, doping with cations with a strong B-site preference such as Mn^{3+} [2] could also in addition to changing the exchange coupling, displace some of the Co^{2+} from the B-sites to the A-sites. This study reports on the effect of nonmagnetic Al^{3+} substitution on Co-ferrite ($\text{CoAl}_x\text{Fe}_{2-x}\text{O}_4$). Al^{3+} is expected to weaken the exchange coupling which would result in a decrease in Curie temperature. Moreover, $d\lambda/dH$ could also, in addition increase as in the case Ge^{4+} , Ga^{3+} , Cr^{3+} and Mn^{3+} . This is because weakening of the exchange coupling results in a decrease of the magnetocrystalline anisotropy which also results in a steeper response of strain to applied magnetic field. Unlike other trivalent and tetravalent cations with defined A-site or B-site preferences, Al^{3+} has been said to have no preference for either type of site [8].

II. EXPERIMENTAL DETAILS

Pure CoFe_2O_4 and $\text{CoAl}_x\text{Fe}_{2-x}\text{O}_4$ ($x = 0$ to 0.9) were prepared by mixing the constituent metallic oxides at appropriate ratios, calcining twice at 1000°C and sintering at 1350°C , all in air. The crystal structures of the samples were determined using X-ray Diffractometry (XRD). The patterns were recorded at a step size of 0.02° on a Philips PW1710 automated powder diffractometer with copper ($\text{CuK}\alpha$) radiation at 35 kV and 40 mA. The microstructures and final compositions of the samples were studied using the FEI XL30 FEG Environmental Scanning Electron Microscope (ESEM) with an Oxford Instrument Inca X-ray analyzer attached for Energy Dispersive X-ray Spectroscopy (EDX).

Magnetization (M) versus applied magnetic field (H) was measured at 300 K with a Vibrating Sample Magnetometer (VSM) up to a maximum applied field, $\mu_0 H = 1.6$ T. The samples were nominally $2.5 \times 2.5 \times 1.5 \pm 0.1$ mm in dimension. Room temperature magnetostriction (λ) was measured parallel to the applied field using piezo-resistive strain gauges attached to the samples. Samples for magnetostriction measurement were cylindrical with diameter 9.2 ± 0.2 mm and height 6.0 ± 0.2 mm.

Manuscript received March 06, 2009. Current version published September 18, 2009. Corresponding author: I. C. Nlebedim (e-mail: nlebedimci@cardiff.ac.uk).

Digital Object Identifier 10.1109/TMAG.2009.2021846

0018-9464/526.00 © 2009 IEEE

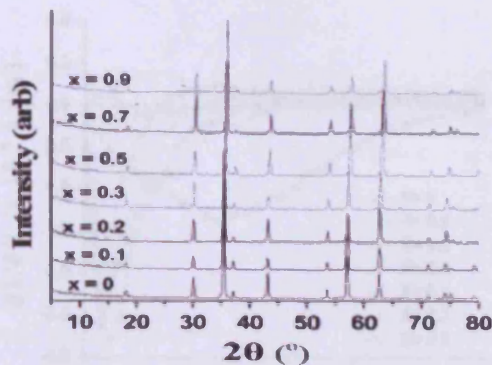


Fig. 1. XRD patterns for $\text{CoAl}_x\text{Fe}_{2-x}\text{O}_4$ with x ranging from 0 to 0.9. Pattern shows a shift to higher 2θ with increase in x .

TABLE I
COMPOSITION OF $\text{CoAl}_x\text{Fe}_{2-x}\text{O}_4$ AS DETERMINED BY EDX

Target Compositions	EDX Compositions		
	Co	Al	Fe
CoFe_2O_4	1.02	-	1.98
$\text{CoAl}_{0.1}\text{Fe}_{1.9}\text{O}_4$	1.03	0.08	1.89
$\text{CoAl}_{0.2}\text{Fe}_{1.8}\text{O}_4$	1.03	0.18	1.79
$\text{CoAl}_{0.3}\text{Fe}_{1.7}\text{O}_4$	1.03	0.25	1.72
$\text{CoAl}_{0.5}\text{Fe}_{1.5}\text{O}_4$	1.03	0.49	1.48
$\text{CoAl}_{0.7}\text{Fe}_{1.3}\text{O}_4$	1.04	0.73	1.23
$\text{CoAl}_{0.9}\text{Fe}_{1.1}\text{O}_4$	0.99	0.87	1.14

III. RESULTS AND DISCUSSIONS

The XRD patterns of the samples as shown in Fig. 1, showed single phase spinel structure for all the samples with a shift to higher 2θ as x increases from 0 to 0.9 in $\text{CoAl}_x\text{Fe}_{2-x}\text{O}_4$. The shift indicates a decrease in the lattice parameter as Al^{3+} is introduced into the spinel structure. The ionic radius of Al^{3+} in A-sites and B-sites ($r_A = 0.39 \text{ \AA}$, $r_B = 0.54 \text{ \AA}$) is smaller than those of Fe^{3+} ($r_A = 0.49 \text{ \AA}$, $r_B = 0.65 \text{ \AA}$) and Co^{2+} ($r_A = 0.58 \text{ \AA}$, $r_B = 0.74 \text{ \AA}$) [9]. It is expected that as the smaller ionic radii Al^{3+} are introduced into the cation sites, the lattice parameter should decrease and be seen as a shift in the XRD pattern.

The SEM micrographs showed uniform microstructure which indicates that the samples are single phase as also seen from the X-ray diffractometry results. The final compositions of the samples as determined by the EDX analysis are shown in Table I.

Fig. 2 shows the variation of magnetization (M) against aluminum composition (x) measured at 300 K and $\mu_0 H = 1.6 \text{ T}$ for the $\text{CoAl}_x\text{Fe}_{2-x}\text{O}_4$ system. The plot shows an approximately linear decrease in M with increase in x . The change in magnetization with applied field, temperature and composition in spinel structured materials is governed by several factors (exchange interaction, site occupancy of the cations (in this case Al^{3+} , Fe^{3+} , Co^{2+}), and thermal agitation) and has been detailed in another study [10].

The variation of λ with H is shown in Fig. 3. This shows that from $x = 0$ to 0.9, the amplitude of λ decreased with x ,

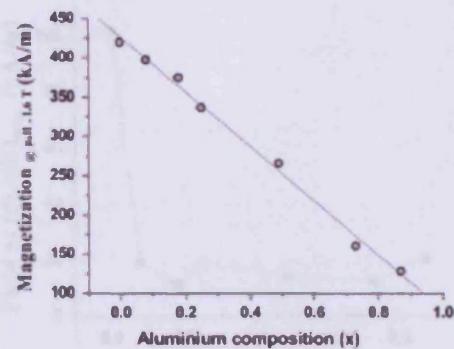


Fig. 2. Variation of magnetization as a function of aluminum composition at 300 K and $\mu_0 H = 1.6 \text{ T}$. The plot shows an approximately linear decrease of M with increase in x .

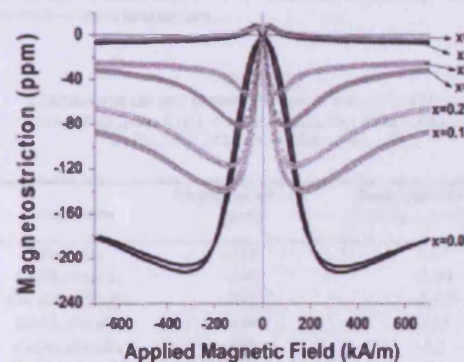


Fig. 3. Variation of magnetostriction with applied magnetic field for the $\text{CoAl}_x\text{Fe}_{2-x}\text{O}_4$ system. Note that the absolute values of magnetostriction are, for $x = 0$ (212 ppm at 328 kA/m) and for $x = 0.1$ (140 ppm at 171 kA/m).

and the magnetic field required to attain this amplitude also decreased with x . For certain applications, such as linear displacement sensors, amplitude of λ between 30 ppm and 100 ppm is quite adequate [11]. Changes in the sign of the $\lambda(H)$ curves as x increased are also observed in the Fig. 3. This indicates a change of the sign of the first cubic anisotropy constant or a change of the signs of both λ_{111} and λ_{100} . From $x = 0$ to 0.5, the slope of the curve was initially negative and later positive. The initial part of the curve represents a region in which the contribution of λ_{100} to the amplitude of λ is dominant. This continues until all magnetic domains align parallel to the easy axes (100). After this, on further application of magnetic field, the contribution of λ_{111} to the amplitude of λ is observed. The reverse is the case for $x = 0.7$ and 0.9, the slope was initially positive and finally negative signifying λ_{111} and λ_{100} being dominant at lower and higher fields respectively or that they have both changed signs. Similar behavior was observed in a previous study on Ge-doped Co-ferrite [5].

With sufficient magnetostriction amplitude for application, the derivative $d\lambda/dH$ becomes a crucial factor for device development. Fig. 4 shows the variation of $d\lambda/dH$ with applied magnetic field. It shows that doping of Co-ferrite with Al resulted in

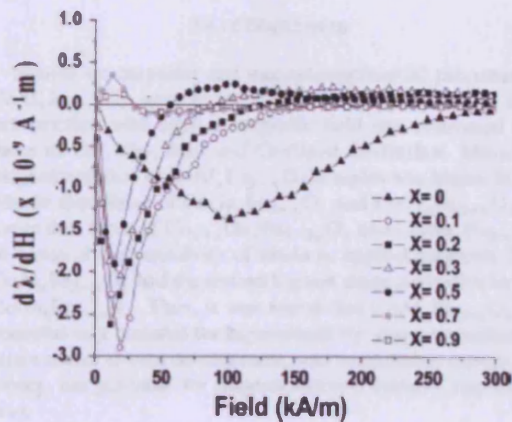


Fig. 4. Strain-field for aluminum compositions, $x = 0$ to 0.9 measured at room temperature. Note that at $x = 0, 0.1$ and 0.2 , $d\lambda/dH = 1.37 \times 10^{-9} \text{ A}^{-1} \text{ m}$, $2.90 \times 10^{-9} \text{ A}^{-1} \text{ m}$ and $2.63 \times 10^{-9} \text{ A}^{-1} \text{ m}$ respectively.

an increase in $d\lambda/dH$ compared with un-doped cobalt ferrite. Maximum strain derivative $(d\lambda/dH)_{\text{max}}$ for Al doped Co-ferrite was found to be higher than $(d\lambda/dH)_{\text{max}}$ for the un-doped samples for Al compositions, $x = 0.1$ to 0.5. Due to the form of their magnetostriction curve, Al compositions $x = 0.7$ and 0.9 both have positive $(d\lambda/dH)_{\text{max}}$ values. The result shows that the $(d\lambda/dH)_{\text{max}}$ value for Al doped Co-ferrite was over 110% more than the $(d\lambda/dH)_{\text{max}}$ of the un-doped sample (Al-doped ($x = 0.1$) = $-2.90 \times 10^{-9} \text{ A}^{-1} \text{ m}$; un-doped ($x = 0.0$) = $-1.37 \times 10^{-9} \text{ A}^{-1} \text{ m}$). This increase can be explained in terms of magnetocrystalline anisotropy. Substitution of nonmagnetic cations for Fe^{3+} in Co-ferrite reduces the super-exchange interaction between the A-sites and B-sites which also lowers the magnetocrystalline anisotropy [5]. It has been suggested that a decrease in magnetocrystalline anisotropy could be responsible for the increase in $(d\lambda/dH)_{\text{max}}$ [12].

From Fig. 5, it can be seen that apart from being higher in magnitude, the $(d\lambda/dH)_{\text{max}}$ of $\text{CoAl}_{0.1}\text{Fe}_{1.9}\text{O}_4$ and $\text{CoAl}_{0.2}\text{Fe}_{1.8}\text{O}_4$ were respectively obtained at applied magnetic fields 81% and 89% less than that required for $(d\lambda/dH)_{\text{max}}$ of the un-doped Co-ferrite. Since it can be shown by a thermodynamic relation that the response of a magnetomechanical stress sensor to applied stress $dB/d\sigma$ is equal to $d\lambda/dH$ [6], it follows that $(d\lambda/dH)_{\text{max}}$ is one of the important figures of merit for determining the sensitivity of the sensor. With the high values of $(d\lambda/dH)_{\text{max}}$ and the lower magnetic fields at which the maximum magnetostriction and $(d\lambda/dH)_{\text{max}}$ were obtained, it is obvious that $\text{CoAl}_x\text{Fe}_{2-x}\text{O}_4$ with x in the range $0 < x \leq 0.2$ is a promising candidate for the development of a more sensitive magnetomechanical stress sensor device than the un-doped Co-ferrite.

Table II summarizes the magnetostriction and strain derivative of applied field for the Al-doped samples ($x = 0.1, 0.2$), the undoped sample and samples doped with other cations. The amplitude of λ obtained for $\text{Co}_{1.1}\text{Ge}_{0.1}\text{Fe}_{1.8}\text{O}_4$ (-241 ppm) was higher than that obtained for $\text{CoAl}_{0.1}\text{Fe}_{1.9}\text{O}_4$ (-140 ppm) but the latter is still sufficient for magnetomechanical

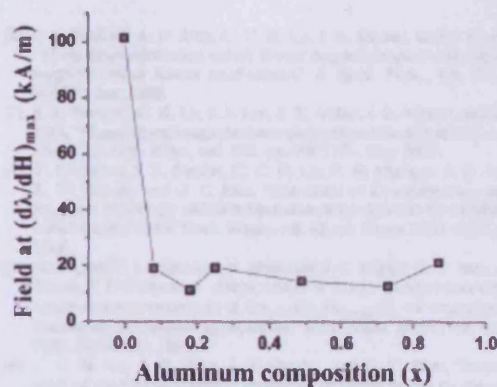


Fig. 5. Applied magnetic field at maximum strain derivative $(d\lambda/dH)_{\text{max}}$ as a function of aluminum composition. The field at $(d\lambda/dH)_{\text{max}}$ are 101 kA/m, 19 kA/m and 11 kA/m for $x = 0.0, 0.1$ and 0.2 respectively. Measurements were made at room temperature.

TABLE II
COMPARISON OF THE MAGNITUDE OF λ AND $(d\lambda/dH)_{\text{max}}$ IN
 $\text{CoAl}_x\text{Fe}_{2-x}\text{O}_4$, $\text{Co}_{1-x}\text{Ge}_x\text{Fe}_{1.8}\text{O}_4$, $\text{CoGa}_x\text{Fe}_{2-x}\text{O}_4$,
 $\text{CoCr}_x\text{Fe}_{2-x}\text{O}_4$ AND $\text{CoMn}_x\text{Fe}_{2-x}\text{O}_4$.

Composition	Magnetostriction λ (ppm)	Strain-field derivative $(d\lambda/dH)_{\text{max}}$ ($\times 10^{-9} \text{ A}^{-1} \text{ m}$)
CoFe_2O_4	-212	1.37
$\text{CoAl}_{0.1}\text{Fe}_{1.9}\text{O}_4$	-140	-2.90
$\text{Co}_{1.1}\text{Ge}_{0.1}\text{Fe}_{1.8}\text{O}_4$	-241	-2.60
$\text{CoAl}_{0.2}\text{Fe}_{1.8}\text{O}_4$	-120	-2.63
$\text{CoGa}_{0.2}\text{Fe}_{1.8}\text{O}_4$	-100	-3.2
$\text{CoMn}_{0.2}\text{Fe}_{1.8}\text{O}_4$	-150	-2.5
$\text{CoCr}_{0.2}\text{Fe}_{1.8}\text{O}_4$	-80	-1.5

sensor applications. On the other hand, $\text{CoAl}_{0.1}\text{Fe}_{1.9}\text{O}_4$ has a higher $(d\lambda/dH)_{\text{max}}$ value ($-2.90 \times 10^{-9} \text{ A}^{-1} \text{ m}$) than $\text{Co}_{1.1}\text{Ge}_{0.1}\text{Fe}_{1.8}\text{O}_4$ ($-2.60 \times 10^{-9} \text{ A}^{-1} \text{ m}$). Also, to attain maximum magnetostriction, $\text{Co}_{1.1}\text{Ge}_{0.1}\text{Fe}_{1.8}\text{O}_4$ would require 93% less magnetizing power consumption than un-doped Co-ferrite [5] while $\text{CoAl}_{0.1}\text{Fe}_{1.9}\text{O}_4$ would require 97% less. This suggests that in terms of response of magnetostriction to applied magnetic field and power efficiency, $\text{CoAl}_{0.1}\text{Fe}_{1.9}\text{O}_4$ would be better than $\text{Co}_{1.1}\text{Ge}_{0.1}\text{Fe}_{1.8}\text{O}_4$ while maintaining a sizeable magnetostriction sufficient for device application.

For $\text{CoGa}_{0.2}\text{Fe}_{1.8}\text{O}_4$, $(d\lambda/dH)_{\text{max}}$ was $-3.2 \times 10^{-9} \text{ A}^{-1} \text{ m}$ at $H = 15 \text{ kA/m}$ compared to $-2.63 \times 10^{-9} \text{ A}^{-1} \text{ m}$ at $H = 11 \text{ kA/m}$ obtained for $\text{CoAl}_{0.2}\text{Fe}_{1.8}\text{O}_4$. The amplitude λ was about 20 ppm more in $\text{CoAl}_{0.2}\text{Fe}_{1.8}\text{O}_4$ than for $\text{CoGa}_{0.2}\text{Fe}_{1.8}\text{O}_4$. $\text{CoAl}_{0.2}\text{Fe}_{1.8}\text{O}_4$ also gave higher $(d\lambda/dH)_{\text{max}}$ than $\text{CoMn}_{0.2}\text{Fe}_{1.8}\text{O}_4$ ($-2.5 \times 10^{-9} \text{ A}^{-1} \text{ m}$) and $\text{CoCr}_{0.2}\text{Fe}_{1.8}\text{O}_4$ ($-1.5 \times 10^{-9} \text{ A}^{-1} \text{ m}$) [12] with amplitude of λ still higher than that of $\text{CoCr}_{0.2}\text{Fe}_{1.8}\text{O}_4$ but lower than that of $\text{CoMn}_{0.2}\text{Fe}_{1.8}\text{O}_4$ [2]. Comparatively, the $(d\lambda/dH)_{\text{max}}$ value for $\text{CoAl}_{0.1}\text{Fe}_{1.9}\text{O}_4$ was higher than that of $\text{CoCr}_{0.2}\text{Fe}_{1.8}\text{O}_4$ and $\text{CoMn}_{0.2}\text{Fe}_{1.8}\text{O}_4$. This, as in case of $\text{Co}_{1.1}\text{Ge}_{0.1}\text{Fe}_{1.8}\text{O}_4$, infers that $\text{CoAl}_{0.1}\text{Fe}_{1.9}\text{O}_4$ is expected to be more a strain sensitive sensor material than $\text{CoCr}_{0.2}\text{Fe}_{1.8}\text{O}_4$ and $\text{CoMn}_{0.2}\text{Fe}_{1.8}\text{O}_4$ at similar operation conditions.

IV. CONCLUSION

Results on magnetic and magnetomechanical properties of $\text{CoAl}_x\text{Fe}_{2-x}\text{O}_4$ have been presented. The variation of magnetostriction with applied magnetic field was compared with those of Ge-, Ga-, Mn- and Cr-doped Co-ferrites. Maximum magnetostriction in $\text{CoAl}_x\text{Fe}_{2-x}\text{O}_4$ samples was higher in amplitude than those of $\text{CoGa}_x\text{Fe}_{2-x}\text{O}_4$ and $\text{CoCr}_x\text{Fe}_{2-x}\text{O}_4$ but lower than those of $\text{Co}_{1+x}\text{Ge}_x\text{Fe}_{2-2x}\text{O}_4$ and $\text{CoMn}_x\text{Fe}_{2-x}\text{O}_4$. In terms of the sensitivity of strain to applied magnetic field, $\text{CoAl}_x\text{Fe}_{2-x}\text{O}_4$ had the second highest strain derivative behind $\text{CoGa}_x\text{Fe}_{2-x}\text{O}_4$. Thus, it was found that $\text{CoAl}_x\text{Fe}_{2-x}\text{O}_4$ has potential as a material for high-sensitivity magnetomechanical strain sensor device development, and considering energy efficiency, has potential for magnetostrictive actuator application also.

ACKNOWLEDGMENT

This research was supported by the U.K. Engineering and Physical Science Research Council under Grant EP057094 and by the U.S. National Science Foundation under Grant DMR-0402716.

REFERENCES

- [1] Y. Chen, J. E. Snyder, C. R. Schwichtenberg, K. W. Dennis, R. W. McCallum, and D. C. Jiles, "Metal-bonded Co-ferrite composites for magnetostrictive torque sensor applications," *IEEE Trans. Magn.*, vol. 35, pp. 3652–3654, Sept. 1999.
- [2] J. A. Puntzen, A. P. Ring, C. C. H. Lo, J. E. Snyder, and D. C. Jiles, "Manganese-substituted cobalt ferrite magnetostrictive materials for magnetic stress sensor applications," *J. Appl. Phys.*, vol. 97, no. 044502, Jan. 2005.
- [3] S. H. Song, C. C. H. Lo, S. J. Lee, S. T. Akhni, J. E. Snyder, and D. C. Jiles, "Magnetic and magnetoelastic properties of Ga-substituted cobalt ferrite," *J. Appl. Phys.*, vol. 101, pp. 09C517–, May 2007.
- [4] Y. Melikhov, J. E. Snyder, C. C. H. Lo, P. N. Matlage, S. H. Song, K. W. Dennis, and D. C. Jiles, "The effect of Cr-substitution on the magnetic anisotropy and its temperature dependence in Cr-substituted cobalt ferrite," *IEEE Trans. Magn.*, vol. 42, no. 10, pp. 2861–2863, Oct. 2006.
- [5] N. Rauvah, C. I. Nlebedim, Y. Melikhov, J. E. Snyder, D. C. Jiles, A. J. Moses, P. I. Williams, F. Anayi, and S. H. Song, "Temperature dependence of magnetostriction of $\text{Co}_{1+x}\text{Ge}_x\text{Fe}_{2-2x}\text{O}_4$ for magnetostrictive sensor and actuator applications," *IEEE Trans. Magn.*, vol. 44, pp. 3013–3016, Nov. 2008.
- [6] C. C. H. Lo, A. P. Ring, J. E. Snyder, and D. C. Jiles, "Improvement of magnetomechanical properties of cobalt ferrite by magnetic annealing," *IEEE Trans. Magn.*, vol. 41, pp. 3676–3678, Oct. 2005.
- [7] A. S. Vainankar, B. V. Khasburtar, and R. N. Pail, "X-ray spectroscopic study of cobalt ferrite," *J. Phys. F: Metal Phys.*, vol. 10, pp. 1615–1619, July 1980.
- [8] A. A. Younis, M. E. Elzain, H. H. Sutherland, and S. H. Sahh, "Mössbauer studies on Al-ferrites," *Hyperfine Interactions*, vol. 68, pp. 323–328, 1992.
- [9] R. D. Shannon, "Revised effective ionic radii and systematic studies of interatomic distances in halides and chalcogenides," *Acta Crystallographica A*, vol. 32, pp. 751–767, Mar. 1976.
- [10] N. Rauvah, C. I. Nlebedim, Y. Melikhov, J. E. Snyder, P. I. Williams, A. J. Moses, and D. C. Jiles, "Temperature dependence of magnetic properties of $\text{CoAl}_x\text{Fe}_{2-x}\text{O}_4$," Sacramento, California, USA, May 4–8, 2009. Digest ID: 607310. Accepted for INTERMAG.
- [11] A. Affanni, A. Guerra, L. Dall'Agliovanna, and G. Chiarboli, "Design and characterization of magnetostrictive linear displacement sensors," in *Instrumentation and Measurement Technology Conference, IMTC 2004*, Como, Italy, May 18–20, 2004, vol. 206.
- [12] S. J. Lee, C. C. H. Lo, P. N. Matlage, S. H. Song, Y. Melikhov, J. E. Snyder, and D. C. Jiles, "Magnetic and magnetoelastic properties of Cr-substituted cobalt ferrite," *J. Appl. Phys.*, vol. 102, pp. 073910–, Aug. 2007.



Contents lists available at ScienceDirect

Journal of Magnetism and Magnetic Materials

journal homepage: www.elsevier.com/locate/jmmm

Influence of vacuum sintering on microstructure and magnetic properties of magnetostrictive cobalt ferrite

L.C. Nlebedim, N Ranvah, P.J. Williams, Y Melikhov, F Anayi, J.E. Snyder, A.J. Moses, D.C. Jiles*

Wolffson Centre for Magnetism, School of Engineering, Cardiff University, Cardiff CF24 3AA, United Kingdom

ARTICLE INFO

Article history:

Received 8 December 2008
Available online 20 March 2009

Keywords:

Anisotropy coefficient
Cobalt ferrite
Magnetoelastic property
Magnetostriction
Vacuum sintering

ABSTRACT

Differences in the microstructure and magnetic properties of highly magnetostrictive cobalt ferrite resulting from the effects of different vacuum sintering temperatures and times have been investigated. A vacuum environment was chosen to allow direct comparison of results with air-sintered samples which are more often reported in the literature. It was found that vacuum sintering resulted in the development of a solid solution second phase with composition $\text{Co}_{1-x}\text{Fe}_x\text{O}_4$ ($x \sim 0.33$). There was a decrease in magnetostriction as a result of the formation of the second phase. Furthermore, differences in sintering temperatures were found to have a greater effect on the magnetostriction than differences in sintering times. It was found that the first order cubic anisotropy coefficient initially increased with both sintering temperature and time, before peaking and decreasing to its lowest measured value. The lowest anisotropy was therefore achieved with samples sintered at higher temperatures and longer times.

© 2009 Elsevier B.V. All rights reserved.

1. Introduction

The use of magnetostrictive materials for development of non-contact stress sensors and actuators in a wide range of engineering applications has attracted considerable research interest. This includes the need to develop low-cost materials with improved mechanical, thermal and chemical properties of which ferrites are good candidates. Among the ferrites, cobalt ferrites (including the parent material CoFe_2O_4 and derivatives $\text{CoM}_x\text{Fe}_{2-x}\text{O}_4$) have been investigated as practical alternatives to the rare earth based magnetostrictive materials such as Terfenol ($\text{Tb}_x\text{Dy}_{1-x}\text{Fe}_2$) and other magnetostrictive metals such as Galferol ($\text{Fe}_{50}\text{Ga}_{50}$) for sensor and actuator development [1,2].

CoFe_2O_4 has a spinel crystal structure. For normal spinels, all the divalent metallic ions are on A-sites (tetrahedral sites) and all the trivalent ions are on B-sites (octahedral sites). On the other hand, inverse spinels have half of the trivalent ions on the A-site and the other half plus all the divalent metallic ions on the B-site. It is widely accepted [3] that CoFe_2O_4 is neither completely normal spinel nor completely inverse spinel. This is because the cation distribution between the tetrahedral and octahedral sites is intermediate between that of normal and inverse spinel materials. Since the magnetostrictive properties of CoFe_2O_4 depend largely on the position and concentration of the Co^{2+} ions, it follows that changes in the site occupancy of these ions will affect the magnetic and magnetostrictive properties of CoFe_2O_4 . Studies have shown that magnetic and magnetostrictive properties can be

altered by both chemical substitutions of the cations [4–6] and by heat treatment [7,8], the latter leading to a different distribution of cations as they migrate towards their most stable (that is the lowest energy) state. The time constants associated with this process are prohibitively long at room temperature, but are reduced at elevated temperature because of the higher thermal energy per ion which enables them to migrate more easily.

Most of the studies on the improvement of magnetostrictive properties of CoFe_2O_4 have concentrated on samples prepared at a particular temperature in air. Since site occupancy of ions is crucial to the magnetostrictive properties, and this can be altered depending on sintering conditions, there is a need for a systematic approach to vary the heat treatment and sintering conditions to produce desired properties. This can also lead to a better understanding of magnetostrictive properties. Such understanding is particularly important due to the varying levels of magnetostriction reported for CoFe_2O_4 in different studies. Values ranging from 100 to 225 ppm have been reported previously [8–10].

In this work, we present the results of a study on the effect of vacuum sintering, with different sintering temperatures and sintering times, on the microstructure, magnetic and magnetostrictive properties of bulk samples of CoFe_2O_4 . Since oxygen partial pressure influences the compositional variation of CoFe_2O_4 [7], vacuum condition was chosen in order to compare and contrast results with those of air-sintered samples reported [8,10].

2. Experimental details

CoFe_2O_4 powder was ball milled, pressed into buttons and sintered in vacuum at a pressure of 10^{-5} Torr. Nine samples were

* Corresponding author.

E-mail address: jilesd@ac.ac.uk (D.C. Jiles).



studied, comprising three samples sintered at each of three temperatures 800, 1000 and 1200 °C, and for different times of 6, 12 and 24 h. All samples were heated and cooled at the same rate of 250 °C/h.

The crystal structures of the sintered samples were characterized by X-ray diffractometry (XRD) and the microstructures by scanning electron microscopy (SEM). To determine the final sample compositions, energy dispersive X-ray (EDX) analysis was carried out in the SEM. Magnetic properties were measured using a SQUID magnetometer up to a maximum applied field of $H = 4 \times 10^6$ A/m. Magnetostriction was measured at room temperature in the direction parallel to the applied field using foil strain gauges bonded on to the samples.

To evaluate the variation of anisotropy with sintering temperature, the law of approach to saturation was used to determine the first cubic anisotropy coefficient (K_1). It was assumed that as magnetization approached saturation, all irreversible hysteretic processes were completed and that the magnetization process in that region was due to reversible rotational processes which are the result of rotation against magnetic anisotropy. The law of approach as given in [11] is

$$M = M_s \left(1 - \frac{a}{H} - \frac{b}{H^2} - \dots \right) + \kappa H \quad (1)$$

where a and b are the fitting coefficients, M_s and H are the saturation magnetization and applied field, respectively, κH is the forced magnetization term [12]. The coefficient a is related to domain wall pinning and therefore in the higher field region of reversible rotation of magnetization, the value of $a \approx 0$. For randomly oriented polycrystalline samples with a cubic crystal structure, the coefficient b is given [13] as

$$b = \frac{8}{105} \frac{K_1^2}{\mu_0^2 M_s^2} \quad (2)$$

where μ_0 is the permeability of free space. This gives the law of approach up to and including the second order term as

$$M = M_s \left[1 - \frac{8}{105} \left(\frac{K_1}{\mu_0 M_s^2} \right)^2 \right] + \kappa H \quad (3)$$

The high-field region of the curve was used to fit Eq. (3) in order to determine K_1 . The chosen region is in the range $0.97M_s < M < M_s$, in which the law of approach is normally assumed to be valid [14].

3. Results and discussion

The variation of sample density with sintering temperature is shown in Fig. 1. Densities of the samples were obtained from the masses and volumes of the thick disk (or short cylinder) shaped samples. An increase in the sintering temperature or sintering time resulted in an increase in the densities of the samples. The sample sintered at 800 °C for 6 h had the lowest density of 4548 kg/m³, while the sample sintered at 1200 °C for 24 h had the highest density of 5080 kg/m³. The theoretical density of pure cobalt ferrite is 5259 kg/m³.

X-ray diffraction spectra of the unsintered powder and solid samples sintered at 800, 1000 and 1200 °C for 24 h are shown in Fig. 2. Also shown are diffraction spectra of samples sintered at 1000 °C for 6, 12 and 24 h. The patterns were recorded at intervals of 0.02° on a Philips PW1710 automated powder diffractometer with copper (CuK α) radiation at 35 kV and 40 mA. Vacuum sintering resulted in the development of additional peaks which match the CoO pattern. These peaks are marked with the "◆" symbol. Similar results were observed for all the sintered samples. Those additional peaks were not observed for samples sintered in

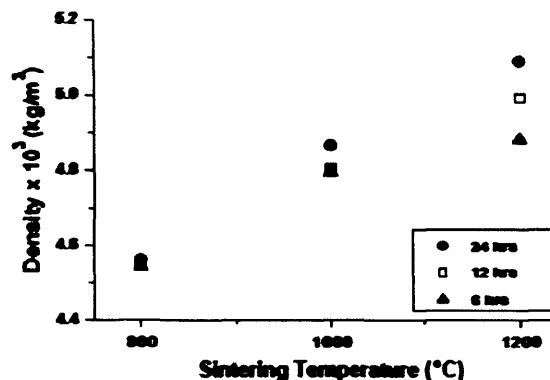


Fig. 1. Variation of density with sintering temperature.

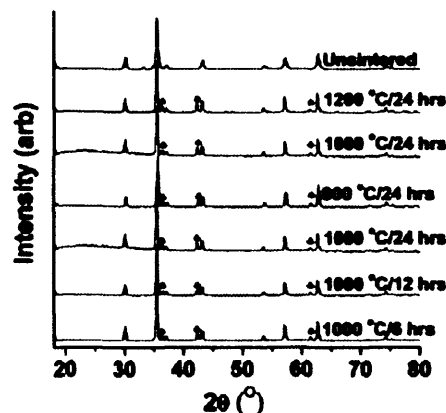


Fig. 2. X-ray diffraction patterns for the CoFe_2O_4 samples sintered for 24 h and the unsintered sample. Unmarked peaks correspond to the spinel cobalt ferrite pattern. Peaks marked with ◆ correspond to the CoO pattern.

air [9] or for the unsintered sample. They could be the result of the reducing effect of the vacuum sintering environment. It has been stated by others [15] that heat treatment of CoFe_2O_4 in a reducing environment helps the development of an additional phase. To understand the origin of these peaks, SEM and EDX analysis of the samples were made.

The SEM micrographs in Fig. 3 show that the samples possess an additional phase as shown by XRD results. Micrographs marked A, B and C are for samples sintered at 1000 °C for 6, 12 and 24 h, respectively, while those marked I, II and III are for samples sintered for 24 h at 800, 1000 and 1200 °C, respectively. In general, the samples sintered at a lower sintering temperature, or held for a shorter time (or both), showed less of the additional light colored phase.

Table 1 shows the EDX results for the samples sintered at 1000 °C and held for 6, 12 and 24 h while Table 2 shows the results for samples held for 24 h at 800, 1000 and 1200 °C. In both cases, the results show that vacuum sintering of CoFe_2O_4 resulted in two phases: a spinel phase slightly richer in Fe and a $\text{Co}_{1-x}\text{Fe}_x\text{O}$ second phase. The second phase may be due to the reducing effect of the vacuum environment. It is a single phase of solid solution CoO/FeO in which $x \approx 0.33$. Both CoO and FeO have the rocksalt structure with similar ionic radii ($\text{Co}^{2+} = 0.75 \text{ \AA}$, $\text{Fe}^{2+} = 0.78 \text{ \AA}$)

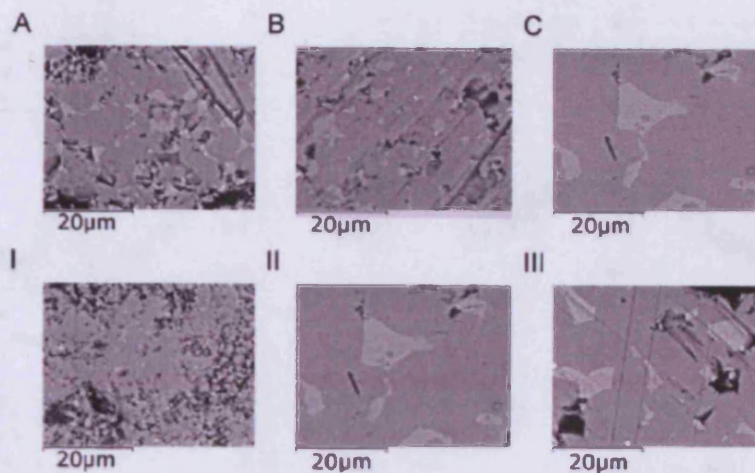


Fig. 3. SEM micrographs of samples held at constant sintering temperature for different times (A, B and C) and for constant sintering times at different sintering temperatures (I, II and III).

Table 1

EDX results for the samples sintered at constant sintering temperature and different sintering times.

Sintering temperature/time	Spinel phase	Second phase
1000 °C/6 h	Co _{0.93} Fe _{0.07} O ₄	Co _{0.65} Fe _{0.35} O
1000 °C/12 h	Co _{0.88} Fe _{0.12} O ₄	Co _{0.67} Fe _{0.33} O
1000 °C/24 h	Co _{0.84} Fe _{0.16} O ₄	Co _{0.66} Fe _{0.34} O

Table 2

EDX results for the samples sintered at different sintering temperatures and constant sintering time.

Sintering temperature/time	Spinel phase	Second phase
800 °C/24 h	Co _{0.98} Fe _{0.02} O ₄	Co _{0.67} Fe _{0.33} O
1000 °C/24 h	Co _{0.94} Fe _{0.06} O ₄	Co _{0.66} Fe _{0.34} O
1200 °C/24 h	Co _{0.85} Fe _{0.15} O ₄	Co _{0.66} Fe _{0.34} O

and molar volumes ($\text{Co}^{2+} = 11.708 \text{ cm}^3/\text{mol}$, $\text{Fe}^{2+} = 11.974 \text{ cm}^3/\text{mol}$). For all compositions in the temperature range from 300 to 2000 K, the CoO/FeO system has a negative free energy and has neither maxima nor minima in its chemical potential versus composition plots over the same temperature range [16]. It is then obvious that CoO/FeO forms a solid solution which is completely miscible and in all compositions it forms a single phase over the range 300–2000 K. Analysis of the X-ray diffraction spectra gave the $\text{Co}_{1-x}\text{Fe}_x\text{O}$ peaks as a CoO peak because the solid solution is ~67% Co, thus its lattice parameter is closer to CoO than to FeO.

The variation of magnetostriction with magnetic field is shown in Fig. 4 for different sintering temperatures at constant sintering time (upper plots) and with different sintering times at constant sintering temperature (lower plots). Comparing these, it is seen that differences in sintering time have less influence on the magnetostriction of the samples than differences in sintering temperature. The highest magnitude of magnetostriction, 125 ppm, was achieved for samples sintered at 800 °C. This value falls into the mid-range of values reported in the literature

for air-sintered samples [8,10]. The magnetostriction amplitude may have been reduced by the detrimental effect of the $\text{Co}_{1-x}\text{Fe}_x\text{O}$ second phase as shown by XRD, SEM and EDX results. The $\text{Co}_{1-x}\text{Fe}_x\text{O}$ phase contains more of antiferromagnetic CoO with a Néel temperature at 297 K [17]. Magnetostriction of CoO has been reported to be -5.4 ppm at 77 K [17,18] and would be expected to be negligible at room temperature. In such a system containing a magnetostrictive composite, it is expected that the effective magnetostriction would decrease with an increase in the volume fraction of the $\text{Co}_{1-x}\text{Fe}_x\text{O}$ second phase. Moreover, according to the single-ion crystalline-field model, magnetostriction in CoFe_2O_4 is due primarily to Co^{2+} located on the B-sites of the spinel crystal structure. Any deviation from stoichiometry resulting in a decrease of Co^{2+} on these sites would therefore result in a lower magnetostriction and it can be seen that the compositions of the spinel phases in Tables 1 and 2 are all deficient in Co^{2+} . This provides a second reason why the magnetostriction is lower in the materials in which the second phase is present.

The variation of coercive field with sintering temperature is shown in Fig. 5. The coercive field was found to decrease with increasing sintering temperature and sintering time. This was expected as coercivity is related to grain size, with larger grains providing less pinning of domain walls because of the lower volume fraction of grain boundaries. Higher sintering temperature and longer sintering time are expected to result in larger grains and consequently lower coercive field. The maximum coercive field (25.2 kA/m) was observed for the sample sintered at 800 °C for 6 h and the least (3.7 kA/m) was observed for the sample sintered at 1200 °C for 24 h.

The variation of K_1 with sintering temperature is plotted in Fig. 6. The lowest value of K_1 , $3.21 \times 10^3 \text{ J/m}^3$, was observed for the sample sintered at 1200 °C for 24 h whereas the highest value, $4.57 \times 10^3 \text{ J/m}^3$, was observed for the sample sintered at 1000 °C for 12 h. The anisotropy coefficient showed a trend, initially increasing and later decreasing, with an increase in sintering temperature and time. The high anisotropy coefficient achieved when the samples were held at 1000 °C for 12 h is not easily explainable from this study but requires further investigation. In general, it was observed that the anisotropy coefficient was lowest for samples sintered at 1200 °C.

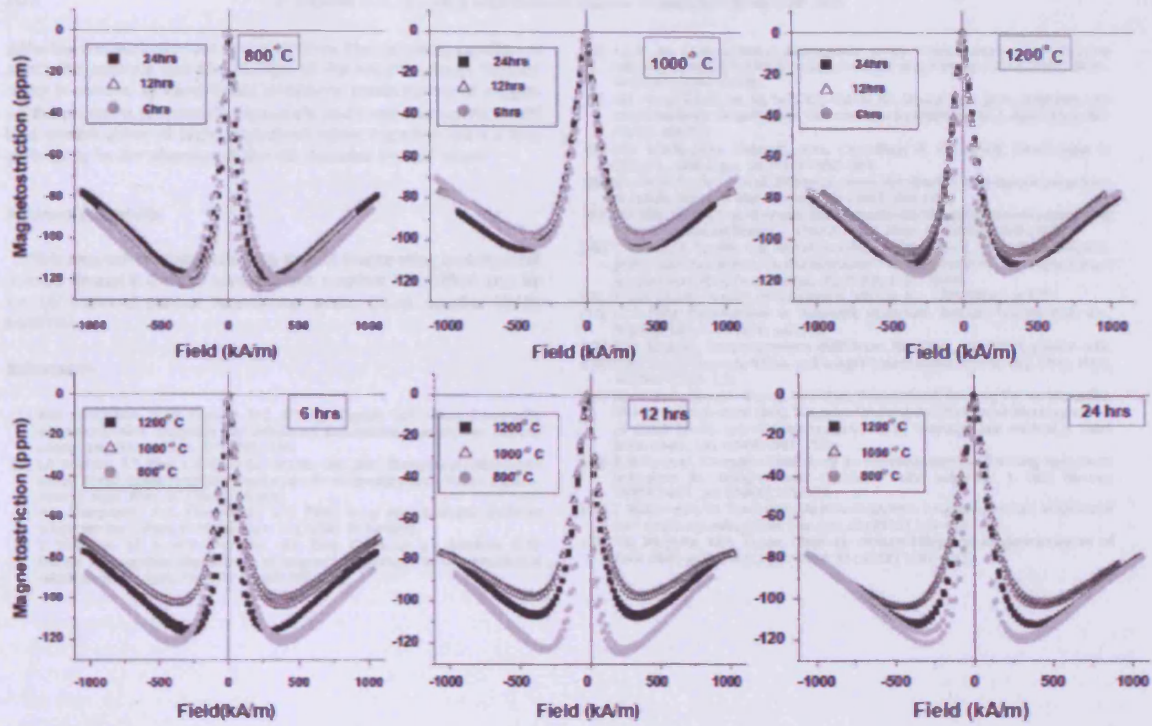


Fig. 4. Variation of magnetostriction with sintering times at constant sintering temperatures (upper) and variation of magnetostriction with sintering temperatures at constant sintering times (lower).

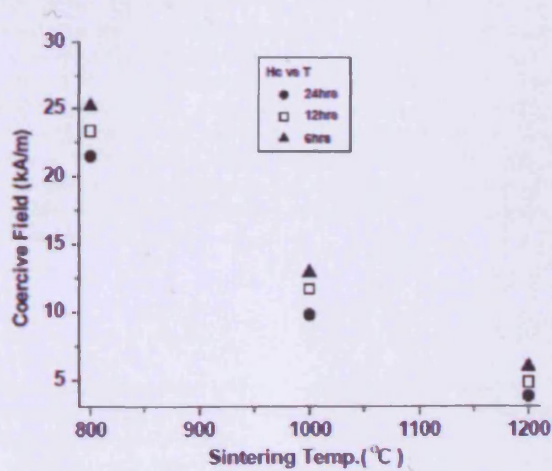


Fig. 5. Variation of coercive field with sintering temperature.

4. Conclusions

The results of a study on the influence of vacuum sintering on microstructure and magnetic properties of magnetostrictive cobalt ferrite and its cation substituted derivatives have been

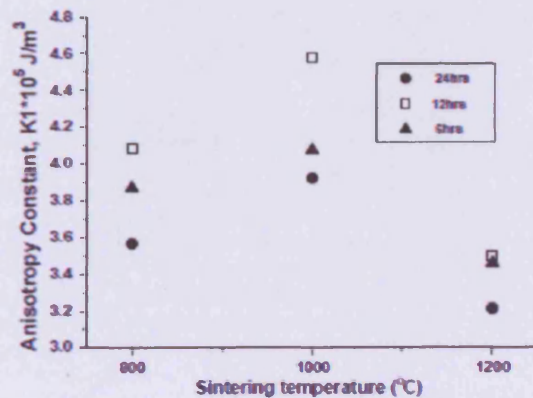


Fig. 6. Variation of the first cubic anisotropy coefficient with sintering temperature.

presented. Samples sintered in vacuum showed comparable values of magnetostriction with some of those sintered in air but the samples sintered in vacuum developed a second phase of $Co_{1-x}Fe_xO$ solid solution system with $x=0.33$, which reduced the overall magnetostriction. Magnetostriction was largest for lower sintering temperatures and longer sintering times. The anisotropy coefficient initially increased and later decreased with increasing



sintering temperature and sintering time. The sintering conditions affect the amount and distribution of the second phase. Further study is needed to identify the necessary combination of oxygen partial pressure, sintering temperature and time that would result in a combination of high magnetostriction together with a low anisotropy in the absence of the detrimental second phase.

Acknowledgments

This research was supported by the UK Engineering and Physical Science Research Council under Grant number EP/J057094 and by the US National Science Foundation under Grant number DMR-0402716.

References

- [1] R.W. McCallum, K.W. Dennis, D.C. Jiles, J. Snyder, Y.H. Chen, Composite magnetostrictive materials for advanced automotive magnetomechanical sensor, *Low Temp. Phys.* 27 (2001) 266.
- [2] J.A. Pousen, A.P. Ring, C.C.H. Lo, J.E. Snyder, D.C. Jiles, Manganese-substituted cobalt ferrite magnetostrictive materials for magnetic stress sensor applications, *J. Appl. Phys.* 97 (2005) 044502.
- [3] A.S. Vaingankar, B.V. Khasbaidar, R.N. Pail, X-ray spectroscopic study of cobalt ferrite, *J. Phys. F: Metal Phys.* 10 (1980) 1615–1619.
- [4] Y. Melnikov, J.E. Snyder, D.C. Jiles, A.P. Ring, C.C.H. Lo, J.A. Pousen, K.W. Dennis, Temperature dependence of magnetic anisotropy in Mn-substituted cobalt ferrite, *J. Appl. Phys.* 99 (2006) 08R102.
- [5] C.C.H. Lo, Compositional dependence of the magnetoelastic effect in substituted cobalt ferrite for magnetostatic stress sensors, *IEEE Trans. Magn.* 43 (2007) 2367–2369.
- [6] S.H. Song, C.C.H. Lo, S.J. Lee, S.T. Ahlani, J.E. Snyder, D.C. Jiles, Magnetic and magnetoelastic properties of Ga-substituted cobalt ferrite, *J. Appl. Phys.* 101 (2007) 08C317.
- [7] G.D. Rieck, J.J.M. Thijssen, Acta Crystallogr. B, the cation distribution in CoFe_2O_4 , *Acta Cryst.* 34 (1968) 982–983.
- [8] J.G. Ho, T.D. Lee, S.J. Park, Effects of cation distribution on magnetic properties in cobalt ferrite, *J. Mat. Sci. Lett.* 12 (1993) 961–962.
- [9] S.D. Bhanu, P.A. Joy, Magnetic and magnetostrictive properties of manganese substituted cobalt ferrite, *J. Phys.D: Appl. Phys.* 40 (2007) 3263–3267.
- [10] Y. Chen, J.E. Snyder, C.R. Schlichtenberg, K.W. Dennis, R.W. McCallum, D.C. Jiles, Metal-bonded Co-ferrite composites for magnetostrictive torque sensor applications, *IEEE Trans. Magn.* 35 (1999) 3652–3654.
- [11] S. Chikazumi, *Physics of Magnetism*, Wiley, Inc., USA, 1964, pp.227.
- [12] D. Culhity, *Introduction to Magnetic Materials*, Addison-Wesley Pub. Co., Reading MA, USA, 1972, pp. 342.
- [13] R.M. Bozorth, *Ferromagnetism*, IEEE Press, New York, USA, 1993, pp.486–487.
- [14] E.W. Lee, Magnetostriction and magnetoelastic effects, *Rep. Prog. Phys.* 18 (1955) 184–229.
- [15] Lijun Zhao, Hongjie Zhang, Yan Qing, Shuyan Song, Shiyong Yu, Weidong Shi, Xianmin Gao, Jianhui Yang, Yungqian Lei, Feng Cao, Studies on the magnetism of cobalt ferrite nanocrystals synthesized by hydrothermal method, *J. Solid State Chem.* 181 (2008) 245–252.
- [16] S. B Pongsa, Computational study on thermodynamics of mixing and phase behaviour for CoO/FeO and CoO/MnO solid solutions, *J. Mol. Struct.: THEOCHEM*, 761 (2006) 171–175.
- [17] T. Nakamichi, M. Yamamoto, Antiferromagnetic magnetostriction in CoO and NiO single crystals, *J. Phys. Soc. Jpn.* 16 (1961) 126–127.
- [18] T.R. McGuire, W.A. Crapo, Magnetic susceptibility and magnetostriction of CoO , MnO and NiO , *J. Appl. Phys.* 33 (1962) 1291–1292.

Temperature Dependence of Magnetostriction of $\text{Co}_{1+x}\text{Ge}_x\text{Fe}_{2-2x}\text{O}_4$ for Magnetostrictive Sensor and Actuator Applications

Naresh Ravvah¹, I. C. Nlebedim¹, Y. Melikhov¹, J. E. Snyder¹, D. C. Jiles¹, Fellow, IEEE, A. J. Moses¹, P. I. Williams¹, F. Anayi¹, and Sang-Hoon Song²

¹Wolfson Centre for Magnetism, Cardiff University, Wales CF24 3AA, U.K.

²Materials Science Engineering Department, Iowa State University, Ames, IA 50010 USA

The temperature dependence of the magnetoelastic properties of a series of germanium/cobalt co-substituted cobalt ferrite samples has been measured. Magnetostriction loops of the compositions $\text{Co}_{1+x}\text{Ge}_x\text{Fe}_{2-2x}\text{O}_4$ ($x = 0.1, 0.3, \text{ and } 0.6$) were measured over a temperature range of 250–400 K. Germanium/cobalt co-substitution was found to change the Curie temperature, anisotropy, and the magnetostriction coefficients in the crystal directions of [100] and [111]. Both magnetostriction and strain sensitivity were seen to decrease in magnitude with increasing temperature. $\text{Co}_{1.1}\text{Ge}_{0.1}\text{Fe}_{1.8}\text{O}_4$ was found to have a maximum sensitivity $(d\lambda/dH)_\sigma$ of $2.6 \times 10^{-11} \text{ A}^{-1}\text{m}$, which is twice the value obtained for pure cobalt ferrite, without any decrease in maximum magnetostriction in the linear region.

Index Terms—Cobalt ferrite, germanium substitution, magnetostriction, stress sensor.

I. INTRODUCTION

COBALT ferrite based materials have generated considerable interest for applications in magnetostrictive torque and stress sensor and actuator applications [1]–[4]. Magnetoelastic stress sensors work on the principle that basic magnetic properties such as permeability and magnetization are altered in the presence of stress due to the magnetoelastic coupling which results in a stress dependent contribution to the anisotropy that alters the permeability of the material. This contribution is sometimes represented as an equivalent field H_σ although the analogy with magnetic field is not exact. Thus, stress can be detected by using a non-contact magnetic field sensor to measure the altered magnetic properties of a magnetoelastic material [1].

An ideal non-contact magnetoelastic sensor material will have a high sensitivity of magnetic flux density to applied stress $(dB/d\sigma)_H$ (where B is the magnetic flux density and σ is the stress, λ is the magnetostrictive strain, and H is the magnetic field) and negligible hysteresis. The relationship between strain derivative and the sensitivity of magnetization to applied stress can be expressed as [5]

$$\left(\frac{d\lambda}{dH}\right)_\sigma = \mu_0 \left(\frac{dB}{d\sigma}\right)_H \quad (1)$$

where μ_0 is the permeability of free space. Thus, a high strain derivative is indicative of promising characteristics for both a magnetoelastic sensor and an actuator material.

Giant magnetostrictive materials such as Terfenol have high magnetostriction coefficients, but not a very high sensitivity of magnetic flux density to stress for a stress sensor material [1]. Cobalt ferrite-based materials have a high sensitivity of magnetization to applied stress and an excellent chemical stability,

which indicate their potential for non-contact magnetostrictive sensor and actuator applications [1], [6], [7]. The niche area of application of these materials is in situations with low strain requiring high sensitivity [1]. Chemical substitutions have been used to selectively tailor the properties of these materials. Substitution for Fe^{3+} -cations with trivalent M^{3+} -cations ($\text{M} = \text{Mn}, \text{Cr}, \text{ and } \text{Ga}$), to obtain $\text{CoM}_x\text{Fe}_{2-x}\text{O}_4$, produces lower Curie temperature and improved magnetic and magnetoelastic properties [3], [4], [8]. Cobalt ferrite has a cubic spinel-type structure in which the O^{2-} ions form an fcc-like lattice. The Co^{2+} and Fe^{3+} ions occupy either of the two interstitial sites—tetrahedral (A sites) or octahedral (B sites). Magnetic and magnetoelastic properties of cobalt ferrite-based materials depend on the exchange interactions, which in turn depends on the cation distribution in the lattice. The cobalt ions in cobalt ferrite have a preference for the octahedral (B) sites and the actual distribution depends on how close to equilibrium these distributions get, and that in turn depends on the thermal treatment during processing [9]. In the present work, the effect of germanium/cobalt-substitution on the temperature dependence of the magnetoelastic properties of $\text{Co}_{1+x}\text{Ge}_x\text{Fe}_{2-2x}\text{O}_4$ has been studied over a temperature range of 250–400 K for $x = 0.1, 0.3, \text{ and } 0.6$. The substitution of a tetravalent Ge^{4+} -ion and divalent Co^{2+} -ion for two trivalent Fe^{3+} -ions was expected to produce a cation distribution that is different from that of previously tested trivalent substitutions and hence the material was expected to exhibit different properties from those of the previous materials.

II. SAMPLE PREPARATION

A series of polycrystalline Ge/Co-substituted cobalt ferrite samples, $\text{Co}_{1+x}\text{Ge}_x\text{Fe}_{2-2x}\text{O}_4$, was prepared by standard powder ceramic techniques using a final sintering at a temperature of 1623 K for 24 hours, followed by furnace cooling to room temperature [1], [2]. Energy dispersive x-ray spectroscopy (EDS/EDX) was used to determine the actual chemical compositions, which were found to be close to the target compositions (see Table I) [10].

TABLE I
COMPOSITION OF $\text{Co}_{1-x}\text{Ge}_x\text{Fe}_{2-2x}\text{O}_4$ DETERMINED BY EDS [10]

Target compositions	Composition by EDS		
	Fe	Co	Ge
$\text{Co}_{1.1}\text{Ge}_{0.1}\text{Fe}_{1.8}\text{O}_4$	1.77	1.11	0.12
$\text{Co}_{1.3}\text{Ge}_{0.3}\text{Fe}_{1.4}\text{O}_4$	1.29	1.33	0.38
$\text{Co}_{1.6}\text{Ge}_{0.6}\text{Fe}_{0.8}\text{O}_4$	0.70	1.63	0.67

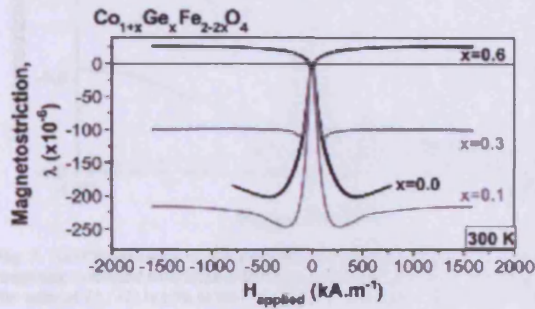


Fig. 1. Field induced magnetostriction of $\text{Co}_{1-x}\text{Ge}_x\text{Fe}_{2-2x}\text{O}_4$ ($x = 0.0$ from [2]) at 300 K.

III. EXPERIMENTAL DETAILS

The Curie temperatures were determined by vibrating sample magnetometry and they were found to decrease with increasing Ge-content. Curie temperatures of samples with Ge-content of $x = 0.1, 0.3,$ and 0.6 were measured to be 715 K, 558 K and 407 K respectively. The Curie temperature of pure cobalt ferrite prepared by the same process was 784 K [3]. The field-induced magnetostriction was measured with a strain gauge setup. 350 Ω strain gauges and M-Bond 610 strain gauge adhesive from Vishay Micromeritics were used; both function over the entire temperature range of the experiment. Magnetostriction loops ($\lambda - H$) were measured over a field range of $-2 \text{ T} \leq \mu_0 H \leq 2 \text{ T}$ within a temperature range of 250–400 K.

IV. RESULTS AND DISCUSSION

The magnetostriction curves at room temperature of all the measured compositions are shown in Fig. 1. Fig. 2 shows the variation of the sensitivity parameter $d\lambda/dH$ with field and composition.

A. Shapes of the Curves

Over the temperature range of 250–400 K, three different shapes of magnetostriction curves were observed and classified as shown in Fig. 3(a) and (b). Cobalt ferrite has two independent magnetostriction coefficients, λ_{100} and λ_{111} , along the two crystal directions of [100] and [111] respectively. At 300 K, it is known that $\lambda_{100} < 0$, $\lambda_{111} > 0$, and $|\lambda_{100}| > (3/2)|\lambda_{111}|$ in pure cobalt ferrite. Furthermore, the first order cubic anisotropy constant K_1 for pure cobalt ferrite is positive at all temperatures, making [100] the easy-direction. At low field values, the field-induced strain $\lambda(H)$ has a large negative slope due to a dominant contribution from λ_{100} . After the alignment of domain magnetizations with the local easy axes, a further increase

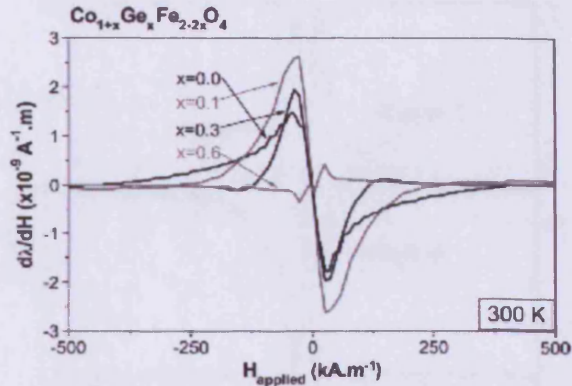


Fig. 2. Strain derivative ($d\lambda/dH$) of $\text{Co}_{1-x}\text{Ge}_x\text{Fe}_{2-2x}\text{O}_4$ ($x = 0.0$ from [2]) at 300 K.

in field causes $\lambda(H)$ to increase slowly with a positive slope because of the contribution from λ_{111} as some magnetization vectors are forced away from the easy axes towards the hard axes in order to align with the magnetic field. These variations and the contributions of the two magnetostriction coefficients to the shape of the field-induced magnetostriction curve of pure cobalt ferrite under different conditions have been discussed by others [11].

The three shapes found in the magnetostriction curves of germanium/cobalt substituted cobalt ferrite are due to the changes in K_1 , λ_{100} and λ_{111} with temperature and composition. Shape-A was obtained when the contribution of λ_{100} to strain increased faster with increasing field than the λ_{111} contribution, at low fields. This initial high negative slope continued until complete alignment of domains with the easy [100] axes. An increase in field beyond this point results in λ_{111} making a contribution to the positive slope of $\lambda(H)$ at these fields. The positive slope at high fields is much less than the negative slope at low fields. Shape-A was observed for samples with Ge-content of $x = 0.1$ at all observed temperatures, and for $x = 0.3$ at 250 and 300 K.

Shape-B was observed when the contribution of λ_{100} to $\lambda(H)$ was dominant at all fields. At high field values, the contribution of λ_{111} was either negligible or small and negative. Shape-B was observed for samples with Ge-content of $x = 0.3$ at 350 and 400 K.

Shape-C is an inverted form of Shape-B. Such characteristic shape of $\lambda(H)$ curve can be obtained when either the contribution of λ_{100} to the field induced magnetostriction becomes negligible, or when λ_{100} or K_1 switches sign. Shape C was observed for $\text{Co}_{1.6}\text{Ge}_{0.6}\text{Fe}_{0.8}\text{O}_4$ over the entire temperature range of the experiment.

B. Strain Amplitude and Strain Derivative

The field-induced magnetostrictive strain amplitude $\lambda_{\text{max,linear}}$, for the initial high-sensitivity “linear” region of the $\lambda(H)$ characteristic, was determined. For Shape-A, the maximum of $\lambda(H)$ at the end of the linear region was chosen as the value of $\lambda_{\text{max,linear}}$. For Shape-B and C, the end of “linear”

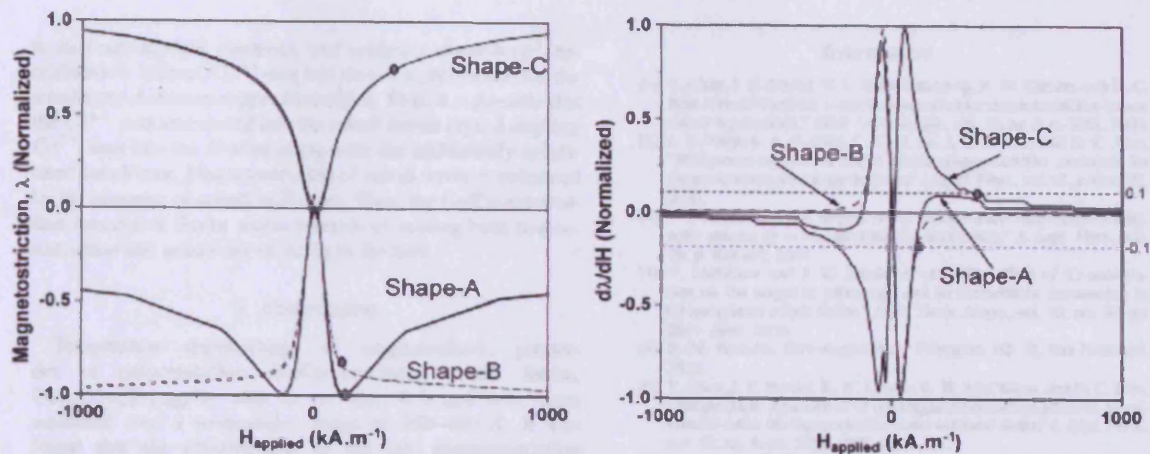


Fig. 3. (a) Classification of different shapes of magnetostriction $\lambda - H$ curves. (b) Corresponding $d\lambda/dH - H$ curves. Field induced magnetostrictive strain amplitude is marked with filled dots onto both the curves. For Shape-B and Shape-C, the value of magnetostrictive strain amplitude was chosen as the point where the value of $d\lambda/dH$ is 10% of the $(d\lambda/dH)_{max}$ for that sample. Such points have been marked with filled dots on curves corresponding for Shape-B and Shape-C.

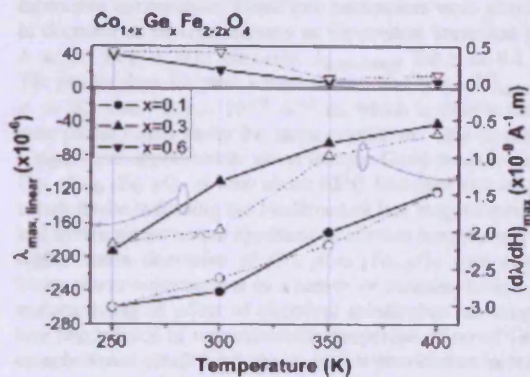


Fig. 4. Solid lines and solid symbols show the field induced magnetostrictive strain amplitude $\lambda_{max,linear}$. Dotted lines and hollow symbols show amplitude of field-induced strain derivative $(d\lambda/dH)_{max}$. Note that the sample with Ge-content of $x = 0.6$ had a positive magnetostriction, whereas all other samples had negative magnetostriction. For pure cobalt ferrite, the value of $\lambda_{max,linear}$ is -225×10^{-6} and the value of $(d\lambda/dH)_{max}$ is $-1.3 \times 10^{-9} \text{ A}^{-1} \cdot \text{m}$ [1].

region was chosen as the point where $(d\lambda/dH)$ has decreased to 10% of $(d\lambda/dH)_{max}$ [see Fig. 3(a) and (b)]. Fig. 4 shows the temperature dependence of $\lambda_{max,linear}$ and $(d\lambda/dH)_{max}$ for the various measured compositions. Please note that the sign of magnetostriction is also shown in the figure.

$|\lambda_{max,linear}|$ decreased for all samples with temperature increasing towards the Curie temperature T_C . $(d\lambda/dH)_{max}$ also followed the same trend with temperature. At room temperature, for the $\text{Co}_{0.9}\text{Ge}_{0.1}\text{Fe}_{1.8}\text{O}_4$ sample, the value of $\lambda_{max,linear}$ is -241×10^{-6} , which is 7% higher than for pure cobalt ferrite (-225×10^{-6}). Also the value of $(d\lambda/dH)_{max}$ for the sample with Ge-content of $x = 0.1$ was 102% higher ($-2.6 \times 10^{-9} \text{ A}^{-1} \cdot \text{m}$ vs. $-1.3 \times 10^{-9} \text{ A}^{-1} \cdot \text{m}$) than the value for pure cobalt ferrite [1]. Thus the sample with Ge-content of $x = 0.1$ achieved a value of $\lambda_{max,linear}$ comparable to that of pure cobalt

ferrite at less than half (27%) of the field needed by pure cobalt ferrite to achieve its maximum magnetostriction. In design of a sensor, this would translate to 93% less power consumption in comparison to pure cobalt ferrite.

In comparison to results of previous studies, the amplitude of strain derivative $(d\lambda/dH)_{max}$ of $\text{Co}_{0.9}\text{Ge}_{0.1}\text{Fe}_{1.8}\text{O}_4$ is comparable to that of $\text{CoMn}_{0.2}\text{Fe}_{1.8}\text{O}_4$ and $\text{CoCr}_{0.2}\text{Fe}_{1.8}\text{O}_4$ and less than that of $\text{CoGa}_{0.2}\text{Fe}_{1.8}\text{O}_4$ ($(d\lambda/dH)_{max} = -3.2 \times 10^{-9} \text{ A}^{-1} \cdot \text{m}$) [8], [12]. However, its amplitude of field induced magnetostriction $\lambda_{max,linear}$ is more than that of $\text{CoGa}_{0.2}\text{Fe}_{1.8}\text{O}_4$ ($\lambda_{max,linear} = -192 \times 10^{-6}$), $\text{CoCr}_{0.2}\text{Fe}_{1.8}\text{O}_4$ ($\lambda_{max,linear} = -78 \times 10^{-6}$), and $\text{CoMn}_{0.2}\text{Fe}_{1.8}\text{O}_4$ ($\lambda_{max,linear} = -184 \times 10^{-6}$) [8], [13].

C. Effect of Anisotropy

The field induced strain derivative is an important characteristic of a magnetoelastic sensor/actuator material and it has been suggested that the strain derivative of a material depends on both magnetostriction and magnetic anisotropy. Anisotropy can be considered as the spring constant against which the field is producing a strain in the material [14]. The high sensitivity region of magnetostriction characteristics is obtained as a result of the domain magnetization processes caused by applied field or stress. These processes occur more readily in a material with a lower anisotropy. A lower polycrystalline magnetic anisotropy therefore should result in a higher sensitivity of strain to applied field. Previously, it was found that the randomly oriented magnetocrystalline anisotropy for polycrystalline materials reduces with increasing substitution of $M = \text{Cr, Mn, and Ga}$ for Fe [3], [4], [15]. The anisotropy in cubic spinel materials, which is dependent on the exchange interaction, can be reduced due to the weakening of $A - B$ exchange interaction on substitution of other cations for Fe [13]. It is probable that such a process is responsible for the high strain derivatives observed in chemically substituted cobalt ferrite-based materials. Ge tends to have tetrahedral coordination in solid structures due

to its four unpaired electrons, and tendency towards sp^3 hybridization. Indeed, Co^{3+} ion has shown a preference for the tetrahedral A -sites in copper ferrite [16]. Thus, it is possible that the Ge^{4+} ions introduced into the cobalt ferrite crystal displace Co^{2+} ions into the B -sites along with the additionally substituted cobalt ions. Magnetostriction of cobalt ferrite is enhanced by the presence of cobalt in B -sites. Thus, the Ge/Co-substitution into cobalt ferrite works towards increasing both magnetostriction and sensitivity of strain to the field.

V. CONCLUSION

Temperature dependences of magnetoelastic properties of polycrystalline Ge/Co-substituted cobalt ferrite, $Co_{1-x}Ge_xFe_{2-2x}O_4$ with ($x = 0.1, 0.3, \text{ and } 0.6$), were measured over a temperature range of 250–400 K. It was found that the contributions of the two magnetostriction coefficients, λ_{100} and λ_{111} , to field-induced strain $\lambda(H)$ changed with chemical composition and temperature. The field-induced strain amplitude λ_{max} and strain derivative $(d\lambda/dH)_{max}$ were observed to decrease in magnitude with increasing temperature. These two parameters were also seen to decrease at all temperatures as Ge-content increased from $x = 0.1$ to $x = 0.6$. However, λ_{max} for $x = 0.1$ was 7% greater than for pure cobalt ferrite, and $(d\lambda/dH)_{max}$ for $x = 0.1$ was $-2.6 \times 10^{-2} \text{ A}^{-1}\text{m}$, which is double that of pure cobalt ferrite under the same conditions. This represents a significant improvement given that the Curie temperature of $Co_{0.9}Fe_{1.1}O_4$ is also about 65°C less than that of pure cobalt ferrite indicating the likelihood of less magnetomechanical hysteresis for sensor applications at room temperature. The higher strain derivative of $Co_{0.9}Fe_{1.1}O_4$ also ensures lower power consumption in a sensor or actuator device. The understanding of effect of chemical substitution on temperature dependence of magnetoelastic properties of novel Ge/Co co-substituted cobalt ferrite has therefore provided an increased understanding of the potential of cobalt ferrite based materials for sensor and actuator applications over a range of temperature.

ACKNOWLEDGMENT

This research was supported in part by the UK Engineering and Physical Sciences Research Council under Grant EP/D057094 and in part by the US National Science Foundation under Grant DMR-0402716.

REFERENCES

- [1] Y. Chen, J. E. Snyder, C. R. Schwichtenberg, K. W. Calhoun, and D. C. Jiles, "Metal-bonded Co-ferrite composites for magnetostrictive torque sensor applications," *IEEE Trans. Magn.*, vol. 35, no. 5, p. 3652, 1999.
- [2] J. A. Ptasnik, A. P. Ring, C. C. H. Lo, J. E. Snyder, and D. C. Jiles, "Manganese-substituted cobalt ferrite magnetostrictive materials for magnetic stress sensor applications," *J. Appl. Phys.*, vol. 97, p. 044502, 2005.
- [3] Y. Melikhov and J. E. Snyder *et al.*, "Temperature dependence of magnetic anisotropy in Mn-substituted cobalt ferrite," *J. Appl. Phys.*, vol. 99, p. 08R102, 2006.
- [4] Y. Melikhov and J. E. Snyder *et al.*, "The effect of Cr-substitution on the magnetic anisotropy and its temperature dependence in Cr-substituted cobalt ferrite," *IEEE Trans. Magn.*, vol. 42, no. 10, pp. 2861–2863, 2006.
- [5] R. M. Bozorth, *Ferromagnetism*. Princeton, NJ: D. Van Nostrand, 1951.
- [6] Y. Chen, J. E. Snyder, K. W. Dennis, R. W. McCullum, and D. C. Jiles, "Temperature dependence of the magnetomechanical effect in metal-bonded cobalt ferrite composites under torsional strain," *J. Appl. Phys.*, vol. 87, no. 9, pp. 5798–5800, 2000.
- [7] B. Zhou and Y.-W. Zhang *et al.*, "Enhanced magneto-optical Kerr effects and decreased Curie temperature in Co-Mn ferrite thin films," *Appl. Phys. Lett.*, vol. 79, no. 12, pp. 1849–1851, 2001.
- [8] N. Rawah and Y. Melikhov *et al.*, "Variation of magnetoelastic properties of $Co_{1-x}Ge_xFe_{2-2x}O_4$ with temperature," in *Proceedings ICG-08 52nd Conf. Magnetism and Mag. Mater.*, Tampa, FL, 5–9, 2007.
- [9] G. A. Sawatzky, F. Van Der Woude, and A. H. Morrish, "Inhomogeneous study of several ferrimagnetic spinets," *Phys. Rev.*, vol. 187, no. 2, pp. 747–757, Nov. 1969.
- [10] S. H. Song, "Magnetic and magnetoelastic properties of M-substituted cobalt ferrites ($M = Ni, Cr, Ga, Ge$)," Ph.D. dissertation, Iowa State Univ., Ames, IA, 2007.
- [11] R. M. Bozorth, E. F. Tilden, and A. J. Williams, "Anisotropy and magnetostriction of some ferrites," *Phys. Rev.*, vol. 99, no. 6, pp. 1788–1798, Sep. 1955.
- [12] C. C. H. Lo, "Compositional dependence of the magnetoelastic effect in substituted cobalt ferrite for magnetoelastic stress sensors," *IEEE Trans. Magn.*, vol. 43, no. 6, 2007.
- [13] S. J. Lee and C. C. H. Lo *et al.*, "Magnetic and magnetoelastic properties of Cr-substituted cobalt ferrite," *J. Appl. Phys.*, vol. 102, no. 7, p. 073910, 2007.
- [14] Y. Chen, B. K. Kriegermeier-Sutton, J. E. Snyder, K. W. Dennis, R. W. McCullum, and D. C. Jiles, "Magnetoelastic effects under torsional strain in iron, cobalt and nickel," *J. Magnetism Magn. Mater.*, vol. 236, no. 1–2, pp. 131–138, Oct. 2001.
- [15] N. Rawah and Y. Melikhov *et al.*, "Temperature dependence of magnetic anisotropy of Ga-substituted cobalt ferrite," *J. Appl. Phys.*, vol. 103, no. 7, p. 07E506, 2008. [Online]. Available: <http://link.aip.org/link/JAP10307E506>
- [16] A. D. Al-Rawah and A. Rais *et al.*, "Magnetic properties of $Co_{1-x}Ni_xFe_{2-2x}O_4$ mixed ferrites ($M = Co, Ni, 0 \leq x \leq 0.4$)," *J. Magnetism Magn. Mater.*, vol. 269, no. 2, pp. 168–175, 2004.

Manuscript received March 03, 2008. Current version published December 17, 2008. Corresponding author: N. Rawah (e-mail: RawahN@cf.ac.uk; RawahN@cariff.ac.uk).

Temperature dependence of magnetic anisotropy of germanium/cobalt cosubstituted cobalt ferrite

N. Ravva,^{a)} Y. Melikhov, I. C. Nlebedim, D. C. Jiles, J. E. Snyder, A. J. Moses, and P. I. Williams
Wolfson Centre for Magnetics, Cardiff University, Cardiff CF24 3AA, United Kingdom

(Presented 14 November 2008; received 22 September 2008; accepted 4 January 2009; published online 9 March 2009)

The variations in magnetization and magnetic anisotropy of $\text{Ge}^{4+}/\text{Co}^{2+}$ cosubstituted cobalt ferrite with temperature were investigated for a series of compositions $\text{Co}_{1-x}\text{Ge}_x\text{Fe}_{2-2x}\text{O}_4$ ($0 \leq x \leq 0.4$). The magnetization at 5 T and low temperature were observed to increase for all Ge/Co cosubstituted samples compared to pure CoFe_2O_4 . Hysteresis loops were measured for each sample over the magnetic field range of -5 T to $+5$ T for temperatures in the range of 10–400 K. The high field regions of these loops were modeled using Law of Approach to saturation, which represents the rotational and forced magnetization processes. The first order cubic magnetocrystalline anisotropy coefficient K_1 was calculated from these fits. K_1 decreased with increasing Ge content at all temperatures. Anisotropy increased substantially as temperature decreased. Below 150 K, for certain compositions ($x=0, 0.1, 0.2,$ and 0.3), the maximum applied field of $\mu_0 H=5$ T was less than the anisotropy field and therefore insufficient to saturate the magnetization. In these cases, the use of the Law of Approach model can give values of K_1 that are lower than the correct values and this method cannot be used to estimate anisotropy accurately under these conditions. © 2009 American Institute of Physics. [DOI: 10.1063/1.3077201]

I. INTRODUCTION

There has been a recent interest in cobalt ferrite based materials because of their high magnetostrictive strain amplitude, high magnetostrictive strain derivative (rate of change in magnetostrictive strain with applied field), and low hysteresis, which makes them a candidate material for high performance stress/torque sensor and actuator applications.^{1–6} Chemical substitution can enhance the properties of cobalt ferrite by altering the cation distribution in the cubic spinel structure, therefore, influencing the magnetoelastic properties of these materials. Previous studies have shown that the substitution of M^{3+} (Mn^{3+} , Cr^{3+} , and Ga^{3+})^{2,3,7} in place of some of Fe^{3+} reduces the hysteresis and increases the strain derivative of cobalt ferrite for certain compositions with, however, a decline or no improvement in the magnitude of magnetostrictive strain amplitude. The change in magnetoelastic properties of these materials can be explained in terms of the change in important magnetic properties such as the magnetization characteristics and magnetocrystalline anisotropy.

In the present study, we have investigated a new cosubstitution of $\text{Ge}^{4+}/\text{Co}^{2+}$ in place of some of Fe^{3+} in cobalt ferrite. The high tetrahedral site preference of Ge^{4+} in the cubic spinel lattice of cobalt ferrite and the additional substitution of Co^{2+} produced a more favorable change in properties in comparison to previously tried substitutions.

II. EXPERIMENT AND RESULTS

A series of randomly oriented polycrystalline $\text{Ge}^{4+}/\text{Co}^{2+}$ cosubstituted cobalt ferrite samples with general composition

of $\text{Co}_{1-x}\text{Ge}_x\text{Fe}_{2-2x}\text{O}_4$ was made by standard powder ceramic techniques with a final sintering at 1350 °C for 24 h, followed by furnace cooling to room temperature.^{1,3} The target compositions had a germanium content of $x=0, 0.1, 0.2, 0.3,$ and 0.4 . The actual compositions were determined using energy dispersive x-ray spectroscopy (EDS) in a scanning electron microscope (SEM) and were found to be close to the target compositions, as shown in Table I. The Curie temperatures of Ge/Co cosubstituted cobalt ferrite have been found to decrease with increasing x .⁸

The variation in technical saturation of magnetization with temperature was measured using a superconducting quantum interference device (SQUID) magnetometer at an applied field of $\mu_0 H=5$ T. As can be seen in Fig. 1, the magnetization increased monotonically with decreasing temperature over the range of 400–160 K for all samples. The apparent saturation magnetization decreased for CoFe_2O_4 below 160 K, for $\text{Co}_{1.1}\text{Ge}_{0.1}\text{Fe}_{1.8}\text{O}_4$ below 128 K, and for $\text{Co}_{1.2}\text{Ge}_{0.2}\text{Fe}_{1.6}\text{O}_4$ below 78 K. For all other samples, saturation magnetization was observed to increase with decreasing temperature throughout the entire temperature range.

TABLE I. Comparison of target and actual compositions in $\text{CoGe}_x\text{Fe}_{2-2x}\text{O}_4$.

Target compositions	Composition by EDS		
	Fe	Co	Ge
CoFe_2O_4	2.05	0.95	...
$\text{Co}_{1.1}\text{Ge}_{0.1}\text{Fe}_{1.8}\text{O}_4$	1.77	1.11	0.12
$\text{Co}_{1.2}\text{Ge}_{0.2}\text{Fe}_{1.6}\text{O}_4$	1.57	1.21	0.22
$\text{Co}_{1.3}\text{Ge}_{0.3}\text{Fe}_{1.4}\text{O}_4$	1.29	1.33	0.38
$\text{Co}_{1.4}\text{Ge}_{0.4}\text{Fe}_{1.2}\text{O}_4$	1.10	1.43	0.47

^{a)}Electronic mail: ravva@cf.ac.uk.

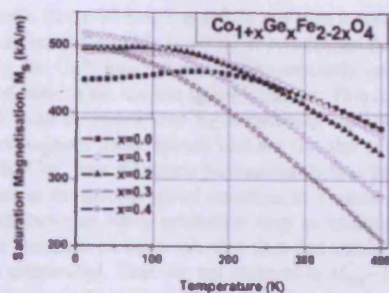


FIG. 1. The variation in technical saturation magnetization with temperature.

Symmetric magnetic hysteresis loops were measured with a SQUID magnetometer for temperatures 10, 50, 100, 150, 200, 250, 300, 350, and 400 K using a maximum applied field of $\mu_0 H = 5$ T.

For calculation of anisotropy, the high field regions of the M - H loops were fitted to the Law of Approach to saturation.⁹ The underlying assumption is that this high field regime represents the processes of reversible rotation of magnetization against anisotropy and forced magnetization. According to the Law of Approach, the high field regions ($H \gg H_{\text{coercivity}}$) of M - H loops can be described by

$$M = M_s \left[1 - \frac{8 K_1^2}{105 \mu_0 M_s^2 H^2} \right] + \kappa H, \quad (1)$$

where M is the magnetization, M_s is the saturation magnetization, H is the applied field, κ is the forced magnetization coefficient that describes the linear increase in spontaneous magnetization at high fields, and K_1 is the first order cubic anisotropy coefficient. The constant $8/105$ is specific to cubic anisotropy of randomly oriented polycrystalline materials. At temperatures above 150 K, data from the field region $\mu_0 H \geq 1$ T were fitted to Eq. (1) to determine the values of parameters M_s , K_1 , and κ . At temperatures below 150 K, the field range for fitting was restricted to $\mu_0 H \geq 2$ T, and, in some cases, the forced magnetization term was set to zero, i.e., $\kappa = 0$, with M_s and K_1 being the only fitting parameters (see discussion below).

III. DISCUSSION

The analysis of temperature dependence of cubic anisotropy of germanium/cobalt cosubstituted cobalt ferrite can be divided into two temperature zones, above and below 150 K. Above 150 K, the maximum applied field is sufficiently large compared to the anisotropy field so as to give good approach to saturation and good fits. The anisotropy of all samples was observed to increase as the temperature decreased. This is so because during cooling, as we move further away from the Curie temperature of these samples, the ratio of exchange interaction to thermal energy increases, which contributes to the increase in anisotropy. As the temperature was reduced from 400 K, the cubic anisotropy for every sample increased slowly at first and steeply below a certain temperature. As can be seen in Fig. 2, the region of steep increase in K_1

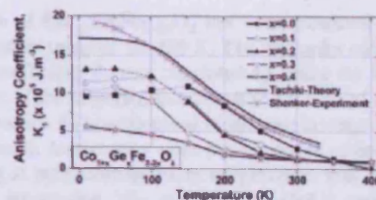


FIG. 2. Temperature dependence of cubic anisotropy coefficient K_1 calculated by fitting the experimental data to Law of Approach for $\text{Co}_{1+x}\text{Ge}_x\text{Fe}_{2-2x}\text{O}_4$. Experimental data (Ref. 11) marked as Shenker experiment and theoretically calculated data (Ref. 12) marked as Tachiki theory are presented for comparison.

moved to lower temperatures as the Ge/Co ratio increased from $x=0.0$ to $x=0.4$. It is possible that this effect is correlated with the decrease in Curie temperature of Ge/Co cosubstituted cobalt ferrite with increasing germanium/cobalt ratio.

Below 150 K, the first order magnetocrystalline cubic anisotropy coefficient K_1 appears to decrease with decreasing temperature for CoFe_2O_4 below 150 K, for $\text{Co}_{1.1}\text{Ge}_{0.1}\text{Fe}_{1.8}\text{O}_4$ below 100 K, and for $\text{Co}_{1.2}\text{Ge}_{0.2}\text{Fe}_{1.6}\text{O}_4$ and $\text{Co}_{1.3}\text{Ge}_{0.3}\text{Fe}_{1.4}\text{O}_4$ below 50 K. This apparent decrease can be explained by the presence of anisotropy fields higher than the applied field of $\mu_0 H = 5$ T. This high anisotropy prevents the rotation against it, therefore, causing the apparent saturation magnetization to decrease for CoFe_2O_4 below 160 K, for $\text{Co}_{1.1}\text{Ge}_{0.1}\text{Fe}_{1.8}\text{O}_4$ below 128 K, and for $\text{Co}_{1.2}\text{Ge}_{0.2}\text{Fe}_{1.6}\text{O}_4$ below 78 K, and preventing from complete saturation being reached in these cases (see Fig. 1). The estimated value of anisotropy field $H_A = 2K_1/(\mu_0 M)$ (Ref. 10) for pure cobalt ferrite at 150 K is 4.8 T and is expected to rise above the maximum applied field of 5 T at temperatures below 150 K. Therefore, in these cases, the anisotropy coefficient could not be calculated accurately by fitting the data available to the Law of Approach even using special adjustment procedures.⁶ As anisotropy field increased significantly close to 150 K, the region of hysteresis loop where rotation of magnetization against anisotropy takes place shifts to higher field values; therefore, the field range for fitting was restricted to $\mu_0 H \geq 2$ T. Additionally, the force magnetization coefficient was set to zero, i.e., $\kappa = 0$, as in the presence of such high anisotropy fields, the maximum applied field of $\mu_0 H = 5$ T was not sufficient to cause forced magnetization, but rather is still rotating magnetization against the high anisotropy field. Despite these adjustment procedures the values of anisotropy coefficient K_1 , calculated with $\kappa = 0$, are suspect and are connected with dotted lines in Fig. 2. The results from Shenker,¹¹ who determined cubic anisotropy of CoFe_2O_4 using single crystals and torque measurements near their easy axes, support our hypothesis of high anisotropy fields. Additionally, the room temperature value of K_1 for CoFe_2O_4 we determined ($K_1 = 2.66 \times 10^5 \text{ J m}^{-3}$) is consistent with the theoretical predictions made by Tachiki.¹²

As can be seen from Fig. 1, the sample with Ge concentration of $x=0.1$ has higher technical saturation magnetization than pure cobalt ferrite at room temperature. Furthermore, the extrapolated 0 K saturation magnetization $M(0 \text{ K})$ appears to increase initially as we substitute Ge/Co into co-

balt ferrite (for $x=0.1, 0.2,$ and 0.3) and then it reduces with high concentration of Ge ($x=0.4$). This indicates that at least initially, the Ge^{4+} ions substitute predominantly into the tetrahedral sites in the inverse spinel structure. This increase in $M(0\text{ K})$ can be understood by considering the structure of the ferrimagnetic cubic spinels and the fact that at least initially the Ge^{4+} ions substitute predominantly into the tetrahedral sites in the inverse spinel structure. In a spinel structure, there are twice as many octahedral sites as tetrahedral sites, and the moments on the octahedral sites and tetrahedral sites couple antiparallel. Thus the net moment is $M_{\text{oct}} - M_{\text{tet}}$. Pure cobalt ferrite is an inverse spinel, meaning that Co^{2+} has an energetic preference for the octahedral sites; however, it tends not to be 100% inverse, meaning that some smaller amount of Co does reside on the tetrahedral sites. Ge^{4+} , on the other hand, is expected to have a natural preference for the tetrahedral sites due to its tetravalence and tendency toward sp^3 hybridization.¹³ So although in $\text{Ge}^{4+}/\text{Co}^{2+}$ co-substitution for Fe^{3+} much of the Co^{2+} might be substituting into the octahedral sites and decreasing M_{oct} by a little, most of the Ge^{4+} indeed appears to be substituting into the tetrahedral sites, decreasing M_{tet} by much more (since Ge^{4+} has no magnetic moment). Thus the net moment goes up. For high content of Ge ($x=0.4$), $M(0\text{ K})$ appears to decrease again. This could be due to either some of the additional Ge^{4+} substituting into the octahedral sites or due to decrease in the tetrahedral-octahedral exchange coupling to the point that a noncollinear spin arrangement occurs.¹⁴

The substitution of Ge^{4+} reduces the exchange coupling between the octahedral and tetrahedral sites, as can be seen from the steep decrease in Curie temperature with Ge content.⁸ It is probable that this reduction in exchange coupling is responsible for the reduction in the magnitude of magnetic anisotropy, despite the fact that upon Ge/Co co-substitution, the amount of Co in the octahedral sites most likely increases. The crystalline anisotropy in cobalt ferrite acts like the spring constant against which applied field is acting while producing magnetostriction. Thus, with reduction in anisotropy, the strain derivative (i.e., rate of change in magnetostrictive strain with applied field) increases.¹⁵ This has been indeed observed in the case of Ge/Co co-substitution.⁸

As opposed to all our previously investigated substitutions of Mn^{3+} ,³ Cr^{3+} ,⁴ and Ga^{3+} (Ref. 7) for Fe^{3+} in cobalt ferrite, for small amounts of Ge/Co co-substitution ($x=0.1$), the maximum magnetostriction actually increases, rather than decreasing, and then falls off initially more slowly.⁸ This is likely due to increased amount of Co^{2+} in the octahedral sites. This combination of both increasing strain derivative and increasing magnetostriction amplitude with small amounts of Ge/Co co-substitution makes this material series favorable out of those we have investigated for stress sensor and actuator applications.

IV. SUMMARY AND CONCLUSION

The temperature dependence of magnetic properties of a series of Ge/Co co-substituted cobalt ferrite with a general

formula of $\text{Co}_{1-x}\text{Ge}_x\text{Fe}_{2-2x}\text{O}_4$ has been measured within a temperature range of 10–400 K. The first order cubic anisotropy coefficient K_1 was calculated by fitting the high field regimes of the magnetization curves to the Law of Approach to saturation. K_1 was observed to increase in magnitude with decrease in temperature with the region of steep increase coming at progressively lower temperatures with increasing Ge/Co substitution. The anisotropy of Ge/Co co-substituted cobalt ferrite was seen to decrease with increasing germanium concentration at all temperatures. The saturation magnetization at 10 K was seen to increase with germanium concentration for $0 \leq x \leq 0.3$, indicating that for these compositions, Ge^{4+} substitutes predominantly into the tetrahedral sites. It was found that in certain cases of low temperature, the anisotropy of samples with germanium concentration of $x=0, 0.1, 0.2,$ and 0.3 was so high that it prevents complete approach to saturation in the presence of maximum applied field of 5 T. For Ge/Co co-substituted compositions in the region of $\text{Co}_{1-x}\text{Ge}_x\text{Fe}_{2-2x}\text{O}_4$, the combination of higher magnetostrictive strain derivative brought about by lower anisotropy than pure cobalt ferrite and the increased maximum magnetostriction make this material a favorable candidate for stress sensor and actuator applications.

ACKNOWLEDGMENTS

This research was supported by the UK Engineering and Physical Sciences Research Council under Grant No. EP/D057094 and by the U.S. National Science Foundation under Grant No. DMR-0402716.

- ¹Y. Chen, J. E. Snyder, C. R. Schwichtenberg, K. W. Collins, and D. C. Jiles, *IEEE Trans. Magn.* 35, 3652 (1999).
- ²S. J. Lee, C. C. H. Lo, P. N. Mudge, S. H. Song, Y. Melikhov, J. E. Snyder, and D. C. Jiles, *J. Appl. Phys.* 102, 073910 (2007).
- ³J. A. Paulsen, A. P. Ring, C. C. H. Lo, J. E. Snyder, and D. C. Jiles, *J. Appl. Phys.* 97, 044502 (2005).
- ⁴Y. Melikhov, J. E. Snyder, C. C. H. Lo, P. N. Mudge, S. H. Song, K. W. Dennis, and D. C. Jiles, *IEEE Trans. Magn.* 42, 2861 (2006).
- ⁵Y. Melikhov, J. E. Snyder, C. C. H. Lo, A. P. Ring, J. A. Paulsen, K. W. Dennis, and D. C. Jiles, *J. Appl. Phys.* 99, 08R102 (2006).
- ⁶N. Rawwah, Y. Melikhov, D. C. Jiles, J. E. Snyder, A. J. Moses, P. I. Williams, and S. H. Song, *J. Appl. Phys.* 103, 07E506 (2008).
- ⁷N. Rawwah, Y. Melikhov, J. E. Snyder, S. H. Song, D. C. Jiles, A. J. Moses, and P. I. Williams, 52nd Conference on Magnetism and Magnetic Materials, Tampa, Florida, 2007 (unpublished).
- ⁸N. Rawwah, I. C. Nlebedim, Y. Melikhov, J. E. Snyder, D. C. Jiles, A. J. Moses, P. I. Williams, F. Anayi, and S.-H. Song, *IEEE Trans. Magn.* 44, 3013 (2008).
- ⁹S. Chikazumi, *Physics of Ferromagnetism*, 2nd ed. (Oxford University Press, New York, 1997), pp. 503–508.
- ¹⁰B. D. Cullity, *Introduction to Magnetic Materials* (Addison-Wesley, Reading, MA, 1972), p. 233.
- ¹¹H. Sherringer, *Phys. Rev.* 107, 1246 (1957).
- ¹²M. Tachiki, *Prog. Theor. Phys.* 23, 1055 (1960).
- ¹³A. D. Al-Rawaf, A. Rais, A. A. Younis, A. M. Gimnoch, M. E. Elzain, S. Manen, and A. Al-Falaky, *J. Magn. Magn. Mater.* 269, 168 (2004).
- ¹⁴J. Smit and H. P. J. Wijn, *Ferrites* (N.V. Philips, Eindhoven, Holland, 1959), p. 163.
- ¹⁵D. C. Jiles, J. B. Thoele, and M. K. Devine, *IEEE Trans. Magn.* 28, 27 (1992).

Dependence of Magnetomechanical Performance of $\text{CoGa}_x\text{Fe}_{2-x}\text{O}_4$ on Temperature Variation
Accepted for presentation at the 55th MMM Conference, Atlanta Georgia, USA, November, 2010
Submitted for publication in the *J. Appl. Phys.*, April, 2011

I.C Nlebedim, Y. Melikhov, J. E Snyder, N. Ranvah, A.J Moses and D.C Jiles

Wolfson Centre for Magnetics, School of Engineering, Cardiff University, CF24 3AA, Cardiff, United Kingdom

The temperature dependence of the magnetoelastic properties of the $\text{CoGa}_x\text{Fe}_{2-x}\text{O}_4$ system (for $x = 0.0, 0.2$ and 0.4) has been studied. It has been shown that both increase in temperature and applied magnetic field resulted in reduced magnetostrictive hysteresis. In both $\text{CoGa}_{0.2}\text{Fe}_{1.8}\text{O}_4$ and $\text{CoGa}_{0.4}\text{Fe}_{1.6}\text{O}_4$, measurement at 250 K gave higher magnetostriction amplitude than at 150 K. It was also shown that $\text{CoGa}_{0.2}\text{Fe}_{1.8}\text{O}_4$ is more stable under temperature variation than other compositions studied which is important for sensor applications. The highest strain sensitivity was obtained for $\text{CoGa}_{0.2}\text{Fe}_{1.8}\text{O}_4$ at 250 K. Results demonstrate the possibility of tailoring magnetomechanical properties of the material to suit intended applications under varying temperature conditions.

Index Terms: Cobalt Gallium ferrite, Magnetostriction, Magnetostrictive hysteresis, Strain sensitivity, Curie, Temperature

I. INTRODUCTION

Cobalt ferrite and its derivatives are very promising materials for stress sensor and actuator applications. The need to control the magnetostrictive properties has resulted in several studies including the influence of vacuum sintering [1], annealing and quenching heat treatment [2], metal bonding [3] and cation substitutions [4, 5, 6, 7]. Of these, cation substitution has been found very useful for improving the strain response of cobalt ferrite to applied magnetic field. Substitution of non-magnetic cations alters the concentration and site occupancy of Co^{2+} and thereby alters the magnetocrystalline anisotropy and magnetostrictive properties. As a result, the desired properties for specific magnetomechanical applications can be controlled by selectively tailoring cation site occupancy via cation substitution.

This study reports on the influence of temperature variation on the properties of $\text{CoGa}_x\text{Fe}_{2-x}\text{O}_4$ for magnetomechanical applications. $\text{CoGa}_x\text{Fe}_{2-x}\text{O}_4$ has over 145% higher magnetomechanical response than CoFe_2O_4 [6] but nothing is known about how the response varies with temperature. Of all cation substitution studies on CoFe_2O_4 , $\text{CoGa}_x\text{Fe}_{2-x}\text{O}_4$ showed the highest strain sensitivity at room temperature [7]. Since devices based on $\text{CoGa}_x\text{Fe}_{2-x}\text{O}_4$ would need to work under varying temperature conditions, understanding the dependence of performance on temperature is crucial. This study therefore reports on the dependence of the magnetostrictive properties of $\text{CoGa}_x\text{Fe}_{2-x}\text{O}_4$ on both cation composition and temperature.

II. EXPERIMENTAL DETAILS

The samples were all calcined at 1000 °C and sintered at 1350 °C for 24 hrs in air. The crystal structures were studied by X-ray diffractometry (XRD). To investigate the microstructures of the samples, backscattered electron micrographs were obtained using an analytical scanning electron microscope (ASEM) equipped with an x-ray analyzer for energy dispersive X-ray Spectroscopy (EDX). Magnetostriction (λ) was measured parallel to the applied field with strain gauges attached on the samples, over a

temperature range 50 to 350 K using a Physical Property Measurement System (PPMS). The derivative of the λ -H curve with respect to field ($d\lambda/dH$) was used to determine the strain sensitivity of the materials.

III. RESULTS AND DISCUSSIONS

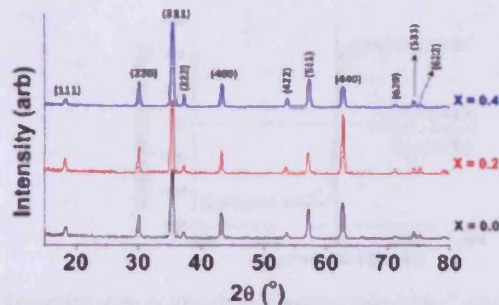


Fig. 1: XRD patterns of the $\text{CoGa}_x\text{Fe}_{2-x}\text{O}_4$ samples ($x = 0.0, 0.2$ and 0.4)

X-ray diffraction patterns of the samples are shown in Fig. 1. The patterns have peaks which are consistent with the cubic spinel phase. They are not shifted relative to the un-substituted ($x = 0$) sample as was the case of $\text{CoAl}_x\text{Fe}_{2-x}\text{O}_4$ [8]. This indicates that the lattice parameters of the samples were similar or even identical. The lattice parameter was found to be 8.38 \AA for all the samples. The preservation of the lattice parameter for $\text{CoGa}_x\text{Fe}_{2-x}\text{O}_4$ in contrast with the $\text{CoAl}_x\text{Fe}_{2-x}\text{O}_4$ system arises because the ionic radii of Ga^{3+} in tetrahedral and octahedral positions ($r_A = 0.47 \text{ \AA}$, $r_B = 0.62 \text{ \AA}$) are similar to those of Fe^{3+} ($r_A = 0.49 \text{ \AA}$, $r_B = 0.65 \text{ \AA}$). Therefore, substituting Ga^{3+} for Fe^{3+} is expected to have little effect on the lattice parameter compared with the substitution of the Al^{3+} with much smaller ionic radii ($r_A = 0.39 \text{ \AA}$, $r_B = 0.54 \text{ \AA}$). From EDX, the sample compositions were shown to be $\text{Co}_{1.02}\text{Fe}_{1.98}\text{O}_4$ (for $x = 0$), $\text{Co}_{1.04}\text{Ga}_{0.2}\text{Fe}_{1.74}\text{O}_4$ (for $x = 0.2$) and $\text{Co}_{1.03}\text{Ga}_{0.39}\text{Fe}_{1.58}\text{O}_4$ (for $x = 0.4$).

Fig. 2 shows the backscattered electron images of the samples. The uniformity in contrast observed for all the samples further confirms that all had a single phase crystal structure. They also appear to be of uniform composition because the image contrast in a backscattered electron image is a function of composition.



Fig. 2: Backscattered scanning electron micrographs for the $\text{CoGa}_x\text{Fe}_{2-x}\text{O}_4$ system ($x = 0.0, 0.2, 0.4$)

The variation of magnetization with applied magnetic field is shown in Fig. 3. In contrast with Al^{3+} substitution [7], the saturation magnetization of the Ga^{3+} substituted cobalt ferrite initially increased at $x = 0.2$ and later decreased at $x = 0.4$. The saturation magnetization at $x = 0.4$ is also higher than that at $x = 0.0$. The increase in saturation magnetization with Ga^{3+} substitution is in agreement with Ga^{3+} having tetrahedral site preference. The net magnetization in un-substituted cobalt ferrite is mainly due to the magnetic moments of Co^{2+} on the octahedral sites as the moments of the Fe^{3+} on the octahedral and

tetrahedral sites almost cancel each other. Substituting non-magnetic Ga^{2+} into the tetrahedral sites will displace either Co^{2+} or Fe^{3+} into the octahedral site. In either case, the consequence will be an increase in saturation magnetization.

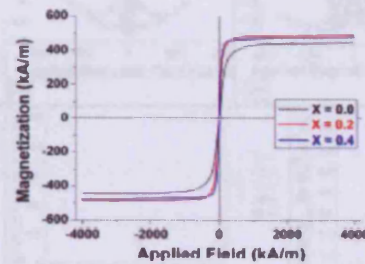


Fig. 3: Variation of magnetization as a function of applied field for Ga^{3+} concentrations $x = 0.0, 0.2$ and 0.4 .

As shown in Fig. 4a for un-substituted cobalt ferrite samples, peak to peak magnetostriction amplitude decreased with increase in the measurement temperature. In the substituted samples, the slope of the high field region of the magnetostriction curve was initially low at 50 K, increased at 150 K and decreased further with increase in measurement temperatures. Also, the contribution of λ_{111} to the resultant magnetostriction increased with increase in measurement temperature. It can be seen from all the results that both increase in temperature and applied magnetic field resulted in reduced magnetostrictive hysteresis. This suggests that the effects of high temperature and high applied field on magnetostrictive hysteresis are similar. Hysteresis in magnetic materials are mainly caused by the difficulty to rotate magnetization past imperfections in the samples. This difficulty reduces with increase in magnetic energy and/or thermal energy making it possible to have less hysteresis with increase in applied field and/or temperature.

In both $\text{CoGa}_{0.2}\text{Fe}_{1.8}\text{O}_4$ (Fig. 4b) and $\text{CoGa}_{0.4}\text{Fe}_{1.6}\text{O}_4$ (Fig. 4c), measurement at 250 K gave higher magnetostriction amplitude than at 150 K. A similar result was obtained for the magnetostriction of $\text{CoAl}_x\text{Fe}_{2-x}\text{O}_4$ at $x = 0.5$ and 0.7 [8]. This result shows that the substitution of Ga^{3+} for Fe^{3+} alters the magnetostrictive behaviors of cobalt ferrite even at different temperatures as shown in Fig. 4d. It could also be seen in Fig. 4d that under temperature variations, $\text{CoGa}_x\text{Fe}_{2-x}\text{O}_4$ is more stable than CoFe_2O_4 which could be essential for sensor applications. In Fig. 4e, it appears that $\text{CoGa}_{0.2}\text{Fe}_{1.8}\text{O}_4$ is more stable with temperature variation than $\text{CoGa}_{0.4}\text{Fe}_{1.6}\text{O}_4$.

Fig. 4f shows the variation of $(d\lambda/dH)_{\text{max}}$ of $\text{CoGa}_x\text{Fe}_{2-x}\text{O}_4$ with temperature. At all temperatures studied except 250 K, $(d\lambda/dH)_{\text{max}}$ decreased with increase in gallium concentration. As in the case of Al^{3+} substituted cobalt ferrite [9], at 250 K, $(d\lambda/dH)_{\text{max}}$ initially increased from $x = 0.0$ to 0.2 and decreased afterwards. This is similar to the observation at 300 K except that the maximum $(d\lambda/dH)_{\text{max}}$ was at $x = 0.4$ rather than 0.2 . A similar trend was observed in previous studies on cation substituted cobalt ferrite samples in which the $(d\lambda/dH)_{\text{max}}$ initially increased at lower concentrations of the substituted cations ($x \leq 0.2$) and finally decreased at higher cation concentrations [4]. The figure also shows that with cation substitution, the maximum strain sensitivity is in the temperature range, 250 to 300 K. These results demonstrate the capability to alter magnetomechanical performance to suit intended applications by adjusting concentration at different temperatures.

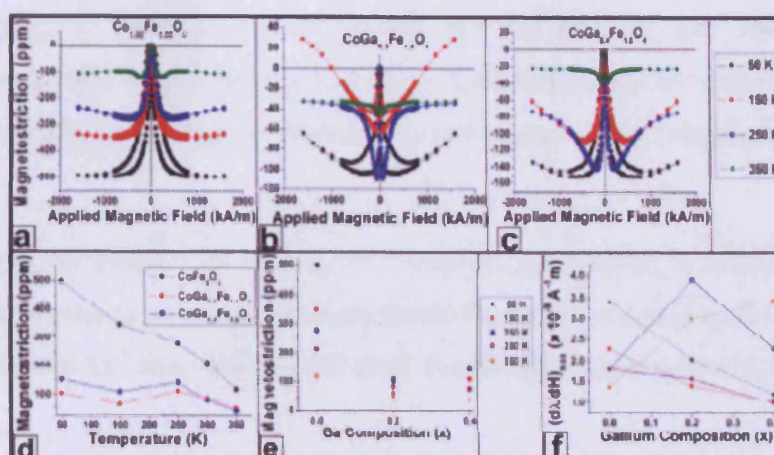


Fig. 4: Magnetostriction curves for the $\text{CoGa}_x\text{Fe}_{2-x}\text{O}_4$ system (a) $x = 0.0$, (b) $x = 0.2$, and (c) $x = 0.4$. Variation of magnetostriction amplitude with (d) temperature and (e) Ga^{3+} composition (f) shows the variation of strain derivative with temperature

CONCLUSION

A study on the dependence of magnetomechanical performance of $\text{CoGa}_x\text{Fe}_{2-x}\text{O}_4$ on temperature variation has shown that magnetostrictive properties of cobalt ferrite can be altered by cation substitution. It was observed from XRD and SEM investigations that substitution of Ga^{3+} does not result in any observable changes in the crystal structure and microstructure of the material. On the other hand, magnetic and magnetostrictive properties have shown strong dependence on Ga^{3+} substitution. The highest strain sensitivity $(d\lambda/dH)_{\max}$ was observed for $\text{CoGa}_{0.2}\text{Fe}_{1.8}\text{O}_4$ in the region 250 to 300 K.

ACKNOWLEDGMENTS

This research was supported by the UK EPSRC (grant no. EP/057094) and by the US NSF (grant no. DMR-0402716).

REFERENCES

- [1] I. C. Nlebedim, N. Ranvah, P. I. Williams, Y. Melikhov, F. Anayi, J. E. Snyder, A. J. Moses, D. C. Jiles, *J. Magn. and Magn. Mater.* **321** (2009) 2528
- [2] I. C. Nlebedim, N. Ranvah, P. I. Williams, Y. Melikhov, J. E. Snyder, A. J. Moses, D. C. Jiles, *J. Magn. Magn. Mater.* **322** (2010) 1929
- [3] Y. Chen, J. E. Snyder, C. R. Schwichtenberg, K. W. Dennis, R. W. McCallum, D. C. Jiles *IEEE Trans. on Magn.*, **35** (1999) 3652
- [4] C. C. H. Lo *IEEE Trans. Magn.* **43** (2007) 2367
- [5] N. Ranvah, C. I. Nlebedim, Y. Melikhov, J. E. Snyder, D. C. Jiles, A. J. Moses, P. I. Williams, F. Anayi, and S. H. Song *IEEE Trans. Magn.*, **44** (2008) 3013
- [6] S. H. Song, C. C. H. Lo, S. J. Lee, S. T. Aldini, J. E. Snyder and D. C. Jiles *J. Appl. Phys.*, **101** (2007) 09C517
- [7] I. C. Nlebedim, N. Ranvah, Y. Melikhov, P. I. Williams, J. E. Snyder, A. J. Moses and D. C. Jiles, *IEEE Trans. Magn.*, **45**, 4120 (2009)
- [8] I. C. Nlebedim, N. Ranvah, Y. Melikhov, P. I. Williams, J. E. Snyder, A. J. Moses, and D. C. Jiles *J. Appl. Phys.* **107** (2010) 09A936

Conference Presentations

1. I.C. Nlebedim, Y. Melikhov, J. E. Snyder, A.J. Moses and D.C. Jiles "Dependence of Magnetomechanical Performance of $\text{CoGa}_x\text{Fe}_{2-x}\text{O}_4$ on Temperature Variation" **Abstract No: DH-07**, 55th Magnetism and Magnetic Materials Conference, Atlanta, Georgia, November 2010
2. I. C. Nlebedim, N. Ranvah, Y. Melikhov, P. I. Williams, J. E. Snyder, A. J. Moses, D. C. Jiles "Effect of Temperature Variation on the Magnetoelastic Properties of $\text{CoAl}_x\text{Fe}_{2-x}\text{O}_4$ " **Abstract No: BT-09**, submitted for the 11th Joint MMM-INTERMAG Conference, Washington DC, January 2010.
3. A. Raghunathan, I. C. Nlebedim, J. E. Snyder, and D. C. Jiles "Growth of Crystalline Cobalt ferrite Thin Films at Lower Temperatures using Pulsed-laser Deposition Technique" **Abstract No: CE-02**, submitted for the 11th Joint MMM-INTERMAG Conference, Washington DC, January 2010.
4. N. Ranvah, I. C. Nlebedim, Y. Melikhov, J. E. Snyder, A. J. Moses, P. I. Williams, and D. C. Jiles "AC Magnetic Property Measurements on Cobalt Ferrite for Sensor Applications", **Abstract No: GU-09**, submitted for the 11th Joint MMM-INTERMAG Conference, Washington DC, January 2010.
5. Jiles, David; Raghunathan, Arun; Nlebedim, Ikenna; and Snyder, John; "Growth of Crystalline Cobalt ferrite Thin Films at Lower Temperatures using Pulsed-laser Deposition Technique" **Abstract No: Q37.00014**, American Physical Society Meeting, Portland, Oregon, March, 2010
6. Jiles, David; Ranvah, Naresh; Nlebedim, Ikenna; Melikhov, Yevgen; Snyder, John; Moses, Anthony; Williams, Paul; "Effect on chemical substitution on properties of magnetoelastic properties of cobalt ferrite" **Abstract No: S1.00098**, American Physical Society Meeting, Portland, Oregon, March, 2010
7. I. C. Nlebedim, N. Ranvah, P. I. Williams, Y. Melikhov, J. E. Snyder, A. J. Moses, D. C. Jiles "Investigation of the Dependence of Sensitivity of Magnetostriction of Cobalt Ferrite to Applied

Field on Cation Ratio and Processing Parameters" Abstract No: M3-15, 19th Soft Magnetic Materials Conference, Torino, September, 2009

8. I. C. Nlebedim "Enhancement of Highly Magnetostrictive Cobalt Ferrite for Advanced Sensor and Actuator Applications" IEEE Magnetic Society Summer School, Nanjing, China, September, 2009.
9. N. Ranvah, I. C. Nlebedim, Y. Melikhov, J. E. Snyder, A. J. Moses, P. I. Williams, and D. C. Jiles, "Investigation of cobalt ferrite based materials for stress sensor and actuator design" N IEEE Magnetic Society Summer School, Nanjing, China, September, 2009.
10. I. C. Nlebedim, N. Ranvah, P. I. Williams, Y. Melikhov, J. E. Snyder, A. J. Moses, D. C. Jiles "Effect of Heat Treatment on the Cation Distribution in Magnetostrictive $\text{CoAl}_x\text{Fe}_{2-x}\text{O}_4$ " Abstract No: 572435, 8th Pacific Rim Conference on Ceramics and Glass Technology, Vancouver, Canada, June, 2009
11. N. Ranvah, Y. Melikhov, I. C. Nlebedim, D. C. Jiles, J. E. Snyder, A. J. Moses, P. I. Williams "Temperature dependence of magnetic properties of $\text{CoAl}_x\text{Fe}_{2-x}\text{O}_4$ for magnetostrictive sensor and actuator applications" Abstract No: EU-04, INTERMAG 2009 conference, Sacramento, California, May 2009.
12. I.C. Nlebedim, N Ranvah, P.I. Williams, Y Melikhov, J.E. Snyder, A.J. Moses, D.C. Jiles "Magnetic and Magnetomechanical Properties of $\text{CoAl}_x\text{Fe}_{2-x}\text{O}_4$ for Stress Sensor and Actuator Applications" Abstract No: AP-11, INTERMAG 2009 conference, Sacramento, California, May 2009.
13. I. C Nlebedim, N. Ranvah, Y. Melikhov, P. I Williams, J. E Snyder, A. J Moses and D. C Jiles "Highly Magnetostrictive $\text{CoAl}_x\text{Fe}_{2-x}\text{O}_4$ for Advanced Magnetomechanical Sensor and Actuator Applications" Materials Network Wales meeting, Technium Springboard, Cwmbran, Torfaen, Wales, May 14, 2009

14. N. Ranvah, Y. Melikhov, I. C. Nlebedim, D. C. Jiles, J. E. Snyder, A. J. Moses, P. I. Williams, "Temperature dependence of magnetic anisotropy of germanium/cobalt co-substituted cobalt ferrite" Abstract No: HE-09, pp. 234, 53rd Magnetism and Magnetic Materials Conference, Austin, Texas, November 2008.

15. N. Ranvah, I. C. Nlebedim, Y. Melikhov, D. C. Jiles, J. E. Snyder, A. J. Moses, P. I. Williams, and S. H. Song "Temperature dependence of magnetostriction of $\text{Co}_{1-x}\text{Ge}_x\text{Fe}_{2-2x}\text{O}_4$ for magnetostrictive sensor and actuator applications", , Abstract No: HG-08, IEEE INTERMAG Conference, Madrid, Spain, May 2008.

16. I.C. Nlebedim, N Ranvah, P.I. Williams, Y Melikhov, F Anayi, J.E. Snyder, A.J. Moses, D.C. Jiles "Enhancement of Magnetoelastic Properties of Highly Magnetostrictive Cobalt Ferrite through Control of Sintering Conditions" Abstract No: EW-07, INTERMAG Europee 2008, Madrid, Spain, May 2008.

17. N. Ranvah, I. C. Nlebedim, Y. Melikhov, D. C. Jiles, J. E. Snyder, A. J. Moses, P. I. Williams, "Magnetic and magnetoelastic properties of Ge-substituted cobalt ferrite" Abstract No: D23.006, American Physical Society Meeting, New Orleans, March 2008.

